SUPPORTING INFORMATION

Selective 1,2-insertion of carbodiimides and substrate-divergent silyl group migration at 1-metallacyclobuta-2,3-dienes

Xinzhe Shi[1,2‡], Sihan Li[2‡], Anke Spannenberg[2], Fabian Reiß[2*], Torsten Beweries[2*]

[1] School of Chemistry and Chemical Engineering, Harbin Institute of Technology, Harbin 150001, P. R. China

[2] Leibniz-Institut für Katalyse e.V., Albert-Einstein-Str. 29a, 18059 Rostock, Germany

Email: fabian.reiss@catalysis.de, torsten.beweries@catalysis.de.

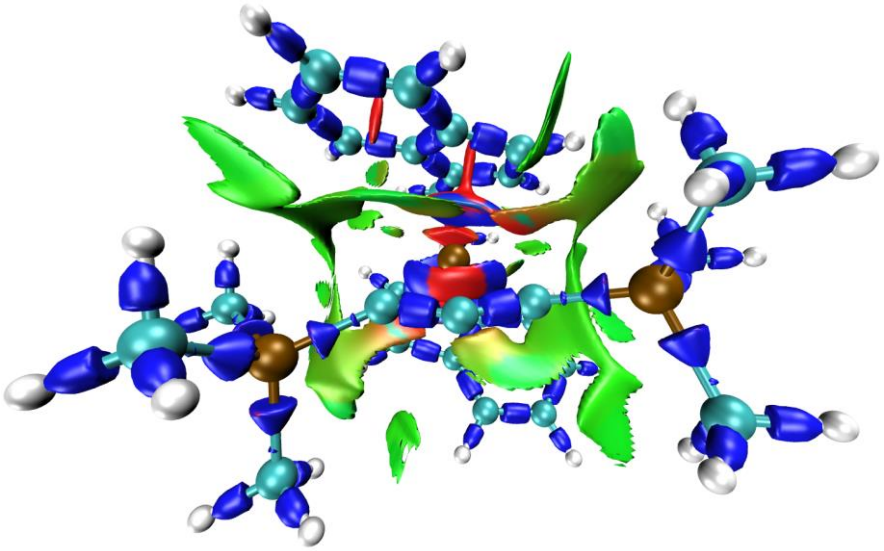

Table of Contents

1. Experimental details

1.1 General information

All manipulations were carried out in an oxygen- and moisture-free argon atmosphere using standard Schlenk and drybox techniques. The solvents were purified with the Grubbs-type column system "Pure Solv MD-5" and dispensed into thick-walled glass Schlenk bombs equipped with Young-type Teflon valve stopcocks. [*rac*-(ebthi)$ZrCl_2$] (MCAT), [*rac*-(sbthi)$ZrCl_2$] (LANXESS), [*rac*-(ebi)$ZrCl_2$] (LANXESS) and [*rac*-(sbi)$ZrCl_2$] (LANXESS) were stored under argon and used as received. [*rac*-(ebi)$TiCl_2$] was prepared according to the literature.[1] N,N'-Diisopropylcarbodiimide (99%, Acros), N,N'-dicyclohexylcarbodiimide (99%, Acros), N,N'-di-*p*-tolylcarbodiimide (95%, MERCK), N,N'-bis(2,6-diisopropylphenyl)carbodiimide (98%, TCI) and N,N'-bis(trimethylsilyl)carbodiimide (98%, Acros) were condensed prior to use into a Schlenk flask and stored under argon. Benzophenone (99%, Fluka) was dried in *vacuo* prior to use and stored under argon. [$Li_2(Me_3SiC_3SiMe_3)$] was prepared according to a literature procedure and isolated as white solid.[2,3] Preparative chromatography was performed by elution from columns of slurry-packed Silica Gel 60 (0.04-0.063 mm, Macherey-Nagel GmbH).

NMR spectra were determined on Bruker AV300 and AV400. ^1H and $^{13}C\{^1H\}$ chemical shifts were referenced to the solvent signal: benzene-d_6 (δ_H 7.16 ppm, δ_C 128.06 ppm).[4]

IR spectra were recorded on a Bruker Alpha FT-IR ATR Spectrometer, placed in a glove box under Ar atmosphere. Spectra are not corrected.

MS analysis was done using a Finnigan MAT 95-XP instrument (Thermo-Electron) in CI^+/CI^- mode (isobutene).

Melting points are uncorrected and were determined in sealed capillaries under Ar atmosphere using a Mettler-Toledo MP 70.

X-Ray diffraction data were collected on a STOE IPDS II (**P$_{2b\text{-}iPr}$** and **P$_{2d\text{-}SiMe3}$**) and a Bruker Kappa APEX II Duo diffractometer (**2c**, **2d**, **P$_{1a\text{-}iPr}$**, **P$_{2a\text{-}iPr}$**, **P$_{2d\text{-}iPr}$**, **P$_{1a\text{-}Cy}$**, **P$_{2c\text{-}Cy}$**, **P$_{2c\text{-}SiMe3}$** and **6**), respectively. The structures were solved by direct methods (SHELXS-97)[5] and refined by full-matrix least-squares procedures on F^2 (SHELXL-2014).[6] Diamond[7] was used for graphical representations. For 2244176 contributions of disordered solvent were removed form the diffraction data using the SQUEEZE procedure in PLATON.[8] 2244181 was refined as a racemic twin.

CHN analysis was using a Leco TruSpec elemental analyser. At this point it should be pointed out that we could not obtain satisfactory elemental analysis in most cases. Despite repeated recrystallisation, repeated measurements with and without oxidiser V_2O_5 and modified furnace temperature, we observed up to 20% less carbon content than calculated/expected. This behaviour might be explained by formation of mixed zircon-silicon-carbides (ceramics) in the furnace and therefore the carbon content dramatically decreases.[9]

All DFT calculations were carried out with the Gaussian 16[11] package of molecular orbital programs further details are given in section 9 Computational details.

2. Synthesis of compounds

2.1 Synthesis of 1,3-bis(trimethylsilyl)propyne[3]

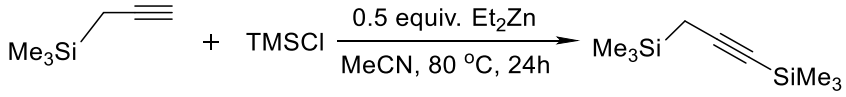

To a 50 mL Schlenk flask trimethyl-(propargyl)-silane (1 eq., 22.8 mmol, 2.56 g), chlorotrimethylsilane (1.2 eq., 27.4 mmol, 2.98 g), MeCN (20 mL) and Et_2Zn (*n*-hexane solution, 1 M, 0.5 eq., 0.5 mL) were added and the mixture was stirred at 80 °C for 24 h. After cooling, the reaction mixture was cannula-filtered and evaporated the solvent on rotary evaporator. Flash silica gel column chromatography with hexane as the eluent afforded the raw product as pink oil. After adding $Na[Et_4Al]$ to dry the product overnight and condensation, a colourless oil was obtained (2.36 g, 56.5 %). Spectroscopic data are in agreement with previously published data.[2,10]

2.2 Synthesis of 1a

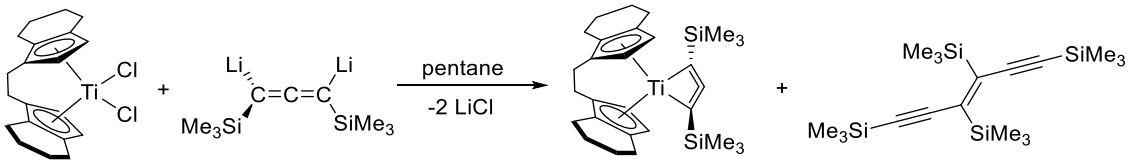

1a **4**

The synthesis of complex **1a** is follows the previously published procedure.[10] During the crystallisation of the concentrated solution at -78 °C, we observed that the desired complex **1a** formed as a dark red solid and the coupling product **4** formed as colourless crystals, which were removed by washing with pentane several times.

Complex **1a**: **^{1}H NMR** (25 °C, benzene-d_6, 400.1 MHz): δ 7.22 (d, $^3J_{H,H}$ = 3.4 Hz, 2H, 2 x C*H* ebthi), 5.27 (d, $^3J_{H,H}$ = 3.4 Hz, 2H, 2 x C*H* ebthi), 2.72-2.52 (m, 4H, 2 x CH_2 ebthi), 2.41-2.25 (m, 4H, CH_2 ebthi), 2.05-1.87 (m, 4H, 2 x CH_2 ebthi), 1.43-1.07 (m, 10H, 5 x CH_2 ebthi), 0.35 (s, $^2J_{H,Si}$ = 6.8 Hz, 18H, 6 x CH_3 $SiMe_3$).

Compound **4**: **^{1}H NMR** (25 °C, benzene-d_6, 400.1 MHz): δ 0.48 (s, $^2J_{H,Si}$ = 7.0 Hz, 18H, 6 x CH_3 $SiMe_3$), 0.20 (s, $^2J_{H,Si}$ = 6.8 Hz, 18H, 6 x CH_3 $SiMe_3$).

2.3 Synthesis of 1c

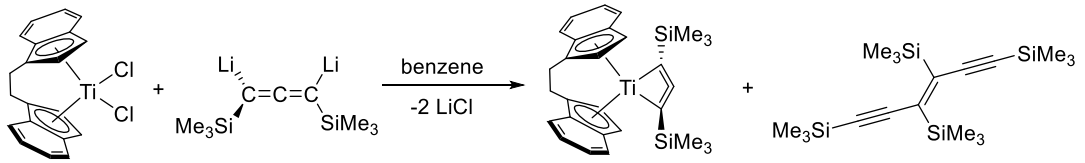

1c **4**

[*rac*-(ebi)$TiCl_2$] (0.18 mmol, 6.8 mg) and [$Li_2(Me_3SiC_3SiMe_3)$] (0.18 mmol, 3.5 mg) were dissolved in benzene-d_6 (0.6 mL) in a Young-NMR tube at room temperature. The colour of the reaction mixture changed from pale green to dark green in 10 minutes and to dark red after 12 hours. The coupling product **4** was also observed during the reaction.

Complex **1c**: **^{1}H NMR** (25 °C, benzene-d_6, 400.1 MHz): δ 6.92-6.82 (m, 4H, 4 x C*H* ebi), 6.81-6.75 (d, $^3J_{H,H}$ = 3.6 Hz, 2H, 2 x C*H* ebi), 6.61-6.41 (m, 4H, 4 x C*H* ebi), 5.77-5.70 (d, $^3J_{H,H}$ = 3.6 Hz, 2H, 2 x C*H* ebi), 3.15-2.93 (m, 4H, 2 x CH_2 ebi), 0.14 (s, $^2J_{H,Si}$ = 6.6 Hz, 18H, 6 x CH_3 $SiMe_3$).

Compound **4**: **^{1}H NMR** (25 °C, benzene-d_6, 400.1 MHz): δ 0.48 (s, $^2J_{H,Si}$ = 7.0 Hz, 18H, 6 x CH_3 $SiMe_3$), 0.20 (s, $^2J_{H,Si}$ = 6.8 Hz, 18H, 6 x CH_3 $SiMe_3$).

2.4 Synthesis of 2c

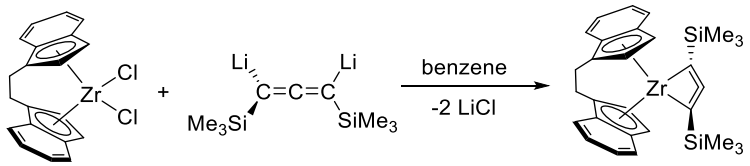

2c

[*rac*-(ebi)$ZrCl_2$] (0.24 mmol, 100 mg) and [$Li_2(Me_3SiC_3SiMe_3)$] (0.24 mmol, 47 mg) were dissolved in benzene (5 mL) at room temperature. After 2 days of stirring at room temperature or 1 hour of stirring at 50 °C, the orange-red solution was filtered and then the solvent was removed in *vacuo*. After dissolving in pentane, the residue was concentrated and stored at -30 °C for recrystallisation to obtain complex **2c** (Isolated yield 90%, 114 mg). Crystals suitable for SC-XRD analysis were grown from pentane.

uncorrected decomposition point: 95-98 °C (Ar.). **^{1}H NMR** (25 °C, benzene-d_6, 400.1 MHz): δ 7.21-7.17 (m, 4H, 4 x C*H* ebi), 6.90-6.86 (m, 2H, 2 x C*H* ebi), 6.61-6.55 (m, 4H, 4 x C*H* ebi), 5.85 (d, $^3J_{H,H}$ = 3.5 Hz, 2H, 2 x C*H* ebi), 3.04-2.86 (m, 4H, 2 x CH_2 ebi), 0.15 (s, $^2J_{H,Si}$ = 6.6 Hz, 18H, 6 x CH_3 $SiMe_3$). **^{13}C{^{1}H} NMR** (25 °C, benzene-d_6, 100.6 MHz): δ 172.7 (*C*=C=*C*), 145.2 (C=*C*=C), 127.1 (2 x *C*H ebi), 126.0 (2 x *C* ebi), 125.3, 122.2, 120.3 (6 x *C*H ebi), 120.0, 112.5 (4 x *C* ebthi), 105.7, 105.3 (4 x *C*H ebi), 27.0 (2 x CH_2 ebi), 2.8 (2 x $SiMe_3$). **^{29}Si-inept NMR** (25 °C, benzene-d_6, 79.5 MHz): δ −13.99 (dec, $^2J_{H,Si}$ = 6.6 Hz, *Si*Me_3). **Elemental analysis** calcd (%) for M($C_{29}H_{34}Si_2Zr$) = 529.99 g mol^{-1}: C 65.72, H 6.47; found: C 63.43, H 6.94. **IR** (ATR, 32 scans, cm^{-1}): 3062 (w), 2950 (w), 2895 (w), 2856 (w), 1834 (w), 1735 (m), 1605 (w), 1443 (w), 1344 (w), 1241 (m), 1191 (w), 1046 (w), 1010 (w), 938 (w), 827 (s), 781 (s), 736 (s), 683 (m), 626 (m), 555 (w), 494 (m), 473

(m). **MS-CI$^+$** (*isobutane*): [M$^+$] 530 (70), [(M−H)$^+$] 529 (100), [ebi$^+$] 259 (14), [($Me_3SiCHCCHSiMe_3$+H)$^+$] 185 (23), [$SiMe_3^+$] 73 (6).

2.5 Synthesis of 2d

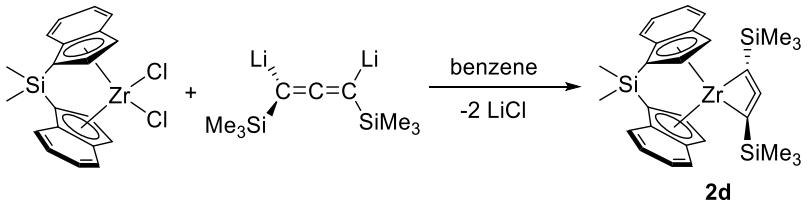

2d

[*rac*-(sbi)$ZrCl_2$] (0.22 mmol, 100 mg) and [$Li_2(Me_3SiC_3SiMe_3)$] (0.22 mmol, 43 mg) were dissolved in benzene (3 mL). After 2 days of stirring at room temperature or 30 minutes of stirring at 50 °C, the red solution was filtered and then the solvent was removed in *vacuo*. After dissolving in pentane, the residue was concentrated and stored at -30 °C for recrystallisation to obtain complex **2d** (Isolated yield 89%, 110 mg). Crystals suitable for SC-XRD analysis were grown from pentane.

uncorrected decomposition point: 75-78 °C (Ar.). **^{1}H NMR** (25 °C, benzene-d_6, 400.1 MHz): δ 7.32 (dd, $^3J_{H,H}$ = 3.4, 1.0 Hz, 2H, 2 x C*H* sbi), 7.25-7.22 (m, 2H, 2 x C*H* sbi), 7.12-7.09 (m, 2H, 2 x C*H* sbi), 6.59-6.5 (m, 4H, 4 x C*H* sbi), 5.97 (d, $^3J_{H,H}$ = 3.4 Hz, 2H, 2 x C*H* sbi), 0.67 (s, $^2J_{H,Si}$ = 7.0 Hz, 6H, 2 x CH_3 $SiMe_2$), 0.14 (s, $^2J_{H,Si}$ = 6.6 Hz, 18H, 6 x CH_3 $SiMe_3$). **^{13}C{^{1}H} NMR** (25 °C, benzene-d_6, 100.6 MHz): δ 180.1 (*C*=C=*C*), 140.2 (C=*C*=C), 128.6 (2 x *C* sbi), 127.4, 125.7, 123.7 (6x *C*H sbi), 123.4 (2 x *C* sbi), 122.8, 111.6, 109.4 (6 x *C*H sbi), 85.9 (2 x *C* sbi), 2.6 (2 x $SiMe_3$), −1.9 (2 x $SiMe_2$). **^{29}Si-inept NMR** (25 °C, benzene-d_6, 79.5 MHz): δ −12.99 (dec, $^2J_{H,Si}$ = 6.6 Hz, *Si*Me_3), −14.87 (sep, $^2J_{H,Si}$ = 7.0 Hz, *Si*Me_2). **Elemental analysis** calcd (%) for M($C_{29}H_{36}Si_3Zr$) = 560.09 g mol^{-1}: C 62.19, H 6.48; found: C 58.11, H 4.65 (Measured with V_2O_5. Without V_2O_5: C 52.77, H 4.28). **IR** (ATR, 32 scans, cm^{-1}): 3061 (w), 2950 (w), 2894 (w), 1860 (w), 1732 (m), 1604 (w), 1471 (w), 1442 (w), 1400 (w), 1334 (w), 1296 (w), 1239 (m), 1155 (w), 1135 (w), 1048 (w), 962 (w), 826 (s), 788 (s), 740 (s), 681 (s), 649 (m), 627 (m), 558 (w), 528 (m), 485 (m), 452 (s), 432 (m). **MS-CI$^+$** (*isobutane*): [sbi$^+$] 289 (21), [2x(indenyl)$^+$] 229 (13), [($SiMe_2$+indenyl)$^+$] 173 (100), [(indenyl+2H)$^+$] 117 (55), [Zr$^+$] 91 (28).

3. Reactivity of complexes with carbodiimides

General procedure: 1-metallacyclobuta-2,3-diene complexes (0.20 mmol) and carbodiimides (0.20 mmol) were dissolved in benzene (2 mL) and stirred at room temperature for several hours, then the solvent was removed in *vacuo*. After dissolving in pentane, the residue was concentrated and stored at -30 °C for recrystallisation to obtain the corresponding products.

3.1 Reactivity with N,N'-diisopropylcarbodiimide

3.1.1 Reaction of 1a with N,N'-diisopropylcarbodiimide to $P_{1a\text{-}iPr}$

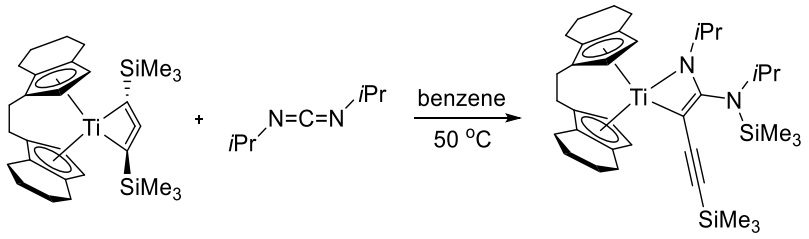

1a **$P_{1a\text{-}iPr}$**

According to general procedure, compound **1a** (0.20 mmol, 99 mg) was reacted with N,N'-diisopropylcarbodiimide (0.20 mmol, 25 mg) at 50 °C. Then the reaction mixture was stirred for 72 hours and **$P_{1a\text{-}iPr}$** (67 mg, 54%) was obtained after recrystallisation. Crystals suitable for SC-XRD analysis were grown from pentane.

uncorrected decomposition point: 154-157 °C (Ar.). **^{1}H NMR** (25 °C, benzene-d_6, 400.1 MHz): δ 7.44 (d, $^3J_{H,H}$ = 3.0 Hz, 1H, C*H* ebthi), 6.91 (d, $^3J_{H,H}$ = 3.1 Hz, 1H, C*H* ebthi), 5.64 (d, $^3J_{H,H}$ = 3.0 Hz, 1H, C*H* ebthi), 5.45 (d, $^3J_{H,H}$ = 3.2 Hz, 1H, C*H* ebthi), 3.71 (m, 1H, C*H* *i*Pr), 3.18 (m, 1H, C*H* *i*Pr), 2.79-2.65 (m, 2H, CH_2 ebthi), 2.63-2.13 (m, 10H, 5 x CH_2 ebthi), 2.09-1.98 (m, 2H, CH_2 ebthi), 1.90-1.64 (m, 4H, 2 x CH_2 ebthi), 1.50 (d, $^3J_{H,H}$ = 6.5 Hz, 3H, CH_3 *i*Pr), 1.42 (d, $^3J_{H,H}$ = 6.3 Hz, 3H, CH_3 *i*Pr), 1.38-1.28 (m, 2H, CH_2 ebthi), 1.26 (d, $^3J_{H,H}$ = 7.1 Hz, 3H, CH_3 *i*Pr), 0.95 (d, $^3J_{H,H}$ = 6.9 Hz, 3H, CH_3 *i*Pr), 0.51 (s, $^2J_{H,Si}$ = 6.5 Hz, 9H, 3 x CH_3 N-SiMe_3), 0.44 (s, $^2J_{H,Si}$ = 6.9 Hz, 9H, 3 x CH_3 C-SiMe_3). **^{13}C{^{1}H} NMR** (25 °C, benzene-d_6, 100.6 MHz): δ 183.1 (Ti-*C*), 140.7 (N*C*N), 129.5, 127.6, 126.0, 125.3, 123.4, 121.1 (6 x *C* ebthi), 119.7 (C≡*C*-SiMe_3), 119.6 (*C*H ebthi), 115.0 (*C*≡C-SiMe_3), 114.4 (*C*H ebthi), 108.3 (*C*H ebthi), 105.2 (*C*H ebthi), 52.7, 49.8 (2 x *C*H *i*Pr), 28.1 (*C*H_2 ebthi), 27.0, 26.7, 25.7 (3 x *C*H_3 *i*Pr), 25.2, 25.0 (2 x *C*H_2 ebthi), 24.5 (*C*H_3 *i*Pr), 24.0, 23.7, 23.4, 22.8, 22.7 (5 x *C*H_2 ebthi), 4.6, 1.6 (2 x SiMe_3). **^{29}Si-inept NMR** (25 °C, benzene-d_6, 79.5 MHz): δ 0.9, −22.4. **Elemental analysis** calcd (%) for M($C_{36}H_{56}N_2Si_2Ti$) = 620.90 g mol^{-1}: C 69.58, H 9.02, N 4.51; found: C 67.01, H 7.94, N 3.55. **IR** (ATR, 32 scans, cm^{-1}): 2949 (w), 2930 (w), 2856 (w), 2046 (m), 1950 (w), 1879 (w), 1594 (w), 1453 (w), 1439 (w), 1376 (w), 1359 (w), 1315 (w), 1241 (m), 1192 (m), 1156 (w), 1142 (w), 1112 (w), 1036 (w), 979 (m), 955 (w), 945 (w), 934 (w), 922 (w), 831 (s), 808 (s), 780 (s), 752 (s), 688 (m), 644 (s), 594 (m), 548 (m), 530 (m), 515 (m), 475 (m), 466 (m), 439 (m), 421 (m). **MS-CI$^+$** (*isobutane*): [(M−N*i*PrSiMe_3−CSiMe_3)$^+$] 405 (86), [(M−2SiMe_3−2H)$^+$] 472 (22), [(M−Ti−ebthi+2H)$^+$] 311 (20), [(*i*PrNCN*i*PrSiMe−4H)$^+$] 167 (100), [SiMe_3^+] 73 (3).

3.1.2 Reaction of 2a with N,N'-diisopropylcarbodiimide to $P_{2a\text{-}iPr}$

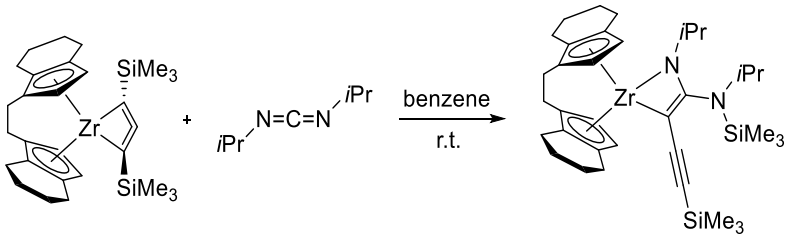

2a **$P_{2a\text{-}iPr}$**

According to general procedure, compound **2a** (0.20 mmol, 108 mg) was reacted with N,N'-diisopropylcarbodiimide (0.20 mmol, 25 mg) at room temperature. The colour of the reaction mixture changed from pale green to dark green in 5 minutes. Then the reaction mixture was stirred for 6 hours and **$P_{2a\text{-}iPr}$** (123 mg, 93%) was obtained after recrystallisation. Crystals suitable for SC-XRD analysis were grown from pentane.

uncorrected decomposition point: 121-124 °C (Ar.). **^{1}H NMR** (25 °C, benzene-d_6, 400.1 MHz): δ 7.00 (d, $^{3}J_{H,H}$ = 3.1 Hz, 1H, C*H* ebthi), 6.28 (d, $^{3}J_{H,H}$ = 3.1 Hz, 1H, C*H* ebthi), 5.58 (d, $^{3}J_{H,H}$ = 3.1 Hz, 1H, C*H* ebthi), 5.47 (d, $^{3}J_{H,H}$ = 3.1 Hz, 1H, C*H* ebthi), 3.65 (hept, $^{3}J_{H,H}$ = 6.5 Hz, 1H, C*H* *i*Pr), 3.24 (hept, $^{3}J_{H,H}$ = 6.7 Hz, 1H, C*H* *i*Pr), 2.80-1.94 (m, 15H, CH_2 ebthi), 1.61-1.44 (m, 1H, CH_2 ebthi), 1.45 (d, $^{3}J_{H,H}$ = 6.5 Hz, 3H, CH_3 *i*Pr), 1.42-1.26 (m, 4H, 2 x CH_2 ebthi), 1.32 (d, $^{3}J_{H,H}$ = 7.1 Hz, 3H, CH_3 *i*Pr), 1.23 (d, $^{3}J_{H,H}$ = 6.2 Hz, 3H, CH_3 *i*Pr), 0.97 (d, $^{3}J_{H,H}$ = 6.7 Hz, 3H, CH_3 *i*Pr), 0.53 (s, $^{2}J_{H,Si}$ = 6.5 Hz, 9H, 3 x CH_3 N-SiMe_3), 0.43 (s, $^{2}J_{H,Si}$ = 6.9 Hz, 9H, 3 x CH_3 C-SiMe_3). **^{13}C{^{1}H} NMR** (25 °C, benzene-d_6, 100.6 MHz): δ 148.8 (N*C*N), 145.1 (Zr-*C*), 128.4, 126.8, 126.1, 124.1, 123.2, 121.2 (6 x *C* ebthi), 117.7 (*C*H ebthi), 115.1 (*C*≡C-SiMe_3), 110.1, 107.0, 105.3 (3 x *C*H ebthi), 103.1 (C≡*C*-SiMe_3), 53.1, 47.9 (2 x *C*H *i*Pr), 27.8, 27.44 (2 x *C*H_2 ebthi), 27.39, 26.3, 26.1 (3 x *C*H_3 *i*Pr), 25.2, 24.5 (2 x *C*H_2 ebthi), 24.2 (*C*H_3 *i*Pr), 23.9, 23.79, 23.76, 23.5, 23.1, 22.6 (6 x *C*H_2 ebthi), 4.4, 1.8 (2 x SiMe_3). **^{29}Si-inept NMR** (25 °C, benzene-d_6, 79.5 MHz): δ 0.66 (dec, $^{2}J_{H,Si}$ = 6.5 Hz, N-*Si*Me_3), −22.83 (dec, $^{2}J_{H,Si}$ = 6.9 Hz, C-*Si*Me_3). **Elemental analysis** calcd (%) for M($C_{36}H_{56}N_2Si_2Zr$) = 664.25 g mol^{-1}: C 65.10, H 8.50, N 4.22; found: C 61.34, H 9.02, N 2.70. **IR** (ATR, 32 scans, cm^{-1}): 2942 (w), 2854 (w), 2064 (m), 1449 (w), 1370 (w), 1357 (w), 1312 (w), 1241 (m), 1207 (m), 1137 (w), 1118 (m), 1035 (w), 986 (m), 945 (w), 922 (w), 833 (s), 780 (s), 754 (m), 685 (w), 642 (s), 546 (m), 513 (w), 478 (m), 425 (w). **MS-CI^{+}** (*isobutane*): [M^{+}] 664 (72), [(M−2H)$^{+}$] 662 (100), [(M−Zr−ebthi+2H)$^{+}$] 311 (18), [SiMe_3^{+}] 73 (4).

3.1.3 Reaction of 2b with N,N′-diisopropylcarbodiimide to $P_{2b\text{-}iPr}$

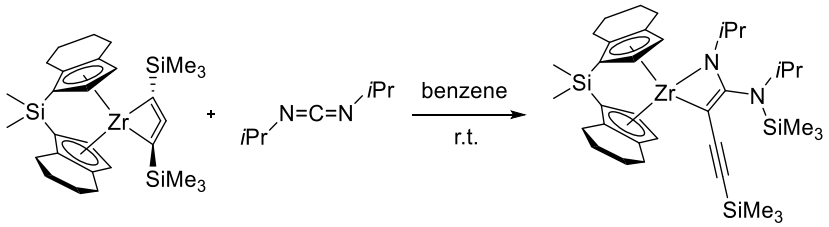

2b **$P_{2b\text{-}iPr}$**

According to general procedure, compound **2b** (0.20 mmol, 114 mg) was reacted with N,N′-diisopropylcarbodiimide (0.20 mmol, 25 mg) at room temperature. The colour of the reaction mixture changed from pale green to dark green in 5 minutes. Then the reaction mixture was stirred for 1 hour and **$P_{2b\text{-}iPr}$** (122 mg, 88%) was obtained after recrystallisation. Crystals suitable for SC-XRD analysis were grown from pentane.

uncorrected decomposition point: 122-125 °C (Ar.). **^{1}H NMR** (25 °C, benzene-d_6, 400.1 MHz): δ 7.32 (d, $^{3}J_{H,H}$ = 3.1 Hz, 1H, C*H* sbthi), 6.52 (d, $^{3}J_{H,H}$ = 3.1 Hz, 1H, C*H* sbthi), 5.67 (d, $^{3}J_{H,H}$ = 3.1 Hz, 1H, C*H* sbthi), 5.61 (d, $^{3}J_{H,H}$ = 3.1 Hz, 1H, C*H* sbthi), 3.66 (hept, $^{3}J_{H,H}$ = 6.5 Hz, 1H, C*H* *i*Pr), 3.24 (hept, $^{3}J_{H,H}$ = 6.9 Hz, 1H, C*H* *i*Pr), 2.69-2.47 (m, 3H, CH_2 sbthi), 2.42-2.39 (m, 2H, CH_2 sbthi), 2.35-2.28 (m, 2H, CH_2 sbthi), 2.17-2.10 (m, 1H, CH_2 sbthi), 2.04-1.91 (m, 2H, CH_2 sbthi), 1.60-1.23 (m, 6H, 3x CH_2 sbthi), 1.47 (d, $^{3}J_{H,H}$ = 6.5 Hz, 3H, CH_3 *i*Pr), 1.32 (d, $^{3}J_{H,H}$ = 7.2 Hz, 3H, CH_3 *i*Pr), 1.26 (d, $^{3}J_{H,H}$ = 6.2 Hz, 3H, CH_3 *i*Pr), 0.97 (d, $^{3}J_{H,H}$ = 6.8 Hz, 3H, CH_3 *i*Pr), 0.58 (s, $^{2}J_{H,Si}$ = 6.9 Hz, 3H, CH_3 $SiMe_2$), 0.55 (s, $^{2}J_{H,Si}$ = 6.6 Hz, 9H, 3 x CH_3 N-$SiMe_3$), 0.43 (s, $^{2}J_{H,Si}$ = 6.9 Hz, 3H, CH_3 $SiMe_2$), 0.42 (s, $^{2}J_{H,Si}$ = 6.9 Hz, 9H, 3 x CH_3 C-$SiMe_3$). **^{13}C{^{1}H} NMR** (25 °C, benzene-d_6, 100.6 MHz): δ 147.7 (N*C*N), 147.3 (Zr-*C*), 130.6, 128.8, 128.2, 125.3 (4 x *C* sbthi), 123.3, 117.3 (2 x *C*H sbthi), 114.4 (*C*≡C-$SiMe_3$), 111.4, 110.1 (2 x *C*H sbthi), 107.5, 104.7 (2 x *C* sbthi), 104.3 (C≡*C*-$SiMe_3$), 53.1, 48.1 (2 x *C*H *i*Pr), 27.5 (*C*H_3 *i*Pr), 26.9 (*C*H_2 sbthi), 26.2 (*C*H_3 *i*Pr), 26.2 (*C*H_2 sbthi), 25.8 (*C*H_3 *i*Pr), 25.5 (*C*H_2 sbthi), 24.2 (*C*H_3 *i*Pr), 24.0, 23.9, 23.6, 23.0, 22.9 (5 x *C*H_2 sbthi), 4.4, 1.7 (2 x $SiMe_3$), −1.4, −2.7 (2 x $SiMe_2$). **^{29}Si-inept NMR** (25 °C, benzene-d_6, 79.5 MHz): δ 0.73 (dec, $^{2}J_{H,Si}$ = 6.6 Hz, N-*Si*Me_3), −15.48 (sep, $^{2}J_{H,Si}$ = 6.9 Hz, *Si*Me_2), −22.61 (dec, $^{2}J_{H,Si}$ = 6.9 Hz, C-*Si*Me_3). **Elemental analysis** calcd (%) for M($C_{36}H_{58}N_2Si_3Zr$) = 694.35 g mol^{-1}: C 62.27, H 8.42, N 4.03; found: C 62.35, H 8.42, N 3.70 (Measured with V_2O_5. Without V_2O_5: C 57.45, H 8.670, N 2.320). **IR** (ATR, 32 scans, cm^{-1}): 3064 (w), 2929 (m), 2894 (w), 2861 (w), 2066 (m), 1845 (w), 1616 (w), 1562 (w), 1458 (w), 1418 (w), 1361 (w), 1322 (w), 1292 (w), 1242 (m), 1207 (m), 1137 (m), 1119 (m), 1041 (w), 986 (m), 965 (w), 923 (w), 830 (s), 800 (s), 781 (s), 754 (m), 676 (m), 660 (m), 645 (s), 601 (w), 548 (m), 473 (m), 445 (m), 423 (m). **MS-CI^{+}** (*isobutane*): [M^{+}] 694 (73), [(M−2H)$^{+}$] 692 (100), [(M−C_3H_7)$^{+}$] 651 (11).

3.1.4 Reaction of 2c with N,N'-diisopropylcarbodiimide to $P_{2c\text{-}iPr}$

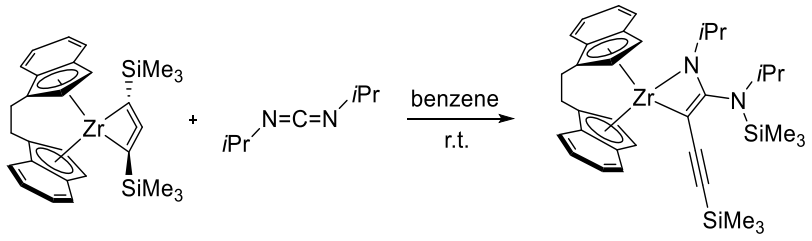

2c **$P_{2c\text{-}iPr}$**

According to general procedure, compound **2c** (0.20 mmol, 106 mg) was reacted with N,N'-diisopropylcarbodiimide (0.20 mmol, 25 mg) at room temperature. The colour of the reaction mixture changed from red to dark green in 5 minutes. Then the reaction mixture was stirred for 1 hour and the solvent was removed in *vacuo* to obtain **$P_{2c\text{-}iPr}$** as green powder (126 mg, 96%).

uncorrected decomposition point: 92-95 °C (Ar.). **^{1}H NMR** (25 °C, benzene-d_6, 400.1 MHz): δ 7.44 (dd, $^3J_{H,H}$ = 3.4, 0.8 Hz, 1H, C*H* ebi), 7.40 (dt, $^3J_{H,H}$ = 8.5, 1.0 Hz, 1H, C*H* ebi), 7.22 (dt, $^3J_{H,H}$ = 8.7, 1.1 Hz, 1H, C*H* ebi), 7.10-7.06 (m, 3H, 3 x C*H* ebi), 6.98-6.94 (m, 1H, C*H* ebi), 6.73 (ddd, $^3J_{H,H}$ = 8.7, 6.5, 1.0 Hz, 1H, C*H* ebi), 6.53 (d, $^3J_{H,H}$ = 3.5 Hz, 1H, C*H* ebi), 6.50 (ddd, $^3J_{H,H}$ = 8.6, 6.5, 1.0 Hz, 1H, C*H* ebi), 6.02 (d, $^3J_{H,H}$ = 3.5 Hz, 1H, C*H* ebi), 5.92 (d, $^3J_{H,H}$ = 3.4 Hz, 1H, C*H* ebi), 3.31 (hept, $^3J_{H,H}$ = 6.5 Hz, 1H, C*H* *i*Pr), 3.14 (m, 1H, CH_2 ebi), 3.06-2.97 (m, 2H, C*H* *i*Pr and CH_2 ebi), 2.95-2.88 (m, 2H, CH_2 ebi), 1.40 (d, $^3J_{H,H}$ = 6.4 Hz, 3H, CH_3 *i*Pr), 1.24 (d, $^3J_{H,H}$ = 7.2 Hz, 3H, CH_3 *i*Pr), 1.14 (d, $^3J_{H,H}$ = 6.2 Hz, 3H, CH_3 *i*Pr), 0.45 (d, $^3J_{H,H}$ = 6.8 Hz, 3H, CH_3 *i*Pr), 0.44 (s, $^2J_{H,Si}$ = 6.9 Hz, 9H, 2 x CH_3 C-SiMe$_3$), 0.41 (s, $^2J_{H,Si}$ = 6.6 Hz, 9H, 3 x CH_3 N-SiMe$_3$). **^{13}C{^{1}H} NMR** (25 °C, benzene-d_6, 100.6 MHz): δ 150.3 (N*C*N), 148.4 (Zr-*C*), 126.5, 125.16, 125.15, 125.06, 124.7 (5 x *C*H ebi), 123.84, 123.78, 123.5, 123.3 (4 x *C* ebi), 122.1, 120.5, 119.2 (3 x *C*H ebi), 116.7, 116.4 (2 x *C* ebi), 112.8 (*C*≡C-SiMe$_3$), 110.6, 110.4, 109.3 (3 x *C*H ebi), 102.8 (C≡*C*-SiMe$_3$), 101.8 (*C*H ebi), 54.3, 47.1 (2 x *C*H *i*Pr), 27.3, 27.2 (2 x *C*H$_2$ ebi), 26.4, 25.9, 25.6, 24.0 (4 x *C*H$_3$ *i*Pr), 4.5, 1.8 (2 x SiMe$_3$). **^{29}Si-inept NMR** (25 °C, benzene-d_6, 79.5 MHz): δ −0.19 (dec, $^2J_{H,Si}$ = 6.6 Hz, N-*Si*Me$_3$), −23.03 (dec, $^2J_{H,Si}$ = 6.9 Hz, C-*Si*Me$_3$). **Elemental analysis** calcd (%) for M($C_{36}H_{48}N_2Si_2Zr$) = 656.19 g mol^{-1}: C 65.90, H 7.37, N 4.27; found: C 65.14, H 7.55, N 2.96 (Measured with V_2O_5. Without V_2O_5: C 57.73, H 5.30, N 1.15). **IR** (ATR, 32 scans, cm^{-1}): 3064 (w), 2952 (w), 2924 (w), 2861 (w), 2065 (m), 1842 (w), 1582 (w), 1461 (w), 1446 (w), 1375 (w), 1352 (w), 1241 (m), 1219 (m), 1137 (w), 1117 (m), 1049 (w), 1010 (w), 984 (m), 923 (w), 831 (s), 782 (s), 735 (s), 687 (m), 645 (m), 546 (m), 515 (w), 472 (m), 443 (s). **MS-CI$^+$** (*isobutane*): [M$^+$] 656 (33), [ebi$^+$] 259 (100), [SiMe$_3^+$] 73 (41).

3.1.5 Reaction of 2d with N,N′-diisopropylcarbodiimide to $P_{2d\text{-}iPr}$

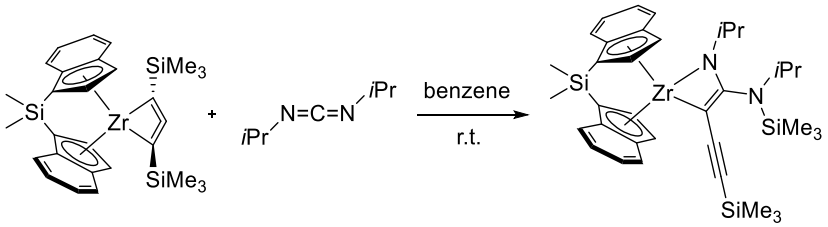

2d **$P_{2d\text{-}iPr}$**

According to general procedure, compound **2d** (0.20 mmol, 112 mg) was reacted with N,N′-diisopropylcarbodiimide (0.20 mmol, 25 mg) at room temperature. The colour of the reaction mixture changed from red to brown in 5 minutes. Then the reaction mixture was stirred for 1 hour and **$P_{2d\text{-}iPr}$** (123 mg, 90%) was obtained after recrystallisation. Crystals suitable for SC-XRD analysis were grown from pentane.

uncorrected decomposition point: 77-80 °C (Ar.). **^{1}H NMR** (25 °C, benzene-d_6, 400.1 MHz): δ 7.66 (dd, $^{3}J_{H,H}$ = 3.4, 0.9 Hz, 1H, C*H* sbi), 7.52 (dt, $^{3}J_{H,H}$ = 8.4, 1.1 Hz, 1H, C*H* sbi), 7.29 (dt, $^{3}J_{H,H}$ = 8.5, 1.1 Hz, 1H, C*H* sbi), 7.25 (dq, $^{3}J_{H,H}$ = 8.7, 1.0 Hz, 1H, C*H* sbi), 7.21 (dq, $^{3}J_{H,H}$ = 8.6, 1.0 Hz, 1H, C*H* sbi), 7.10 (ddd, $^{3}J_{H,H}$ = 8.6, 6.7, 1.1 Hz, 1H, C*H* sbi), 6.97 (ddd, $^{3}J_{H,H}$ = 8.4, 6.7, 1.1 Hz, 1H, C*H* sbi), 6.85 (dd, $^{3}J_{H,H}$ = 3.4, 0.9 Hz, 1H, C*H* sbi), 6.69 (ddd, $^{3}J_{H,H}$ = 8.7, 6.6, 1.1 Hz, 1H, C*H* sbi), 6.54 (ddd, $^{3}J_{H,H}$ = 8.5, 6.6, 1.0 Hz, 1H, C*H* sbi), 6.15 (d, $^{3}J_{H,H}$ = 3.4 Hz, 1H, C*H* sbi), 6.12 (d, $^{3}J_{H,H}$ = 3.4 Hz, 1H, C*H* sbi), 3.30 (hept, $^{3}J_{H,H}$ = 6.5 Hz, 1H, C*H* *i*Pr), 3.00 (hept, $^{3}J_{H,H}$ = 6.8 Hz, 1H, C*H* *i*Pr), 1.42 (d, $^{3}J_{H,H}$ = 6.5 Hz, 3H, CH_3 *i*Pr), 1.24 (d, $^{3}J_{H,H}$ = 7.2 Hz, 3H, CH_3 *i*Pr), 1.16 (d, $^{3}J_{H,H}$ = 6.2 Hz, 3H, CH_3 *i*Pr), 0.74 (s, $^{2}J_{H,Si}$ = 6.9 Hz, 3H, CH_3 SiMe$_2$), 0.61 (s, $^{2}J_{H,Si}$ = 6.9 Hz, 3H, CH_3 SiMe$_2$), 0.43 (s, $^{2}J_{H,Si}$ = 6.8 Hz, 9H, 3 x CH_3 C-SiMe$_3$), 0.42 (s, $^{2}J_{H,Si}$ = 6.5 Hz, 9H, 3 x CH_3 N-SiMe$_3$), 0.40 (d, $^{3}J_{H,H}$ = 6.9 Hz, 3H, CH_3 *i*Pr). **^{13}C{^{1}H} NMR** (25 °C, benzene-d_6, 100.6 MHz): δ 152.3 (Zr-*C*), 150.0 (N*C*N), 128.3 (*C* sbi), 127.4 (*C*H sbi), 127.1, 126.5, 126.2 (3 x *C* sbi), 125.60, 125.57, 125.4, 125.3, 123.2, 122.9, 122.3, 115.9, 115.1, 114.5 (10 x *C*H sbi), 112.3 (*C*≡C-SiMe$_3$), 109.3 (*C*H sbi), 104.9 (C≡*C*-SiMe$_3$), 92.0, 90.4 (2 x *C* sbi), 54.3, 47.3 (2 x *C*H *i*Pr), 26.1, 25.8, 25.3, 24.0 (4 x *C*H$_3$ *i*Pr), 4.5, 1.8 (2 x SiMe$_3$), −1.8, −2.1 (2 x SiMe$_2$). **^{29}Si-inept NMR** (25 °C, benzene-d_6, 79.5 MHz): δ −0.26 (dec, $^{2}J_{H,Si}$ = 6.5 Hz, N-*Si*Me$_3$), −15.00 (sep, $^{2}J_{H,Si}$ = 6.9 Hz, *Si*Me$_2$), −22.87 (dec, $^{2}J_{H,Si}$ = 6.8 Hz, C-*Si*Me$_3$). **Elemental analysis** calcd (%) for M($C_{36}H_{50}N_2Si_3Zr$) = 686.29 g mol^{-1}: C 63.00, H 7.34, N 4.08; found: C 62.95, H 7.63, N 3.83 (Measured with V_2O_5. Without V_2O_5: C 58.83, H 8.09, N 3.67). **IR** (ATR, 32 scans, cm^{-1}): 3065 (w), 2955 (w), 2924 (w), 2069 (w), 1849 (w), 1785 (w), 1595 (w), 1446 (w), 1404 (w), 1362 (w), 1334 (w), 1299 (w), 1243 (m), 1219 (m), 1141 (m), 1118 (w), 1051 (w), 986 (w), 964 (w), 828 (s), 803 (s), 741 (s), 681 (s), 643 (s), 547 (m), 451 (s). **MS-CI^{+}** (*isobutane*): [M^{+}] 686 (90), [(M−H)$^{+}$] 685 (100), [(M−Zr−sbi+2H)$^{+}$] 311 (7), [SiMe$_3^{+}$] 73 (3).

3.2 Reaction with N,N'-dicyclohexylcarbodiimide

3.2.1 Reaction of 1a with N,N'-dicyclohexylcarbodiimide to $P_{1a\text{-}Cy}$

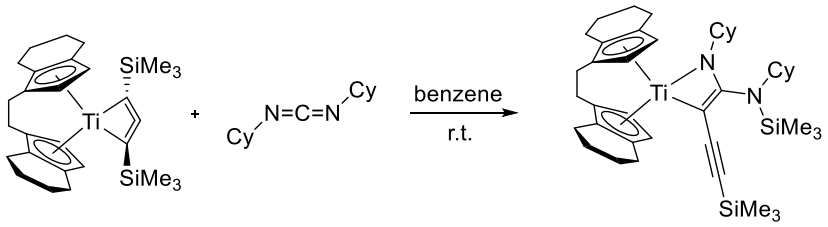

1a **$P_{1a\text{-}Cy}$**

According to general procedure, compound **1a** (0.20 mmol, 99 mg) was reacted with N,N'-dicyclohexylcarbodiimide (0.20 mmol, 41 mg) at room temperature. Then the reaction mixture was stirred for 72 hours and **$P_{1a\text{-}Cy}$** (124 mg, 88%) was obtained after recrystallisation. Crystals suitable for SC-XRD analysis were grown from pentane.

uncorrected decomposition point: 145-148 °C (Ar.). **^{1}H NMR** (25 °C, benzene-d_6, 400.1 MHz): δ 7.30 (d, $^{3}J_{H,H}$ = 3.0 Hz, 1H, C*H* ebthi), 6.96 (d, $^{3}J_{H,H}$ = 3.0 Hz, 1H, C*H* ebthi), 5.77 (d, $^{3}J_{H,H}$ = 2.9 Hz, 1H, C*H* ebthi), 5.55 (d, $^{3}J_{H,H}$ = 3.2 Hz, 1H, C*H* ebthi), 3.30 (m, 1H, C*H* cy), 2.82-2.21 (m, 15H CH_2 C*H* cy and ebthi), 2.18-1.99 (m, 4H, 2 x CH_2 ebthi), 1.92-1.01 (m, 22H CH_2 cy and ebthi), 0.52 (s, $^{2}J_{H,Si}$ = 6.8 Hz, 9H, 3 x CH_3 N-SiMe$_3$), 0.45 (s, $^{2}J_{H,Si}$ = 7.0 Hz, 9H, 3 x CH_3 C-SiMe$_3$). **^{13}C{^{1}H} NMR** (25 °C, benzene-d_6, 75.5 MHz): δ 185.1 (Ti-*C*), 140.5 (N*C*N), 129.6, 127.23, 125.9, 124.8, 123.6, 121.2 (6 x *C* ebthi), 119.8 (C≡*C*-SiMe$_3$), 118.8 (*C*H ebthi), 115.7 (*C*≡C-SiMe$_3$), 114.3 (*C*H ebthi), 108.6 (*C*H ebthi), 105.4 (*C*H ebthi), 62.1, 60.0 (2 x *C*H cy), 28.4, 28.0, 28.0, 27.4, 26.9, 26.6, 26.5, 25.3, 25.2, 24.8, 23.5, 23.4, 22.8, 22.7, 22.6 (20 x CH_2 ebthi and cy), 4.7, 1.7 (2 x SiMe$_3$). **^{29}Si NMR** (25 °C, benzene-d_6, 59.6 MHz): δ 0.9, −22.5. **Elemental analysis** calcd (%) for ($C_{42}H_{64}N_2Si_2Ti$) = 701.03 g mol^{-1}: C 71.86, H 9.13, N 3.99; found: C 63.63, H 8.59, N 2.84. **IR** (ATR, 32 scans, cm^{-1}): IR (ATR, neat, cm-1): 3014 (w), 2927 (w), 2857 (w), 2057 (m), 1605 (w), 1554 (w), 1502 (m), 1461 (m), 1404 (w), 1307 (m), 1240 (m), 1214 (m), 1205 (m), 1172 (m), 1125 (w), 1105 (w), 1014 (m), 954 (w), 933 (w), 911 (w), 880 (w), 833 (s), 793 (s), 747 (m), 715 (m), 690 (m), 647 (s), 574 (w), 536 (w), 523 (m), 498 (m), 461 (m). **MS-CI^{+}** (*isobutane*): [(M)$^{+}$] 701 (88), [(M−SiMe$_3$)$^{+}$] 627 (40), [(M−Ti−ebthi+2H)$^{+}$] 391 (78), [(CyNSiMe$_3$+SiMe$_3$+3H)$^{+}$] 247 (100), [SiMe$_3^{+}$] 73 (10).

3.2.2 Reaction of 2a with N,N'-dicyclohexylcarbodiimide to $P_{2a\text{-}Cy}$

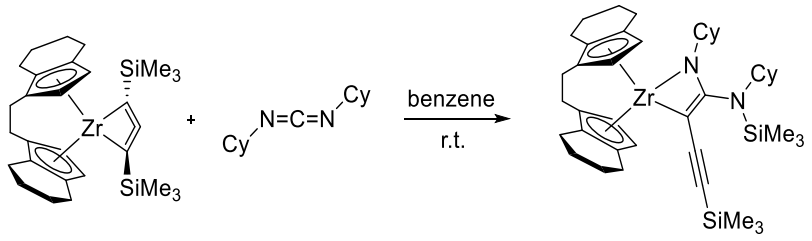

2a **$P_{2a\text{-}Cy}$**

According to general procedure, compound **2a** (0.20 mmol, 108 mg) was reacted with N,N'-dicyclohexylcarbodiimide (0.20 mmol, 41 mg) at room temperature. The colour of the reaction mixture changed from pale green to dark green in 5 minutes. Then the reaction mixture was stirred for 1 hour and the solvent was removed in *vacuo* to obtain **$P_{2a\text{-}Cy}$** as green powder (143 mg, 96%).

uncorrected decomposition point: 83-86 °C (Ar.). **^{1}H NMR** (25 °C, benzene-d_6, 400.1 MHz): δ 6.88 (d, $^3J_{H,H}$ = 3.1 Hz, 1H, C*H* ebthi), 6.32 (d, $^3J_{H,H}$ = 3.1 Hz, 1H, C*H* ebthi), 5.65 (d, $^3J_{H,H}$ = 3.1 Hz, 1H, C*H* ebthi), 5.56 (d, $^3J_{H,H}$ = 3.1 Hz, 1H, C*H* ebthi), 3.23 (tt, $^3J_{H,H}$ = 11.2, 3.6 Hz, 1H, C*H* cy), 2.80-2.37 (m, 11H, C*H* cy and CH_2 cy and ebthi), 2.25-0.95 (m, 30H, CH_2 cy and ebthi), 0.54 (s, $^2J_{H,Si}$ = 6.5 Hz, 9H, 3 x CH_3 N-SiMe$_3$), 0.44 (s, $^2J_{H,Si}$ = 6.9 Hz, 9H, 3 x CH_3 C-SiMe$_3$). **^{13}C{^{1}H} NMR** (25 °C, benzene-d_6, 100.6 MHz): δ 148.5 (N*C*N), 145.7 (Zr-*C*), 128.7, 126.7, 125.9, 124.1, 123.3, 120.9 (6 x *C* ebthi), 117.2 (*C*H ebthi), 115.2 (*C*≡C-SiMe$_3$), 110.0, 107.1, 105.6 (3 x *C*H ebthi), 102.9 (C≡*C*-SiMe$_3$), 62.3, 57.4 (2 x *C*H cy), 38.1, 37.2, 36.6, 35.7, 28.3, 27.8, 27.45, 27.44, 26.8, 26.6, 26.5, 26.2, 25.2, 24.8, 24.6, 23.8, 23.7, 23.6, 23.1, 22.6 (20 x *C*H$_2$ ebthi and cy), 4.5, 1.9(2 x SiMe$_3$). **^{29}Si-inept NMR** (25 °C, benzene-d_6, 79.5 MHz): δ 0.78 (dec, $^2J_{H,Si}$ = 6.5 Hz, N-*Si*Me$_3$), −22.85 (dec, $^2J_{H,Si}$ = 6.9 Hz, C-*Si*Me$_3$). **Elemental analysis** calcd (%) for ($C_{42}H_{64}N_2Si_2Zr$) = 744.38 g mol^{-1}: C 67.77, H 8.67, N 3.76; found: C 66.60, H 8.16, N 3.59 (Measured with V_2O_5. Without V_2O_5: C 66.44, H 8.73, N 3.61). **IR** (ATR, 32 scans, cm^{-1}): 2924 (m), 2850 (m), 2118 (w), 2064 (m), 1836 (w), 1569 (w), 1446 (m), 1342 (w), 1241 (m), 1198 (m), 1176 (m), 1139 (w), 1088 (m), 983 (m), 953 (w), 887 (w), 832 (s), 776 (s), 753 (m), 688 (m), 643 (m), 622 (m), 528 (m), 497 (w), 473 (m), 414 (m). **MS-CI$^+$** (*isobutane*): [M$^+$] 744 (87), [(M−2H)$^+$] 742 (100), [(M−Zr−ebthi+2H)$^+$] 391 (39).

3.2.3 Reaction of 2b with N,N'-dicyclohexylcarbodiimide to $P_{2b\text{-}Cy}$

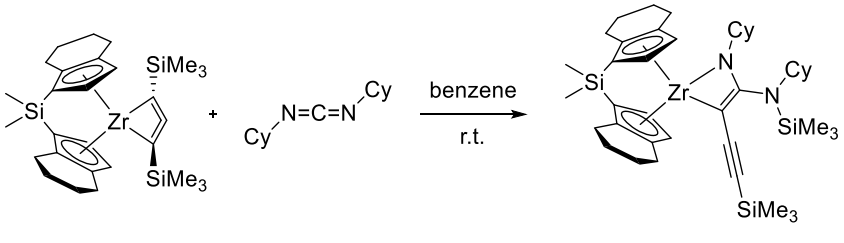

2b **$P_{2b\text{-}Cy}$**

According to general procedure, compound **2b** (0.20 mmol, 114 mg) was reacted with N,N'-dicyclohexylcarbodiimide (0.20 mmol, 41 mg) at room temperature. The colour of the reaction

mixture changed from pale green to dark green in 5 minutes. Then the reaction mixture was stirred for 4 hours and **$P_{2b\text{-}Cy}$** (139 mg, 90%) was obtained after recrystallisation.

uncorrected decomposition point: 85-88 °C (Ar.). **^{1}H NMR** (25 °C, benzene-d_6, 400.1 MHz): δ 7.20 (d, $^3J_{H,H}$ = 3.0 Hz, 1H, C*H* sbthi), 6.55 (d, $^3J_{H,H}$ = 3.1 Hz, 1H, C*H* sbthi), 5.73 (d, $^3J_{H,H}$ = 3.1 Hz, 1H, C*H* sbthi), 5.72 (d, $^3J_{H,H}$ = 3.0 Hz, 1H, C*H* sbthi), 3.25 (tt, $^3J_{H,H}$ = 11.4, 3.6 Hz, 1H, C*H* cy), 2.74 (tt, $^3J_{H,H}$ = 11.9, 3.4 Hz, 1H, C*H* cy), 2.66-2.41 (m, 6H, 3 x CH_2 cy and sbthi), 2.37-2.29 (m, 1H, CH_2 cy and sbthi), 2.22-2.10 (m, 2H, CH_2 cy and sbthi), 2.06-0.92 (m, 27H, CH_2 cy and sbthi), 0.60 (s, $^2J_{H,Si}$ = 6.9 Hz, 3H, CH_3 SiMe$_2$), 0.56 (s, $^2J_{H,Si}$ = 6.6 Hz, 9H, 3 x CH_3 N-SiMe$_3$), 0.44 (s, $^2J_{H,Si}$ = 6.9 Hz, 3H, CH_3 SiMe$_2$), 0.43 (s, $^2J_{H,Si}$ = 6.9 Hz, 9H, 3 x CH_3 C-SiMe$_3$). **^{13}C{^{1}H} NMR** (25 °C, benzene-d_6, 100.6 MHz): δ 147.33 (N*C*N), 147.28 (Zr-*C*), 131.2, 128.7, 128.4, 124.7 (4 x *C* sbthi), 122.4, 117.2 (2 x *C*H sbthi), 114.5 (*C*≡C-SiMe$_3$), 111.8, 110.3 (2 x *C*H sbthi), 108.2, 104.7 (2 x *C* sbthi), 103.9 (C≡*C*-SiMe$_3$), 62.3, 57.5 (2 x *C*H cy), 38.3, 36.71, 36.66, 35.7 (4 x CH_2 cy), 28.3, 27.4, 27.2, 26.8, 26.6, 26.5, 26.11, 26.09, 25.6, 24.8, 23.9, 23.6, 23.1, 22.8 (14 x CH_2 sbthi and cy), 4.5, 1.8 (2 x SiMe$_3$), −1.1, −2.9 (2 x SiMe$_2$). **^{29}Si-inept NMR** (25 °C, benzene-d_6, 79.5 MHz): δ 0.82 (dec, $^2J_{H,Si}$ = 6.6 Hz, N-*Si*Me$_3$), −15.52 (sep, $^2J_{H,Si}$ = 6.9 Hz, *Si*Me$_2$), −22.63 (dec, $^2J_{H,Si}$ = 6.9 Hz, C-*Si*Me$_3$). **Elemental analysis** calcd (%) for ($C_{42}H_{66}N_2Si_3Zr$) = 774.48 g mol^{-1}: C 65.14, H 8.59, N 3.62; found: C 64.64, H 7.61, N 3.06 (Measured with V_2O_5. Without V_2O_5: C 62.73, H 6.79, N 2.86). **IR** (ATR, 32 scans, cm^{-1}): 2929 (m), 2853 (w), 2119 (w), 2070 (m), 1899 (w), 1853 (w), 1450 (w), 1293 (w), 1243 (m), 1199 (m), 1176 (w), 1138 (w), 1085 (w), 984 (w), 886 (w), 831 (s), 805 (s), 781 (s), 754 (m), 691 (m), 676 (m), 644 (m), 624 (w), 554 (w), 529 (m), 473 (m), 446 (m). **MS-CI$^+$** (*isobutane*): [(M−CH$_3$)$^+$] 759 (13), [(sbthi)$^+$] 297 (48), [(Me$_2$Si(thi))$^+$] 177 (100), [SiMe$_3^+$] 73 (14).

3.2.4 Reaction of 2c with N,N'-dicyclohexylcarbodiimide to $P_{2c\text{-}Cy}$

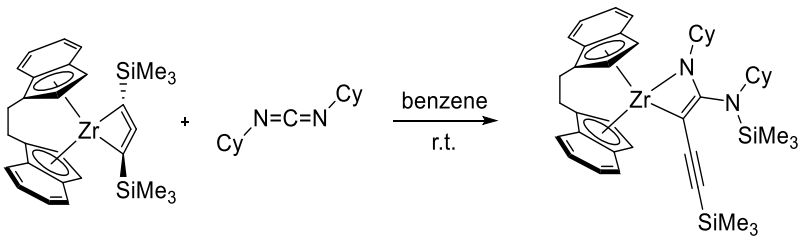

2c **$P_{2c\text{-}Cy}$**

According to general procedure, compound **2c** (0.20 mmol, 106 mg) was reacted with N,N'-dicyclohexylcarbodiimide (0.20 mmol, 41 mg) at room temperature. The colour of the reaction mixture changed from red to brown in 5 minutes. Then the reaction mixture was stirred for 1 hours and **$P_{2c\text{-}Cy}$** (119 mg, 81%) was obtained after recrystallisation. Crystals suitable for SC-XRD analysis were grown from pentane.

uncorrected decomposition point: 89-92 °C (Ar.). **^{1}H NMR** (25 °C, benzene-d_6, 400.1 MHz): δ 7.44 (dt, $^3J_{H,H}$ = 8.5, 1.0 Hz, 1H, C*H* ebi), 7.36-7.34 (m, 2H, 2 x C*H* ebi), 7.14-7.07 (m, 3H, 3 x C*H* ebi), 6.98 (ddd, $^3J_{H,H}$ = 8.5, 6.5, 1.2 Hz, 1H, C*H* ebi), 6.77 (ddd, $^3J_{H,H}$ = 8.6, 6.5, 1.0 Hz, 1H, C*H* ebi), 6.59-6.55 (m, 2H, 2 x C*H* ebi), 6.05 (d, $^3J_{H,H}$ = 3.4 Hz, 1H, C*H* ebi), 6.00 (d, $^3J_{H,H}$ = 3.4 Hz, 1H, C*H* ebi), 3.18-2.88 (m, 6H, C*H* cy and CH_2 ebi), 2.60-2.52 (m, 1H, CH_2 cy), 2.42-2.39 (m, 1H, CH_2 cy),

2.06-2.03 (m, 1H, CH_2 cy), 1.86-1.53 (m, 10H, 5 x CH_2 cy), 1.46-1.00 (m, 6H, 3 x CH_2 cy), 0.97-0.86 (m, 1H, CH_2 cy), 0.44 (s, $^2J_{H,Si}$ = 6.9 Hz, 9H, 3 x CH_3 C-SiMe$_3$), 0.42 (s, $^2J_{H,Si}$ = 6.6 Hz, 9H, 3 x CH_3 N-SiMe$_3$). **^{13}C{^{1}H} NMR** (25 °C, benzene-d_6, 100.6 MHz): δ 150.4 (N*C*N), 149.3 (Zr-*C*), 126.4, 125.2, 125.0, 124.9, 124.7 (5 x *C*H ebi), 123.8, 123.7, 123.6, 123.3 (4 x *C* ebi), 122.2, 120.7, 119.7 (3 x *C*H ebi), 117.0, 116.7 (2 x *C* ebi), 113.0 (*C*≡C-SiMe$_3$), 111.5, 111.1, 108.6 (3 x *C*H ebi), 102.7 (C≡*C*-SiMe$_3$), 101.6 (*C*H ebi), 63.0, 57.0 (2 x *C*H cy), 37.2, 35.95, 35.88, 35.7 (4 x CH_2 cy), 28.3, 27.5, 27.2, 27.0, 26.6, 26.4, 26.2 (8 x CH_2 ebi and cy), 4.7, 1.9 (2 x SiMe$_3$). **^{29}Si-inept NMR** (25 °C, benzene-d_6, 79.5 MHz): δ −0.05 (dec, $^2J_{H,Si}$ = 6.6 Hz, N-*Si*Me$_3$), −23.08 (dec, $^2J_{H,Si}$ = 6.9 Hz, C-*Si*Me$_3$). **Elemental analysis** calcd (%) for M(C$_{42}$H$_{56}$N$_2$Si$_2$Zr) = 736.32 g mol^{-1}: C 68.51, H 7.67, N 3.80; found: C 68.79, H 7.59, N 3.35 (Measured with V_2O_5. Without V_2O_5: C 67.88, H 6.41, N 3.15). **IR** (ATR, 32 scans, cm^{-1}): 3064 (w), 2922 (m), 2849 (w), 2069 (m), 1842 (w), 1579 (w), 1445 (w), 1342 (w), 1243 (m), 1204 (m), 1178 (w), 1083 (w), 1010 (w), 982 (w), 887 (w), 832 (s), 777 (m), 737 (s), 688 (m), 645 (m), 625 (m), 551 (w), 526 (m), 473 (m), 442 (m). **MS-CI$^+$** (*isobutane*): [(M−ebi−2CH$_3$+3H)$^+$] 453 (4), [ebi$^+$] 259 (100).

3.2.5 Reaction of 2d with N,N'-dicyclohexylcarbodiimide to $P_{2d\text{-}Cy}$

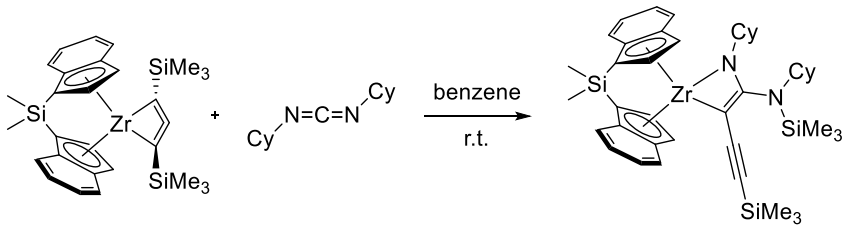

2d **$P_{2d\text{-}Cy}$**

According to general procedure, compound **2d** (0.20 mmol, 112 mg) was reacted with N,N'-dicyclohexylcarbodiimide (0.20 mmol, 41 mg) at room temperature. The colour of the reaction mixture changed from red to brown in 5 minutes. Then the reaction mixture was stirred for 1 hour and the solvent was removed in *vacuo* to obtain **$P_{2d\text{-}Cy}$** as brown powder (143 mg, 93%).

uncorrected decomposition point: 87-90 °C (Ar.). **^{1}H NMR** (25 °C, benzene-d_6, 400.1 MHz): δ 7.59 (dd, $^3J_{H,H}$ = 3.4, 0.9 Hz, 1H, C*H* sbi), 7.55 (dt, $^3J_{H,H}$ = 8.4, 1.1 Hz, 1H, C*H* sbi), 7.47 (dt, $^3J_{H,H}$ = 8.6, 1.1 Hz, 1H, C*H* sbi), 7.31 (dq, $^3J_{H,H}$ = 8.7, 1.0 Hz, 1H, C*H* sbi), 7.25 (dq, $^3J_{H,H}$ = 8.6, 1.0 Hz, 1H, C*H* sbi), 7.10 (ddd, $^3J_{H,H}$ = 8.4, 6.8, 1.1 Hz, 1H, C*H* sbi), 7.00 (ddd, $^3J_{H,H}$ = 8.0, 6.8, 1.0 Hz, 1H, C*H* sbi), 6.86 (dd, $^3J_{H,H}$ = 3.4, 0.9 Hz, 1H, C*H* sbi), 6.73 (ddd, $^3J_{H,H}$ = 8.7, 6.6, 1.0 Hz, 1H, C*H* sbi), 6.60 (ddd, $^3J_{H,H}$ = 8.6, 6.6, 1.0 Hz, 1H, C*H* sbi), 6.18 (d, $^3J_{H,H}$ = 3.4 Hz, 1H, C*H* sbi), 6.16 (d, $^3J_{H,H}$ = 3.3 Hz, 1H, C*H* sbi), 2.89 (tt, $^3J_{H,H}$ = 11.3, 3.7 Hz, 1H, C*H* cy), 2.56 (tt, $^3J_{H,H}$ = 11.9, 3.6 Hz, 1H, C*H* cy), 2.44-2.40 (m, 1H, CH_2 cy), 2.06-2.03 (m, 1H, CH_2 cy), 1.89-1.78 (m, 3H, CH_2 cy), 1.73-1.21 (m, 12H, 6 x CH_2 cy), 1.14-0.99 (m, 3H, CH_2 cy), 0.76 (s, $^2J_{H,Si}$ = 7.0 Hz, 3H, CH_3 SiMe$_2$), 0.62 (s, $^2J_{H,Si}$ = 7.0 Hz, 3H, CH_3 SiMe$_2$), 0.43 (s, $^2J_{H,Si}$ = 6.8 Hz, 9H, 3 x CH_3 C-SiMe$_3$), 0.42 (s, $^2J_{H,Si}$ = 6.5 Hz, 9H, 3 x CH_3 N-SiMe$_3$). **^{13}C{^{1}H} NMR** (25 °C, benzene-d_6, 100.6 MHz): δ 152.7 (Zr-*C*), 150.0 (N*C*N), 127.7, 127.25 (2 x *C* sbi), 127.21 (*C*H sbi), 126.3, 126.1 (2 x *C* sbi), 125.5, 125.4, 123.6, 122.8, 122.6, 116.2, 114.9, 114.8 (10 x *C*H sbi), 112.6 (*C*≡C-SiMe$_3$), 109.2 (*C*H sbi), 104.5 (C≡*C*-SiMe$_3$),

93.1, 91.1 (2 x *C* sbi), 63.0, 57.1 (2 x *C*H cy), 36.8, 35.9, 35.64, 35.57, 28.3, 27.2, 27.1, 26.7, 26.4, 26.1 (10 x CH_2 cy), 4.7, 1.9 (2 x $SiMe_3$), −1.6, −2.2 (2 x $SiMe_2$). **^{29}Si-inept NMR** (25 °C, benzene-d_6, 79.5 MHz): δ −0.24 (dec, $^2J_{H,Si}$ = 6.5 Hz, N-*Si*Me_3), −15.02 (sep, $^2J_{H,Si}$ = 7.0 Hz, *Si*Me_2), −22.93 (dec, $^2J_{H,Si}$ = 6.8 Hz, C-*Si*Me_3). **Elemental analysis** calcd (%) for M($C_{42}H_{58}N_2Si_3Zr$) = 766.42 g mol^{-1}: C 65.82, H 7.63, N 3.66; found: C 65.91, H 7.46, N 3.63 (Measured with V_2O_5. Without V_2O_5: C 65.40, H 7.42, N 3.51). **IR** (ATR, 32 scans, cm^{-1}): 3065 (w), 2924 (m), 2850 (w), 2120 (w), 2069 (w), 1854 (w), 1772 (w), 1593 (w), 1445 (w), 1403 (w), 1334 (w), 1299 (w), 1244 (m), 1204 (m), 1178 (w), 1140 (w), 1084 (m), 982 (w), 964 (w), 887 (w), 829 (s), 803 (s), 740 (s), 681 (m), 643 (m), 552 (m), 527 (m), 451 (s), 431 (m). **MS-CI$^+$** (*isobutane*): [M^+] 766 (60), [$(M-H)^+$] 765 (69), [$(M-SiMe_3-H)^+$] 692 (44), [$(M-SiMe_2-$indenyl$+4H)^+$] 597 (19), [$(M-Zr-$sbi$+2H)^+$]391 (64), [sbi^+] 289 (28), [$(SiMe_2+$indenyl$-H)^+$] 172 (100), [$SiMe_3^+$] 73 (15).

3.3 Reaction with N,N′-di-*p*-tolylcarbodiimide

3.3.1 Reaction of 1a with N,N′-di-*p*-tolylcarbodiimide to $P_{1a\text{-}p\text{-}Tol}$

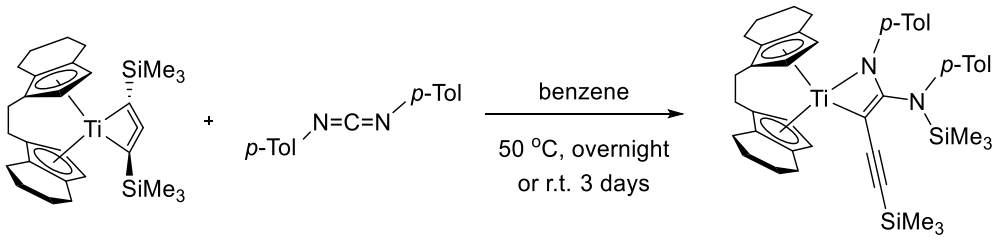

1a **$P_{1a\text{-}Tol}$**

According to general procedure, compound **1a** (0.05 mmol, 25 mg) was reacted with N,N′-di-*p*-tolylcarbodiimide (0.05 mmol, 11 mg) at room temperature for 3 days or 50 °C overnight. The solvent was removed in *vacuo* to obtain **$P_{1a\text{-}p\text{-}Tol}$** as red oil (31 mg, 86%).

^{1}H NMR (25 °C, benzene-d_6, 400.1 MHz): δ 7.51 (d, $^3J_{H,H}$ = 2.9 Hz, 1H, C*H* ebthi), 7.09-7.02 (m, 4H, 4 x C*H* *p*-tol), 6.76-6.63 (m, 4H, 4 x C*H* *p*-tol), 6.08 (d, $^3J_{H,H}$ = 3.2 Hz, 1H, C*H* ebthi), 5.63 (d, $^3J_{H,H}$ = 3.2 Hz, 1H, C*H* ebthi), 5.46 (d, $^3J_{H,H}$ = 3.0 Hz, 1H, C*H* ebthi), 2.93-2.37 (m, 6H, 3 x CH_2 ebthi), 2.28 (s, 3H, 3 x C*H* tol), 2.24-2.03 (m, 2H, CH_2 ebthi), 1.94 (s, 3H, 3 x C*H* tol), 1.89-1.72 (m, 4H, 2 x CH_2 ebthi), 1.58-1.03 (m, 8H, 4 x CH_2 ebthi), 0.59 (s, $^2J_{H,Si}$ = 6.6 Hz, 9H, 3 x CH_3 N-SiMe$_3$), 0.46 (s, $^2J_{H,Si}$ = 7.0 Hz, 9H, 3 x CH_3 C-SiMe$_3$). **^{13}C{^{1}H} NMR** (25 °C, benzene-d_6, 100.6 MHz): δ 168.5 (Ti-*C*), 151.9 (N*C*N), 142.7, 134.8, 134.6, 132.4, 130.4, 130.3, 129.1, 129.1, 129.0, 128.7, 126.7, 124.8, 124.4, 123.3, 1209, 120.1, 118.2 (2 x *C*H ebthi), 116.0 (C≡*C*-SiMe$_3$), 113.2 (*C*≡C-SiMe$_3$), 109.0, 107.9 (2 x *C*H ebthi), 28.5, 27.85, 25.2, 24.8, 23.4, 23.2, 23.1, 22.9, 22.5, 22.5 (10 x *C*H$_2$ ebthi), 21.0, 20.9 (2 x *C*H$_3$ *p*-tol), 1.5, 1.4 (2 x SiMe$_3$). **^{29}Si-inept NMR** (25 °C, benzene-d_6, 79.5 MHz): δ 4.3, −21.8. **Elemental analysis** calcd (%) for ($C_{44}H_{56}N_2Si_2Ti$) = 716.98 g mol^{-1}: C 73.64, H 7.81, N 3.90; found: C 71.34, H 5.64, N 3.15. **IR** (ATR, 32 scans, cm^{-1}): IR (ATR, neat, cm-1): 2924 (m), 2851 (w), 2116 (w), 2052 (w), 1908 (w), 1741 (w), 1556 (w), 1445 (m), 1377 (w), 1341 (w), 1258 (m), 1243 (m), 1190 (w), 1169 (m), 1134 (w), 1084 (m), 1019 (m), 980 (m), 952 (w), 935 (w), 914 (w), 884 (w), 833 (s), 801 (s), 775 (s), 754 (s), 719 (m), 689 (m), 646 (m), 621 (m), 583 (w), 550 (m), 532 (w), 517 (w), 470 (m). **MS-CI$^+$** (*isobutane*): [(M−H)$^+$] 716 (100), [(M−SiMe$_3$+H)$^+$] 645 (22), [(M−Ti−ebthi+2H)$^+$] 407 (59), [SiMe$_3^+$] 73 (6).

3.3.2 Reaction of 2a with N,N′-di-*p*-tolylcarbodiimide to $P_{2a\text{-}p\text{-}Tol}$

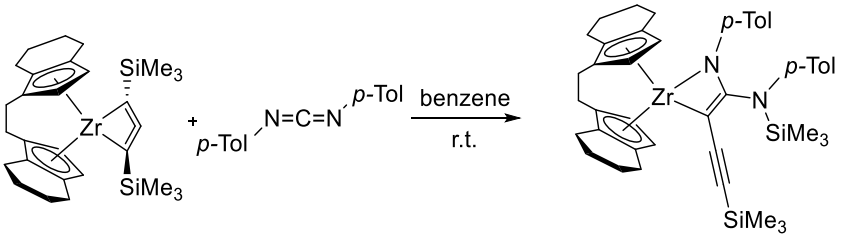

2a **$P_{2a\text{-}Tol}$**

According to general procedure, compound **2a** (0.20 mmol, 108 mg) was reacted with N,N'-di-*p*-tolylcarbodiimide (0.20 mmol, 45 mg) at room temperature. The colour of the reaction mixture changed from pale green to dark green in 5 minutes. Then the reaction mixture was stirred for 4 hours and the solvent was removed in *vacuo* to obtain **$P_{2a\text{-}p\text{-}Tol}$** as green powder (143 mg, 94%).

uncorrected decomposition point: 108-111 °C (Ar.). **^{1}H NMR** (25 °C, benzene-d_6, 400.1 MHz): δ 7.14 (d, $^3J_{H,H}$ = 3.1 Hz, 1H, C*H* ebthi), 7.08-7.05 (m, 2H, 2 x C*H* tol), 7.03-6.98 (m, 2H, 2 x C*H* tol), 6.76-6.72 (m, 2H, 2 x C*H* tol), 6.71-6.66 (m, 2H, 2 x C*H* tol), 5.58 (d, $^3J_{H,H}$ = 3.1 Hz, 1H, C*H* ebthi), 5.54 (d, $^3J_{H,H}$ = 3.1 Hz, 1H, C*H* ebthi), 5.46 (d, $^3J_{H,H}$ = 3.1 Hz, 1H, C*H* ebthi), 2.99-2.90 (m, 1H, CH_2 ebthi), 2.72-2.56 (m, 2H, CH_2 ebthi), 2.49-1.81 (m, 10H, 5 x CH_2 ebthi), 2.27 (s, 3H, CH_3 tol), 1.97 (s, 3H, CH_3 tol), 1.54-1.14 (m, 7H, CH_2 ebthi), 0.62 (s, $^2J_{H,Si}$ = 6.7 Hz, 9H, 3 x CH_3 N-SiMe$_3$), 0.46 (s, $^2J_{H,Si}$ = 6.9 Hz, 9H, 3 x CH_3 C-SiMe$_3$). (Minor impurity of the propargyl complex **3a** was observed due to the slow conversion of **2a** to **3a** at room temperature.) **^{13}C{^{1}H} NMR** (25 °C, benzene-d_6, 100.6 MHz): δ 150.7 (N*C*N), 144.2 (Zr-*C*), 143.2, 142.9 (2 x N-*C* tol), 134.3 (Me-*C* tol), 131.3, 129.3, 129.0 (3 x *C*H tol), 128.9 (Me-*C* tol), 128.2, 127.3, 127.1, 126.5, 123.6, 122.5 (6 x *C* ebthi), 121.1 (*C*H tol), 117.6, 113.8 (2 x *C*H ebthi), 113.4 (*C*≡C-SiMe$_3$), 108.3, 107.7 (2 x *C*H ebthi), 105.9 (C≡*C*-SiMe$_3$), 28.03, 27.96, 24.8, 24.6, 23.8, 23.73, 23.69, 23.6, 22.9, 22.8 (10 x *C*H$_2$ ebthi), 21.0, 20.9 (2 x *C*H$_3$ tol), 1.7, 1.6 (2 x SiMe$_3$). **^{29}Si-inept NMR** (25 °C, benzene-d_6, 79.5 MHz): δ 4.93 (dec, $^2J_{H,Si}$ = 6.7 Hz, N-*Si*Me$_3$), −22.11 (dec, $^2J_{H,Si}$ = 6.9 Hz, C-*Si*Me$_3$). **Elemental analysis** calcd (%) for ($C_{44}H_{56}N_2Si_2Zr$) = 760.34 g mol^{-1}: C 69.44, H 7.37, N 3.68; found: C 67.61, H 7.63, N 2.93. **IR** (ATR, 32 scans, cm^{-1}): 3018 (w), 2925 (w), 2853 (w), 2071 (m), 1895 (w), 1854 (w), 1733 (w), 1607 (w), 1559 (w), 1502 (m), 1487 (m), 1376 (w), 1297 (m), 1243 (m), 1215 (m), 1195 (m), 1106 (w), 1033 (w), 1005 (w), 915 (w), 833 (s), 788 (s), 754 (s), 717 (m), 689 (m), 645 (m), 571 (w), 526 (m), 495 (m), 466 (m). **MS-CI$^+$** (*isobutane*): [M$^+$] 760 (35), [(M−2H)$^+$] 758 (44), [(M−Zr−ebthi+2H)$^+$] 407 (100), [ebthi$^+$] 267 (10), [SiMe$_3^+$] 73 (6).

3.3.3 Reaction of 2b with N,N'-di-*p*-tolylcarbodiimide to $P_{2b\text{-}p\text{-}Tol}$

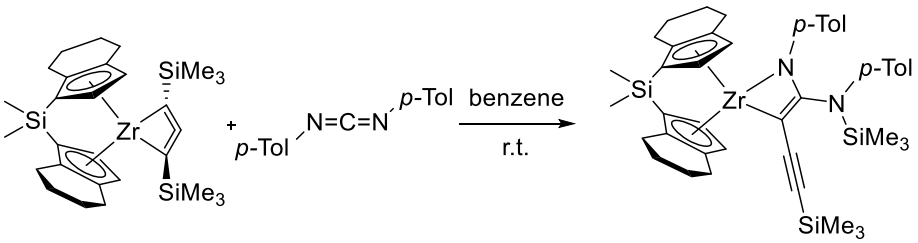

2b **$P_{2b\text{-}Tol}$**

According to general procedure, compound **2b** (0.20 mmol, 114 mg) was reacted with N,N'-di-*p*-tolylcarbodiimide (0.20 mmol, 45 mg) at room temperature. The colour of the reaction mixture changed from pale green to dark green in 5 minutes. Then the reaction mixture was stirred for 4 hours and the solvent was removed in *vacuo* to obtain **$P_{2b\text{-}p\text{-}Tol}$** as green powder (150 mg, 95%).

uncorrected decomposition point: 104-107 °C (Ar.). **^{1}H NMR** (25 °C, benzene-d_6, 400.1 MHz): δ 7.43 (d, $^3J_{H,H}$ = 3.0 Hz, 1H, C*H* sbthi), 7.09-7.05 (m, 2H, 2 x C*H* tol), 7.03-6.99 (m, 2H, 2 x C*H* tol), 6.76-6.72 (m, 2H, 2 x C*H* tol), 6.68-6.65 (m, 2H, 2 x C*H* tol), 5.81 (d, $^3J_{H,H}$ = 3.1 Hz, 1H, C*H* sbthi), 5.56 (d, $^3J_{H,H}$ = 3.1 Hz, 1H, C*H* sbthi), 5.52 (d, $^3J_{H,H}$ = 3.0 Hz, 1H, C*H* sbthi), 2.80-2.71 (m, 1H, CH_2 sbthi), 2.55-1.71 (m, 9H, CH_2 sbthi), 2.28 (s, 3H, CH_3 tol), 1.98 (s, 3H, CH_3 tol), 1.55-1.12 (m, 6H, 3 x CH_2 sbthi), 0.61 (s, $^2J_{H,Si}$ = 6.6 Hz, 9H, 3 x CH_3 N-SiMe$_3$), 0.53 (s, $^2J_{H,Si}$ = 6.9 Hz, 3H, CH_3 SiMe$_2$), 0.45 (s, $^2J_{H,Si}$ = 6.9 Hz, 3H, CH_3 SiMe$_2$), 0.43 (s, $^2J_{H,Si}$ = 6.9 Hz, 9H, 3 x CH_3 C-SiMe$_3$). (Minor impurity of the propargyl complex **3b** was observed due to the slow conversion of **2b** to **3b** at room temperature.) **^{13}C{^{1}H} NMR** (25 °C, benzene-d_6, 100.6 MHz): δ 150.7 (N*C*N), 144.8 (Zr-*C*), 143.0, 142.9 (2 x N-*C* tol), 134.5 (Me-*C* tol), 131.5 (*C*H tol), 131.3, 130.9 (2 x *C* sbthi), 130.3 (Me-*C* tol), 129.2, 129.0 (2 x *C*H tol), 128.5, 126.8 (2 x *C* sbthi), 123.3 (*C*H sbthi), 121.0 (*C*H tol), 120.1(*C*H sbthi), 112.8 (*C*≡C-SiMe$_3$), 112.7, 112.0 (2 x *C*H sbthi), 107.1 (C≡*C*-SiMe$_3$), 105.7, 102.8 (2 x *C* sbthi), 27.1, 26.0, 25.1, 24.1, 23.9, 23.6, 23.2, 22.5 (8 x *C*H$_2$ sbthi), 21.01, 20.97 (2 x *C*H$_3$ tol), 1.7, 1.5 (2 x SiMe$_3$), −1.5, −2.7 (2 x SiMe$_2$). **^{29}Si-inept NMR** (25 °C, benzene-d_6, 79.5 MHz): δ 5.01 (dec, $^2J_{H,Si}$ = 6.6 Hz, N-*Si*Me$_3$), −14.69 (sep, $^2J_{H,Si}$ = 6.9 Hz, *Si*Me$_2$), −21.96 (dec, $^2J_{H,Si}$ = 6.9 Hz, C-*Si*Me$_3$). **Elemental analysis** calcd (%) for ($C_{44}H_{58}N_2Si_3Zr$) = 790.44 g mol^{-1}: C 66.80, H 7.34, N 3.54; found: C 64.76, H 7.35, N 2.77. **IR** (ATR, 32 scans, cm^{-1}): 3017 (w), 2929 (w), 2854 (w), 2072 (m), 1899 (w), 1851 (w), 1607 (w), 1549 (w), 1487 (m), 1443 (w), 1406 (w), 1298 (m), 1243 (s), 1215 (m), 1196 (m), 1157 (w), 1118 (w), 1007 (w), 964 (w), 915 (w), 830 (s), 781 (s), 754 (s), 679 (m), 654 (m), 645 (m), 525 (m), 495 (m), 465 (m), 425 (m). **MS-CI$^+$** (*isobutane*): [M$^+$] 790 (83), [(M−2H)$^+$] 788 (100), [SiMe$_3^+$] 73 (4).

3.3.4 Reaction of 2c with N,N′-di-*p*-tolylcarbodiimide to $P_{2c\text{-}p\text{-}Tol}$

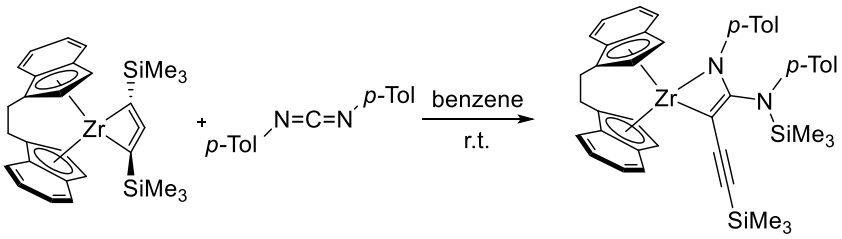

2c **$P_{2c\text{-}Tol}$**

According to general procedure, compound **2c** (0.20 mmol, 106 mg) was reacted with N,N′-di-*p*-tolylcarbodiimide (0.20 mmol, 45 mg) at room temperature. The colour of the reaction mixture changed from red to brown in 5 minutes. Then the reaction mixture was stirred for 1 hour and the solution was filtered, then the solvent was removed in *vacuo* to obtain **$P_{2c\text{-}p\text{-}Tol}$** as brown powder (129 mg, 86%).

uncorrected decomposition point: 107-110 °C (Ar.). **^{1}H NMR** (25 °C, benzene-d_6, 400.1 MHz): δ 7.47-7.44 (m, 2H, 2 x C*H* ebi), 7.13-7.02 (m, 5H, 5 x C*H* ebi+tol), 6.92-6.89 (m, 3H, 3 x C*H* ebi), 6.77-6.71 (m, 4H, 4 x C*H* tol), 6.25-6.19 (m, 3H, 3 x C*H* ebi), 6.01 (d, $^3J_{H,H}$ = 3.5 Hz, 1H, C*H* ebi), 5.97 (d, $^3J_{H,H}$ = 3.4 Hz, 1H, C*H* ebi), 5.69 (d, $^3J_{H,H}$ = 3.5 Hz, 1H, C*H* ebi), 3.16-2.86 (m, 4H, 2 x CH_2 ebi), 2.28 (s, 3H, CH_3 tol), 2.00 (s, 3H, CH_3 tol), 0.50 (s, $^2J_{H,Si}$ = 6.6 Hz, 9H, 3 x CH_3 N-SiMe$_3$), 0.47

(s, $^{2}J_{H,\,Si}$ = 6.9 Hz, 9H, 3 x CH_3 C-SiMe_3). **^{13}C{^{1}H} NMR** (25 °C, benzene-d_6, 100.6 MHz): δ 150.1 (NCN), 146.6 (N-*C* tol), 145.3 (Zr-*C*), 143.6 (N-*C* tol), 134.7 (Me-*C* tol), 131.8, 129.0, 128.9 (3 x *C*H tol), 128.8 (Me-*C* tol), 126.6, 126.5, 125.7, 125.3, 124.7 (5 x *C*H ebi), 124.3, 124.0, 123.9, 123.7 (4 x *C* ebi), 122.4 (*C*H ebi), 121.0 (*C*H tol), 120.3, 119.2 (2 x *C*H ebi), 117.4, 116.4 (2 x *C* ebi), 112.4, 111.8 (2 x *C*H ebi), 111.5 (*C*≡C-SiMe_3), 108.4, 106.2 (2 x *C*H ebi), 105.6 (C≡*C*-SiMe_3), 27.9, 27.6 (2 x CH_2 ebi), 21.0, 20.9 (2 x CH_3 tol), 1.7, 1.6 (2 x SiMe_3). **^{29}Si-inept NMR** (25 °C, benzene-d_6, 79.5 MHz): δ 4.42 (dec, $^{2}J_{H,\,Si}$ = 6.6 Hz, N-*Si*Me_3), −22.35 (dec, $^{2}J_{H,\,Si}$ = 6.9 Hz, C-*Si*Me_3). **Elemental analysis** calcd (%) for M($C_{44}H_{48}N_2Si_2Zr$) = 752.28 g mol^{-1}: C 70.25, H 6.43, N 3.72; found: C 70.32, H 6.80, N 2.97 (Measured with V_2O_5. Without V_2O_5: C 68.92, H 6.63, N 2.87). **IR** (ATR, 32 scans, cm^{-1}): 3019 (w), 2951 (w), 2919 (w), 2857 (w), 2073 (w), 1843 (w), 1605 (w), 1503 (m), 1464 (w), 1345 (w), 1300 (m), 1243 (m), 1215 (m), 1195 (m), 1106 (w), 1047 (w), 1010 (w), 916 (w), 833 (s), 801 (s), 737 (s), 631 (m), 525 (m), 500 (m), 471 (m), 445 (s). **MS-CI^{+}** (*isobutane*): [M^{+}] 752 (2), [(M−Zr−ebi+2H)$^{+}$] 407 (38), [(M−Zr−ebi-SiMe_3+3H)$^{+}$] 335 (41), [ebi^{+}] 259 (100), [(N-*p*tol-SiMe_3+2H)$^{+}$] 180 (47), [SiMe_3^{+}] 73 (36).

3.3.5 Reaction of 2d with N,N′-di-*p*-tolylcarbodiimide to $P_{2d\text{-}p\text{-}Tol}$

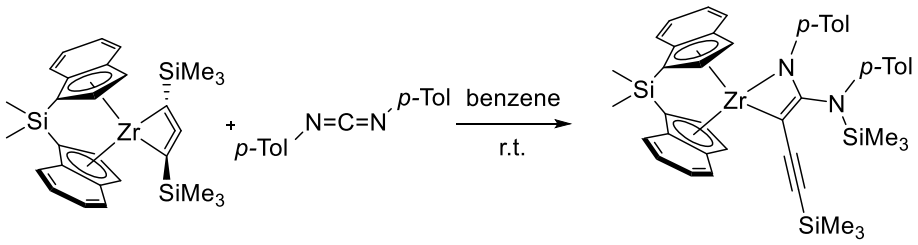

2d **$P_{2d\text{-}Tol}$**

According to general procedure, compound **2d** (0.20 mmol, 112 mg) was reacted with N,N′-di-*p*-tolylcarbodiimide (0.20 mmol, 45 mg) at room temperature. The colour of the reaction mixture changed from red to brown in 5 minutes. Then the reaction mixture was stirred for 1 hour and the solvent was removed in *vacuo* to obtain **$P_{2d\text{-}p\text{-}Tol}$** as brown powder (139 mg, 89%).

uncorrected decomposition point: 107-110 °C (Ar.). **^{1}H NMR** (25 °C, benzene-d_6, 400.1 MHz): δ 7.72 (dd, $^{3}J_{H,\,H}$ = 3.4, 0.9 Hz, 1H, C*H* sbi), 7.57 (dt, $^{3}J_{H,\,H}$ = 8.0, 1.3 Hz, 1H, C*H* sbi), 7.26-7.24 (m, 2H, 2 x C*H* sbi), 7.13-7.06 (m, 2H, 2 x C*H* sbi), 7.05-7.02 (m, 2H, 2 x C*H* tol), 6.94-6.91 (m, 2H, 2 x C*H* tol), 6.84 (dt, $^{3}J_{H,\,H}$ = 8.6, 1.1 Hz, 1H, C*H* sbi), 6.76-6.71 (m, 3H, 3 x C*H* tol and sbi), 6.31 (ddd, $^{3}J_{H,\,H}$ = 8.6, 6.6, 1.0 Hz, 1H, C*H* sbi), 6.18-6.14 (m, 2H, 2 x C*H* tol), 6.10 (d, $^{3}J_{H,\,H}$ = 3.4 Hz, 1H, C*H* sbi), 6.07 (d, $^{3}J_{H,\,H}$ = 3.5 Hz, 1H, C*H* sbi), 5.97 (dd, $^{3}J_{H,\,H}$ = 3.5, 0.8 Hz, 1H, C*H* sbi), 2.29 (s, 3H, CH_3 tol), 2.02 (s, 3H, CH_3 tol), 0.69 (s, $^{2}J_{H,\,Si}$ = 7.0 Hz, 3H, CH_3 SiMe_2), 0.61 (s, $^{2}J_{H,\,Si}$ = 7.0 Hz, 3H, CH_3 SiMe_2), 0.50 (s, $^{2}J_{H,\,Si}$ = 6.6 Hz, 9H, 3 x CH_3 N-SiMe_3), 0.46 (s, $^{2}J_{H,\,Si}$ = 6.9 Hz, 9H, 3 x CH_3 C-SiMe_3). **^{13}C{^{1}H} NMR** (25 °C, benzene-d_6, 100.6 MHz): δ 150.0 (NCN), 147.7 (Zr-*C*), 146.0, 143.6 (2 x N-*C* tol), 134.8 (Me-*C* tol), 131.7 (2 x *C*H tol), 134.0 (*C* sbi), 129.02 (Me-*C* tol), 128.99, 128.9 (4 x *C*H tol), 128.2, 128.1 (2 x *C* sbi), 127.4 (*C*H sbi), 127.0 (*C* sbi), 126.8, 126.2, 125.7, 125.5, 123.1, 123.0, 122.1 (7 x *C*H sbi), 120.8 (2 x *C*H tol), 117.1, 115.8, 114.4, 113.6 (4 x *C*H sbi), 111.0 (*C*≡C-SiMe_3), 107.0 (C≡*C*-SiMe_3), 90.7, 88.5 (2 x *C* sbi), 21.0, 20.9 (2 x *C*H_3 tol), 1.63, 1.62 (2 x

$SiMe_3$), −1.5, −2.4 (2 x $SiMe_2$). **^{29}Si-inept NMR** (25 °C, benzene-d_6, 79.5 MHz): δ 4.41 (dec, $^2J_{H, Si}$ = 6.6 Hz, N-*Si*Me_3), −14.23 (sep, $^2J_{H, Si}$ = 7.0 Hz, *Si*Me_2), −22.25 (dec, $^2J_{H, Si}$ = 6.9 Hz, C-*Si*Me_3). **Elemental analysis** calcd (%) for M($C_{44}H_{50}N_2Si_3Zr$) = 782.38 g mol^{-1}: C 67.55, H 6.44, N 3.58; found: C 67.39, H 6.54, N 3.72 (Measured with V_2O_5. Without V_2O_5: C 66.62, H 6.60, N 3.52). **IR** (ATR, 32 scans, cm^{-1}): 3019 (w), 2952 (w), 2919 (w), 2115 (w), 2073 (w), 1606 (w), 1557 (w), 1503 (m), 1445 (m), 1404 (w), 1299 (m), 1243 (m), 1215 (m), 1200 (m), 1157 (w), 1138 (m), 1106 (w), 1049 (w), 1008 (w), 961 (w), 830 (s), 804 (s), 741 (s), 682 (m), 646 (m), 633 (m), 556 (w), 523 (m), 496 (m), 453 (s). **MS-CI$^+$** (*isobutane*): [M$^+$] 782 (10), [(M−Zr−sbi+2H)$^+$] 407 (71), [(M−Zr−sbi-$SiMe_3$+3H)$^+$] 335 (14), [sbi$^+$] 289 (29), [2x(indenyl)$^+$] 229 (16), [($SiMe_2$+indenyl)$^+$] 173 (100), [(indenyl+2H)$^+$] 117 (20), [$SiMe_3^+$] 73 (10).

3.4 Reaction of N,N′-bis(2,6-diisopropylphenyl)carbodiimide

3.4.1 Reaction of 1a with N,N′-bis(2,6-diisopropylphenyl)carbodiimide

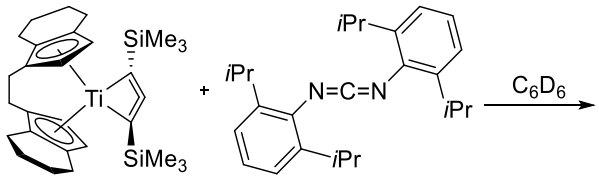

1a

According to general procedure, compound **1a** (0.034 mmol, 16.8 mg) was reacted with N,N′-bis(2,6-diisopropylphenyl)carbodiimide (0.034 mmol, 7.6 mg) in benzene-d_6 (0.6 mL) in a Young-NMR tube. The colour of reaction mixture kept same after 2 days at room temperature and the dark red solution was identified as the mixture of **1a** and N,N′-bis(2,6-diisopropylphenyl)carbodiimide by ^{1}H NMR. After heating the above-mentioned reaction mixture at 80 °C for overnight, the NMR spectrum showed the same.

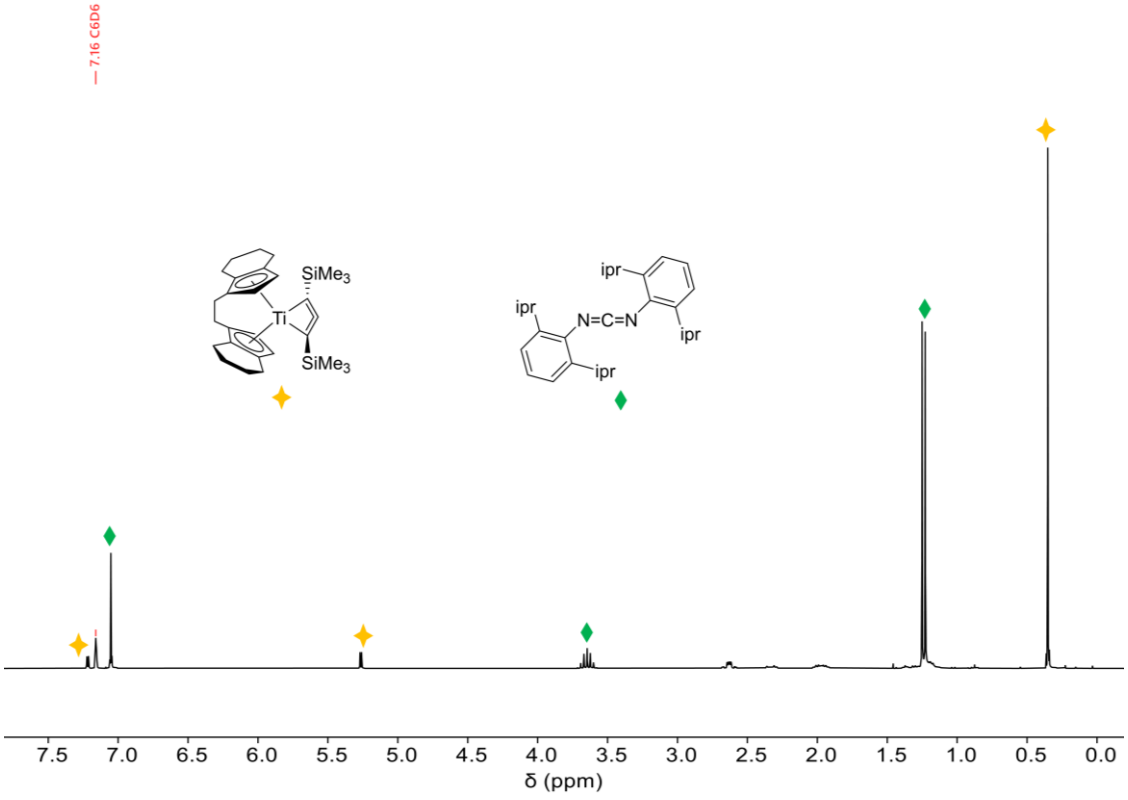

Figure S1. ^{1}H NMR spectrum of the reaction mixture of **1a** with N,N′-bis(2,6-diisopropylphenyl)carbodiimide (25 °C, benzene-d_6, 300.2 MHz).

3.4.2 Reaction of 2a with N,N′-bis(2,6-diisopropylphenyl)carbodiimide

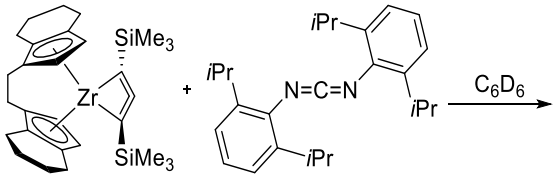

2a

According to general procedure, compound **2a** (0.10 mmol, 54 mg) was reacted with N,N′-bis(2,6-diisopropylphenyl)carbodiimide (0.10 mmol, 36 mg) in benzene-d_6 (0.6 mL) in a Young-NMR tube. The colour of reaction mixture kept same after 2 days at room temperature and the pale green solution was identified as the mixture of **2a**, N,N′-bis(2,6-diisopropylphenyl)carbodiimide and the propargyl complex **3a** by ^{1}H NMR. After heating the above-mentioned reaction mixture at 50 °C for 1 day, the crude NMR spectrum showed that more **3a** was obtained from **2a**, while there was still no formation of any new species.

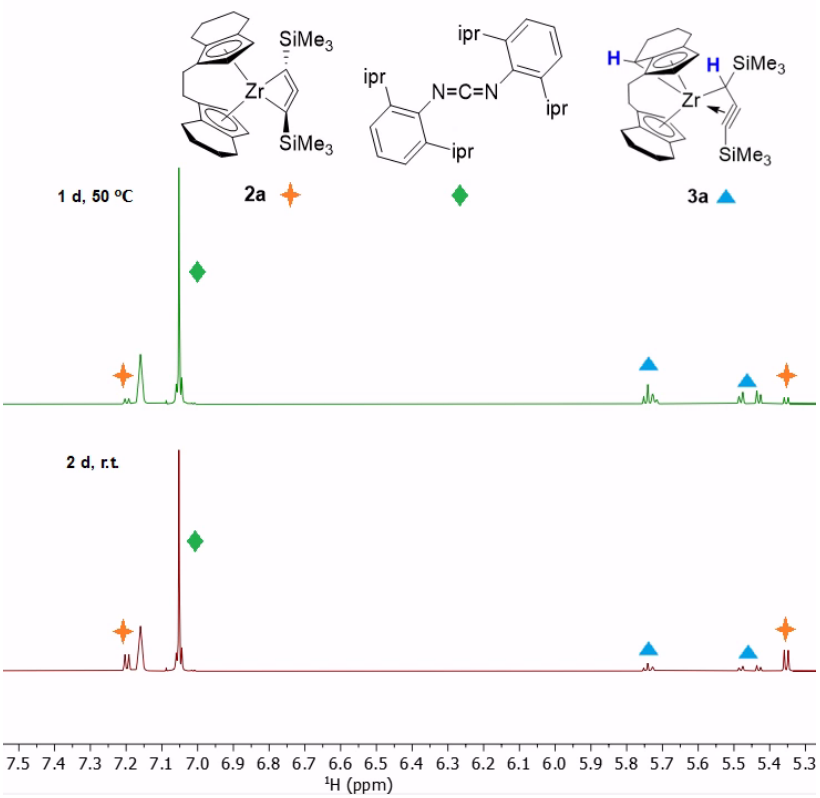

Figure S2. ^{1}H NMR spectrum of the reaction mixture of **2a** with N,N′-bis(2,6-diisopropylphenyl)carbodiimide (25 °C, benzene-d_6, 300.2 MHz).

3.4.3 Reaction of 2b with N,N′-bis(2,6-diisopropylphenyl)carbodiimide

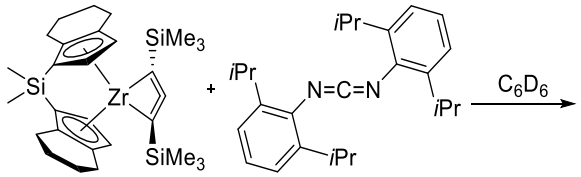

2b

According to general procedure, compound **2b** (0.10 mmol, 57 mg) was reacted with N,N′-bis(2,6-diisopropylphenyl)carbodiimide (0.10 mmol, 36 mg) in benzene-d_6 (0.6 mL) in a Young-NMR tube. The colour of reaction mixture kept same after 2 days at room temperature and the pale green solution was identified as the mixture of **2b**, N,N′-bis(2,6-diisopropylphenyl)carbodiimide and the propargyl complex **3b** by ^{1}H NMR. After heating the above-mentioned reaction mixture at 50 °C for 1 day, the crude NMR spectrum showed that more **3b** was obtained from **2b**, while there was still no formation of any new species.

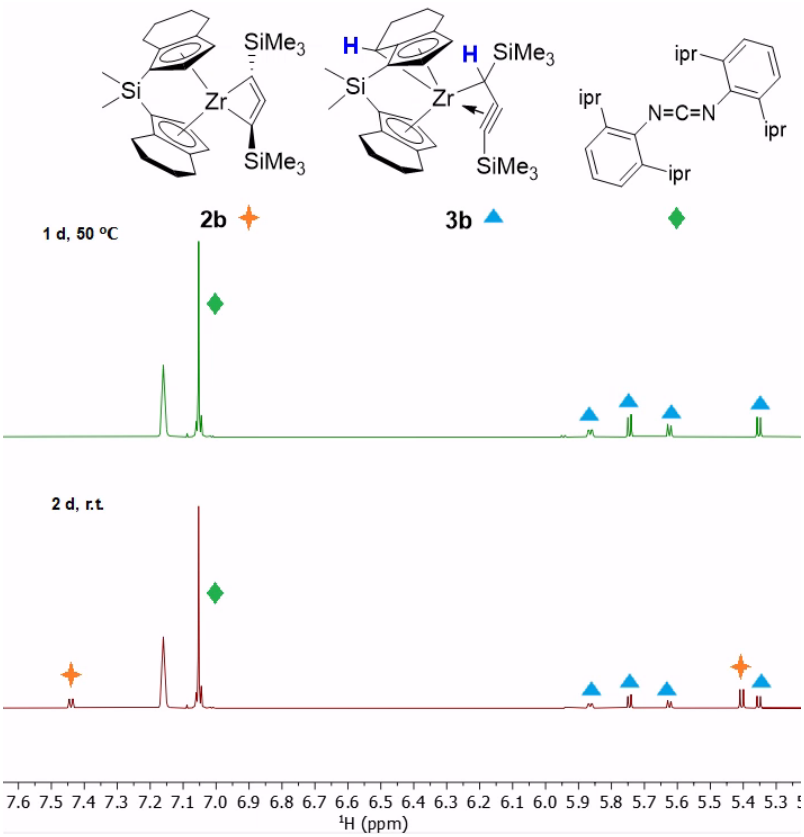

Figure S3. ^{1}H NMR spectrum of the reaction mixture of **2b** with N,N′-bis(2,6-diisopropylphenyl)carbodiimide (25 °C, benzene-d_6, 300.2 MHz).

3.4.4 Reaction of 2c with N,N′-bis(2,6-diisopropylphenyl)carbodiimide

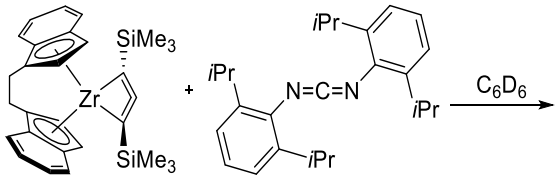

2c

According to general procedure, compound **2c** (0.20 mmol, 106 mg) was reacted with N,N′-bis(2,6-diisopropylphenyl)carbodiimide (0.10 mmol, 36 mg) in benzene-d_6 (0.6 mL) in a Young-NMR tube. The colour of reaction mixture kept same after 2 days at room temperature and the orange-red solution was identified as the mixture of **2c** and N,N′-bis(2,6-diisopropylphenyl)carbodiimide by ^{1}H NMR. After heating the above-mentioned reaction mixture at 80 °C for 1 day, the crude NMR spectrum showed that there is no formation of any new species.

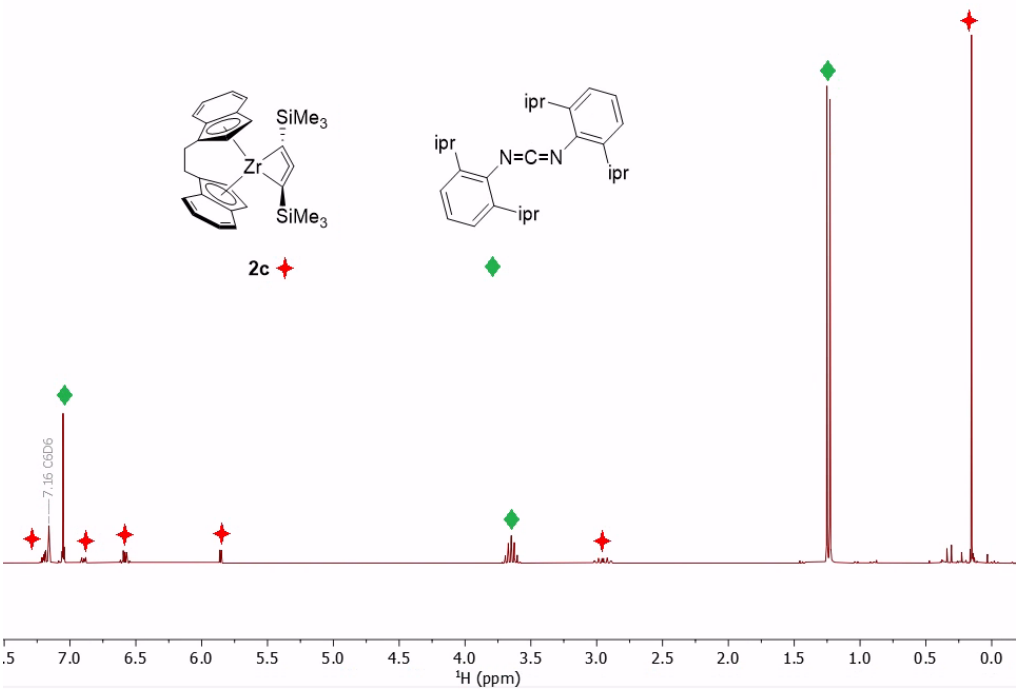

Figure S4. ^{1}H NMR spectrum of the reaction mixture of **2c** with N,N′-bis(2,6-diisopropylphenyl)carbodiimide (25 °C, benzene-d_6, 300.2 MHz).

3.4.5 Reaction of 2d with N,N′-bis(2,6-diisopropylphenyl)carbodiimide

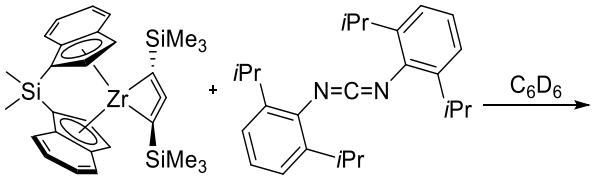

2d

According to general procedure, compound **2d** (0.20 mmol, 112 mg) was reacted with N,N′-bis(2,6-diisopropylphenyl)carbodiimide (0.10 mmol, 36 mg) in benzene-d_6 (0.6 mL) in a Young-NMR tube. The colour of reaction mixture kept same after 2 days at room temperature and the orange-red solution was identified as the mixture of **2d** and N,N′-bis(2,6-diisopropylphenyl)carbodiimide by ^{1}H NMR. After heating the above-mentioned reaction mixture at 80 °C for 1 day, the crude NMR spectrum showed that there is no formation of any new species.

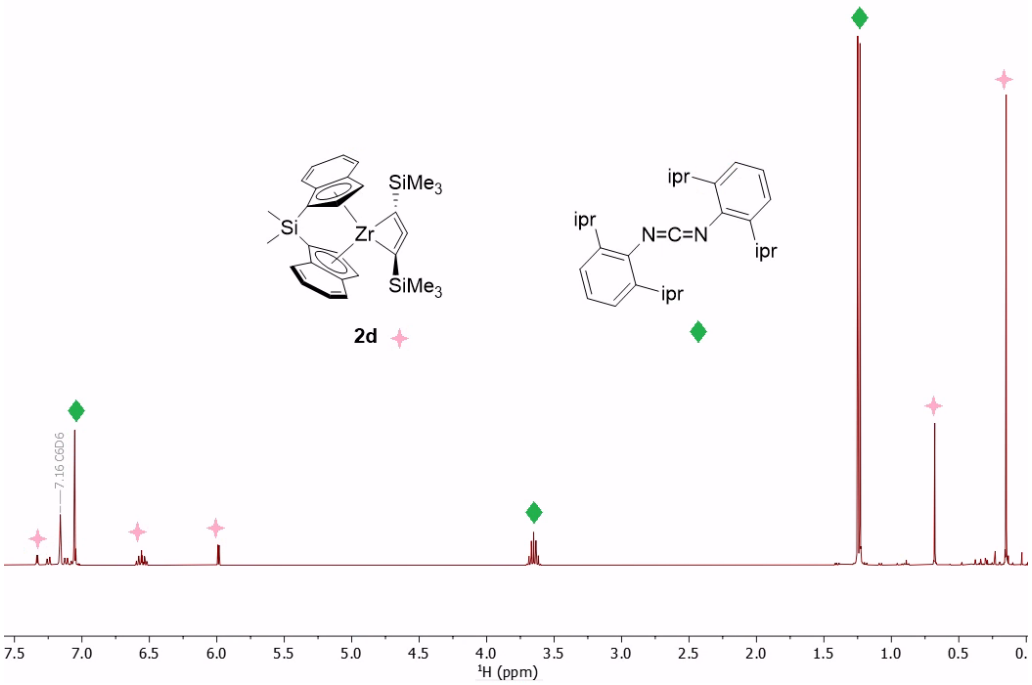

Figure S5. ^{1}H NMR spectrum of the reaction mixture of **2d** with N,N′-bis(2,6-diisopropylphenyl)carbodiimide (25 °C, benzene-d_6, 300.2 MHz).

3.5 Reaction of N,N′-bis(trimethylsilyl)carbodiimide

3.5.1 Reaction of 1a with N,N′-bis(trimethylsilyl)carbodiimide

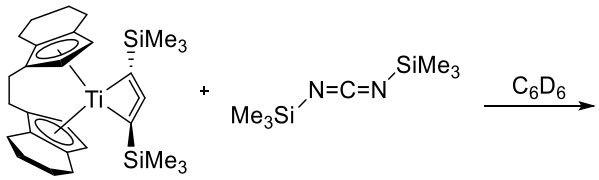

1a

According to general procedure, compound **1a** (0.034 mmol, 16.8 mg) was reacted with N,N′-bis(trimethylsilyl))carbodiimide (0.034 mmol, 8.7 mg) in benzene-d_6 (0.6 mL) in a Young-NMR tube. The colour of reaction mixture kept same after 2 days at room temperature and the dark red solution was identified as the mixture of **1a** and N,N′-bis(trimethylsilyl))carbodiimide by ^{1}H NMR. After heating the above-mentioned reaction mixture at 80 °C for overnight, the NMR spectrum showed the same.

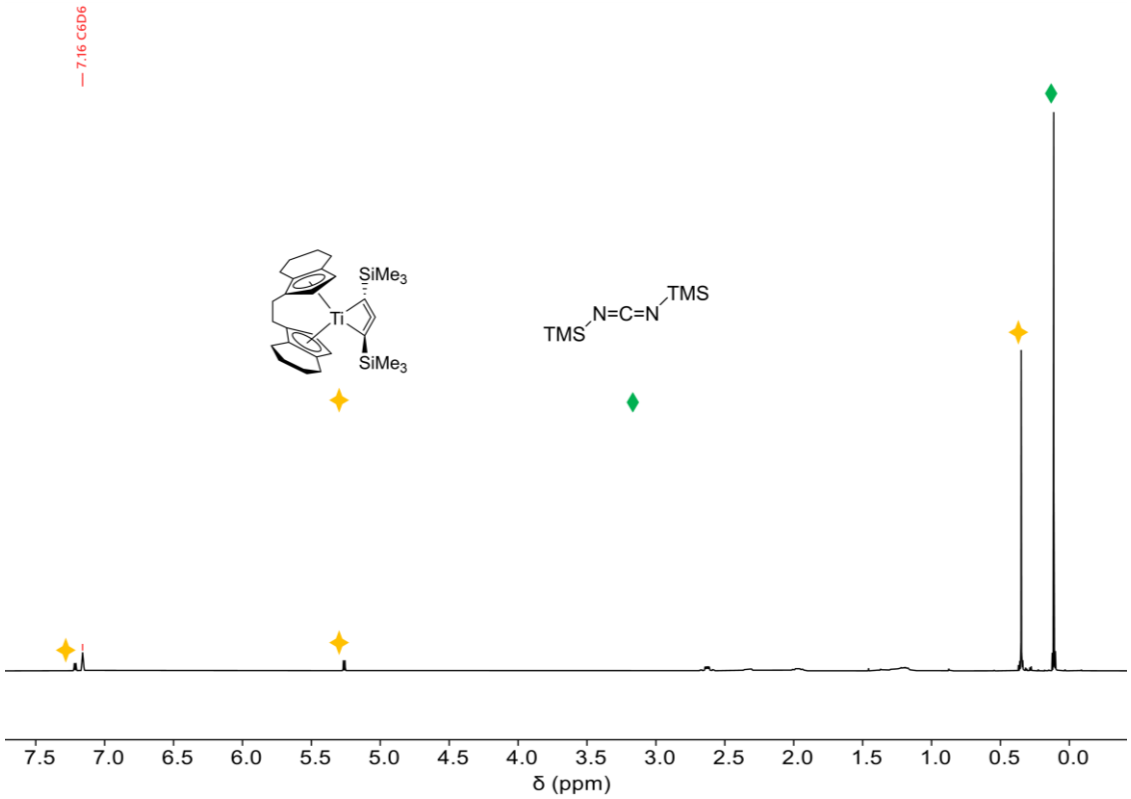

Figure S6. ^{1}H NMR spectrum of the reaction mixture of **1a** with N,N′-bis(trimethylsilyl)carbodiimide (25 °C, benzene-d_6, 300.2 MHz).

3.5.2 Reaction of 2a with N,N′-bis(trimethylsilyl)carbodiimide

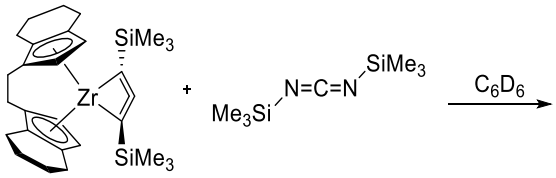

2a

According to general procedure, compound **2a** (0.10 mmol, 54 mg) was reacted with N,N′-bis(trimethylsilyl)carbodiimide (0.10 mmol, 19 mg) in benzene-d_6 (0.6 mL) in a Young-NMR tube. The colour of the reaction mixture changed from pale green to yellow in 2 days at room temperature and the solution was identified as the mixture of **2a**, N,N′-bis(trimethylsilyl)carbodiimide, the propargyl complex **3a** and an unidentified species by ^{1}H NMR. After heating the above-mentioned reaction mixture at 50 °C for 1 day, the crude NMR spectrum showed that more **3a** was obtained from **2a**, while the unidentified species was still too less to be isolated.

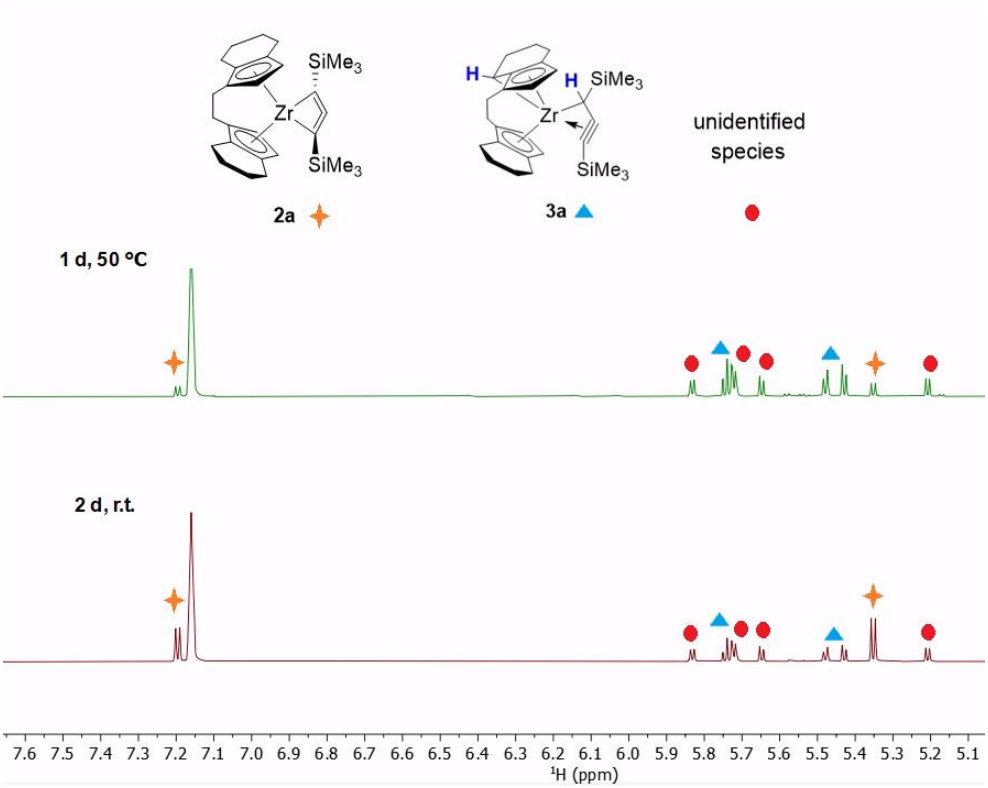

Figure S7. ^{1}H NMR spectrum of the reaction mixture of **2a** with N,N′-bis(trimethylsilyl)carbodiimide (25 °C, benzene-d_6, 300.2 MHz).

3.5.3 Reaction of 2b with N,N′-bis(trimethylsilyl)carbodiimide

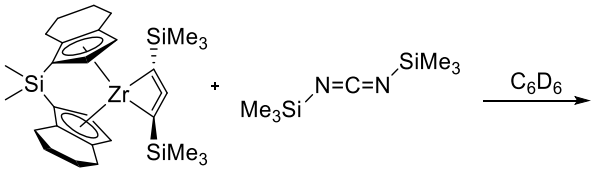

2b

According to general procedure, compound **2b** (0.10 mmol, 57 mg) was reacted with N,N′-bis(trimethylsilyl)carbodiimide (0.10 mmol, 19 mg) in benzene-d_6 (0.6 mL) in a Young-NMR tube. The colour of reaction mixture kept same after 1 day at room temperature and the solution was identified as the mixture of **2b**, N,N′-bis(trimethylsilyl)carbodiimide and the propargyl complex **3b** by ^{1}H NMR. After heating the above-mentioned reaction mixture at 80 °C for 2 days, the crude NMR spectrum showed that more **3b** was obtained from **2b**, while there was still no formation of any new species.

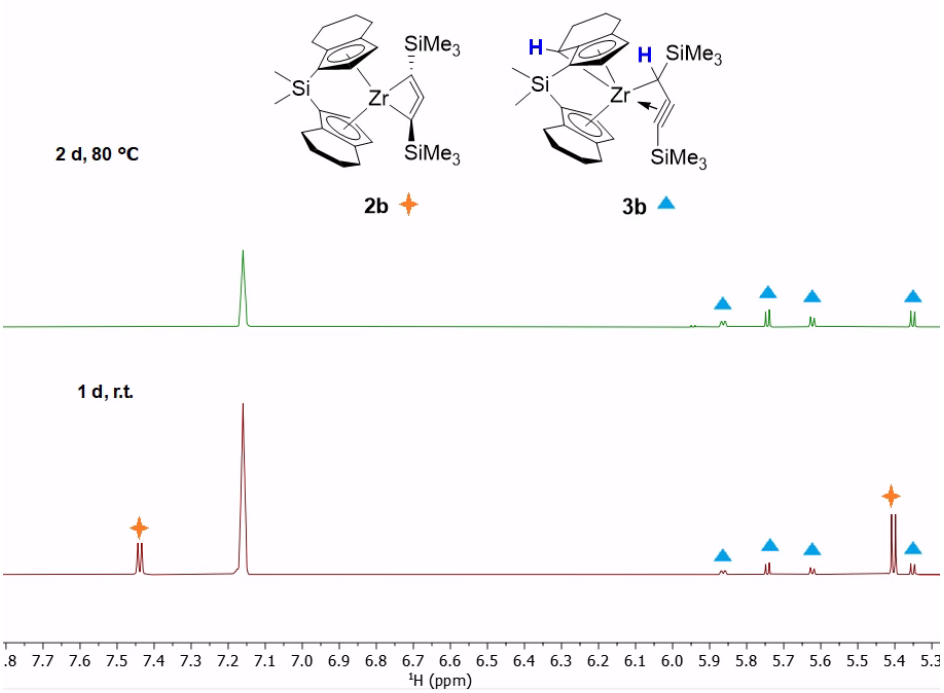

Figure S8. ^{1}H NMR spectrum of the reaction mixture of **2b** with N,N′-bis(trimethylsilyl)carbodiimide (25 °C, benzene-d_6, 300.2 MHz).

3.5.4 Reaction of 2c with N,N'-bis(trimethylsilyl)carbodiimide to $P_{2c\text{-}SiMe3}$

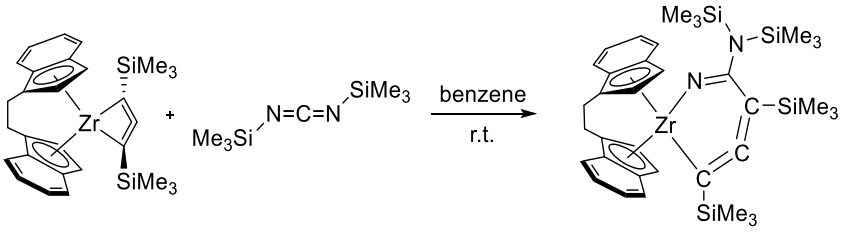

2c **$P_{2c\text{-}SiMe3}$**

According to general procedure, compound **2c** (0.20 mmol, 106 mg) was reacted with N,N'-bis(trimethylsilyl)carbodiimide (0.20 mmol, 38 mg) at room temperature. The colour of the reaction mixture changed from red to brown in 5 minutes. Then the reaction mixture was stirred for 4 hours and **$P_{2c\text{-}SiMe3}$** (122 mg, 85%) was obtained after recrystallisation. Crystals suitable for SC-XRD analysis were grown from pentane. (It is worth noting that pure **$P_{2c\text{-}SiMe3}$** slowly decomposes into **2c** and $Me_3SiN{=}C{=}NSiMe_3$ at room temperature, while a slight excess of $Me_3SiN{=}C{=}NSiMe_3$ can suppress this process).

uncorrected decomposition point: 107-110 °C (Ar.). **^{1}H NMR** (25 °C, benzene-d_6, 400.1 MHz): δ 7.55 (m, 2H, 2 x C*H* ebi), 7.47 (dq, $^3J_{H,H}$ = 8.3, 1.1 Hz, 1H, C*H* ebi), 7.13-7.08 (m, 2H, 2 x C*H* ebi), 7.05-7.01 (m, 1H, C*H* ebi), 6.92 (ddd, $^3J_{H,H}$ = 8.7, 6.6, 1.0 Hz, 1H, C*H* ebi), 6.85 (ddd, $^3J_{H,H}$ = 8.4, 6.7, 1.0 Hz, 1H, C*H* ebi), 6.22 (d, $^3J_{H,H}$ = 3.2 Hz, 1H, C*H* ebi), 6.01 (d, $^3J_{H,H}$ = 3.2 Hz, 1H, C*H* ebi), 5.89 (d, $^3J_{H,H}$ = 3.3 Hz, 1H, C*H* ebi), 5.58 (d, $^3J_{H,H}$ = 3.2 Hz, 1H, C*H* ebi), 3.62-3.43 (m, 2H, CH_2 ebi), 3.32-3.20 (m, 2H, CH_2 ebi), 0.36 (s, $^2J_{H,Si}$ = 6.5 Hz, 9H, 3 x CH_3 C-$SiMe_3$), 0.28 (s, $^2J_{H,Si}$ = 6.6 Hz, 9H, 3 x CH_3 N-$SiMe_3$), 0.25 (s, $^2J_{H,Si}$ = 6.6 Hz, 9H, 3 x CH_3 N-$SiMe_3$), 0.11 (s, $^2J_{H,Si}$ = 6.7 Hz, 9H, 3 x CH_3 C-$SiMe_3$). (Minor impurity of $Me_3SiN{=}C{=}NSiMe_3$ was generally observed as it was used to suppress the decomposition of **$P_{2c\text{-}SiMe3}$**.) **^{13}C{^{1}H} NMR** (25 °C, benzene-d_6, 100.6 MHz): δ 174.4 (C=*C*=C), 159.6 (*C*=N), 130.2 (*C* ebi), 127.2 (*C*H ebi), 127.1 (*C* ebi), 126.6 (*C*H ebi), 125.9 (*C* ebi), 125.3, 123.3, 123.0, 122.7 (4 x *C*H ebi), 122.4 (*C* ebi), 122.3, 121.1 (2 x *C*H ebi), 118.2, 117.1 (2 x *C* ebi), 115.8 (*C*H ebi), 115.7 (*C*-$SiMe_3$), 113.4 (*C*H ebi), 102.2 (*C*-$SiMe_3$), 98.0, 93.2 (2 x *C*H ebi), 31.1, 29.4 (2 x CH_2 ebi), 3.4, 3.3, 2.2, 1.9 (4 x $SiMe_3$). **^{29}Si-inept NMR** (25 °C, benzene-d_6, 79.5 MHz): δ 3.33 (dec, $^2J_{H,Si}$ = 6.5 Hz, C-*Si*Me_3), 2.61 (dec, $^2J_{H,Si}$ = 6.6 Hz, N-*Si*Me_3), −4.81 (dec, $^2J_{H,Si}$ = 6.7 Hz, C-*Si*Me_3), −12.78 (dec, $^2J_{H,Si}$ = 6.6 Hz, N-*Si*Me_3). **Elemental analysis** calcd (%) for M($C_{36}H_{52}N_2Si_4Zr$) = 716.39 g mol^{-1}: C 60.36, H 7.32, N 3.91; found: C 56.66, H 4.75, N 2.79 (Measured with V_2O_5. Without V_2O_5: C 56.35, H 5.17, N 2.73). **IR** (ATR, 32 scans, cm^{-1}): 3066 (w), 2953 (w), 2899 (w), 2853 (w), 2119 (w), 1852 (m), 1437 (w), 1374 (w), 1342 (w), 1240 (m), 1225 (m), 1154 (m), 1027 (m), 933 (m), 875 (m), 829 (s), 775 (s), 745 (s), 710 (m), 679 (s), 655 (m), 627 (m), 531 (m), 474 (m), 436 (m). **MS-CI$^+$** (*isobutane*): [M$^+$] 716 (7), [(M−NCHN($SiMe_3$)$_2$)$^+$] 529 (79), [(M−ebi−H)$^+$] 459 (100), [ebi$^+$] 259 (80), [($Me_3SiCHCCHSiMe_3$+H)$^+$] 185 (67), [$SiMe_3^+$] 73 (52).

3.5.5 Reaction of 2d with N,N′-bis(trimethylsilyl)carbodiimide to $P_{2d\text{-}SiMe3}$

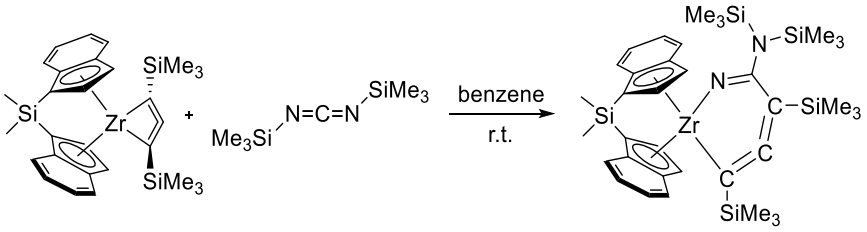

2d **$P_{2d\text{-}SiMe3}$**

According to general procedure, compound **2d** (0.20 mmol, 112 mg) was reacted with N,N′-bis(trimethylsilyl)carbodiimide (0.20 mmol, 38 mg) at room temperature. The colour of the reaction mixture changed from red to brown in 5 minutes. Then the reaction mixture was stirred for 4 hours and **$P_{2d\text{-}SiMe3}$** (133 mg, 89%) was obtained after recrystallisation. Crystals suitable for SC-XRD analysis were grown from pentane. (It is worth noting that pure **$P_{2d\text{-}SiMe3}$** slowly decomposes into **2d** and $Me_3SiN{=}C{=}NSiMe_3$ at room temperature, while a slight excess of $Me_3SiN{=}C{=}NSiMe_3$ can suppress this process).

uncorrected decomposition point: 121-124 °C (Ar.). **^{1}H NMR** (25 °C, benzene-d_6, 400.1 MHz): δ 7.65-7.61 (m, 2H, 2 x C*H* sbi), 7.55 (dq, $^3J_{H,H}$ = 8.6, 1.0 Hz, 1H, C*H* sbi), 7.26 (dq, $^3J_{H,H}$ = 8.3, 1.1 Hz, 1H, C*H* sbi), 7.12 (ddd, $^3J_{H,H}$ = 8.4, 6.7, 1.1 Hz, 1H, C*H* sbi), 7.01 (ddd, $^3J_{H,H}$ = 7.9, 6.7, 1.0 Hz, 1H, C*H* sbi), 6.89-6.82 (m, 2H, 2 x C*H* sbi), 6.57 (d, $^3J_{H,H}$ = 3.3 Hz, 1H, C*H* sbi), 6.40 (d, $^3J_{H,H}$ = 3.2 Hz, 1H, C*H* sbi), 6.30 (d, $^3J_{H,H}$ = 3.2 Hz, 1H, C*H* sbi), 5.95 (d, $^3J_{H,H}$ = 3.3 Hz, 1H, C*H* sbi), 0.89 (s, $^2J_{H,Si}$ = 7.0 Hz, 6H, 2 x CH_3 $SiMe_2$), 0.38 (s, $^2J_{H,Si}$ = 6.6 Hz, 9H, 3 x CH_3 C-$SiMe_3$), 0.26 (s, $^2J_{H,Si}$ = 6.6 Hz, 9H, 3 x CH_3 N-$SiMe_3$), 0.25 (s, $^2J_{H,Si}$ = 6.6 Hz, 9H, 3 x CH_3 N-$SiMe_3$), 0.10 (s, $^2J_{H,Si}$ = 6.7 Hz, 9H, 3 x CH_3 C-$SiMe_3$). (Minor impurity of $Me_3SiN{=}C{=}NSiMe_3$ was generally observed as it was used to suppress the decomposition of **$P_{2d\text{-}SiMe3}$**.) **^{13}C{^{1}H} NMR** (25 °C, benzene-d_6, 100.6 MHz): δ 176.0 (C=*C*=C), 157.9 (*C*=N), 135.2, 131.5, 131.1 (3 x *C* sbi), 127.5, 126.8, 125.13 (3 x *C*H sbi), 125.08 (*C* sbi), 124.9, 124.6, 123.6, 123.5, 123.1, 117.6, 117.2 (7 x *C*H sbi), 114.4 (*C*-$SiMe_3$), 109.1 (*C*H sbi), 103.5 (*C*-$SiMe_3$), 99.5 (*C*H sbi), 90.9, 87.4 (2 x *C* sbi), 3.3, 3.2, 2.2, 1.8 (4 x $SiMe_3$), 0.8, −2.9 (2 x $SiMe_2$). **^{29}Si-inept NMR** (25 °C, benzene-d_6, 79.5 MHz): δ 3.75 (dec, $^2J_{H,Si}$ = 6.6 Hz, C-*Si*Me_3), 2.51 (dec, $^2J_{H,Si}$ = 6.6 Hz, N-*Si*Me_3), −4.88 (dec, $^2J_{H,Si}$ = 6.7 Hz, C-*Si*Me_3), −13.00 (dec, $^2J_{H,Si}$ = 6.6 Hz, N-*Si*Me_3), −15.18 (sep, $^2J_{H,Si}$ = 7.0 Hz, *Si*Me_2). **Elemental analysis** calcd (%) for M($C_{36}H_{54}N_2Si_5Zr$) = 746.49 g mol^{-1}: C 57.92, H 7.29, N 3.75; found: C 53.72, H 8.18, N 3.72 (Measured with V_2O_5. Without V_2O_5: C 49.36, H 8.07, N 2.06). **IR** (ATR, 32 scans, cm^{-1}): 3057 (w), 2953 (w), 2898 (w), 2124 (w), 2065 (w), 1849 (m), 1531 (w), 1399 (w), 1337 (w), 1299 (w), 1243 (m), 1137 (m), 1016 (m), 939 (m), 825 (s), 780 (s), 753 (s), 737 (s), 711 (m), 682 (s), 651 (m), 556 (w), 527 (m), 503 (m), 452 (s), 416 (s). **MS-CI$^+$** (*isobutane*): [M$^+$] 746 (26), [(M−NCHN($SiMe_3$)$_2$)$^+$] 559 (50), [(2x(indenyl)+Si−H)$^+$] 257 (54), [($Me_3SiCHCCHSiMe_3$+H)$^+$] 185 (99), [$SiMe_3^+$] 73 (100).

3.6 Low-temperature NMR spectroscopy

NMR spectra were collected at -50 °C every 10 min until complex **2c** was fully converted into an intermediate species (R = *i*Pr) or after confirming that no reaction occurred (R = $SiMe_3$), After this, the temperature was increased to -40, -30, -20, -10, 0, 10, 25 °C, keeping the temperature constant for 10 min and collecting two NMR spectra.

3.6.1 Reaction of 2c with N,N′-diisopropylcarbodiimide to $P_{2c\text{-}iPr}$

Compound **2c** (0.020 mmol, 10.6 mg) and N,N′-diisopropylcarbodiimide (0.02 mmol, 2.5 mg) were placed in a Young-NMR tube and toluene-d_8 (0.6 mL) was added at -78°C. The sample was kept at this temperature until start of the NMR measurement. Selected NMR spectra are shown below.

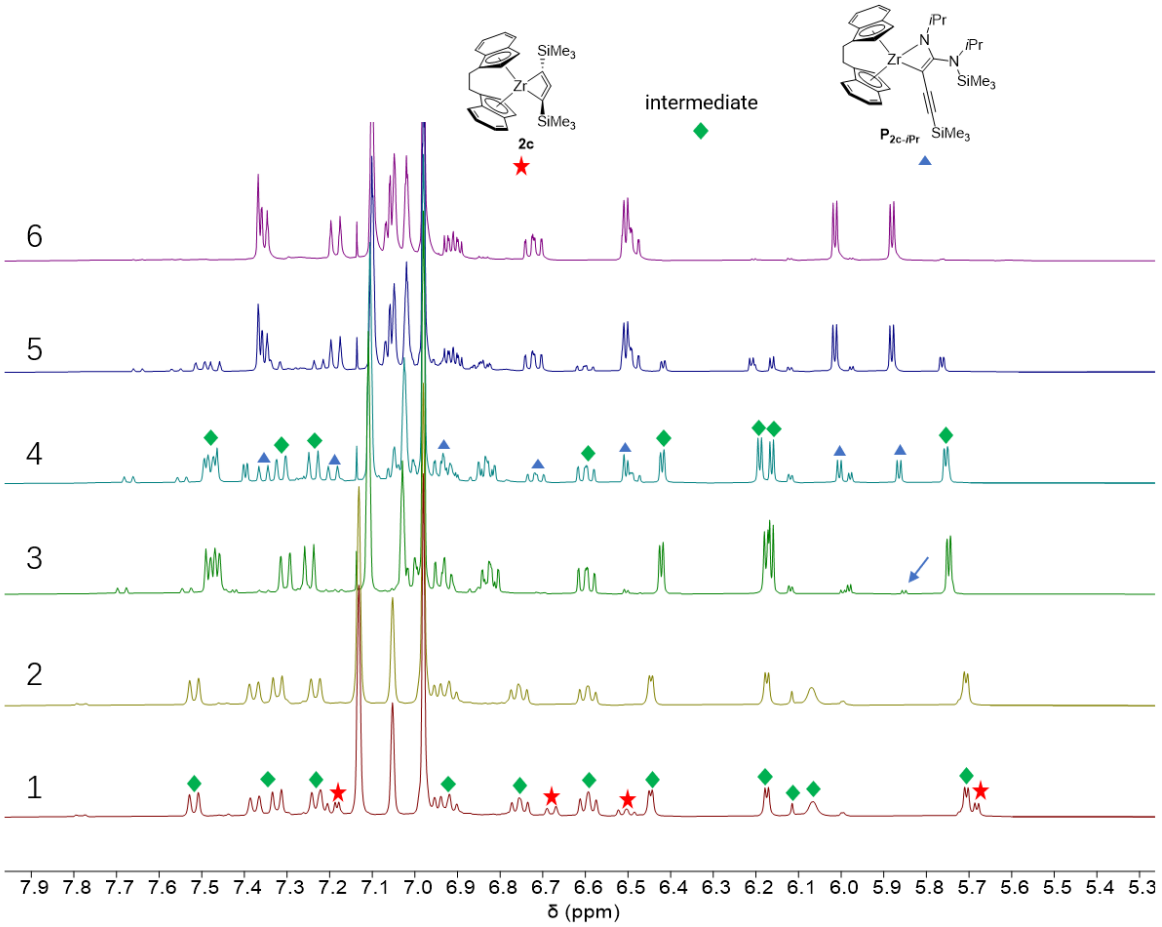

Figure S9. ^{1}H NMR spectra of the reaction of **2c** with N,N′-diisopropylcarbodiimide at different temperatures (toluene-d_8, 400.2 MHz). 1) *T* = -50 °C; 2) *T* = -50 °C for 90 min; 3) *T* = -10 °C; 4) *T* = 10 °C; 5) *T* = 25 °C; 6) *T* = 25 °C for 80 min.

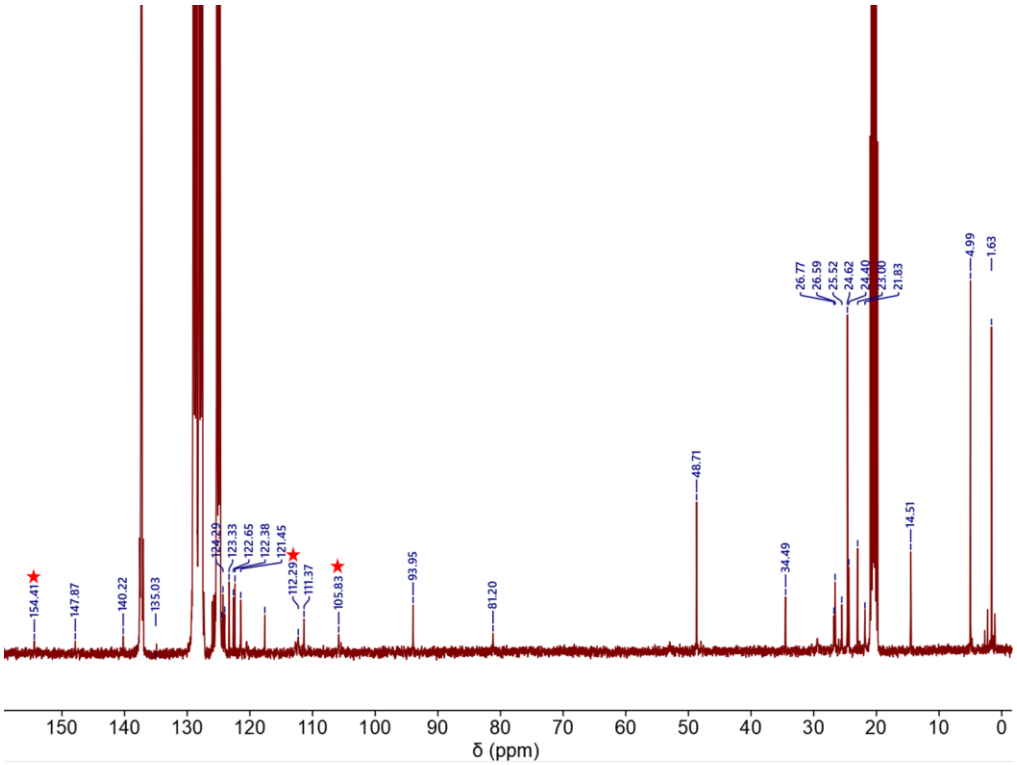

Figure S10. $^{13}C\{^{1}H\}$ NMR spectrum of the intermediate formed during reaction of **2c** with N,N′-diisopropylcarbodiimide at -50 °C (toluene-*d*8, 400.2 MHz). The peaks labelled with a red star are assigned to the allene carbon atoms of the elusive intermediate.

3.6.2 Reaction of 2c with N,N′-bis(trimethylsilyl)carbodiimide to $P_{2c\text{-}SiMe3}$

Compound **2c** (0.020 mmol, 10.6 mg) and N,N′-bis(trimethylsilyl)carbodiimide (0.02 mmol, 3.7 mg) were placed in a Young-NMR tube and toluene-d_8 (0.6 mL) was added at -78°C. The sample was kept at this temperature until start of the NMR measurement. Selected NMR spectra are shown below.

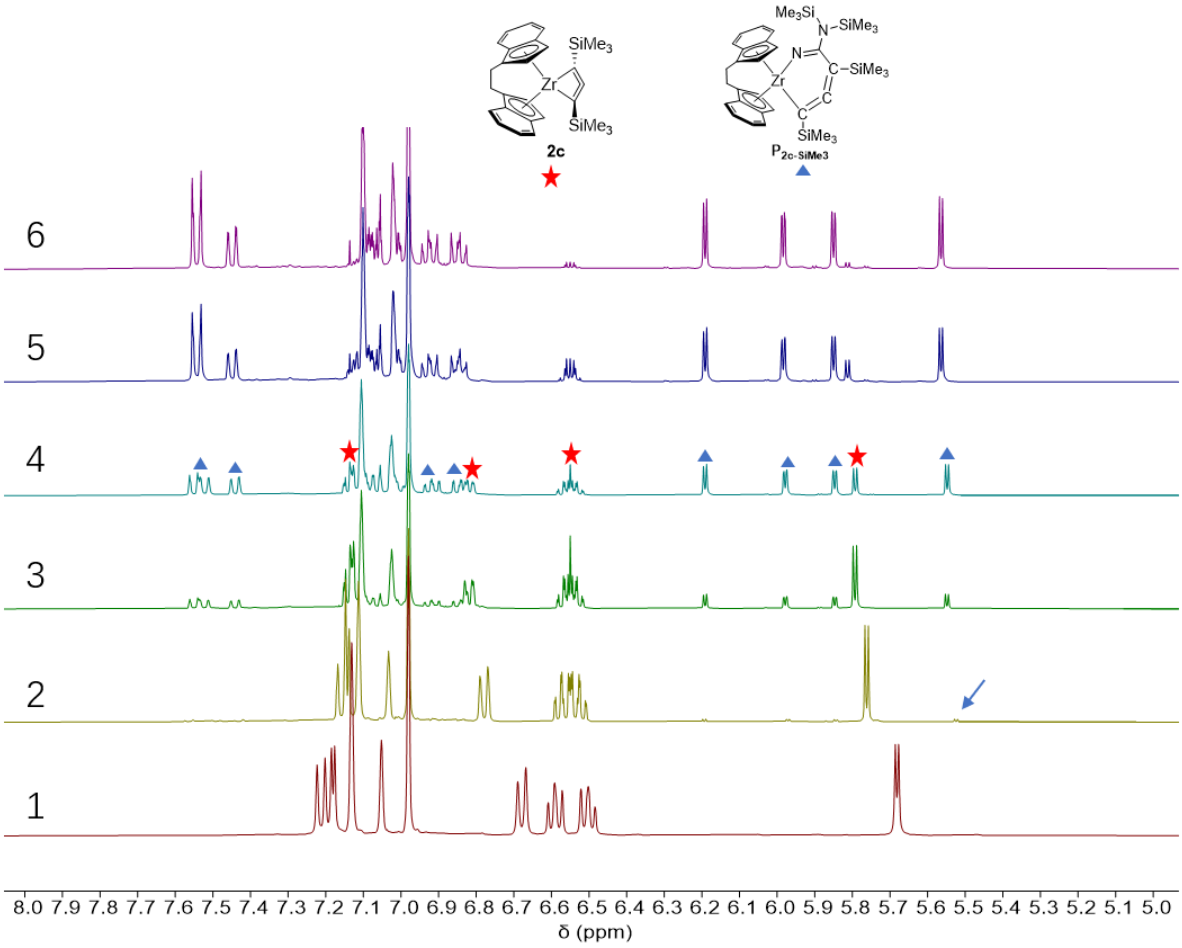

Figure S11. ^{1}H NMR spectra of the reaction of **2c** with N,N′-bis(trimethylsilyl)carbodiimide at different temperatures (toluene-d_8, 400.2 MHz). 1) T = -50 °C for 30 min; 2) T = -10 °C; 3) T = 10 °C for 20 min; 4) T = 10 °C for 130 min; 5) T = 25 °C for 10 min; 6) T = 25 °C for 160 min.

4. Reactivity of $P_{2b\text{-}iPr}$ with benzophenone

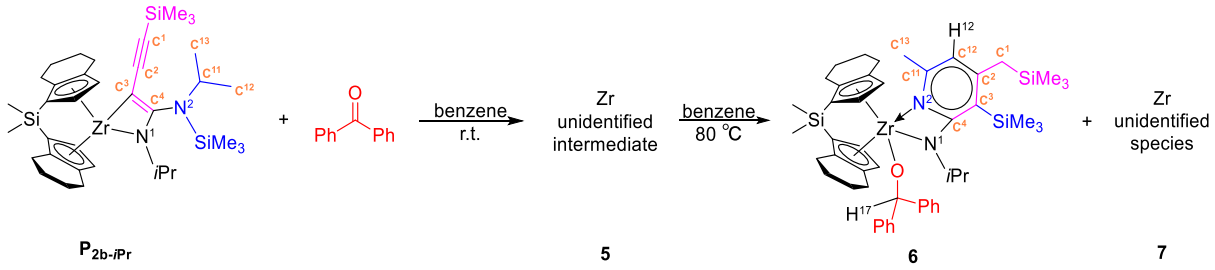

Compound **$P_{2b\text{-}iPr}$** (0.20 mmol, 0.139 g) and benzophenone (0.20 mmol, 37 mg) were dissolved in benzene (2 mL). After 5 days of stirring at room temperature or 1 day of stirring at 60 °C, the solvent was removed in *vacuo*. A NMR sample was taken and the crude NMR spectrum showed that product **5** was the major species (conversion of **$P_{2b\text{-}iPr}$**: 100%). Unfortunately, no crystal suitable for SC-XRD analysis was obtained, and the structure of product **5** hadn't been identified. **^{1}H NMR** (25 °C, benzene-d_6, 300.2 MHz): δ 7.43-7.35 (m, 5H, 5 x C*H* Ph), 7.09-7.00 (m, 3H, 3 x C*H* Ph), 6.71 (d, $^3J_{H,H}$ = 2.7 Hz, 1H, C*H* thi), 6.32 (s, 1H, O-C*H*Ph$_2$), 6.22 (d, $^3J_{H,H}$ = 2.9 Hz, 1H, C*H* thi), 5.80 (d, $^3J_{H,H}$ = 2.7 Hz, 1H, C*H* thi), 5.66 (d, $^3J_{H,H}$ = 3.0 Hz, 1H, C*H* thi), 3.28 (hept, $^3J_{H,H}$ = 6.2 Hz, 1H, C*H* *i*Pr), 1.81 (s, 3H), 1.66 (s, 3H), 1.29 (d, $^3J_{H,H}$ = 6.2 Hz, 3H, C*H*$_3$ *i*Pr), 1.19 (d, $^3J_{H,H}$ = 6.1 Hz, 3H, C*H*$_3$ *i*Pr), 0.69 (s, $^2J_{H,Si}$ = 6.5 Hz, 9H, 3 x C*H*$_3$ SiMe$_3$), 0.55 (s, $^2J_{H,Si}$ = 6.9 Hz, 3H, C*H*$_3$ SiMe$_2$), 0.49 (s, $^2J_{H,Si}$ = 6.9 Hz, 3H, C*H*$_3$ SiMe$_2$), 0.17 (s, $^2J_{H,Si}$ = 6.5 Hz, 9H, 3 x C*H*$_3$ SiMe$_3$) (A more precise assignment was not made, since the signals in the mixture cannot be assigned without any doubt).

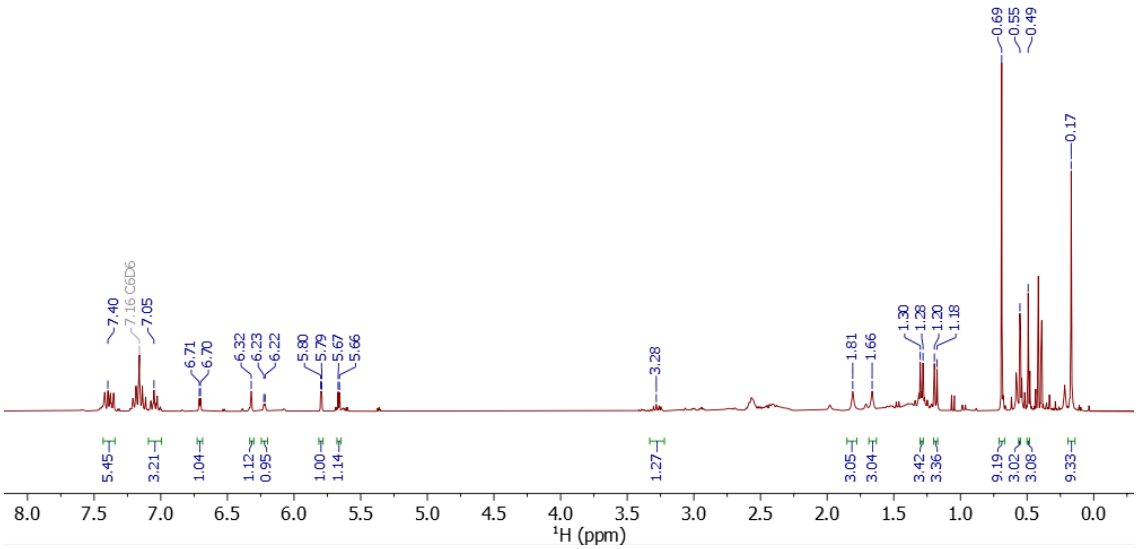

Figure S12. ^{1}H NMR spectrum of the reaction mixture for the formation of **5** (25 °C, benzene-d_6, 300.2 MHz).

After heating the above-mentioned reaction mixture at 80 °C for 2 days, an NMR sample was taken and the crude NMR showed that compound **6** and **7** was the resulting products. Then the yellow residue was dissolved in pentane and stored at -30 °C for crystallisation to obtain the products **6** and **7**. Crystals of compound **6** suitable for SC-XRD analysis were grown from

pentane, which is not the case for product **7**. It should be noted that compound **6** could only be isolated in small amount. Therefore, only ^{1}H NMR and SC-XRD analysis were performed.

^{1}H NMR of 6 (25 °C, benzene-d_6, 300.2 MHz): δ 7.80-7.77 (m, 2H, 2 x C*H* Ph), 7.59-7.37 (m, 3H, 3 x C*H* Ph), 7.26-7.20 (m, 3H, C*H* Ph+pyridine), 7.06-7.01 (m, 3H, 3 x C*H* Ph), 6.27 (d, $^{3}J_{H,H}$ = 2.4 Hz, 1H, C*H* thi), 5.76 (s, 1H, O-C*H*Ph$_2$), 5.57 (d, $^{3}J_{H,H}$ = 2.4 Hz, 1H, C*H* thi), 2.14 (s, 3H, C-C*H*$_3$ pyridine), 1.58 (s, 2H, C*H*$_2$-SiMe$_3$), 0.70 (d, $^{3}J_{H,H}$ = 6.3 Hz, 3H, C*H*$_3$ *i*Pr), 0.54 (d, $^{3}J_{H,H}$ = 4.9 Hz, 3H, C*H*$_3$ *i*Pr), 0.45 (s, $^{2}J_{H,Si}$ = 6.5 Hz, 9H, 3 x C*H*$_3$ SiMe$_3$), 0.25 (s, $^{2}J_{H,Si}$ = 6.9 Hz, 3H, C*H*$_3$ SiMe$_2$), 0.23 (s, $^{2}J_{H,Si}$ = 6.9 Hz, 3H, C*H*$_3$ SiMe$_2$), 0.03 (s, $^{2}J_{H,Si}$ = 6.5 Hz, 9H, 3 x C*H*$_3$ SiMe$_3$). Compound **6** was not isolated in high purity after crystallisation due to unidentified impurities. Therefore, a precise assignment of ^{1}H NMR was not made.

^{1}H NMR of 7 (25 °C, benzene-d_6, 300.2 MHz): δ 7.57-7.46 (m, 3H, C*H* Ph), 6.69 (d, $^{3}J_{H,H}$ = 3.1 Hz, 1H, C*H* thi), 6.39 (s, 1H, O-C*H*Ph$_2$), 6.18 (d, $^{3}J_{H,H}$ = 2.8 Hz, 1H, C*H* thi), 5.46 (d, $^{3}J_{H,H}$ = 2.8 Hz, 1H, C*H* thi), 3.81 (hept, $^{3}J_{H,H}$ = 6.2 Hz, 1H, C*H* *i*Pr), 0.71 (s, $^{2}J_{H,Si}$ = 7.1 Hz, 3H, SiMe$_2$), 0.53 (s, $^{2}J_{H,Si}$ = 6.9 Hz, 3H, SiMe$_2$), 0.38 (s, $^{2}J_{H,Si}$ = 6.5 Hz, 9H, SiMe$_3$), 0.25 (s, $^{2}J_{H,Si}$ = 6.5 Hz, 9H, SiMe$_3$) (A more precise assignment was not made, since the signals in the mixture cannot be assigned without any doubt).

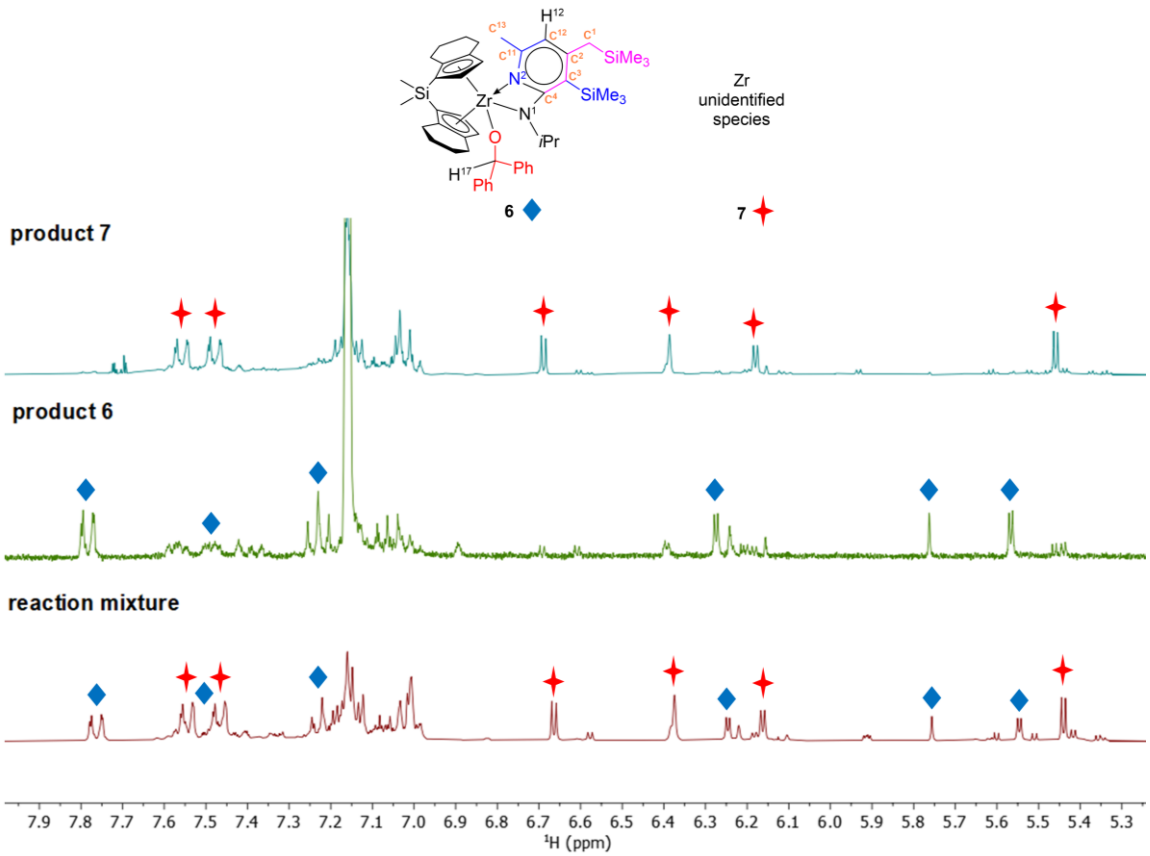

Figure S13. ^{1}H NMR spectra of the reaction mixture for the formation of **6** and **7** (25 °C, benzene-d_6, 300.2 MHz).

5. Proof of stability of compounds

5.1 Stability of 2c

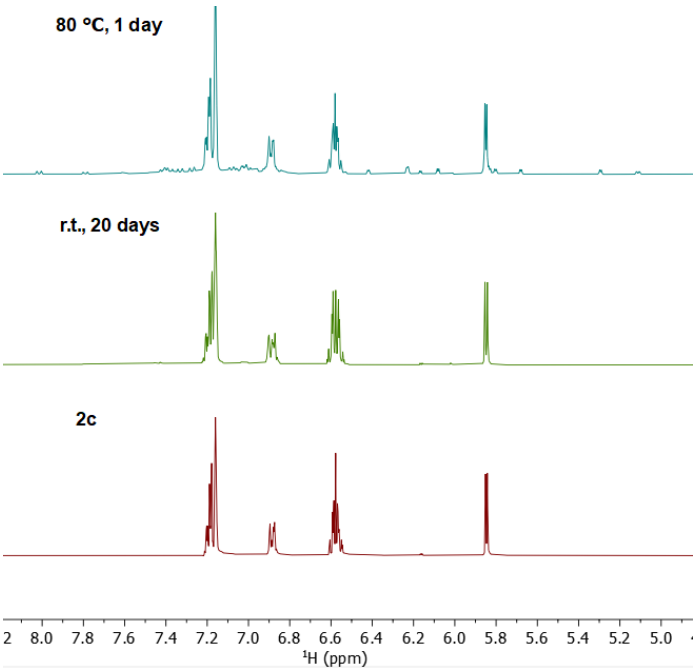

Figure S14. Comparison of ^{1}H NMR spectra of **2c** in benzene-*d*$_6$ at room temperature and 80°C (25 °C, benzene-*d*$_6$, 300.2 MHz).

5.2 Stability of 2d

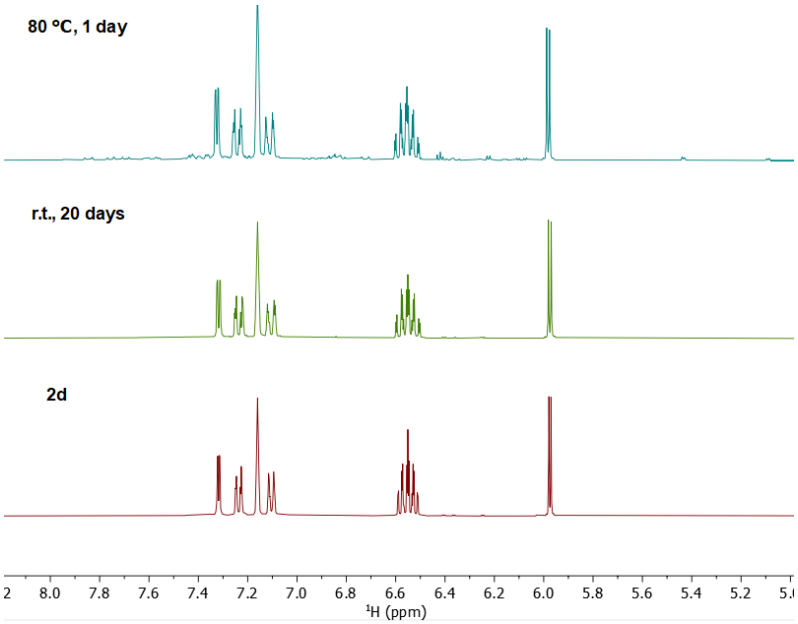

Figure S15. Comparison of ^{1}H NMR spectra of **2d** in benzene-*d*$_6$ at room temperature and 80°C (25 °C, benzene-*d*$_6$, 300.2 MHz).

5.3 Stability of $P_{2c\text{-}SiMe3}$ in benzene at room temperature

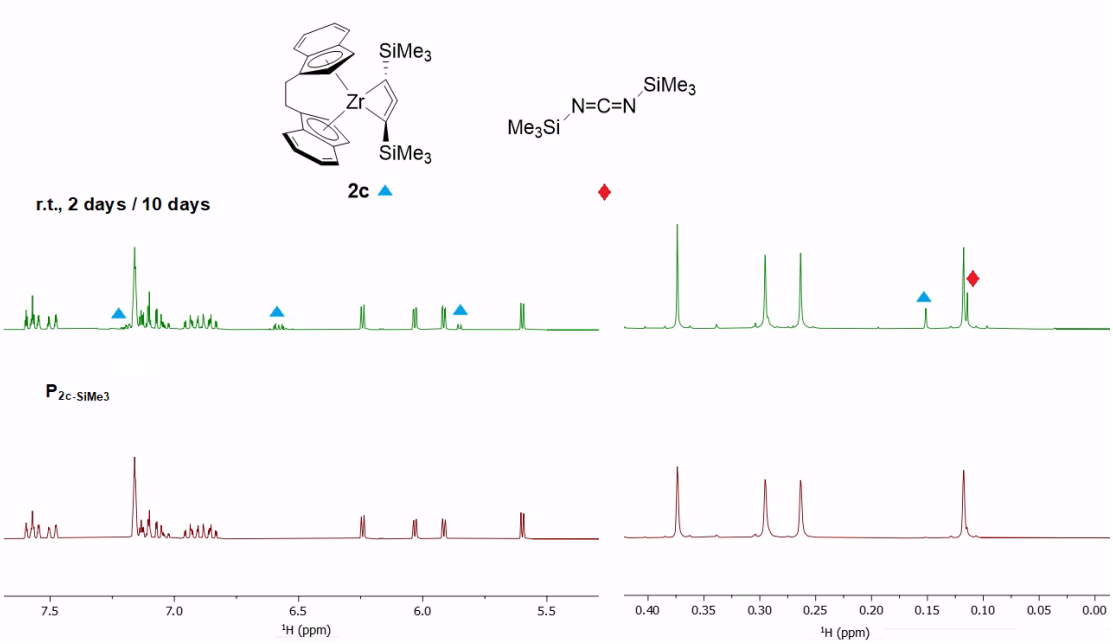

Figure S16. Comparison of ^{1}H NMR spectra of **$P_{2c\text{-}SiMe3}$** in benzene-*d*6 at room temperature (25 °C, benzene-*d*6, 300.2 MHz).

5.4 Stability of $P_{2d\text{-}SiMe3}$ in benzene at room temperature

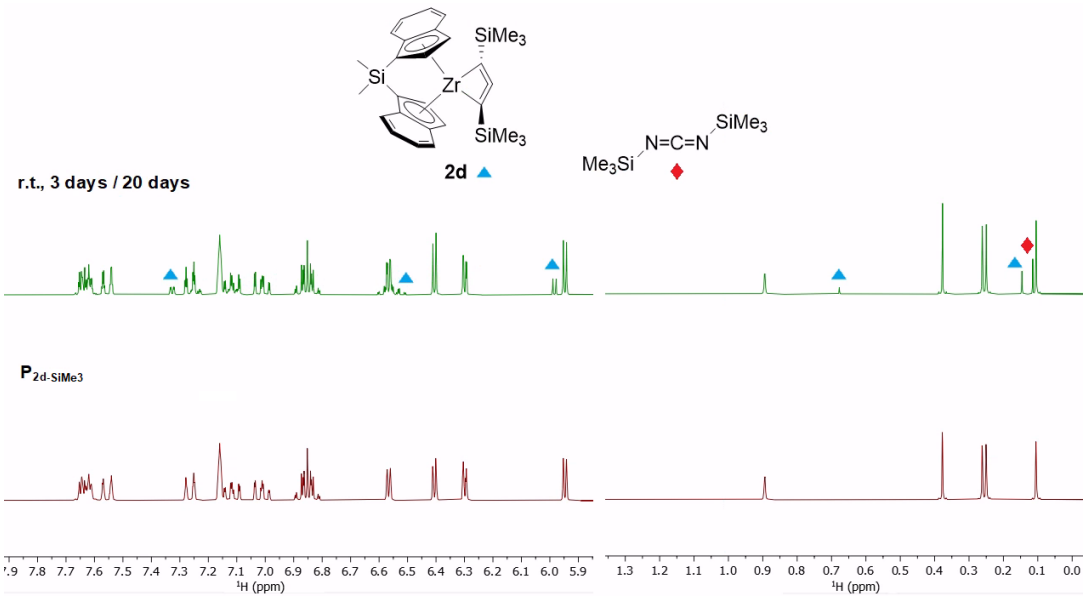

Figure S17. Comparison of ^{1}H NMR spectra of **$P_{2d\text{-}SiMe3}$** in benzene-*d*6 at room temperature (25 °C, benzene-*d*6, 300.2 MHz).

6. Crystallographic details

Table S1. Crystallographic details of 2c, 2d, $P_{1a\text{-}iPr}$, $P_{2a\text{-}iPr}$ and $P_{2b\text{-}iPr}$.

Compound	**2c**	**2d**	**$P_{1a\text{-}iPr}$**	**$P_{2a\text{-}iPr}$**	**$P_{2b\text{-}iPr}$**
Chem. Formula	$C_{29}H_{34}Si_2Zr$	$C_{29}H_{36}Si_3Zr$	$C_{36}H_{56}N_2Si_2Ti$	$C_{36}H_{56}N_2Si_2Zr$	$C_{36}H_{58}N_2Si_3Zr$
Formula weight [g/mol]	529.96	560.07	620.90	664.22	694.33
Colour	red	red	red	green	dark green
Crystal system	triclinic	triclinic	triclinic	triclinic	monoclinic
Space group	$P\bar{1}$	$P\bar{1}$	$P\bar{1}$	$P\bar{1}$	$P2_1/c$
a [Å]	9.154(2)	11.0852(6)	10.5145(12)	10.8751(7)	16.5430(5)
b [Å]	10.966(3)	17.3767(10)	13.1709(15)	12.8716(8)	11.6992(2)
c [Å]	14.773(4)	18.0980(11)	14.5298(17)	15.1684(10)	19.8643(5)
α [°]	75.293(5)	111.5476(12)	76.234(3)	108.3645(12)	90
β [°]	76.747(5)	101.7916(13)	79.028(3)	99.5141(12)	96.448(2)
γ [°]	68.400(5)	106.7712(12)	67.686(3)	96.7831(12)	90
V [Å^3]	1318.4(5)	2910.0(3)	1796.8(4)	1954.3(2)	3820.21(16)
Z	2	4	2	2	4
$\rho_{calcd.}$ [g/cm^3]	1.335	1.278	1.148	1.129	1.207
μ [mm^{-1}]	0.523	0.516	0.330	0.366	0.407
T [K]	150(2)	150(2)	150(2)	150(2)	150(2)
Radiation type	MoKα	MoKα	MoKα	MoKα	MoKα
Measured reflections	66697	99363	73937	71613	60517
Independent reflections	5744	15479	9391	9427	10134
Reflections with $I > 2\sigma(I)$	5412	12735	8219	8277	9059
R_{int}	0.0235	0.0377	0.0281	0.0308	0.0172
F(000)	552	1168	672	708	1480
R_1 [$I > 2\sigma(I)$]	0.0214	0.0276	0.0315	0.0342	0.0323
wR_2 (all data)	0.0577	0.0686	0.0865	0.0923	0.0936
GooF	1.059	1.022	1.031	1.049	1.071
No. of Parameters	295	611	380	399	391
CCDC	2244173	2244174	2244175	2244176	2244177

Table S2. Crystallographic details of $P_{2d\text{-}iPr}$, $P_{1a\text{-}Cy}$, $P_{2c\text{-}Cy}$, $P_{2c\text{-}SiMe3}$, $P_{2d\text{-}SiMe3}$ and 6.

Compound	$\mathbf{P_{2d\text{-}iPr}}$	$\mathbf{P_{1a\text{-}Cy}}$	$\mathbf{P_{2c\text{-}Cy}}$	$\mathbf{P_{2c\text{-}SiMe3}}$	$\mathbf{P_{2d\text{-}SiMe3}}$	**6**
Chem. Formula	$C_{36}H_{50}N_2Si_3Zr$	$C_{42}H_{64}N_2Si_2Ti$	$C_{42}H_{56}N_2Si_2Zr \cdot 0.35\ C_5H_{12}$	$C_{36}H_{52}N_2Si_4Zr$	$C_{36}H_{54}N_2Si_5Zr$	$C_{49}H_{68}N_2OSi_3Zr$
Formula weight [g/mol]	686.27	701.03	761.54	716.37	746.48	876.54
Colour	brown	red	brown	brown	brown	pale yellow
Crystal system	monoclinic	triclinic	triclinic	monoclinic	triclinic	triclinic
Space group	*C*2/*c*	$P\bar{1}$	$P\bar{1}$	$P2_1$	$P\bar{1}$	$P\bar{1}$
a [Å]	41.554(1)	12.5600(7)	10.3013(8)	12.1087(15)	13.4895(4)	10.8285(6)
b [Å]	9.2325(2)	12.8882(7)	11.2587(9)	9.4536(12)	16.7481(5)	11.6013(6)
c [Å]	42.1437(10)	13.1644(7)	36.986(3)	16.977(2)	18.0596(5)	20.3824(11)
α [°]	90	98.2635(14)	84.525(2)	90	79.965(2)	99.912(2)
β [°]	114.639(1)	106.7774(13)	84.314(2)	97.580(2)	87.615(2)	91.290(2)
γ [°]	90	91.0836(14)	87.248(2)	90	78.006(2)	112.7481(19)
V [Å^3]	14696.2(6)	2015.00(19)	4245.8(6)	1926.4(4)	3929.9(2)	2314.9(2)
Z	16	2	4	2	4	2
$\rho_{calcd.}$ [g/cm^3]	1.241	1.155	1.191	1.235	1.262	1.258
μ [mm^{-1}]	3.574	0.302	0.346	0.436	0.459	2.964
T [K]	150(2)	150(2)	150(2)	150(2)	150(2)	150(2)
Radiation type	CuKα	MoKα	MoKα	MoKα	MoKα	CuKα
Measured reflections	108053	65225	120988	81962	41110	37999
Independent reflections	12975	10223	20512	9317	18795	8174
Reflections with $I > 2\sigma(I)$	11786	8686	15466	8997	13448	7656
R_{int}	0.0506	0.0322	0.0602	0.0309	0.0238	0.0367
F(000)	5792	760	1619	756	1576	932
R_1 [$I > 2\sigma(I)$]	0.0269	0.0332	0.0446	0.0205	0.0321	0.0271
wR_2 (all data)	0.0671	0.0897	0.1220	0.0513	0.0799	0.0710
GooF	1.063	1.031	1.022	1.043	0.918	1.045
No. of Parameters	781	482	905	400	821	535
CCDC	2244178	2244179	2244180	2244181	2244182	2244183

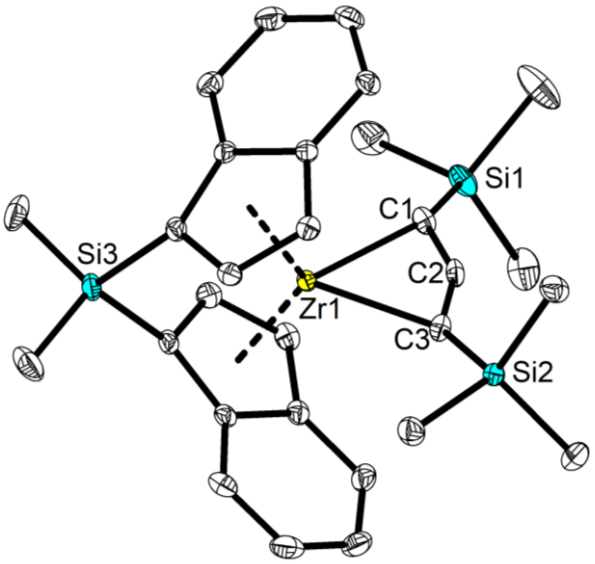

Figure S18. Molecular structure of complex **2d**. Only one of two molecules of the asymmetric unit is depicted. Thermal ellipsoids correspond to 30% probability. Hydrogen atoms are omitted for clarity.

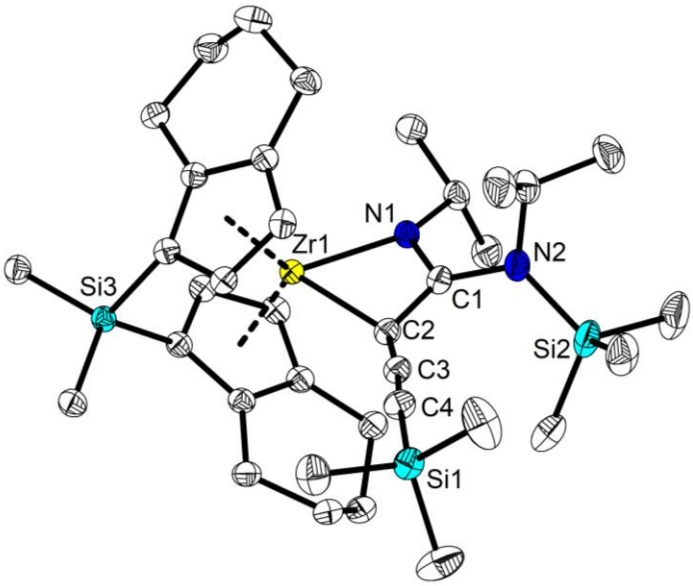

Figure S19. Molecular structure of complex **P2b-*i*Pr**. Thermal ellipsoids correspond to 30% probability. Hydrogen atoms are omitted for clarity.

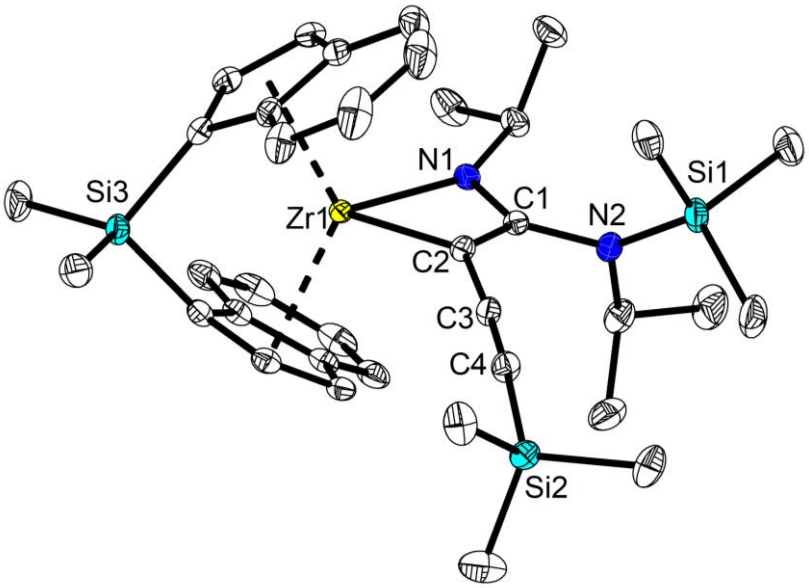

Figure S20. Molecular structure of complex **P2d-*i*Pr**. Only one of two molecules of the asymmetric unit is depicted. Thermal ellipsoids correspond to 30% probability. Hydrogen atoms are omitted for clarity.

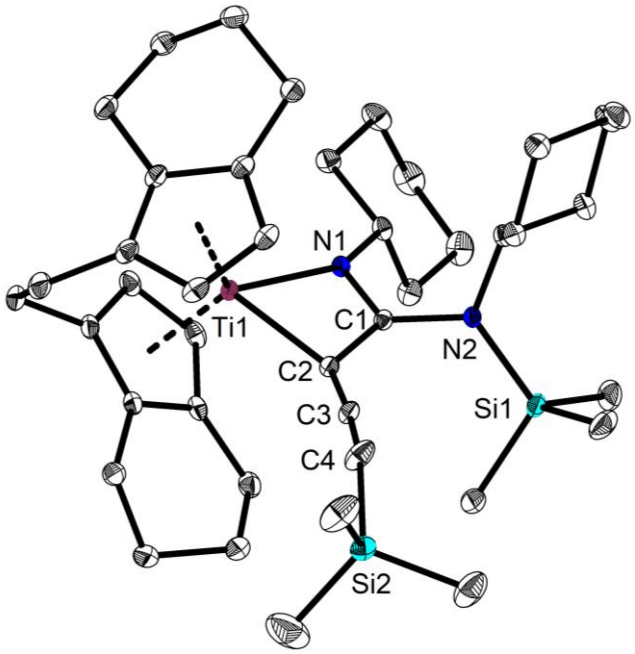

Figure S21. Molecular structure of complex **P1a-Cy**. Thermal ellipsoids correspond to 30% probability. Hydrogen atoms are omitted for clarity.

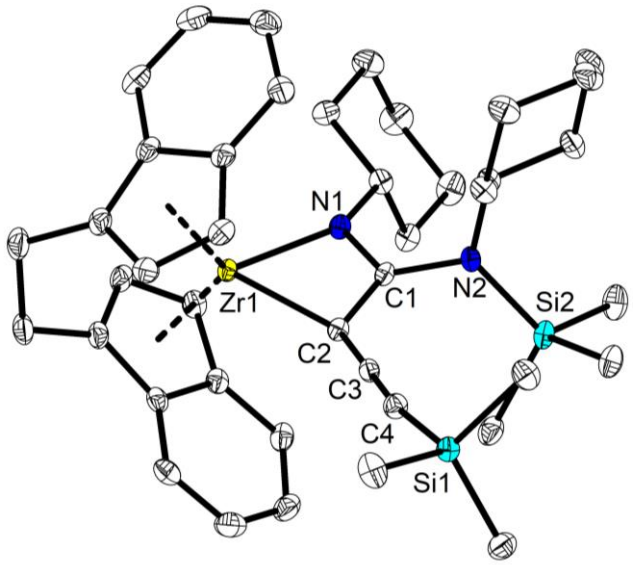

Figure S22. Molecular structure of complex **P2c-Cy**. Only one of two molecules of the asymmetric unit is depicted. Thermal ellipsoids correspond to 30% probability. Hydrogen atoms are omitted for clarity.

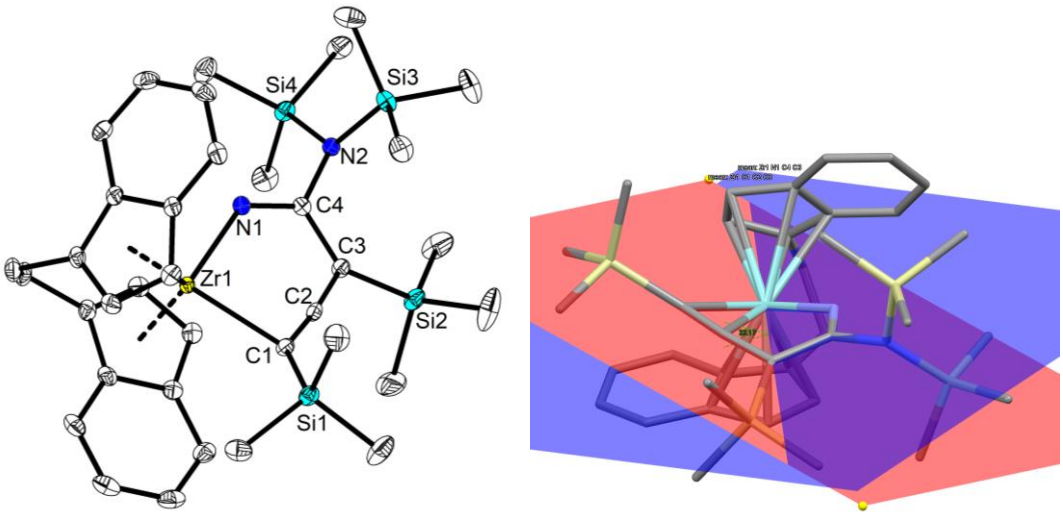

Figure S23. Left: Molecular structure of complex **P2c-SiMe3**. Thermal ellipsoids correspond to 30% probability. Hydrogen atoms are omitted for clarity. Right: Measurement of the angle between the two idealised planes of the metallacycle; red plane defined by Zr1-C1-C2-C3, blue plane defined by Zr1-N1-C4-C3, angle between 33.2° measured with Mercury.[20]

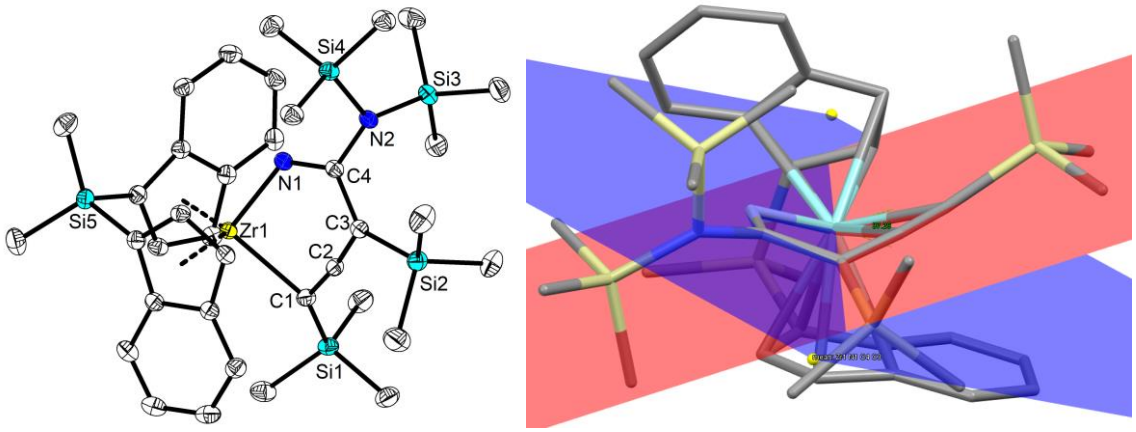

Figure S24. Left: Molecular structure of complex **P2d-SiMe3**. Only one of two molecules of the asymmetric unit is depicted. Thermal ellipsoids correspond to 30% probability. Hydrogen atoms are omitted for clarity. Right: Measurement of the angle between the two idealised planes of the metallacycle; red plane defined by Zr1-C1-C2-C3, blue plane defined by Zr1-N1-C4-C3, angle between 37.3° measured with Mercury.[20]

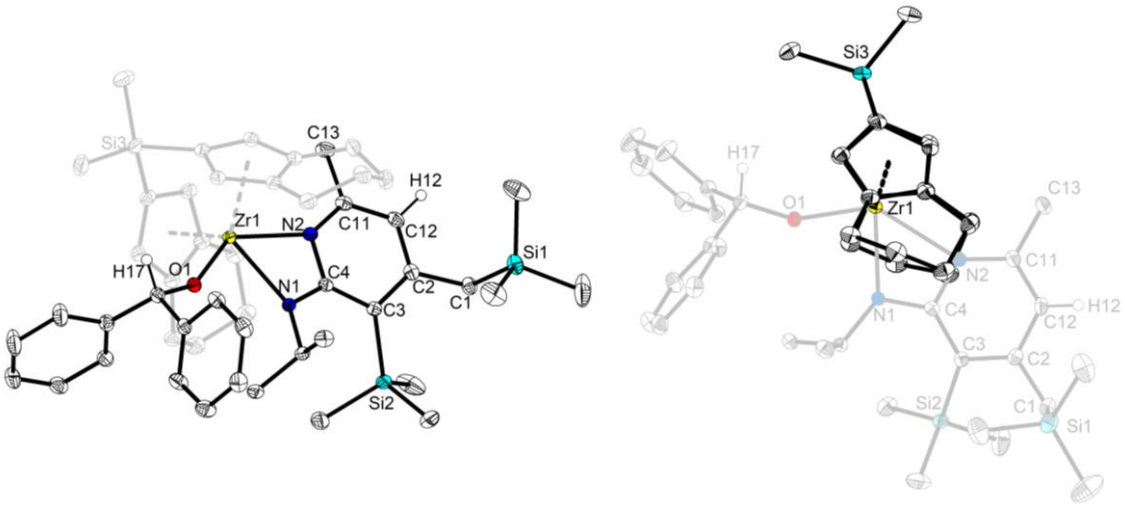

Figure S25. Left: Side view of the molecular structure of complex **6**, the *ansa*-metallocene fragment is depicted in greyscale. Right: Top view of the molecular structure of complex **6**, the *ansa*-metallocene fragment is highlight in black. Thermal ellipsoids correspond to 30% probability. Hydrogen atoms (except H12 and H17) are omitted for clarity.

Table S3. Selected bond lengths (Å), angles (°) and ^{13}C NMR data (ppm) of selected complexes.

	M1-N1	M-C2	M-C1	N1-C1	C1-C2	C1-N2	C2-C3	C3-C4	N1-M-C2	N1-C1-N2	N1-C1-C2	C2-C1-N2	C2-C3-C4	^{13}C NMR	
														C1	C2
P1a-*i*Pr	2.0400(9)	2.1254(11)	2.5007(10)	1.3801(13)	1.3739(14)	1.4341(13)	1.3923(15)	1.2190(17)	66.35(4)	120.38(9)	112.23(9)	126.82(10)	174.30(12)	140.8	183.1
P1a-Cy	2.0562(9)	2.1185(11)	2.5123(11)	1.3751(14)	1.3812(16)	1.4307(14)	1.3880(16)	1.2184(18)	66.18(4)	121.53(10)	111.61(10)	126.37(10)	174.83(14)	140.5	185.1
P1a-*p*-Tol	-	-	-	-	-	-	-	-	-	-	-	-	-	151.9	168.5
P2a-*i*Pr	2.1318(14)	2.2242(18)	2.5800(17)	1.402(2)	1.375(2)	1.432(2)	1.398(2)	1.215(3)	64.70(6)	118.92(13)	114.27(15)	126.35(16)	174.0(2)	148.8	145.1
P2a-Cy	-	-	-	-	-	-	-	-	-	-	-	-	-	148.5	145.7
P2a-*p*-Tol	-	-	-	-	-	-	-	-	-	-	-	-	-	150.7	144.2
P2b-*i*Pr	2.1345(12)	2.2079(14)	2.5803(14)	1.3892(19)	1.384(2)	1.4236(19)	1.395(2)	1.216(20)	64.64(5)	120.13(13)	113.82(12)	125.77(14)	174.74(17)	147.7	147.3
P2b-Cy	-	-	-	-	-	-	-	-	-	-	-	-	-	147.3	147.3
P2b-*p*-Tol	-	-	-	-	-	-	-	-	-	-	-	-	-	150.7	144.8
P2c-*i*Pr	-	-	-	-	-	-	-	-	-	-	-	-	-	150.3	148.4
P2c-Cy	2.116(2)	2.207(2)	2.558(2)	1.389(3)	1.385(3)	1.428(3)	1.406(3)	1.223(4)	65.38(8)	119.8(2)	114.7(2)	125.3(2)	179.5(3)	150.4	149.3
P2c-*p*-Tol	-	-	-	-	-	-	-	-	-	-	-	-	-	150.1	146.6
P2d-*i*Pr	2.1128(16)	2.1923(18)	2.5615(19)	1.395(2)	1.376(3)	1.432(3)	1.401(3)	1.215(3)	65.12(7)	119.25(17)	113.49(17)	126.86(28)	176.3(2)	150.0	152.3
P2d-Cy	-	-	-	-	-	-	-	-	-	-	-	-	-	150.0	152.7
P2d-*p*-Tol	-	-	-	-	-	-	-	-	-	-	-	-	-	150.0	147.7

7. Details of NMR spectroscopy

7.1 NMR spectra of 1a

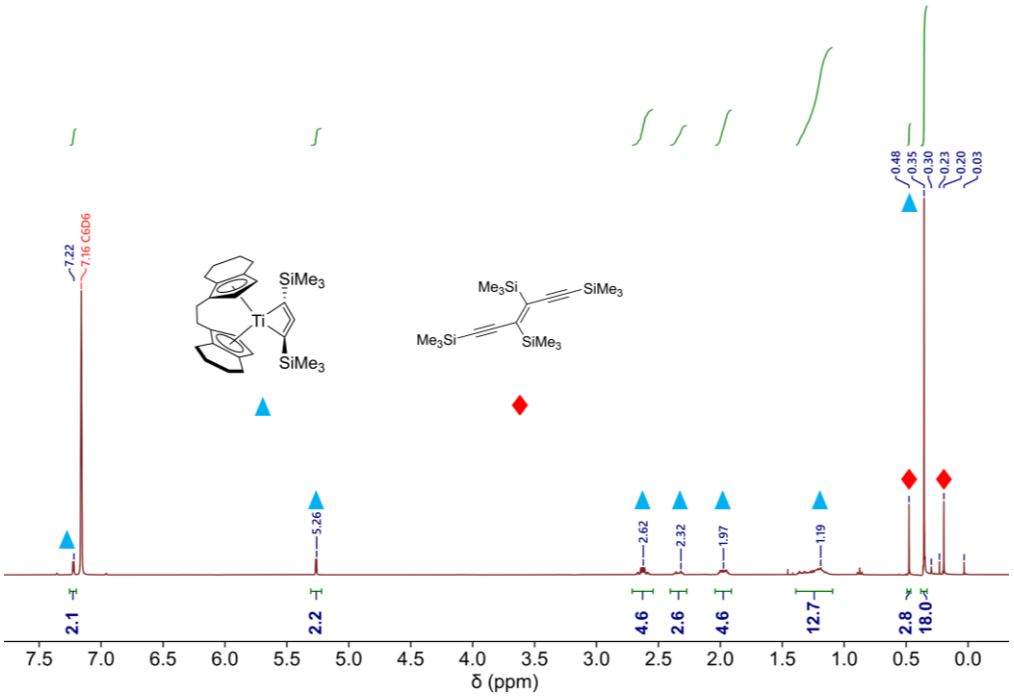

Figure S26. ^{1}H NMR spectrum of **1a**. The sample was taken from the pentane filtrate, followed by removal of the solvent in vacuum (25 °C, benzene-*d*$_6$, 400.1 MHz).

7.2 NMR spectra of 1c

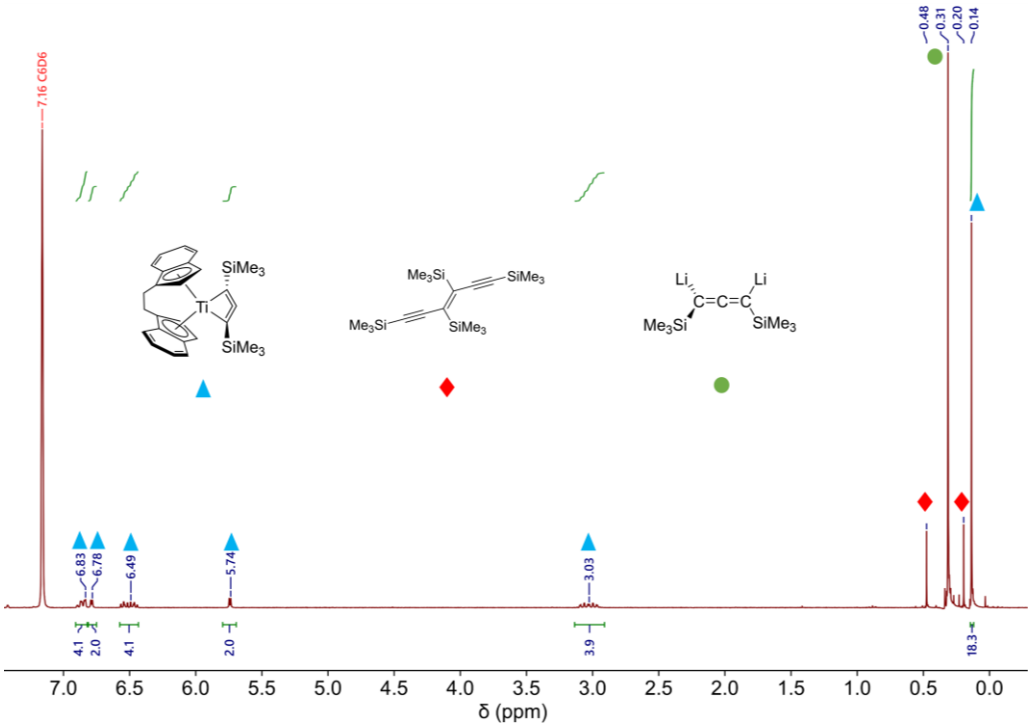

Figure S27. ^{1}H NMR spectrum of **1c** (25 °C, benzene-*d*$_6$, 400.1 MHz).

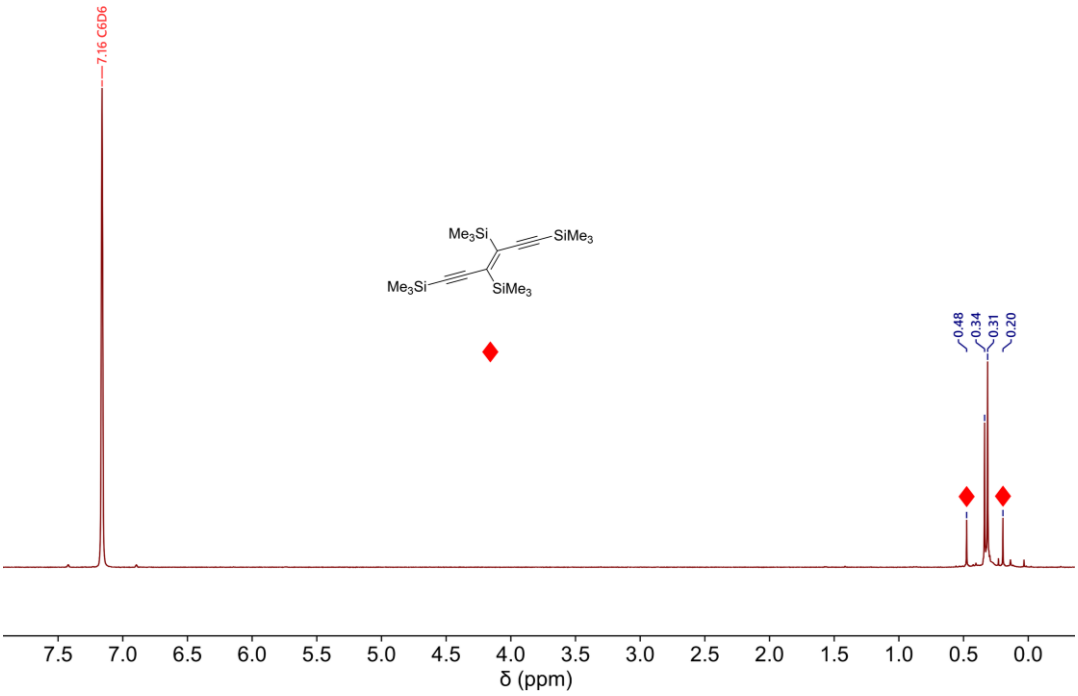

Figure S28. ^{1}H NMR spectrum of **1c** at room temperature after 12 h (25 °C, benzene-*d*$_6$, 400.1 MHz).

7.3 NMR spectra of 2c

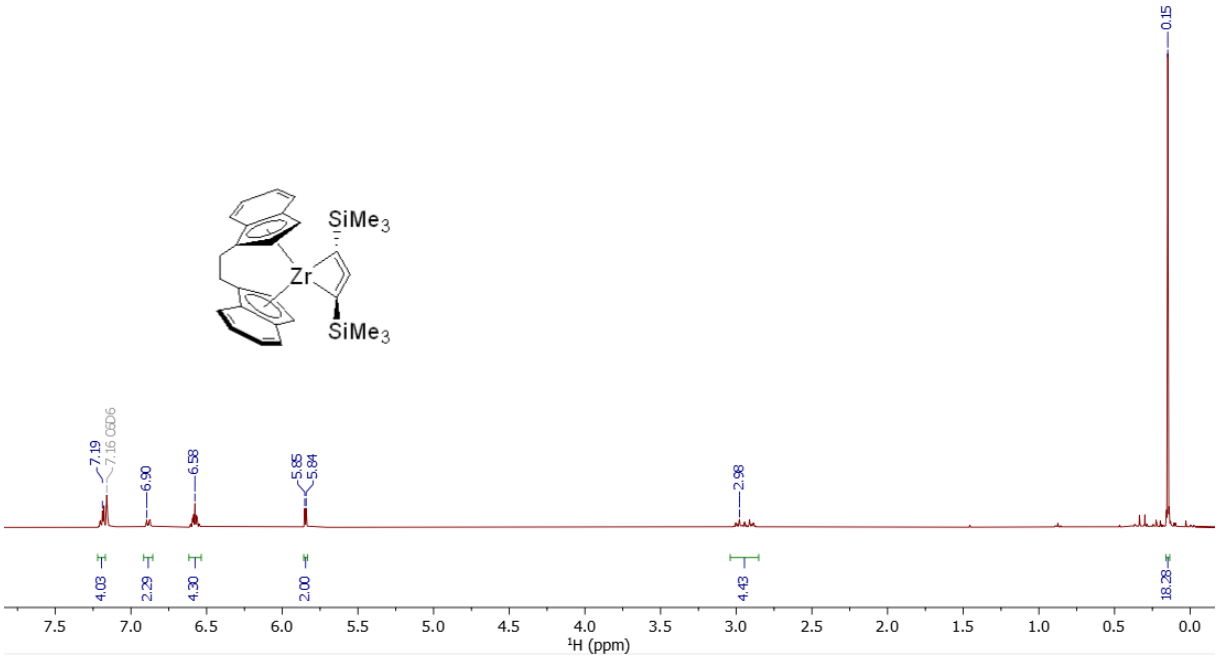

Figure S29. ^{1}H NMR spectrum of **2c** (25 °C, benzene-*d*$_6$, 400.1 MHz).

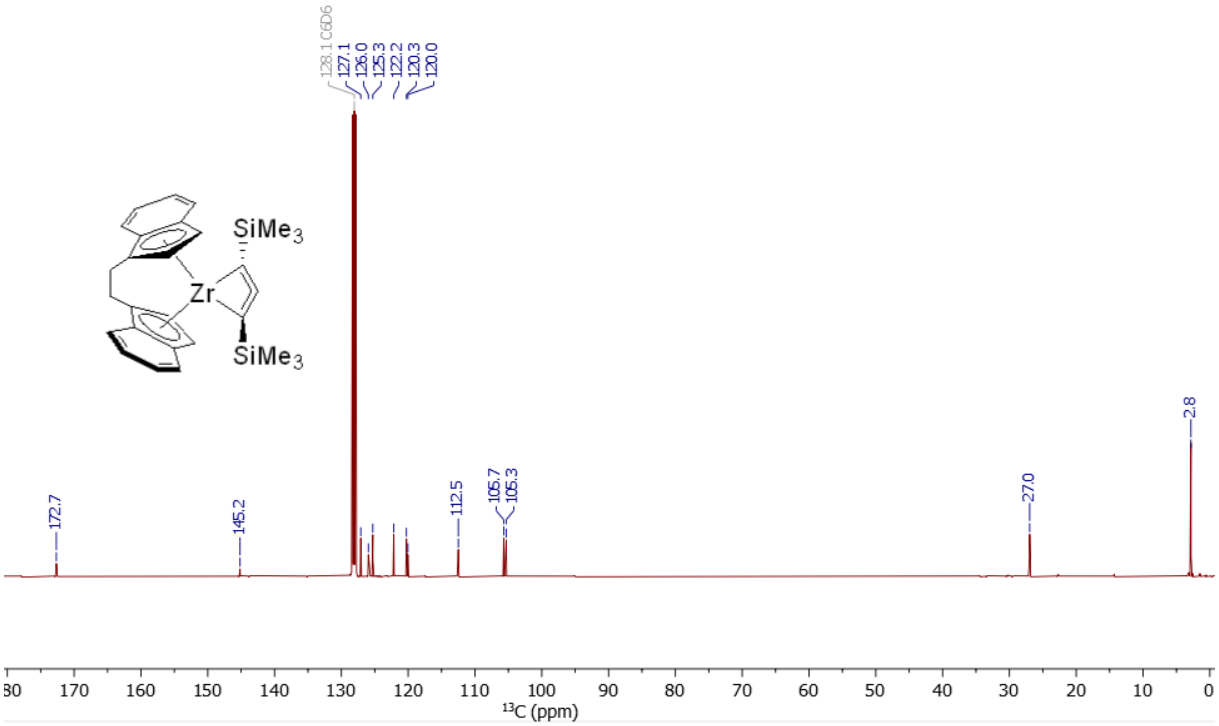

Figure S30. ^{13}C{^{1}H} NMR spectrum of **2c** (25 °C, benzene-*d*$_6$, 100.6 MHz).

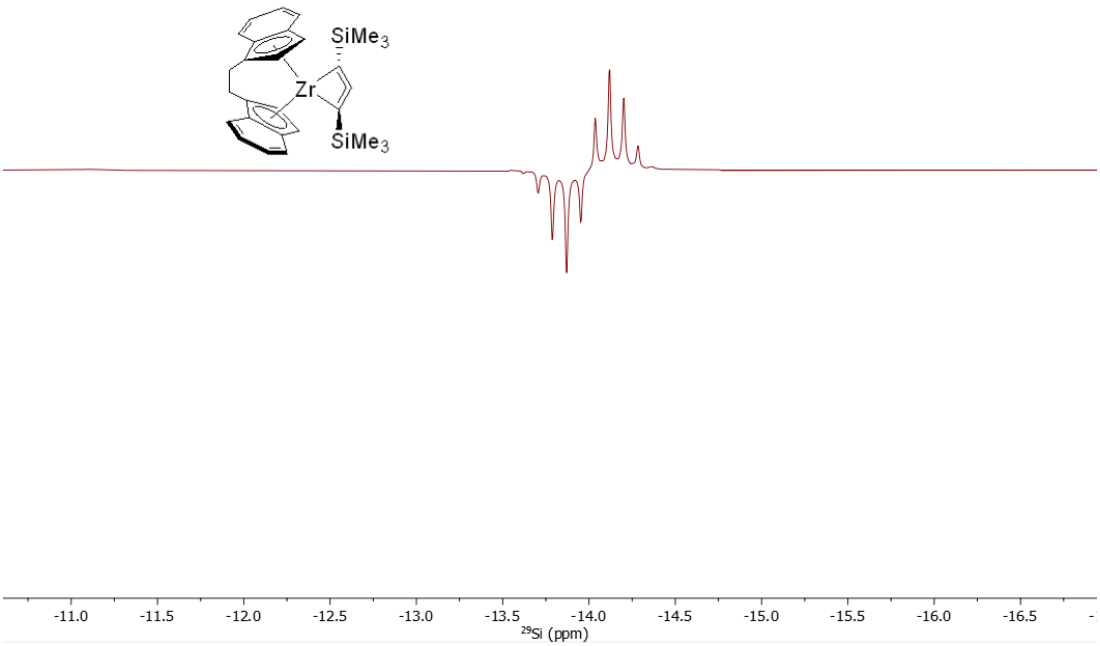

Figure S31. ^{29}Si INEPT NMR spectrum of **2c** (25 °C, benzene-*d*$_6$, 79.5 MHz).

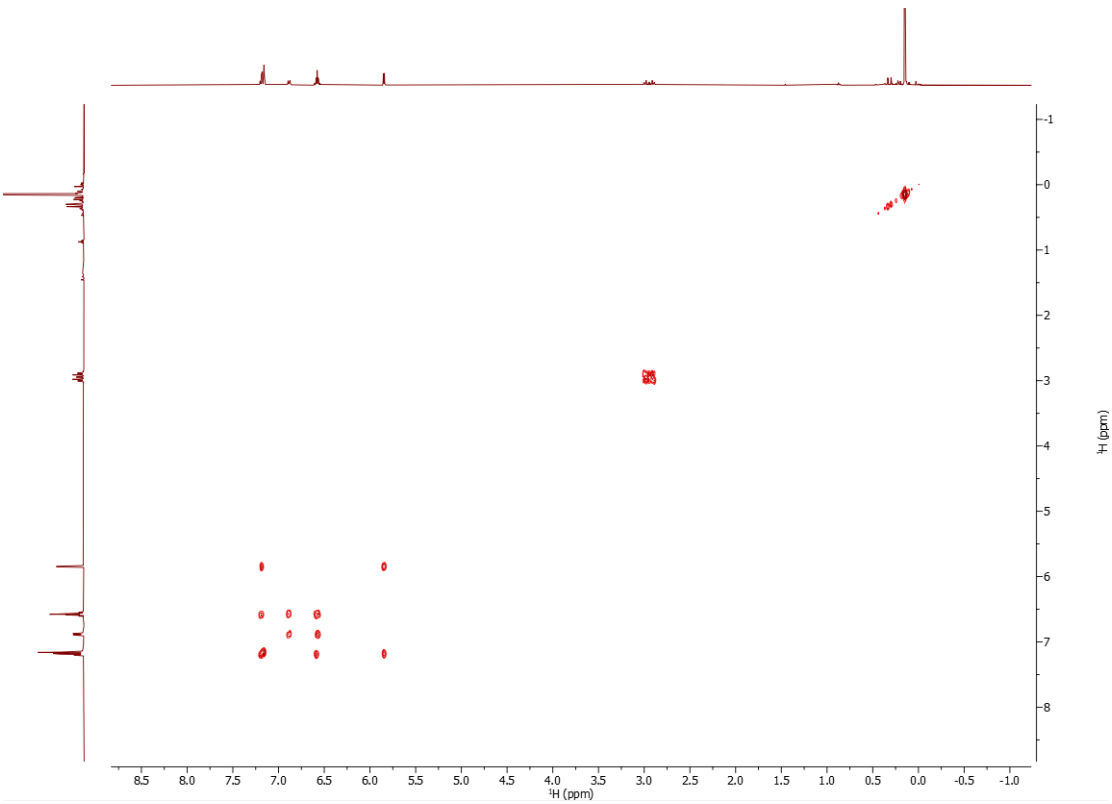

Figure S32. ^{1}H-^{1}H COSY NMR spectrum of **2c** (25 °C, benzene-*d*$_6$, 400.1, 400.1 MHz).

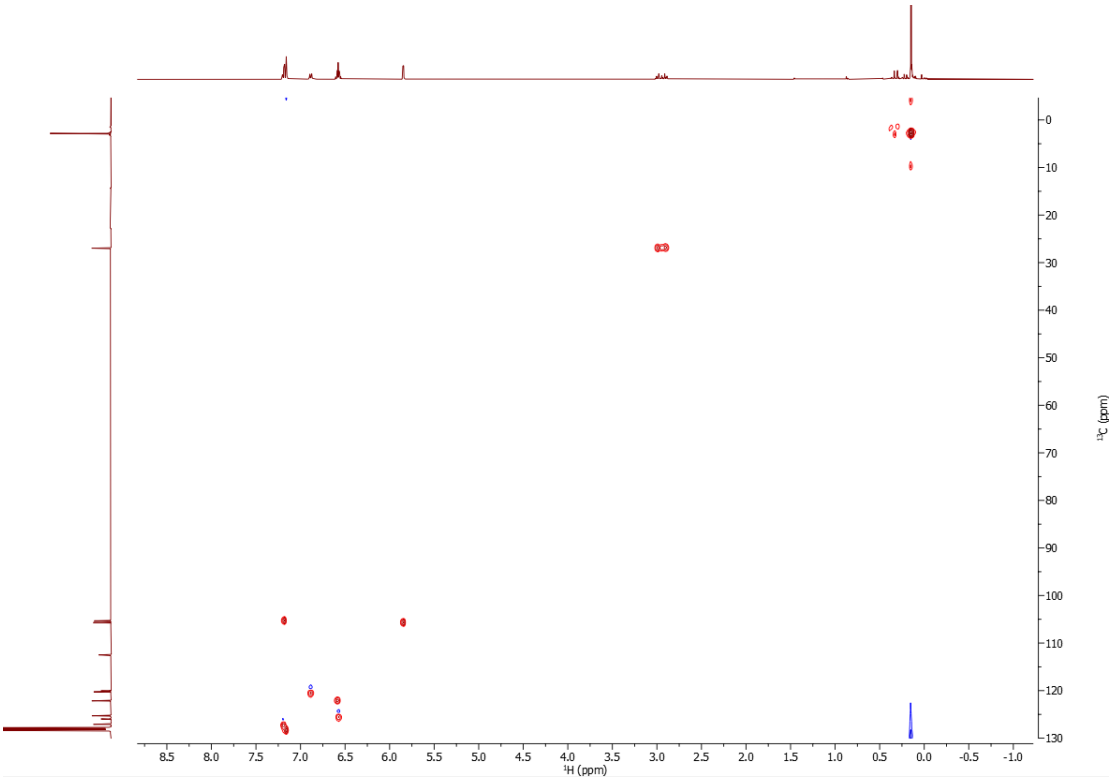

Figure S33. ^{1}H-^{13}C HSQC NMR spectrum of **2c** (25 °C, benzene-d_6, 400.1, 100.6 MHz).

Figure S34. ^{1}H-^{13}C HMBC NMR spectrum of **2c** (25 °C, benzene-d_6, 400.1, 100.6 MHz).

7.4 NMR spectra of 2d

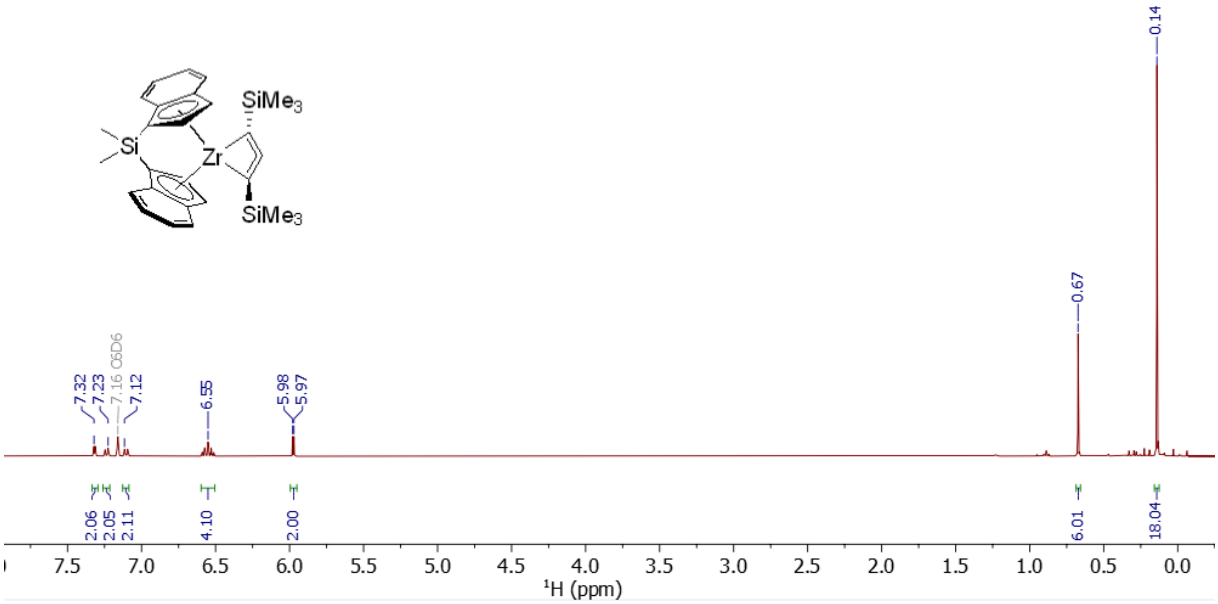

Figure S35. ^{1}H NMR spectrum of **2d** (25 °C, benzene-*d*$_6$, 400.1 MHz).

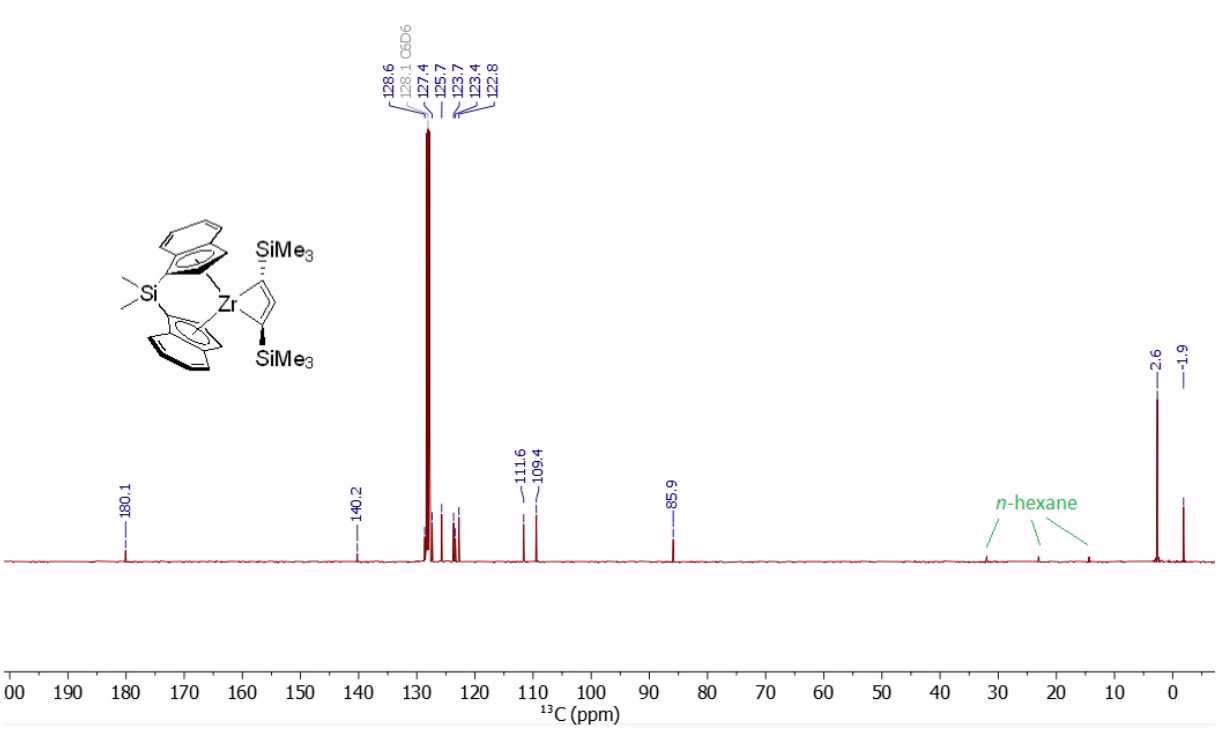

Figure S36. ^{13}C{^{1}H} NMR spectrum of **2d** (25 °C, benzene-*d*$_6$, 100.6 MHz).

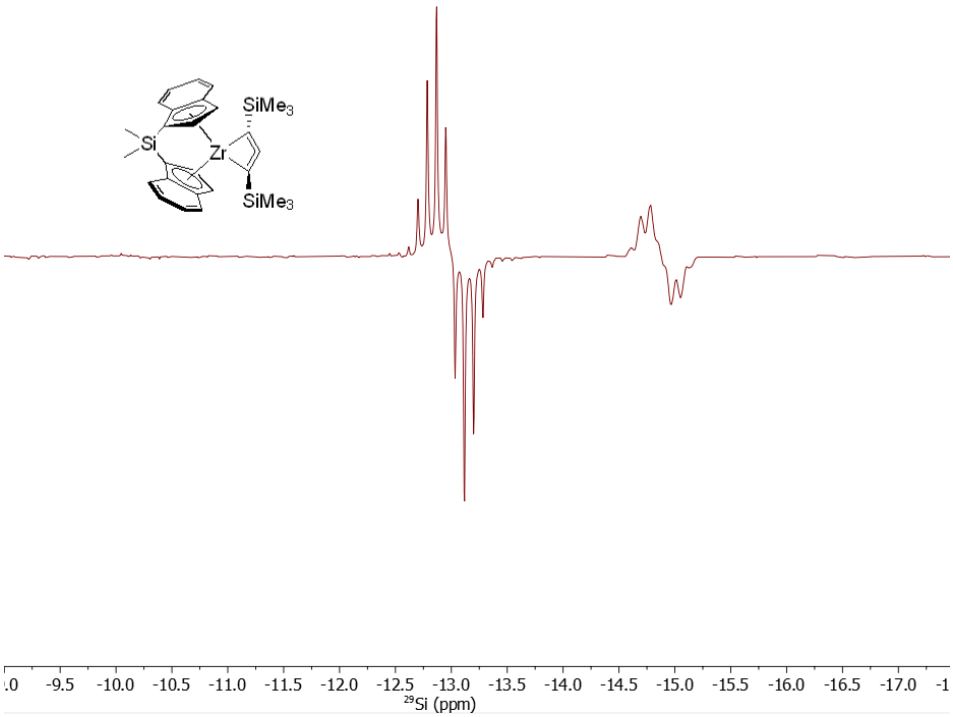

Figure S37. ^{29}Si INEPT NMR spectrum of **2d** (25 °C, benzene-*d*6, 79.5 MHz).

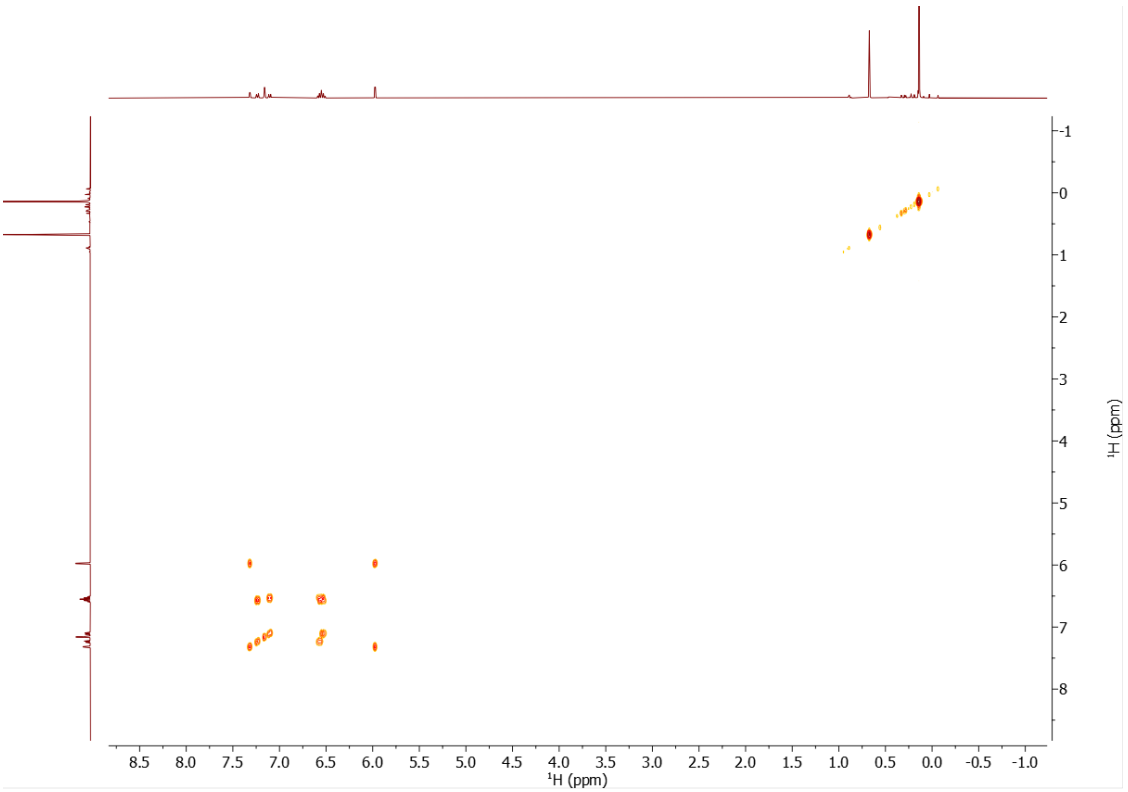

Figure S38. ^{1}H-^{1}H COSY NMR spectrum of **2d** (25 °C, benzene-*d*6, 400.1, 400.1 MHz).

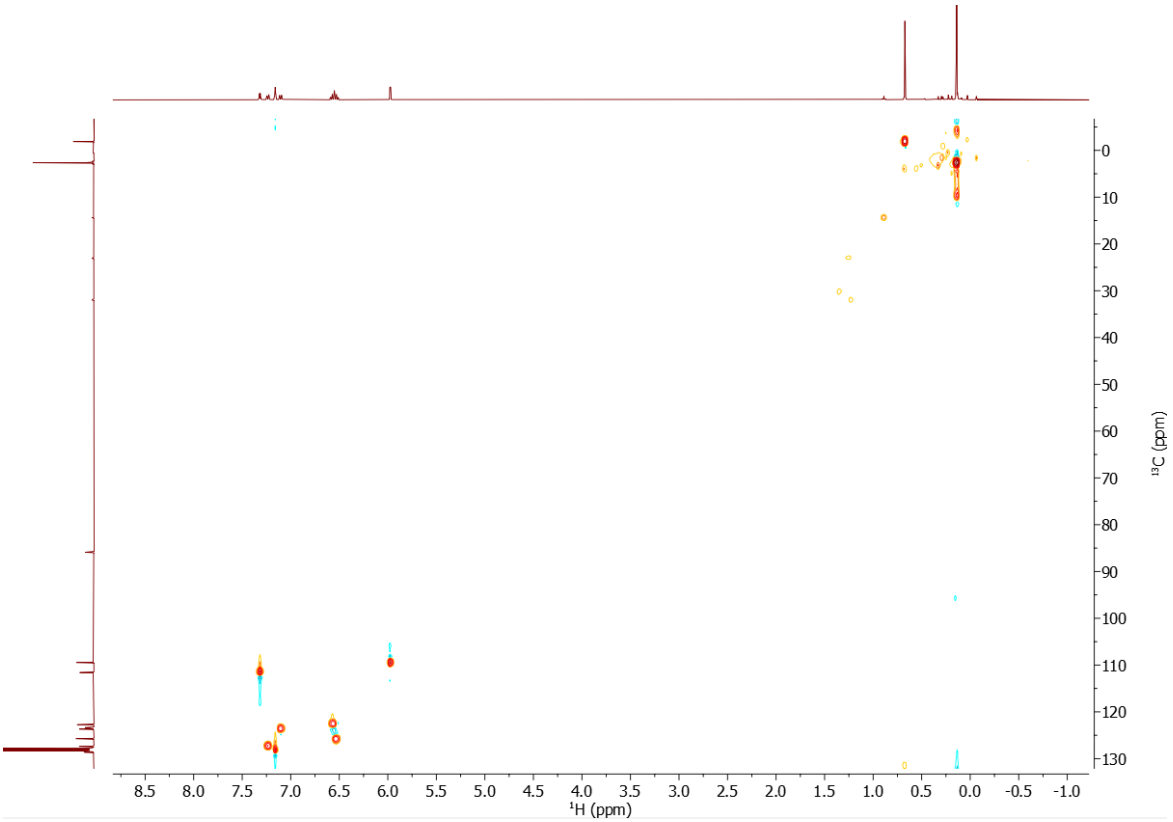

Figure S39. ^{1}H-^{13}C HSQC NMR spectrum of **2d** (25 °C, benzene-d_6, 400.1, 100.6 MHz).

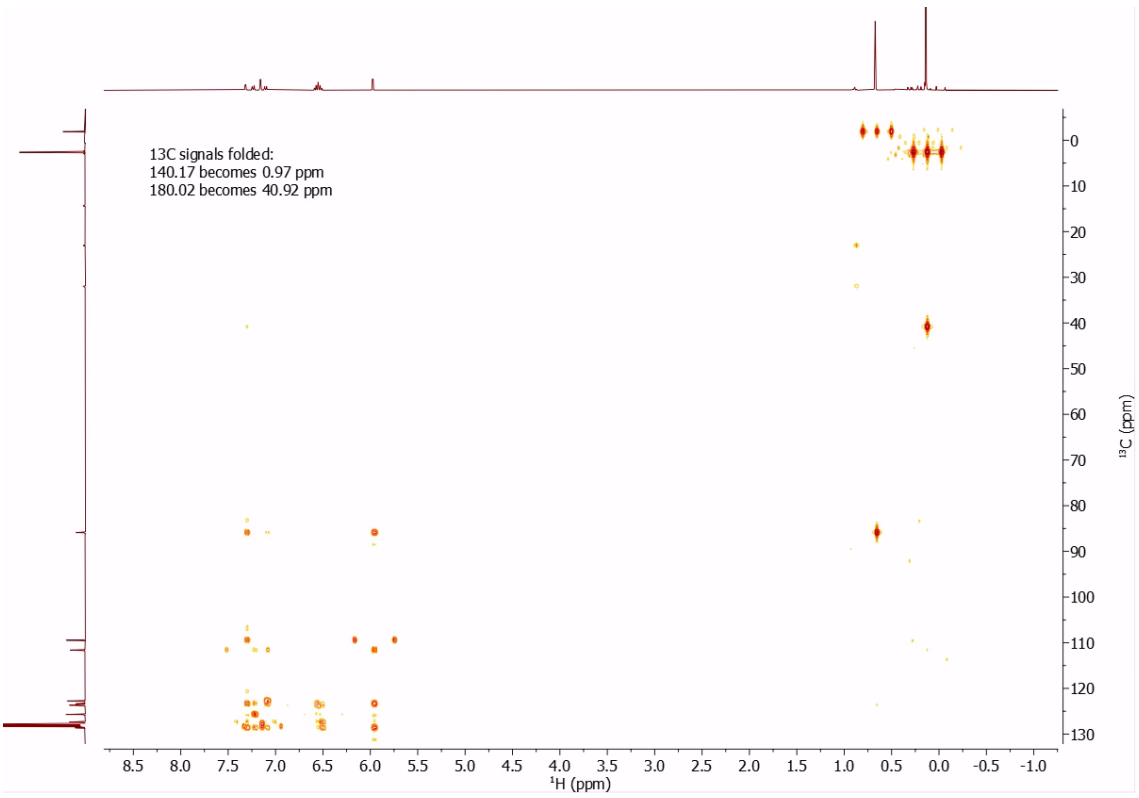

Figure S40. ^{1}H-^{13}C HMBC NMR spectrum of **2d** (25 °C, benzene-d_6, 400.1, 100.6 MHz).

7.5 NMR spectra of $P_{1a\text{-}iPr}$

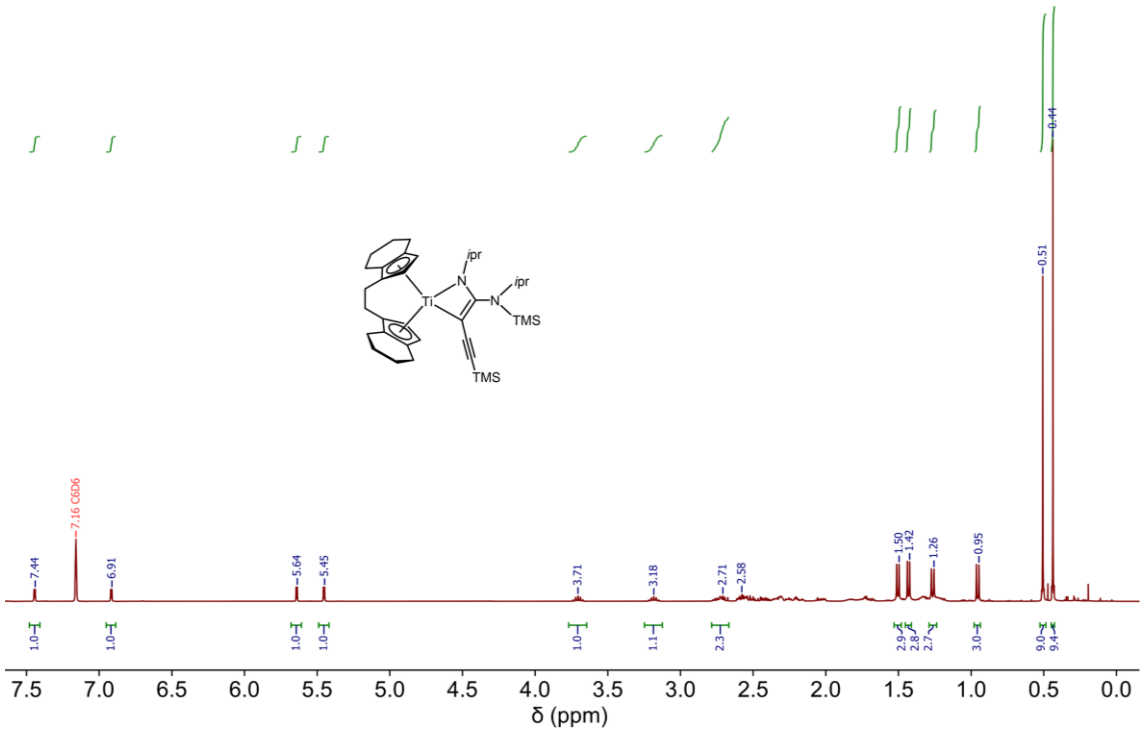

Figure S41. ^{1}H NMR spectrum of **$P_{1a\text{-}iPr}$** (25 °C, benzene-d_6, 400.1 MHz).

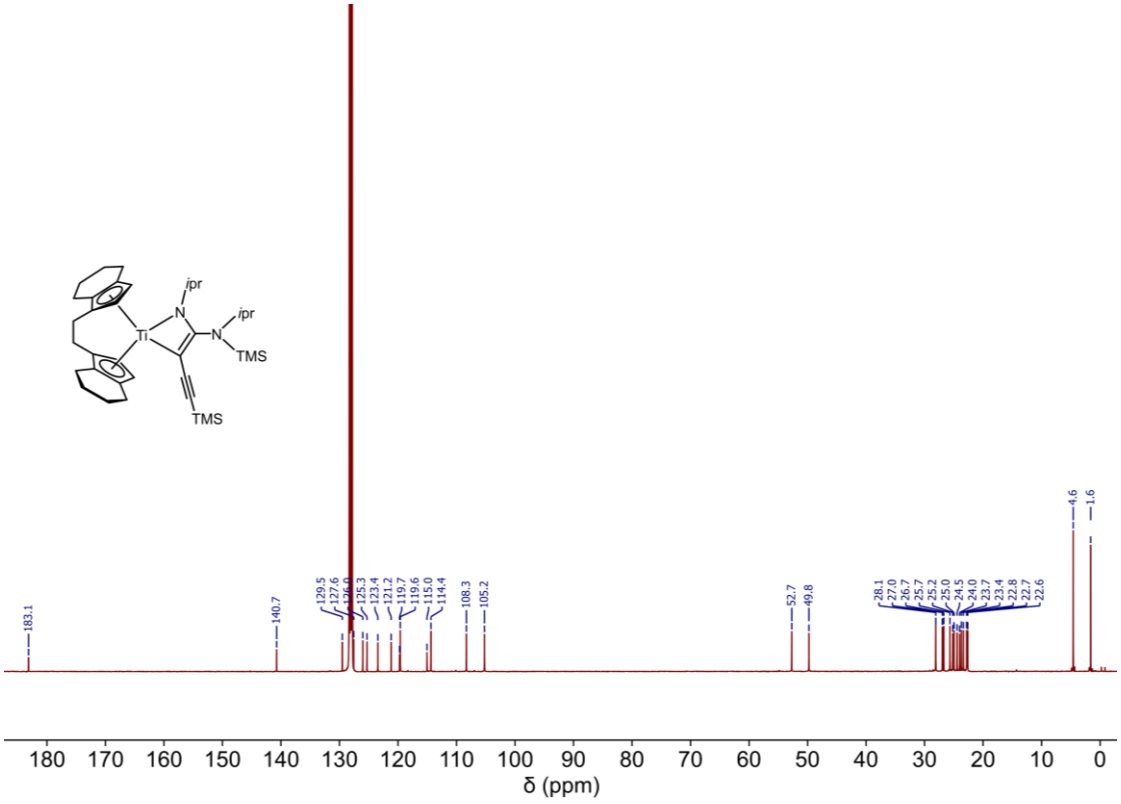

Figure S42. ^{13}C{^{1}H} NMR spectrum of **$P_{1a\text{-}iPr}$** (25 °C, benzene-d_6, 100.6 MHz).

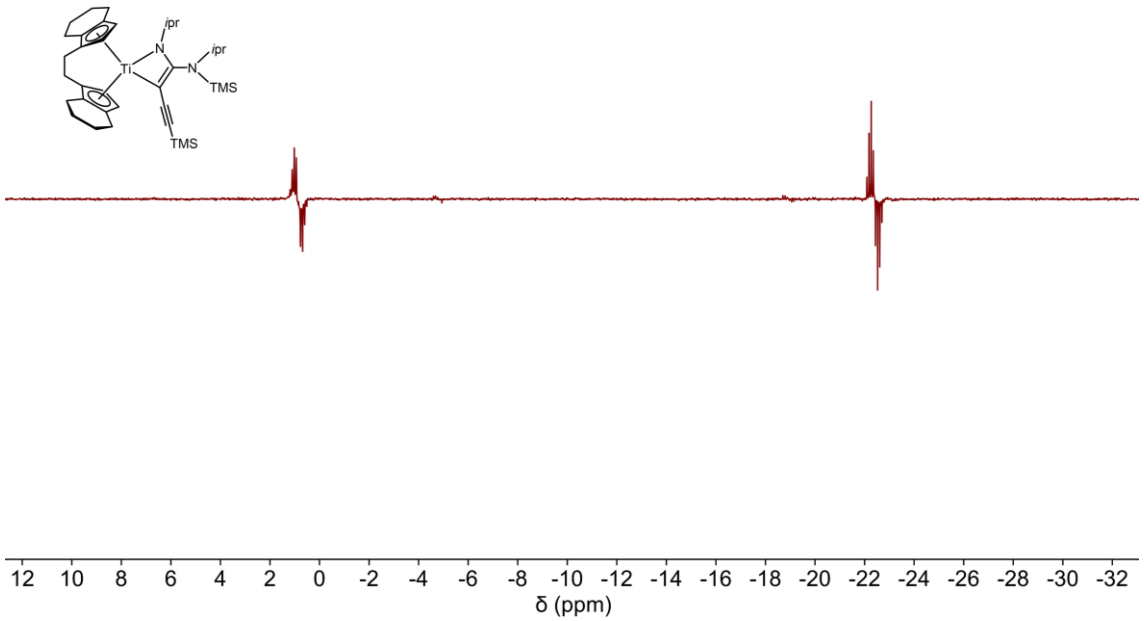

Figure S43. ^{29}Si INEPT NMR spectrum of **P1a-*i*Pr** (25 °C, benzene-*d*6, 79.5 MHz).

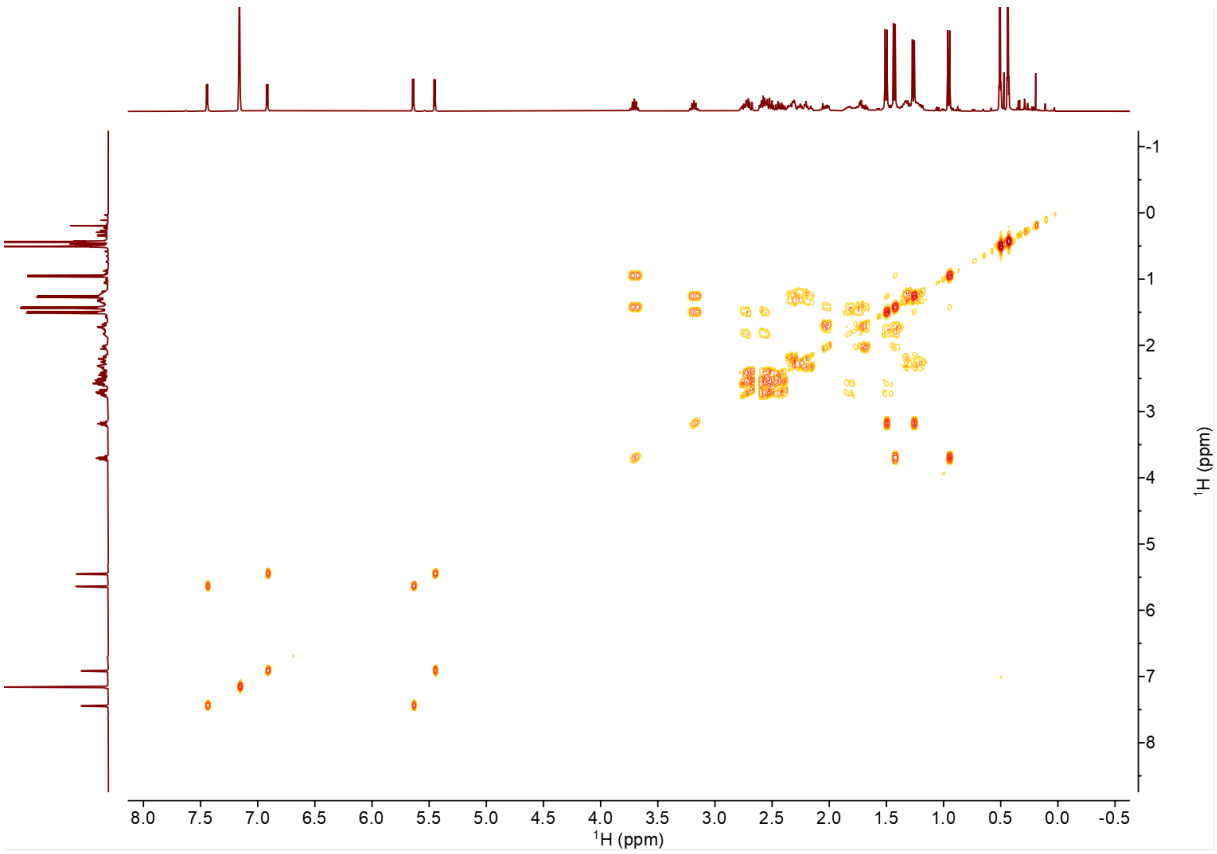

Figure S44. ^{1}H-^{1}H COSY NMR spectrum of **P1a-*i*Pr** (25 °C, benzene-*d*6, 400.1, 400.1 MHz).

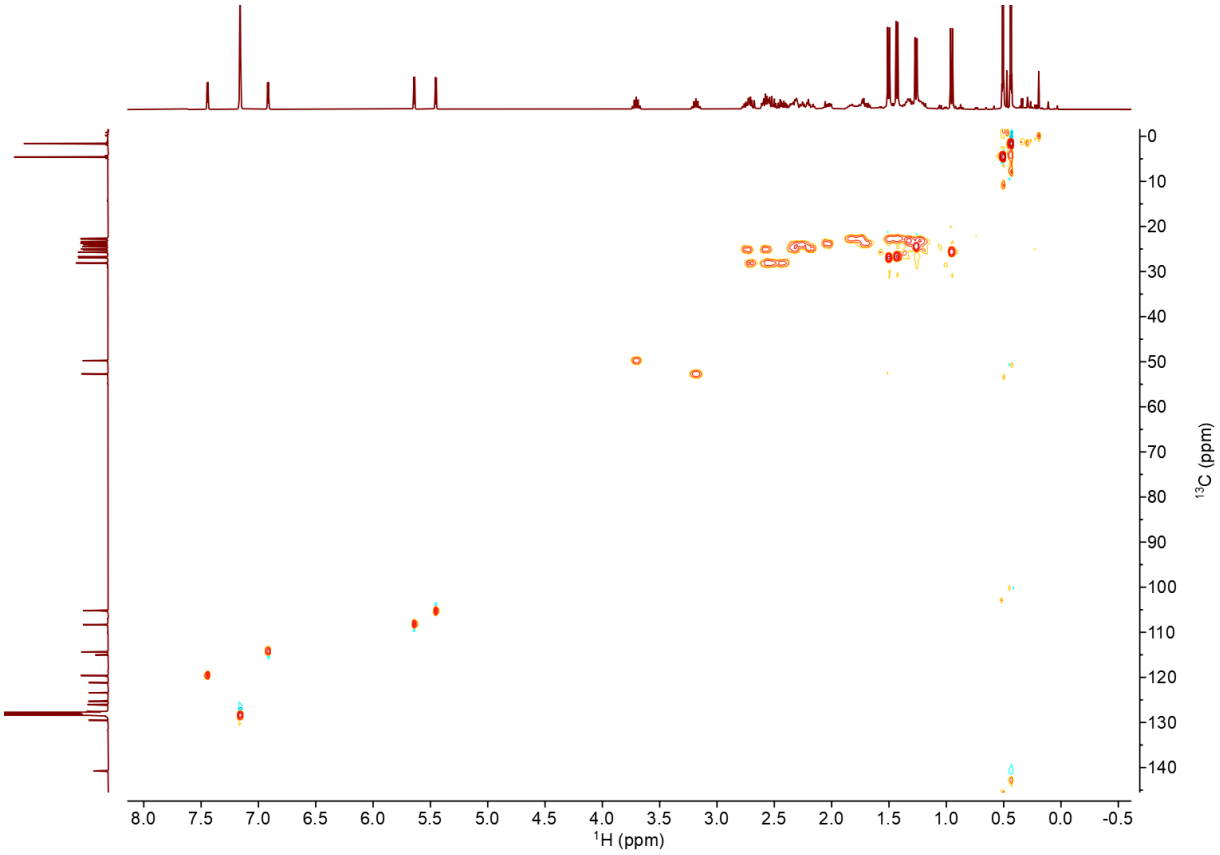

Figure S45. ^{1}H-^{13}C HSQC NMR spectrum of **P1a-*i*Pr** (25 °C, benzene-*d*6, 400.1, 100.6 MHz).

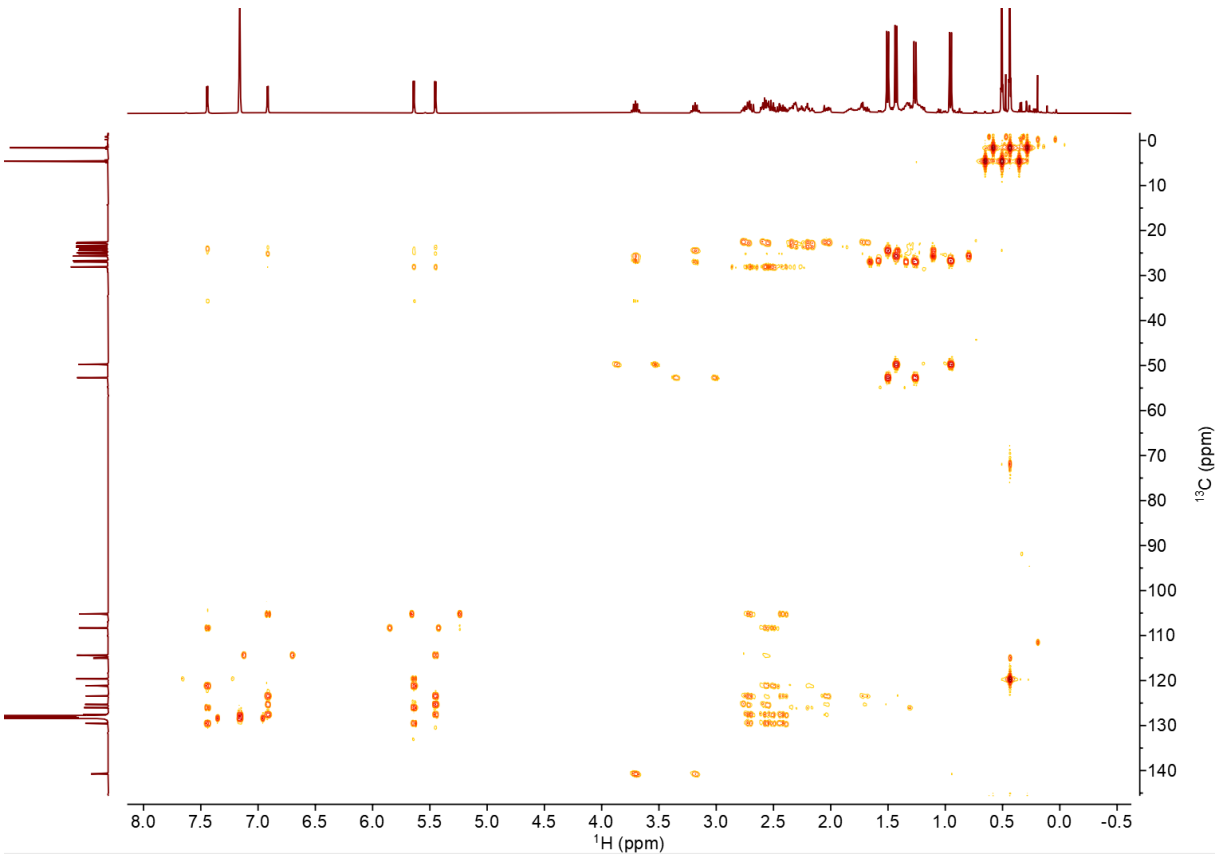

Figure S46. ^{1}H-^{13}C HMBC NMR spectrum of **P1a-*i*Pr** (25 °C, benzene-*d*6, 400.1, 100.6 MHz).

7.6 NMR spectra of $P_{2a\text{-}iPr}$

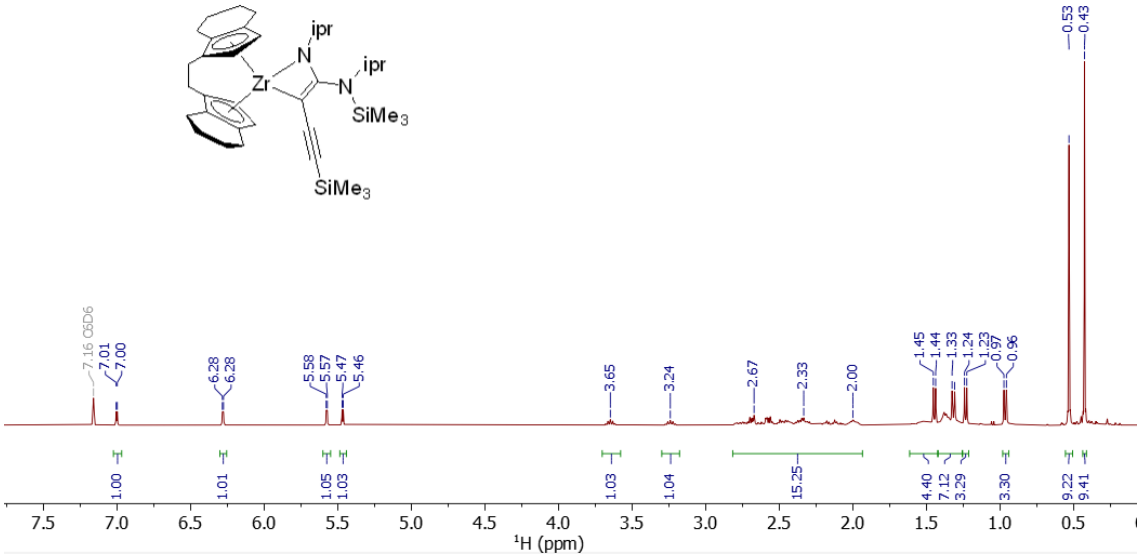

Figure S47. ^{1}H NMR spectrum of **$P_{2a\text{-}iPr}$** (25 °C, benzene-d_6, 400.1 MHz).

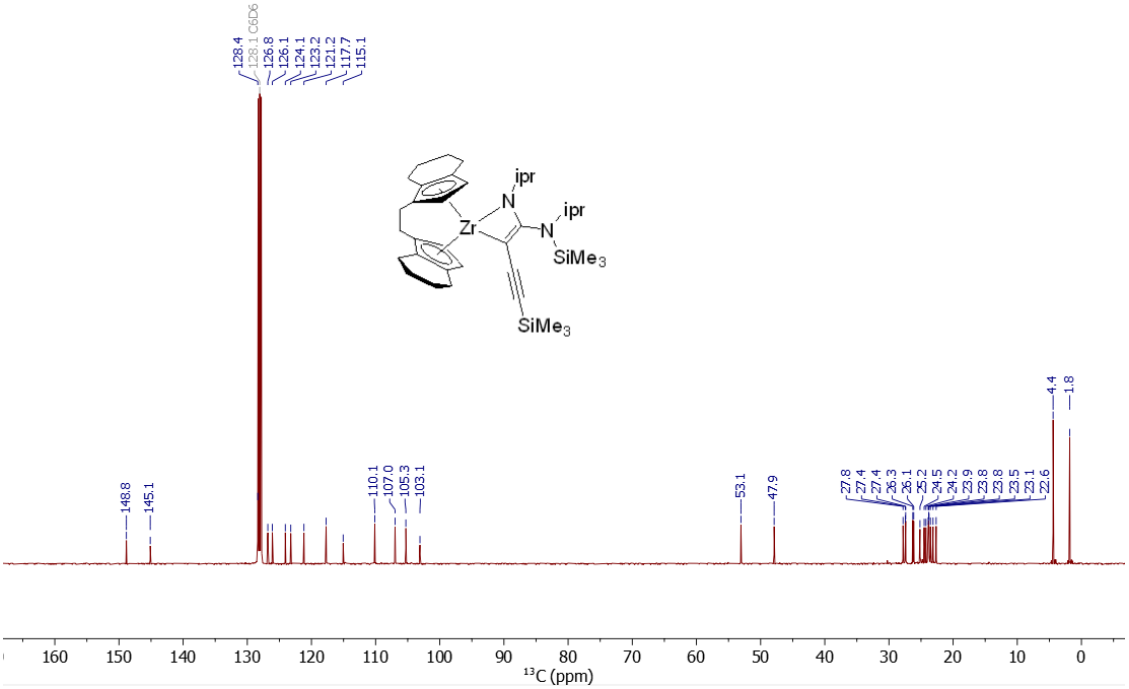

Figure S48. $^{13}C\{^{1}H\}$ NMR spectrum of **$P_{2a\text{-}iPr}$** (25 °C, benzene-d_6, 100.6 MHz).

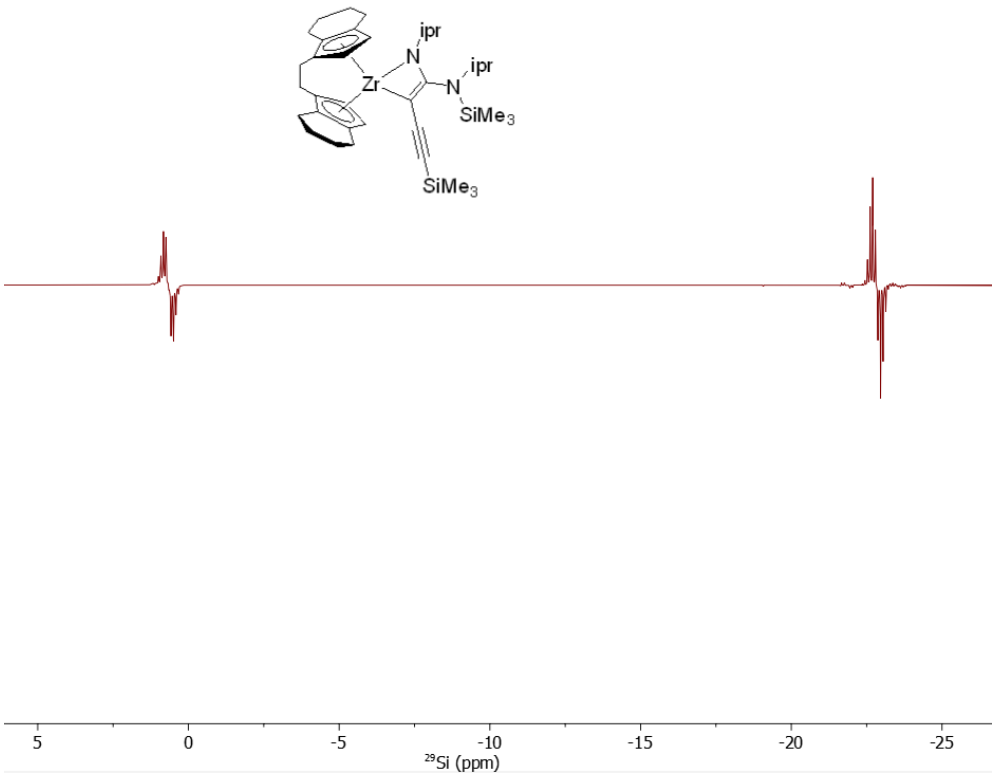

Figure S49. ^{29}Si INEPT NMR spectrum of **P2a-*i*Pr** (25 °C, benzene-*d*6, 79.5 MHz).

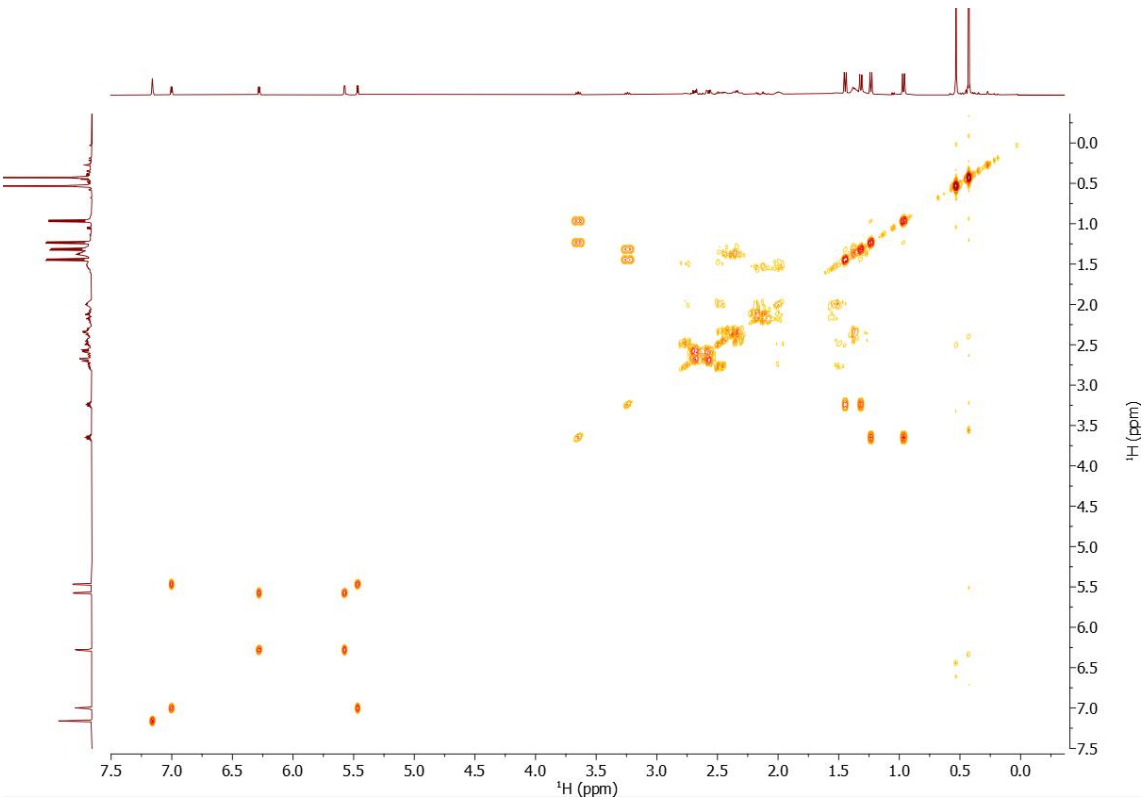

Figure S50. ^{1}H-^{1}H COSY NMR spectrum of **P2a-*i*Pr** (25 °C, benzene-*d*6, 400.1, 400.1 MHz).

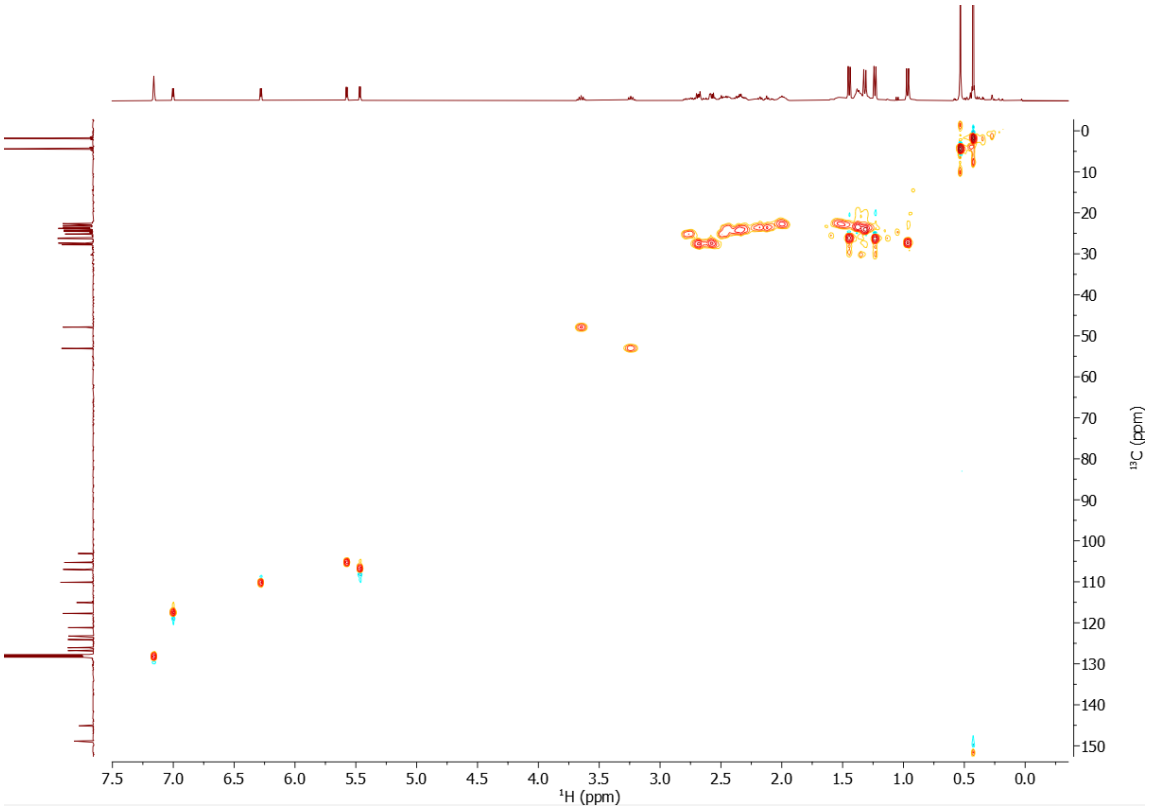

Figure S51. ^{1}H-^{13}C HSQC NMR spectrum of **P2a-*i*Pr** (25 °C, benzene-*d*6, 400.1, 100.6 MHz).

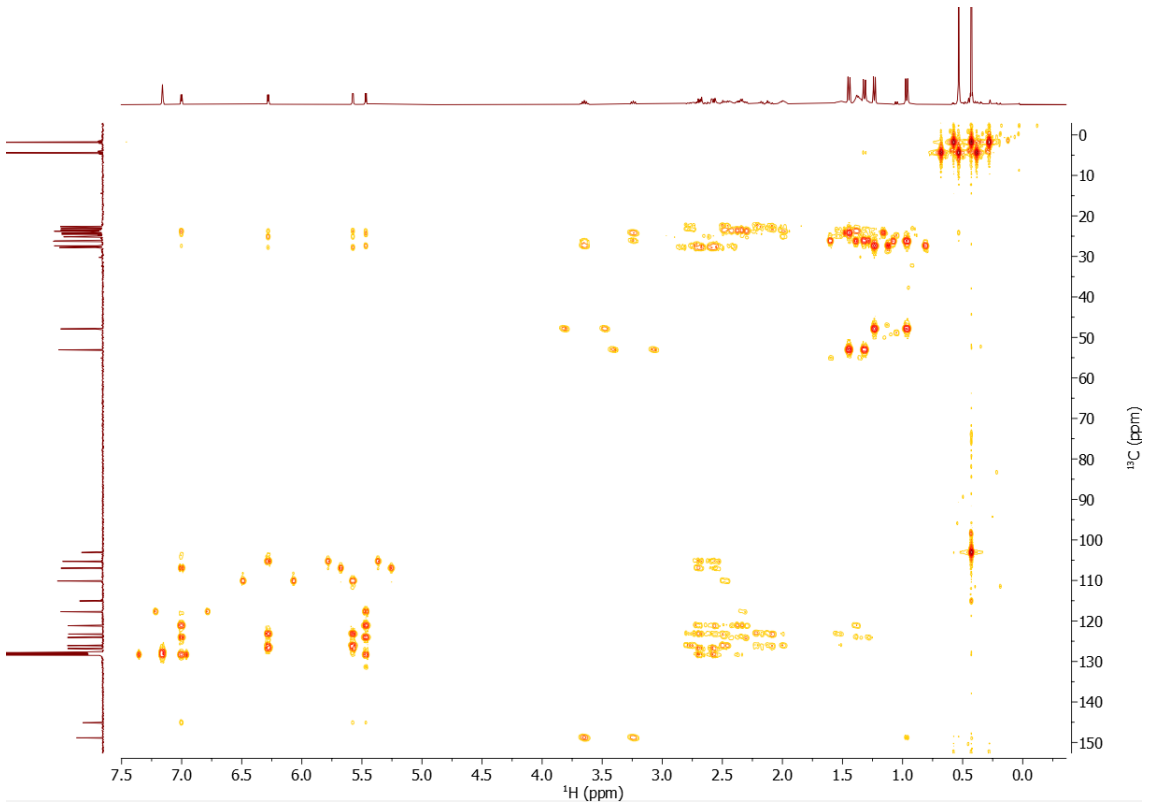

Figure S52. ^{1}H-^{13}C HMBC NMR spectrum of **P2a-*i*Pr** (25 °C, benzene-*d*6, 400.1, 100.6 MHz).

7.7 NMR spectra of $P_{2b\text{-}iPr}$

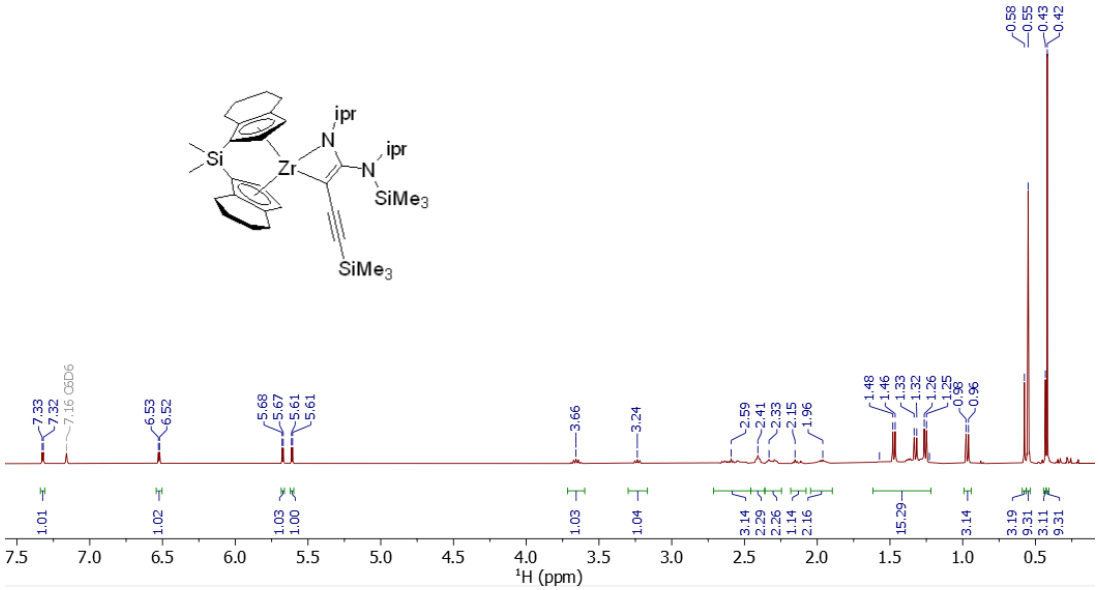

Figure S53. ^{1}H NMR spectrum of **$P_{2b\text{-}iPr}$** (25 °C, benzene-d_6, 400.1 MHz).

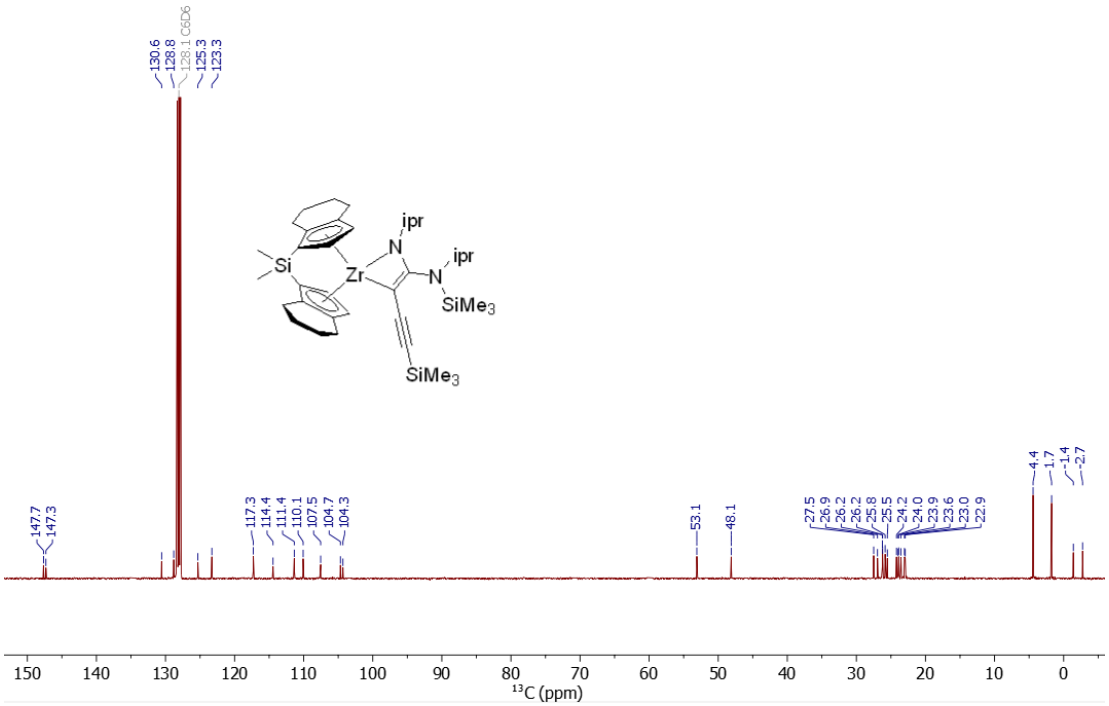

Figure S54. $^{13}C\{^{1}H\}$ NMR spectrum of **$P_{2b\text{-}iPr}$** (25 °C, benzene-d_6, 100.6 MHz).

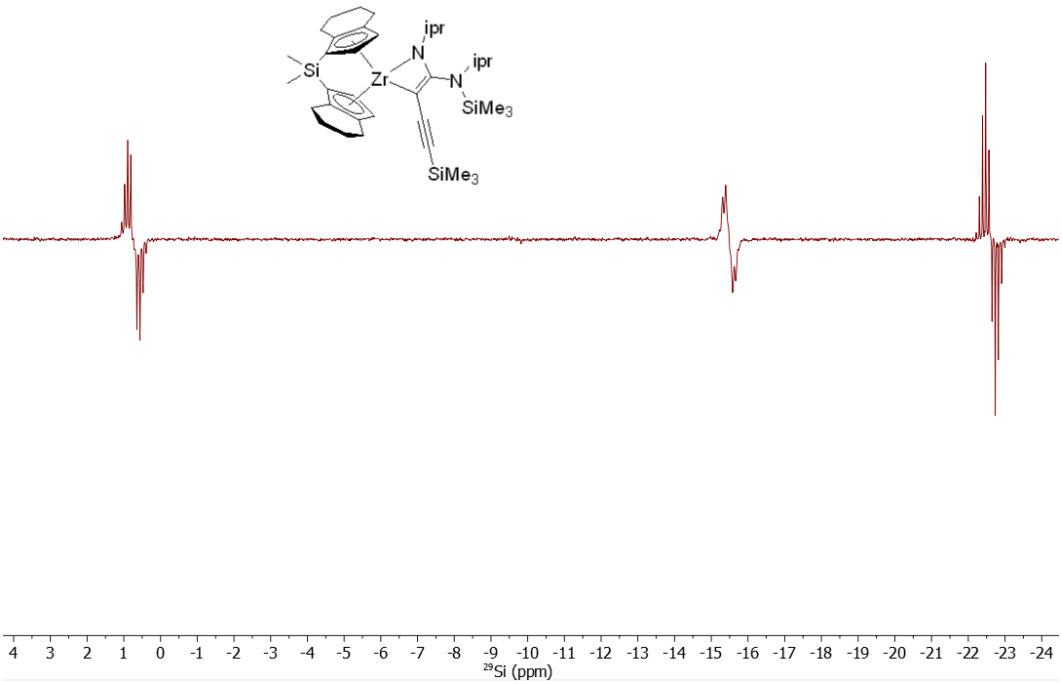

Figure S55. ^{29}Si INEPT NMR spectrum of **P2b-*i*Pr** (25 °C, benzene-*d*6, 79.5 MHz).

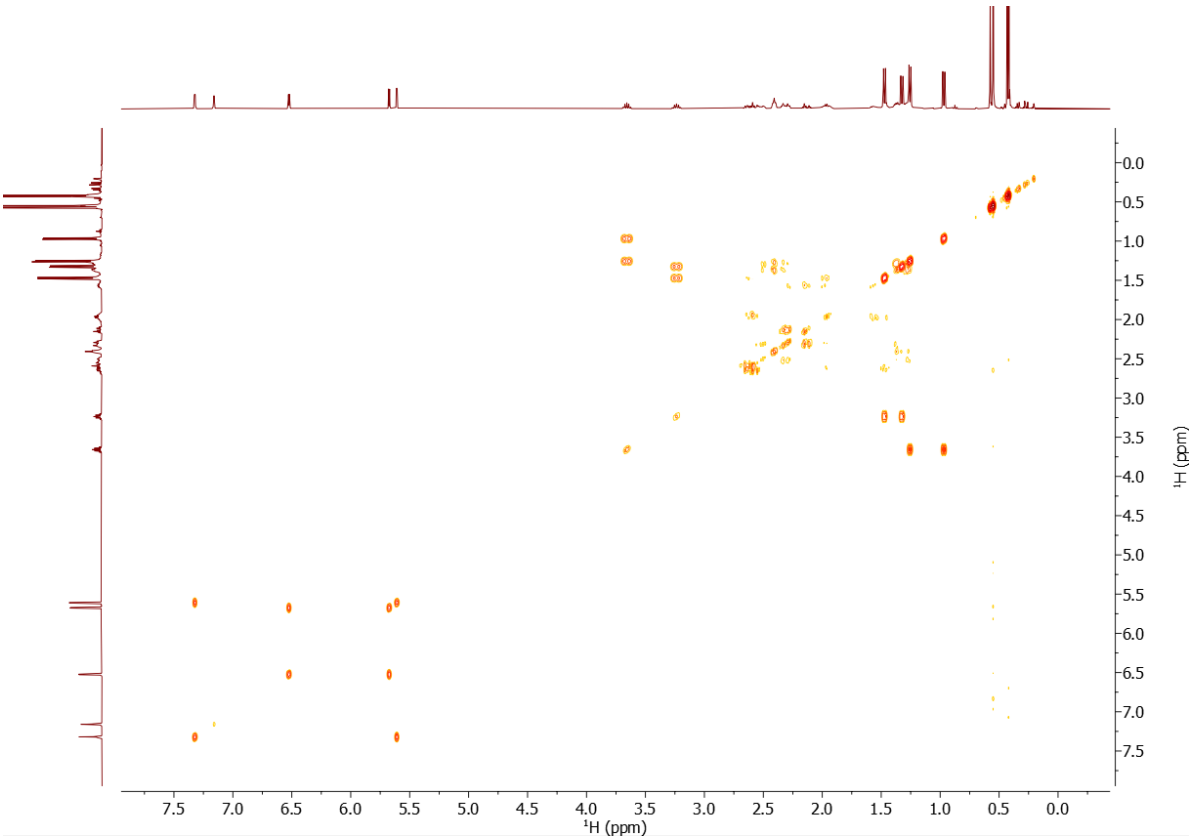

Figure S56. ^{1}H-^{1}H COSY NMR spectrum of **P2b-*i*Pr** (25 °C, benzene-*d*6, 400.1, 400.1 MHz).

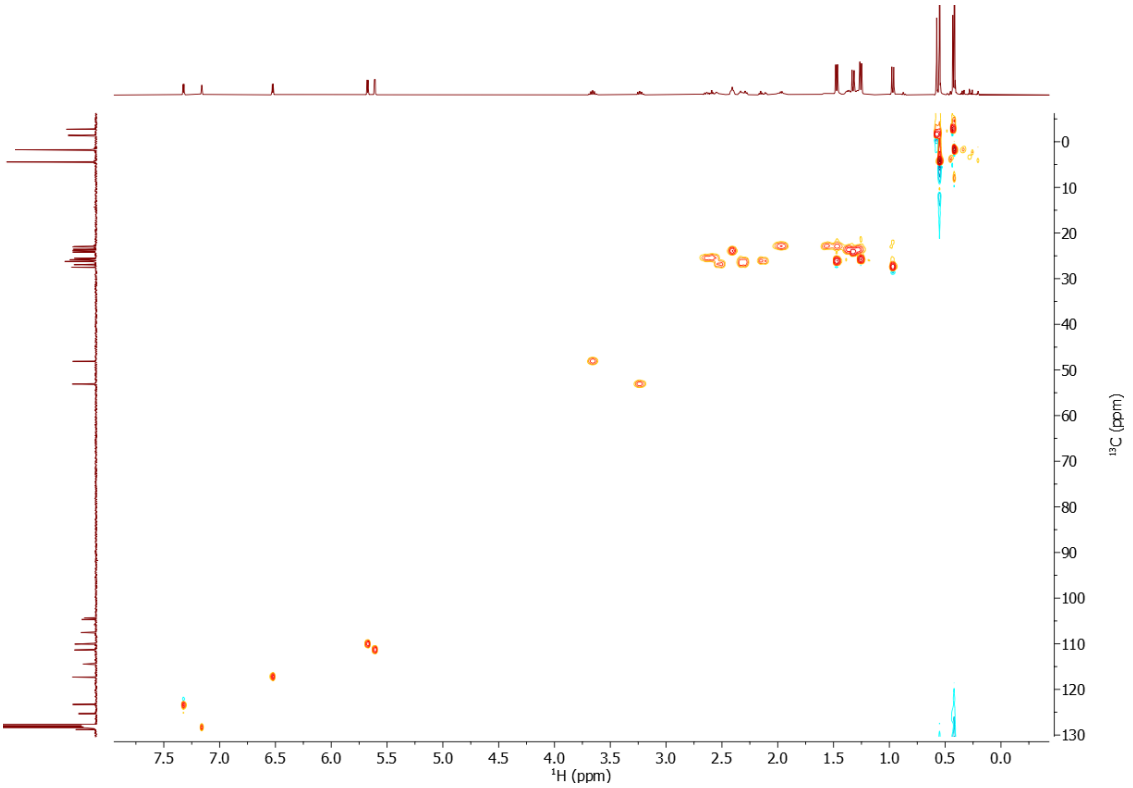

Figure S57. ^{1}H-^{13}C HSQC NMR spectrum of **P2b-*i*Pr** (25 °C, benzene-*d*6, 400.1, 100.6 MHz).

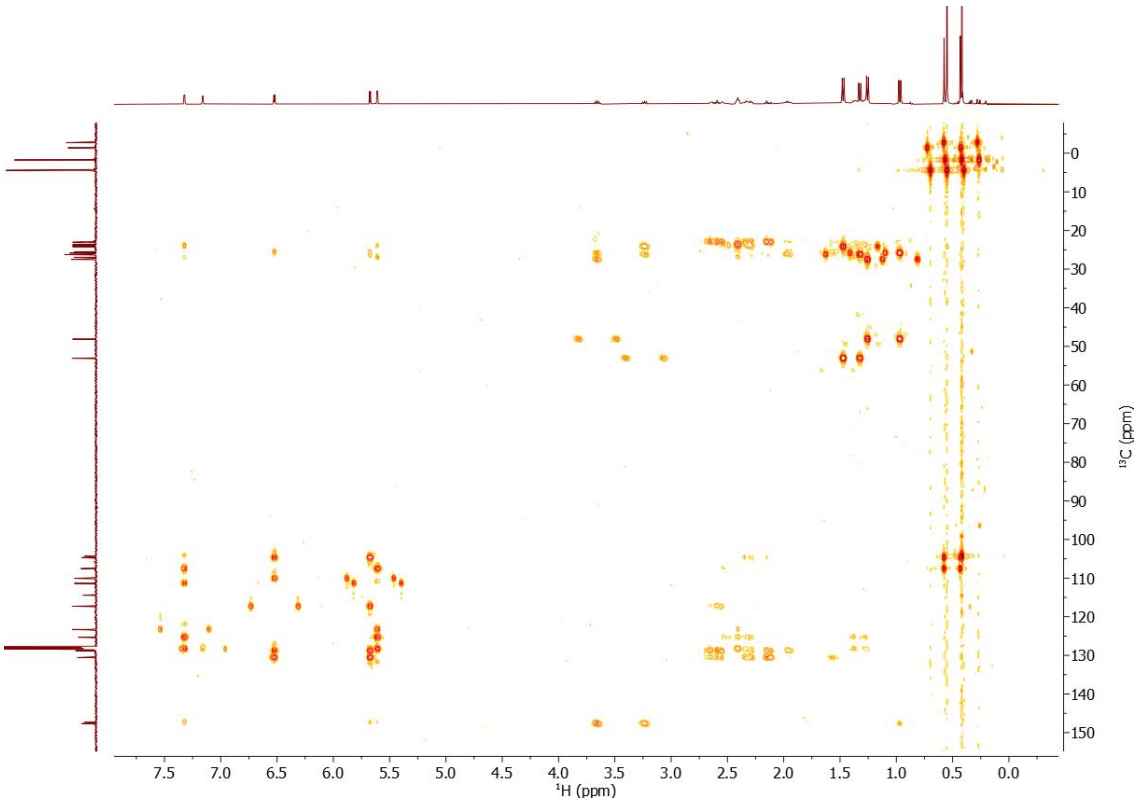

Figure S58. ^{1}H-^{13}C HMBC NMR spectrum of **P2b-*i*Pr** (25 °C, benzene-*d*6, 400.1, 100.6 MHz).

7.8 NMR spectra of $P_{2c\text{-}iPr}$

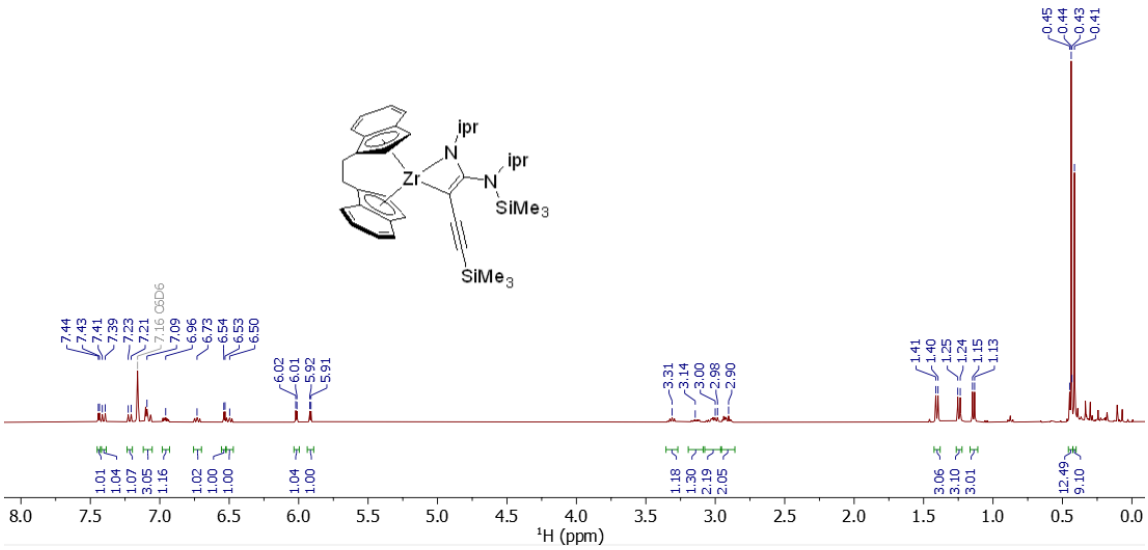

Figure S59. ^{1}H NMR spectrum of **$P_{2c\text{-}iPr}$** (25 °C, benzene-d_6, 400.1 MHz).

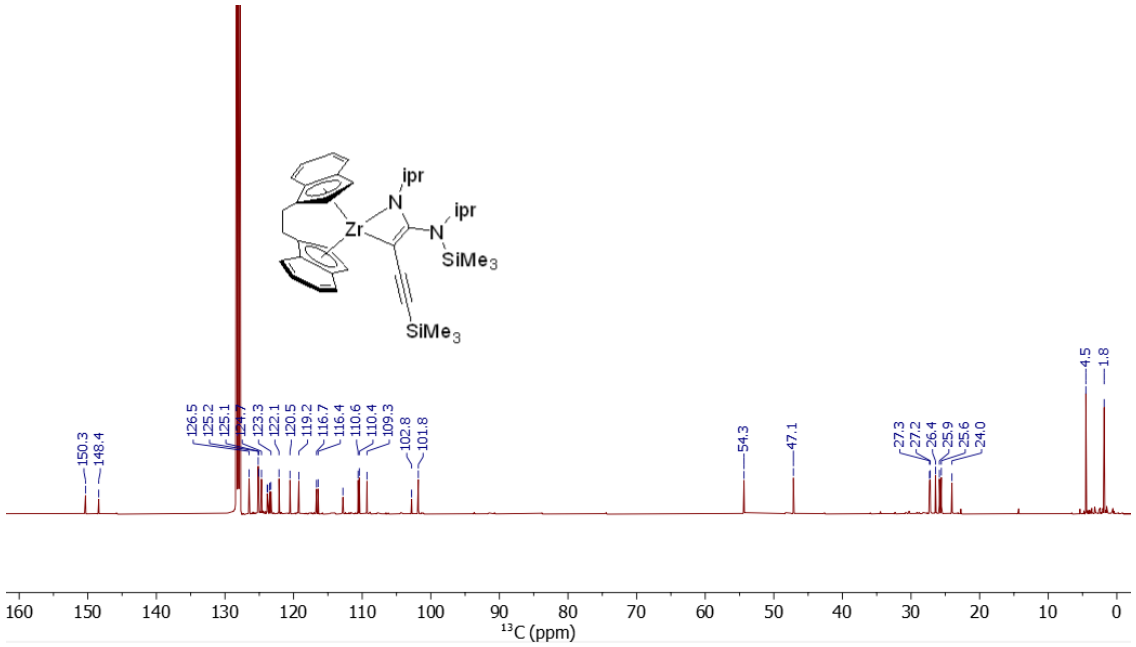

Figure S60. $^{13}C\{^{1}H\}$ NMR spectrum of **$P_{2c\text{-}iPr}$** (25 °C, benzene-d_6, 100.6 MHz).

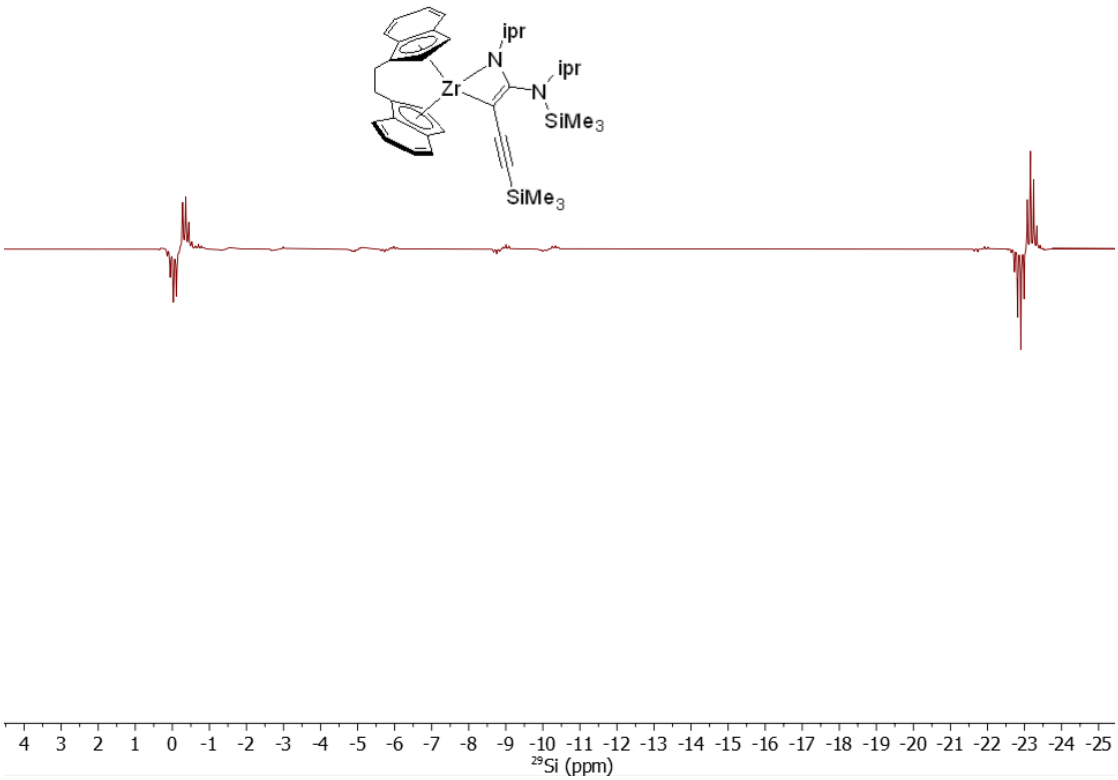

Figure S61. ^{29}Si INEPT NMR spectrum of **P2c-*i*Pr** (25 °C, benzene-*d*6, 79.5 MHz).

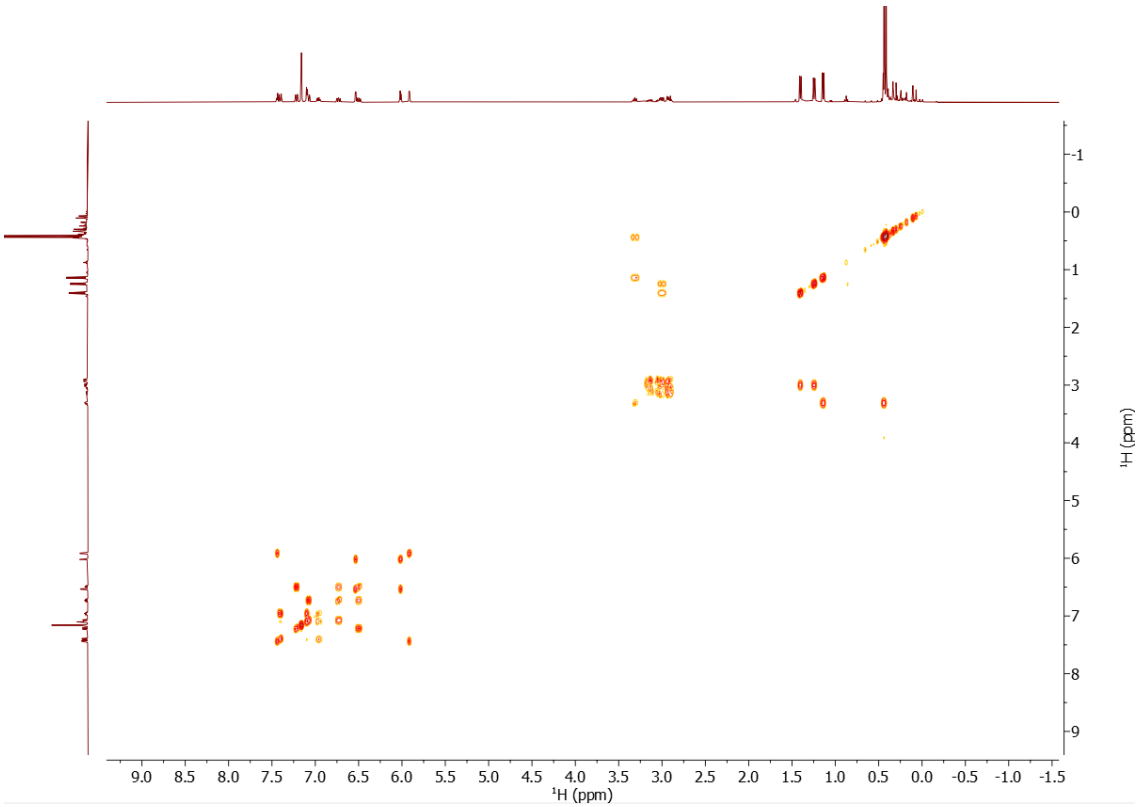

Figure S62. ^{1}H-^{1}H COSY NMR spectrum of **P2c-*i*Pr** (25 °C, benzene-*d*6, 400.1, 400.1 MHz).

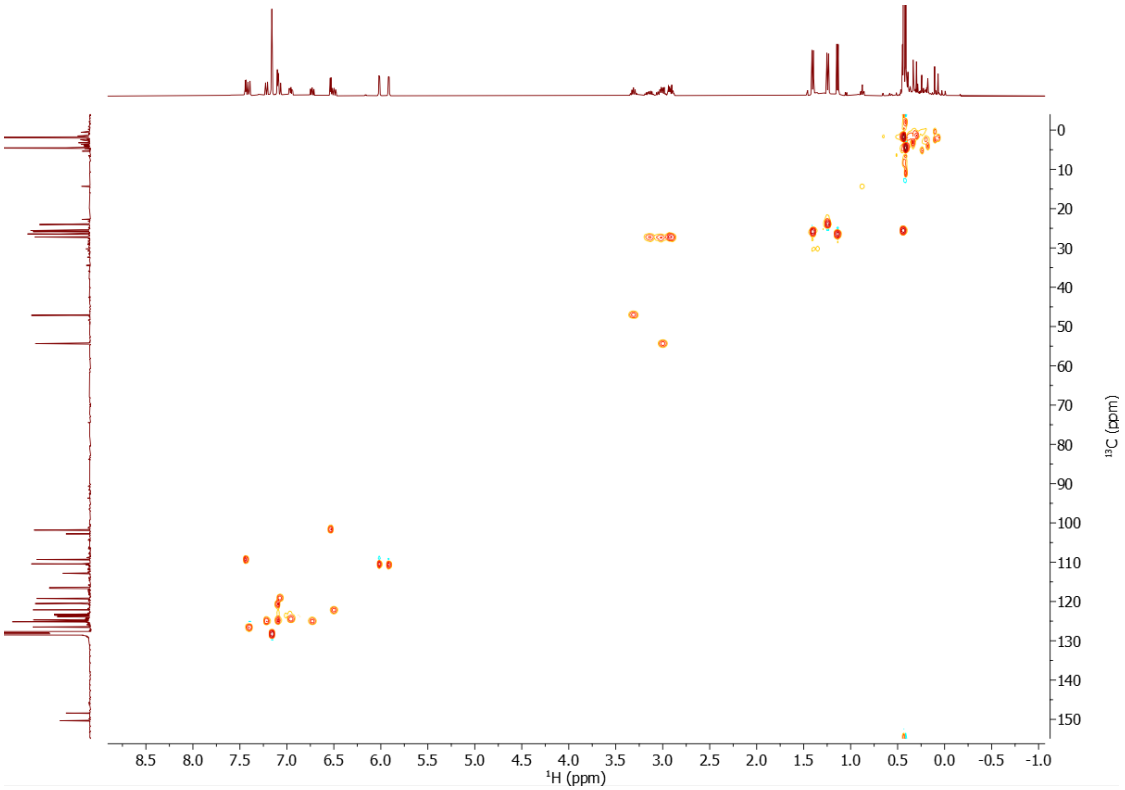

Figure S63. ^{1}H-^{13}C HSQC NMR spectrum of **P2c-*i*Pr** (25 °C, benzene-*d*6, 400.1, 100.6 MHz).

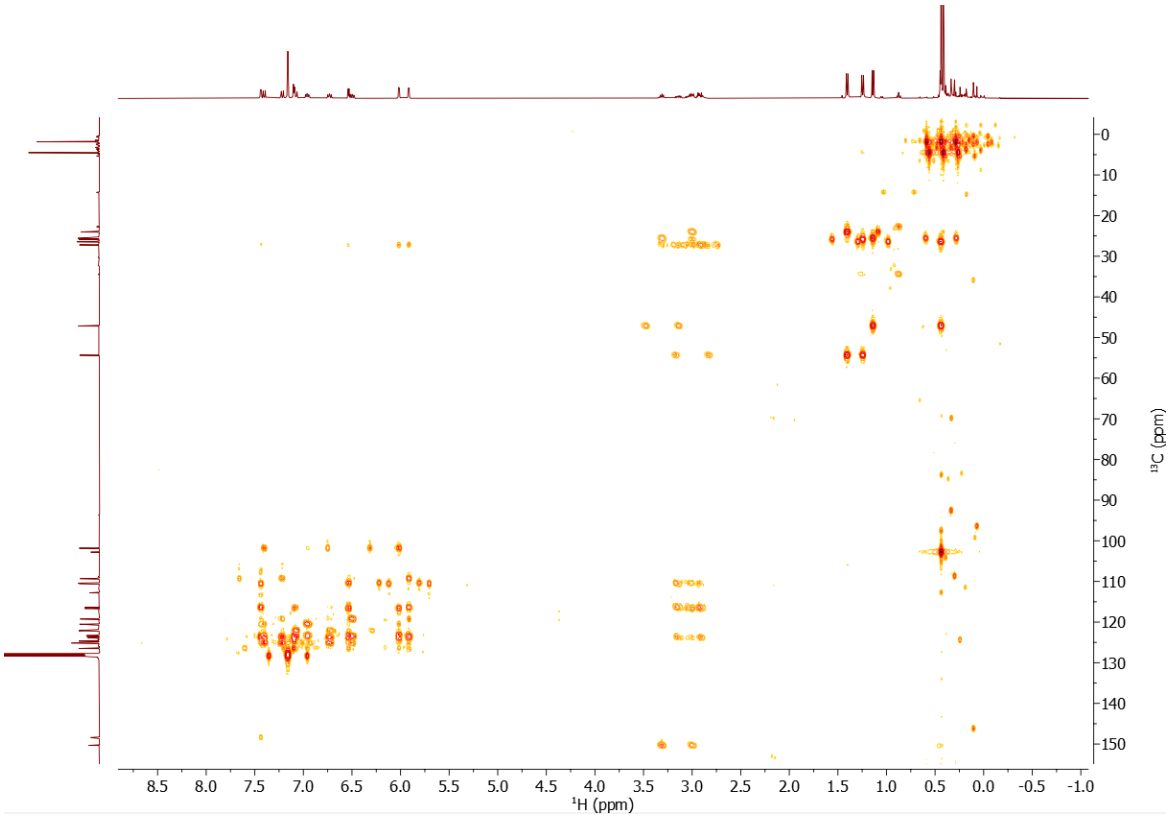

Figure S64. ^{1}H-^{13}C HMBC NMR spectrum of **P2c-*i*Pr** (25 °C, benzene-*d*6, 400.1, 100.6 MHz).

7.9 NMR spectra of $P_{2d\text{-}iPr}$

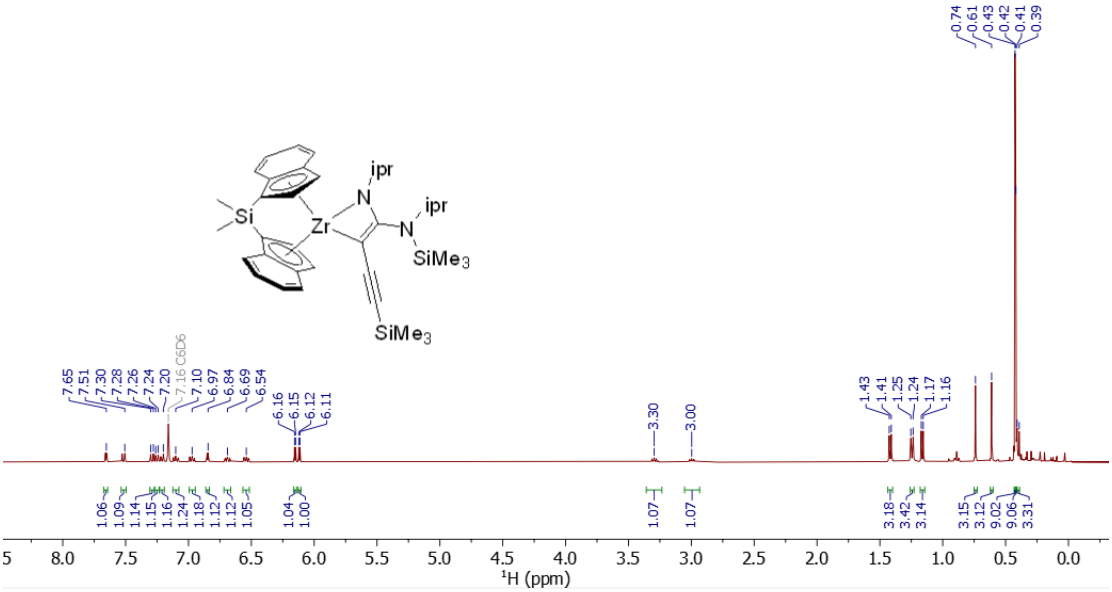

Figure S65. ^{1}H NMR spectrum of **$P_{2d\text{-}iPr}$** (25 °C, benzene-d_6, 400.1 MHz).

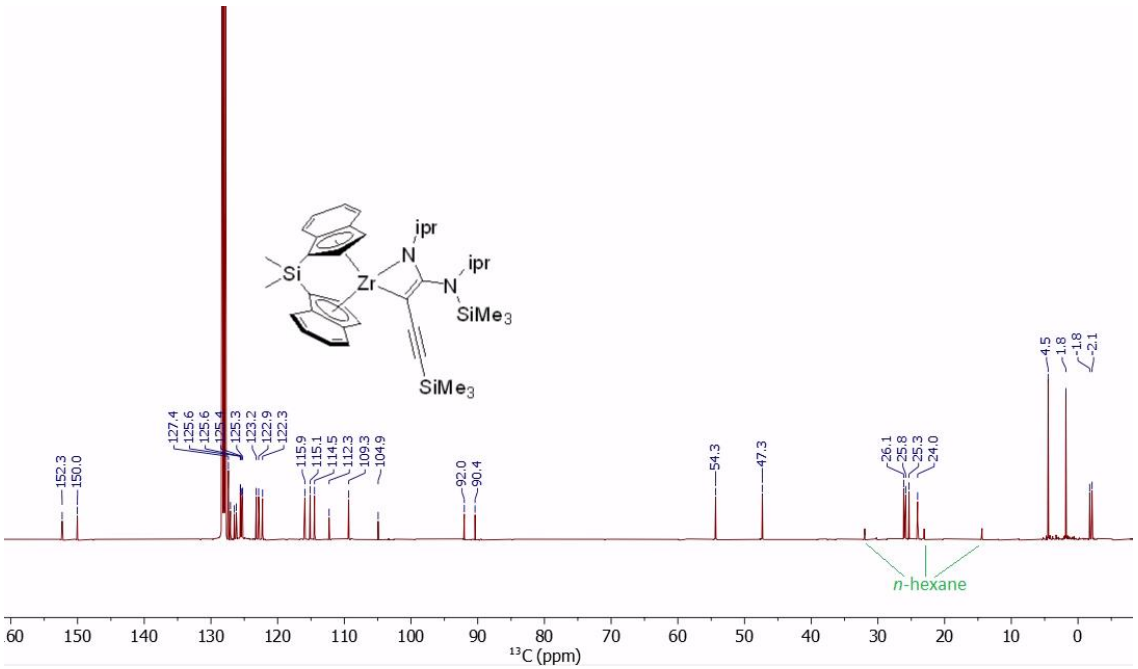

Figure S66. $^{13}C\{^{1}H\}$ NMR spectrum of **$P_{2d\text{-}iPr}$** (25 °C, benzene-d_6, 100.6 MHz).

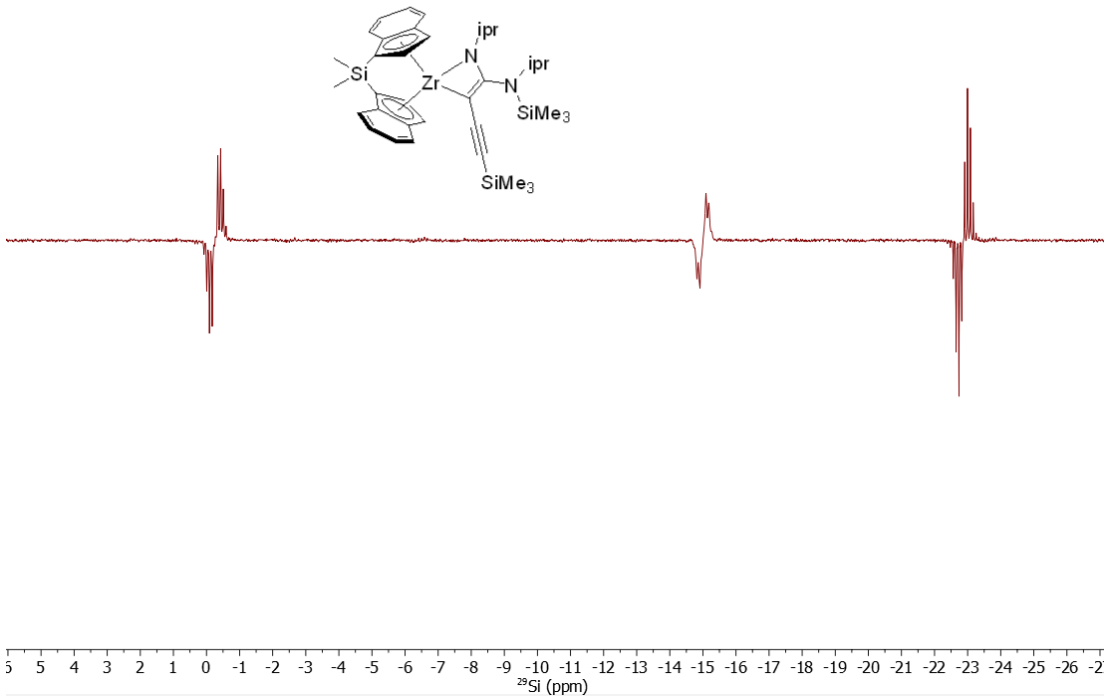

Figure S67. ^{29}Si INEPT NMR spectrum of **P2d-*i*Pr** (25 °C, benzene-*d*6, 79.5 MHz).

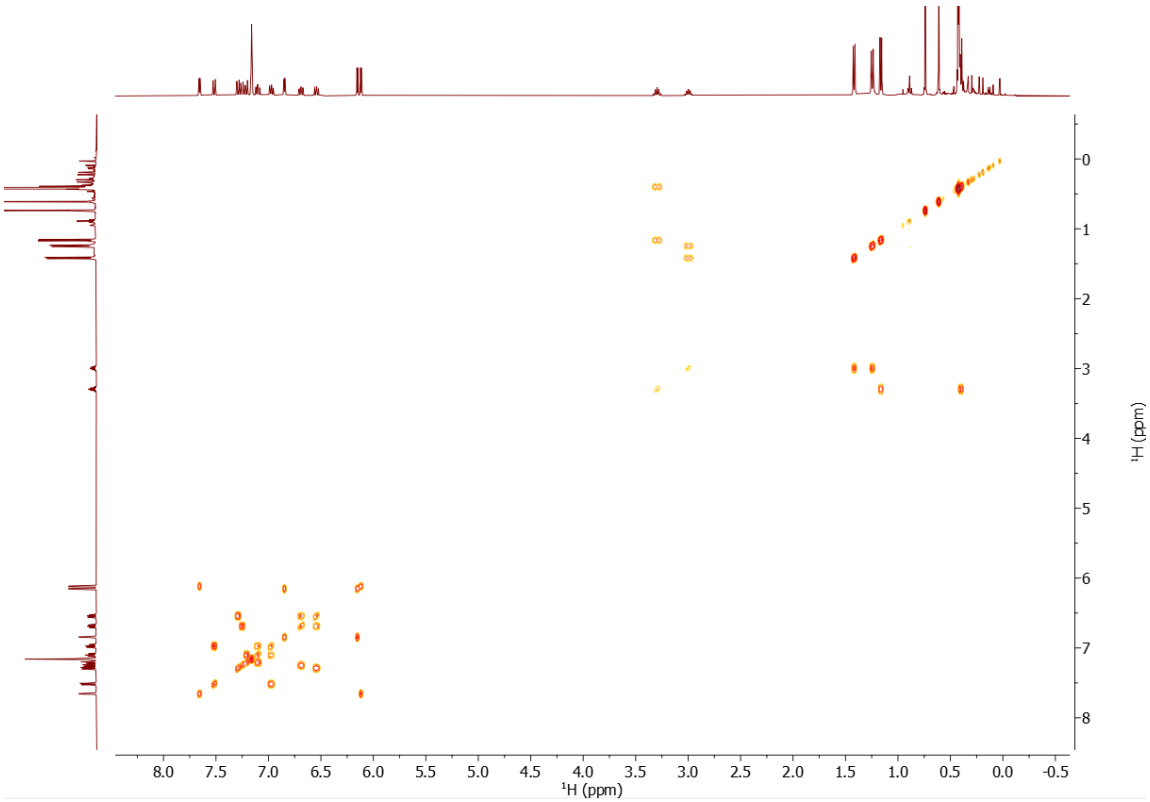

Figure S68. ^{1}H-^{1}H COSY NMR spectrum of **P2d-*i*Pr** (25 °C, benzene-*d*6, 400.1, 400.1 MHz).

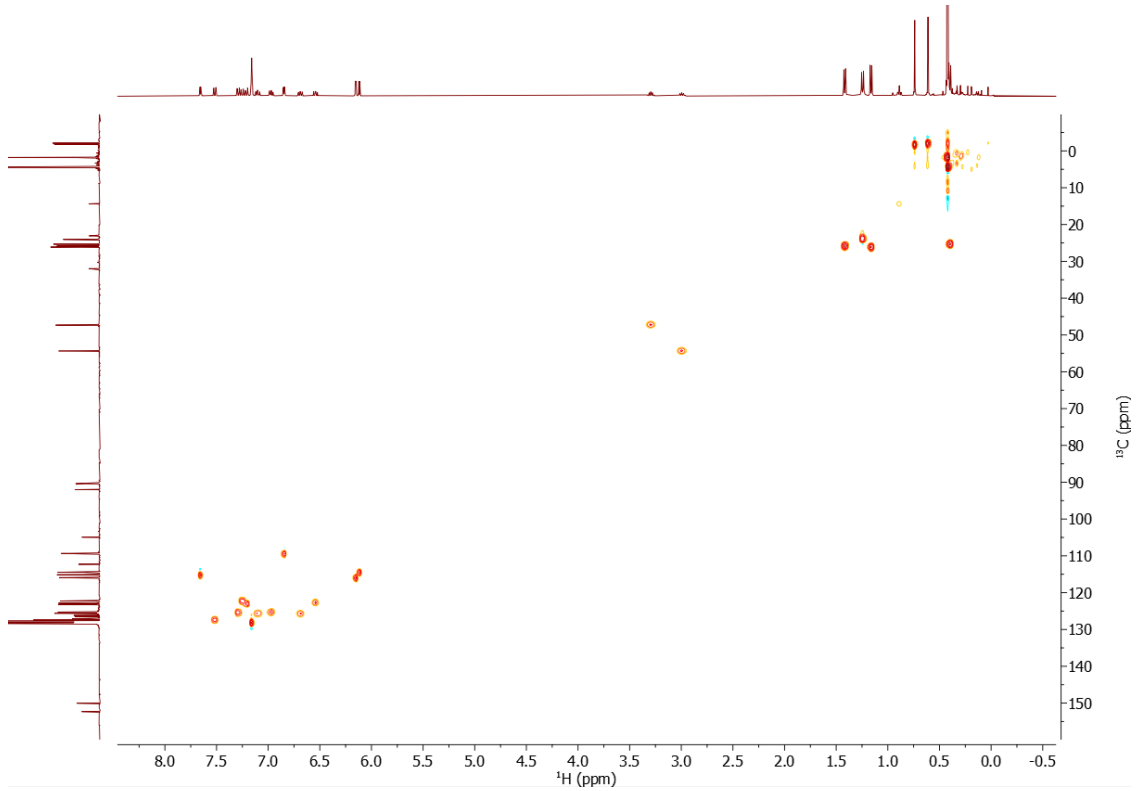

Figure S69. ^{1}H-^{13}C HSQC NMR spectrum of **P2d-*i*Pr** (25 °C, benzene-*d*$_6$, 400.1, 100.6 MHz).

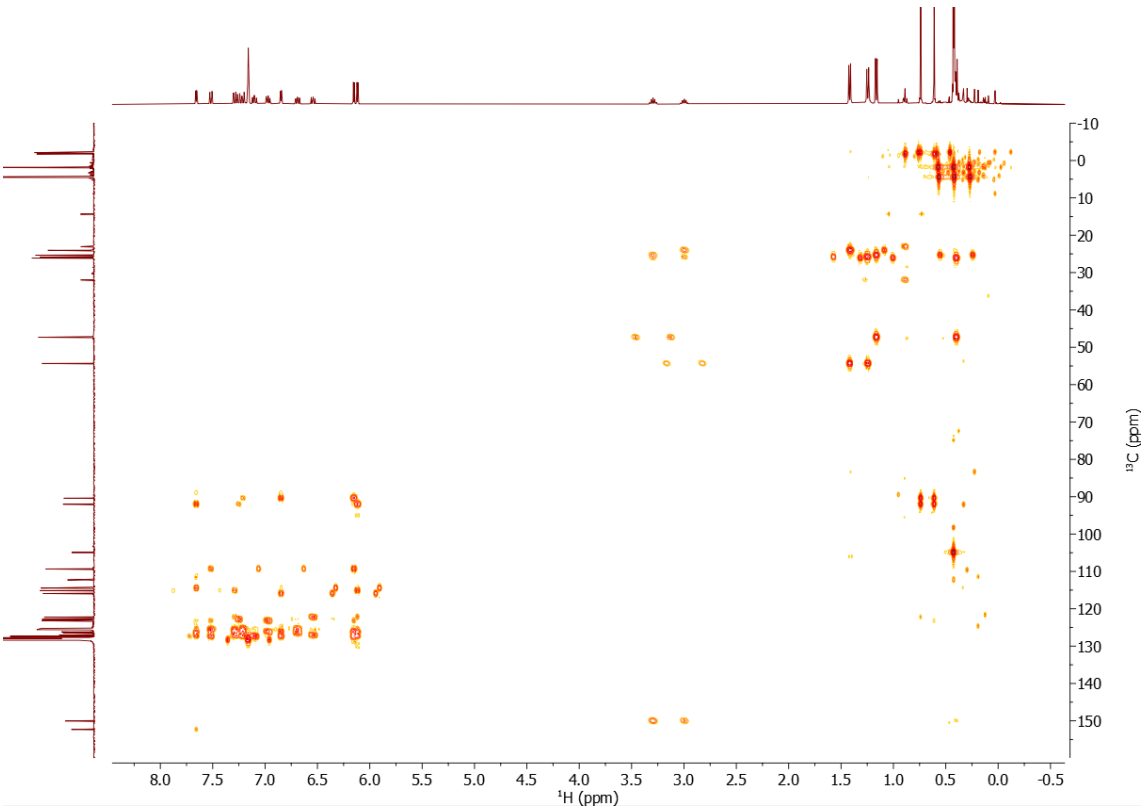

Figure S70. ^{1}H-^{13}C HMBC NMR spectrum of **P2d-*i*Pr** (25 °C, benzene-*d*$_6$, 400.1, 100.6 MHz).

7.10 NMR spectra of $P_{1a\text{-}Cy}$

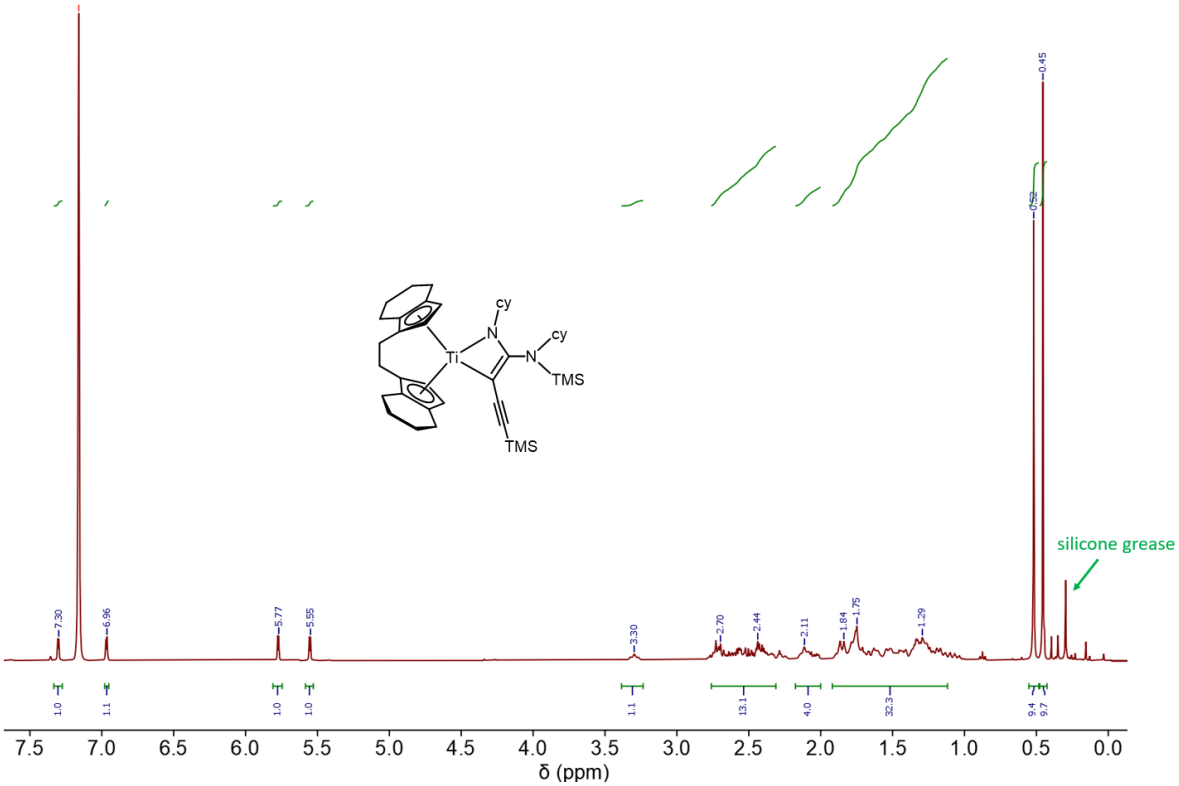

Figure S71. ^{1}H NMR spectrum of **$P_{1a\text{-}Cy}$** (25 °C, benzene-*d*6, 400.1 MHz).

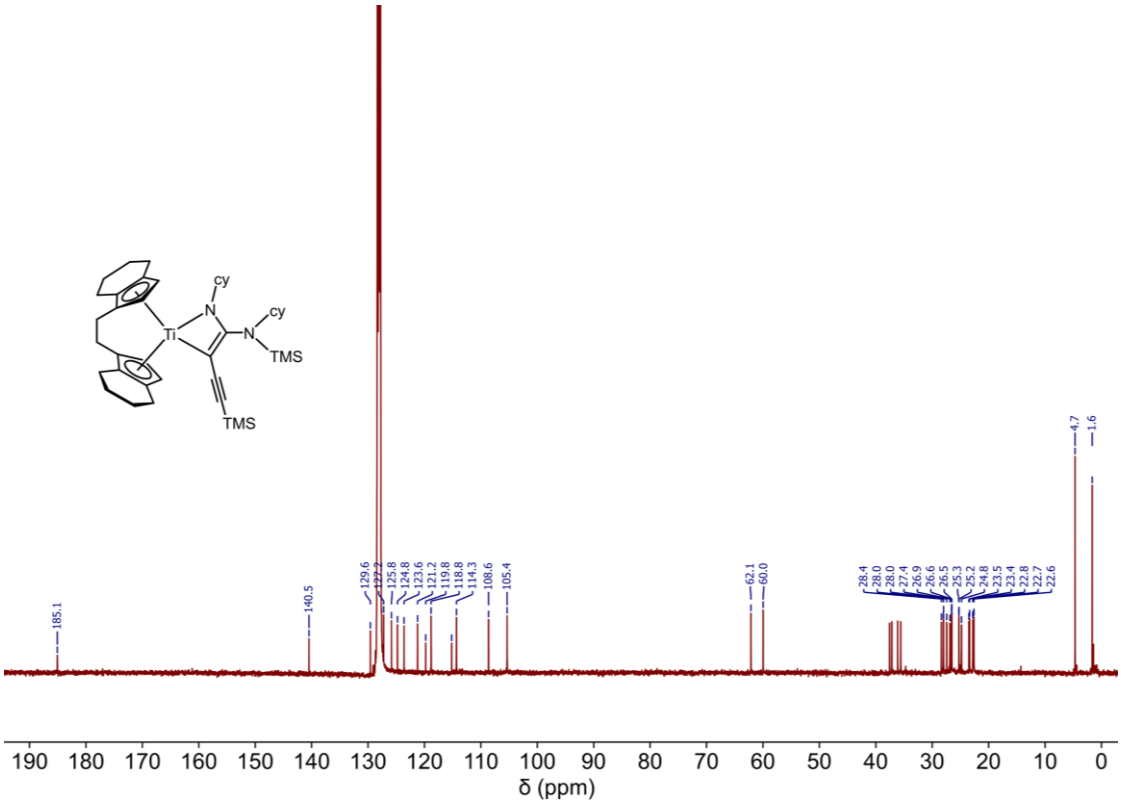

Figure S72. ^{13}C{^{1}H} NMR spectrum of **$P_{1a\text{-}Cy}$** (25 °C, benzene-*d*6, 75.5 MHz).

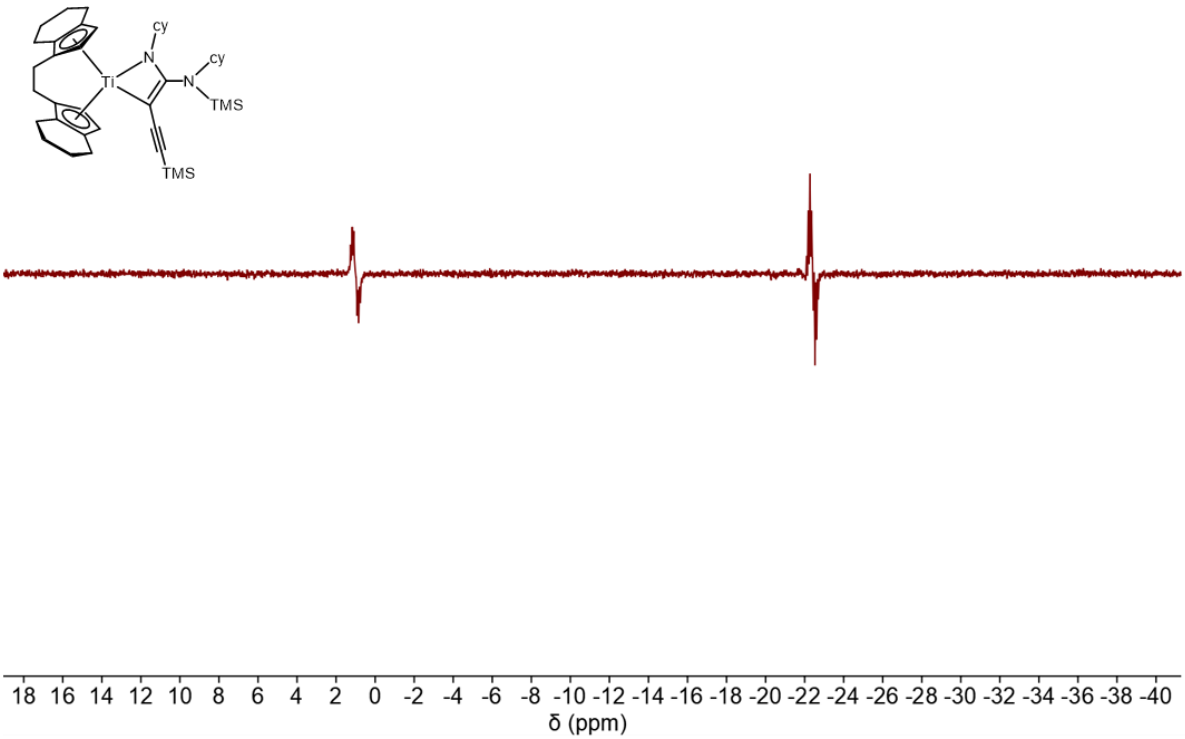

Figure S73. ^{29}Si INEPT NMR spectrum of **P1a-Cy** (25 °C, benzene-*d*6, 79.5 MHz).

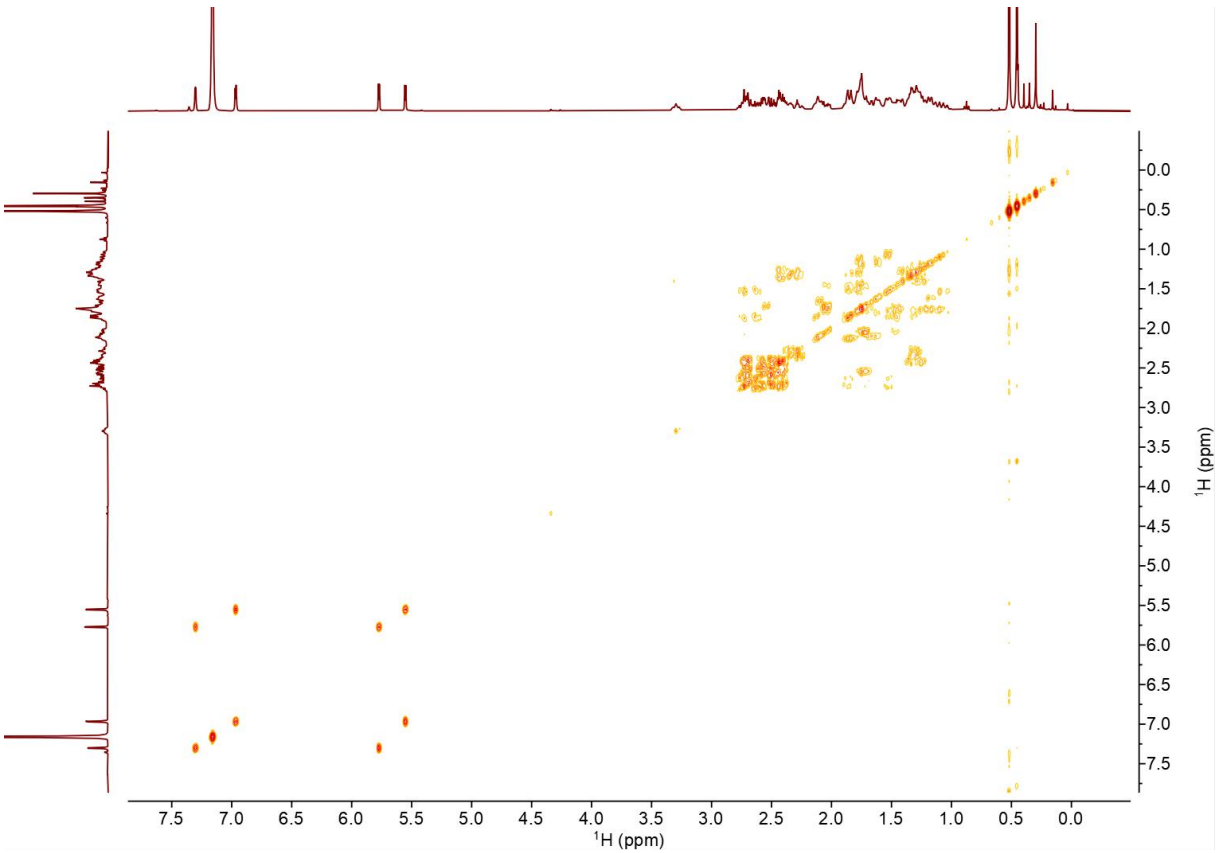

Figure S74. ^{1}H-^{1}H COSY NMR spectrum of **P1a-Cy** (25 °C, benzene-*d*6, 400.1, 400.1 MHz).

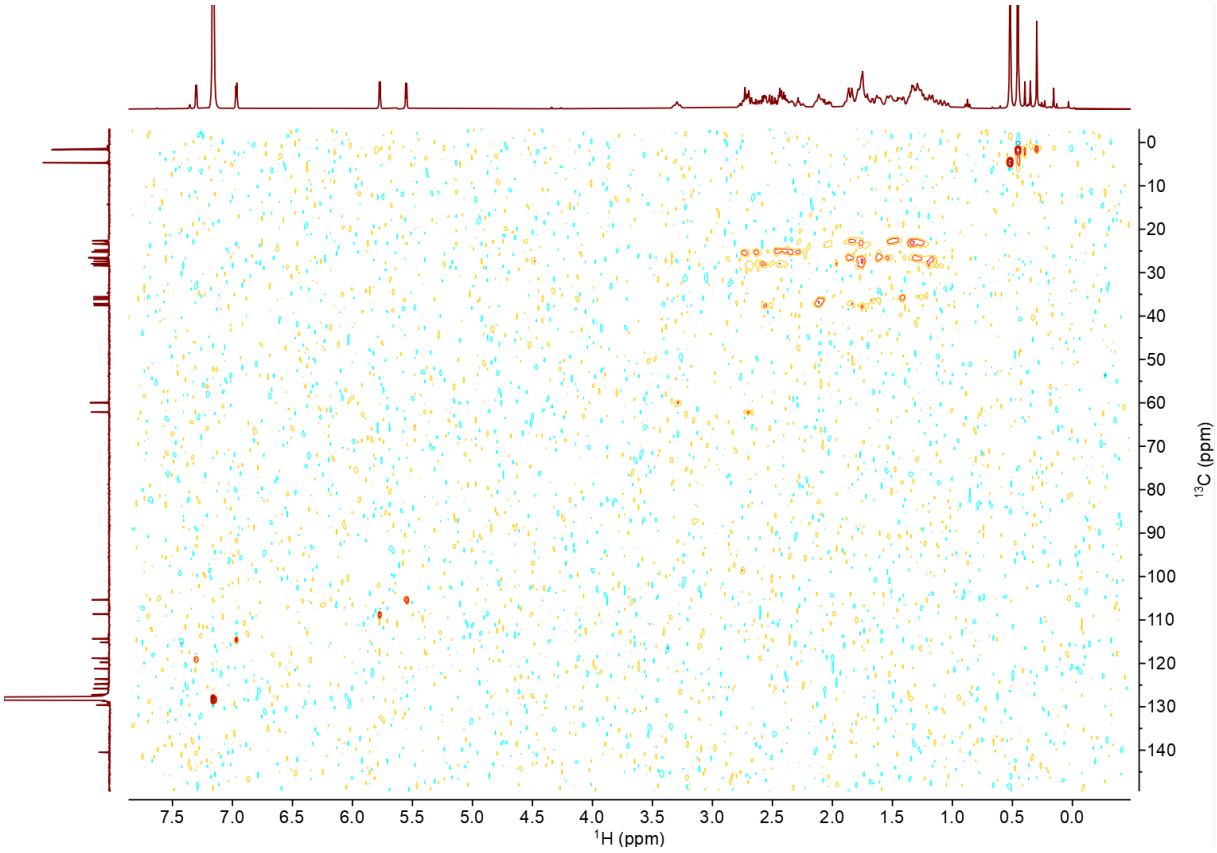

Figure S75. ^{1}H-^{13}C HSQC NMR spectrum of **P$_{1a\text{-}Cy}$** (25 °C, benzene-*d*$_6$, 400.1, 75.5 MHz).

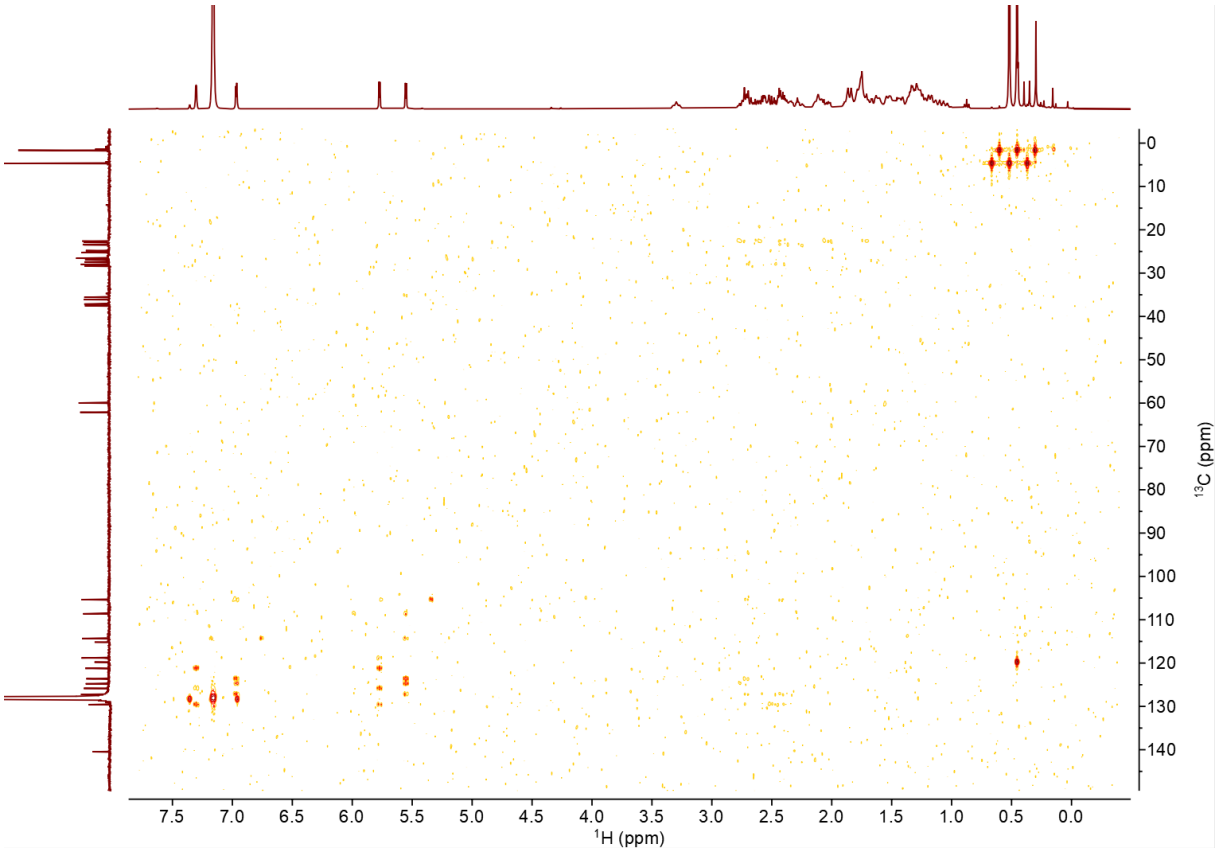

Figure S76. ^{1}H-^{13}C HMBC NMR spectrum of **P$_{1a\text{-}Cy}$** (25 °C, benzene-*d*$_6$, 400.1, 75.5 MHz).

7.11 NMR spectra of $P_{2a\text{-}Cy}$

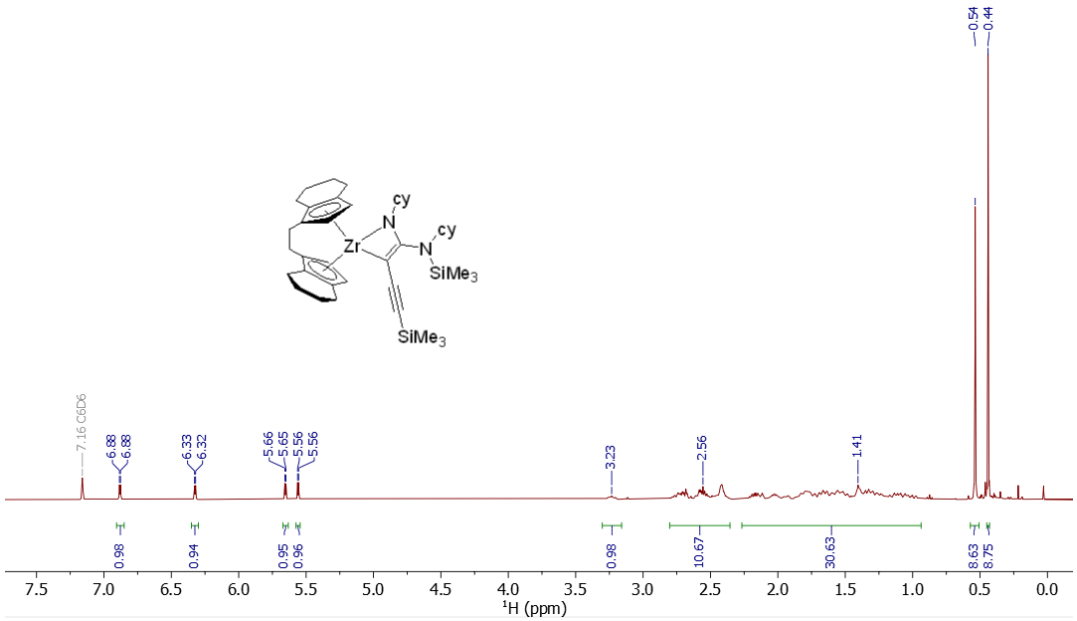

Figure S77. ^{1}H NMR spectrum of **$P_{2a\text{-}Cy}$** (25 °C, benzene-*d*6, 400.1 MHz).

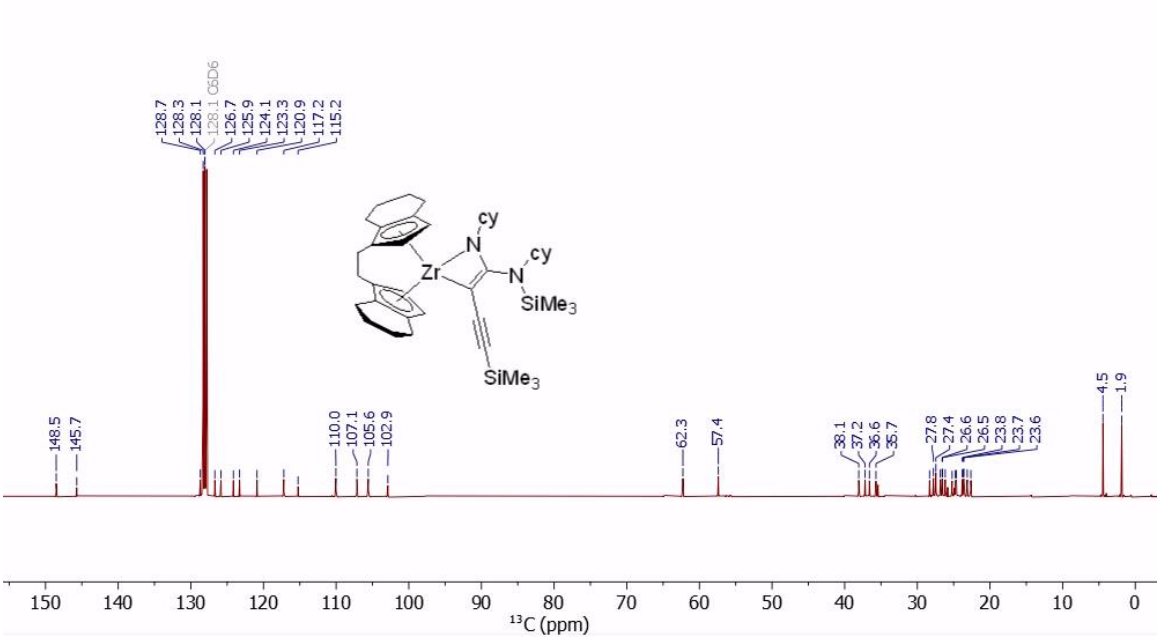

Figure S78. $^{13}C\{^{1}H\}$ NMR spectrum of **$P_{2a\text{-}Cy}$** (25 °C, benzene-*d*6, 100.6 MHz).

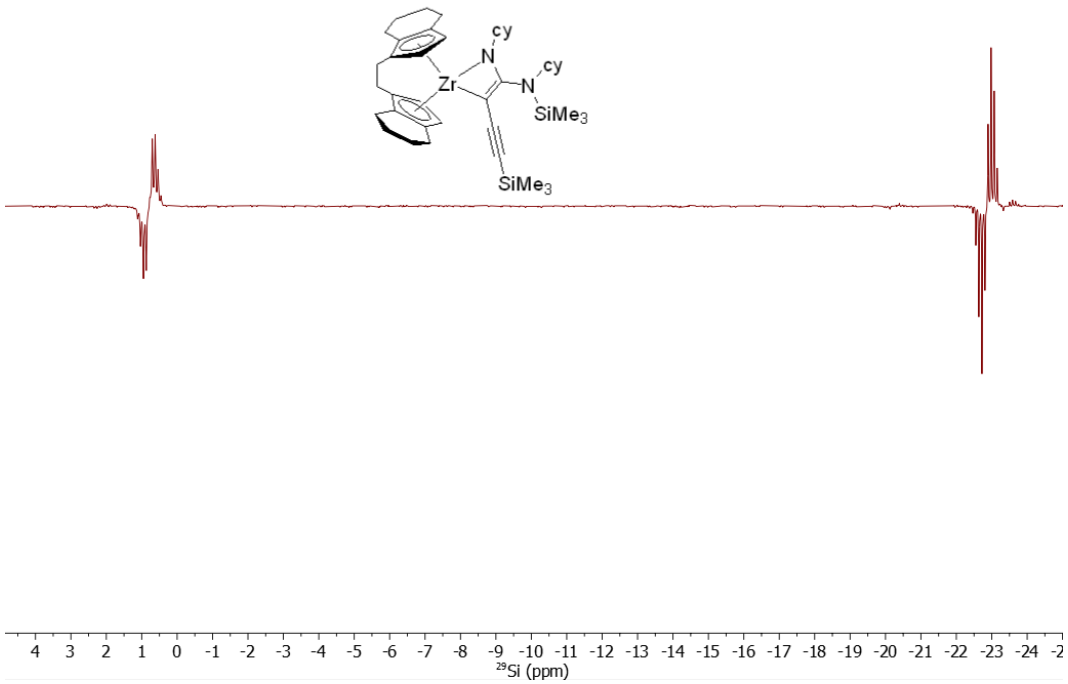

Figure S79. ^{29}Si INEPT NMR spectrum of **P2a-Cy** (25 °C, benzene-*d*6, 79.5 MHz).

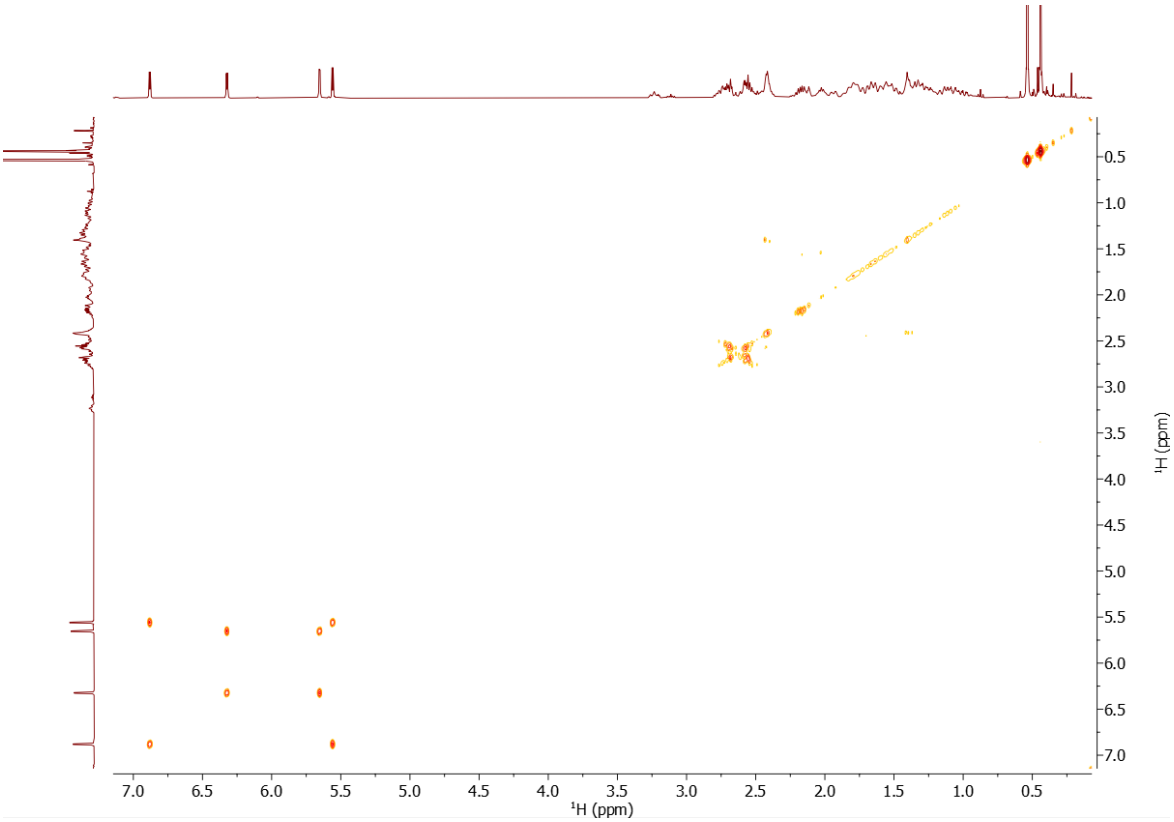

Figure S80. ^{1}H-^{1}H COSY NMR spectrum of **P2a-Cy** (25 °C, benzene-*d*6, 400.1, 400.1 MHz).

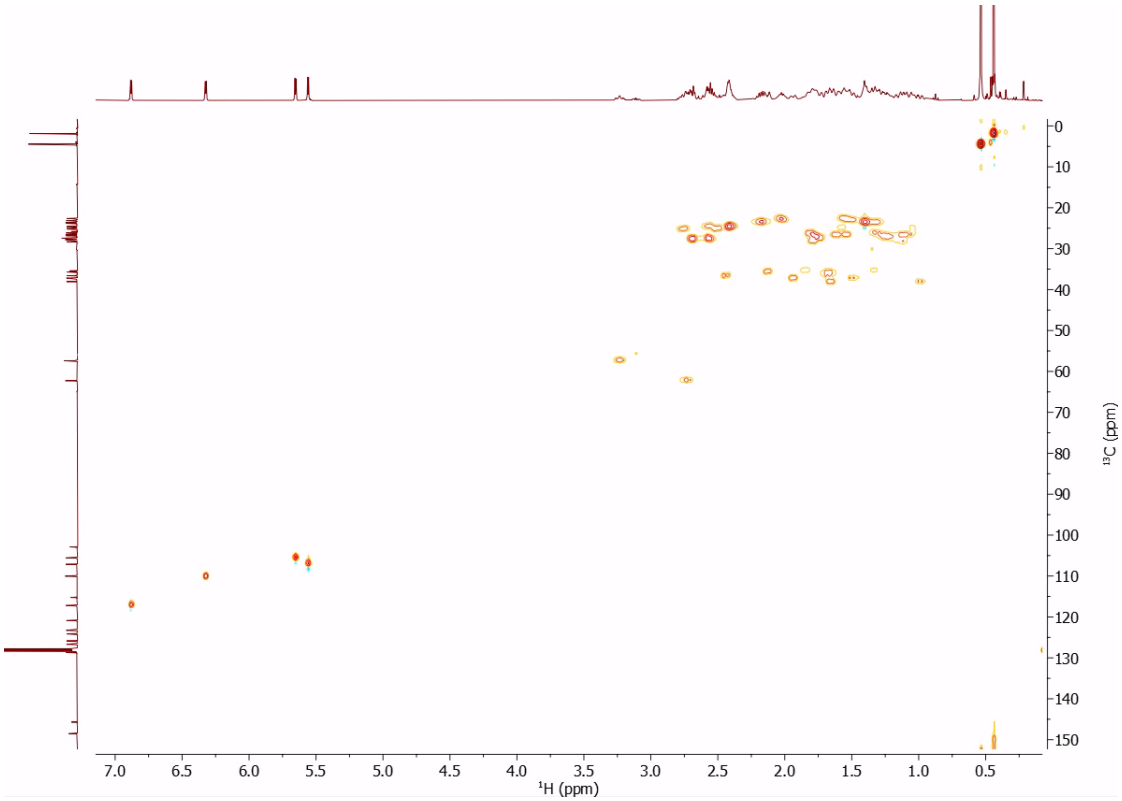

Figure S81. ^{1}H-^{13}C HSQC NMR spectrum of **P2a-Cy** (25 °C, benzene-*d*6, 400.1, 100.6 MHz).

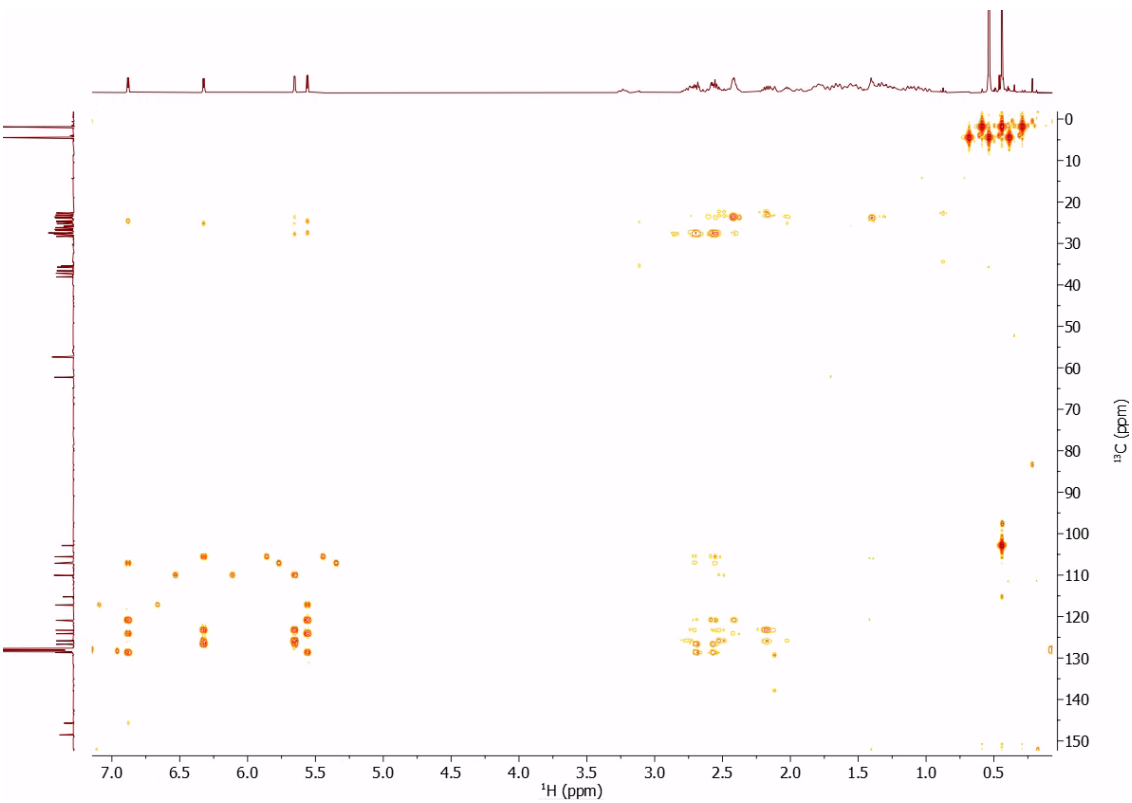

Figure S82. ^{1}H-^{13}C HMBC NMR spectrum of **P2a-Cy** (25 °C, benzene-*d*6, 400.1, 100.6 MHz).

7.12 NMR spectra of $P_{2b\text{-}Cy}$

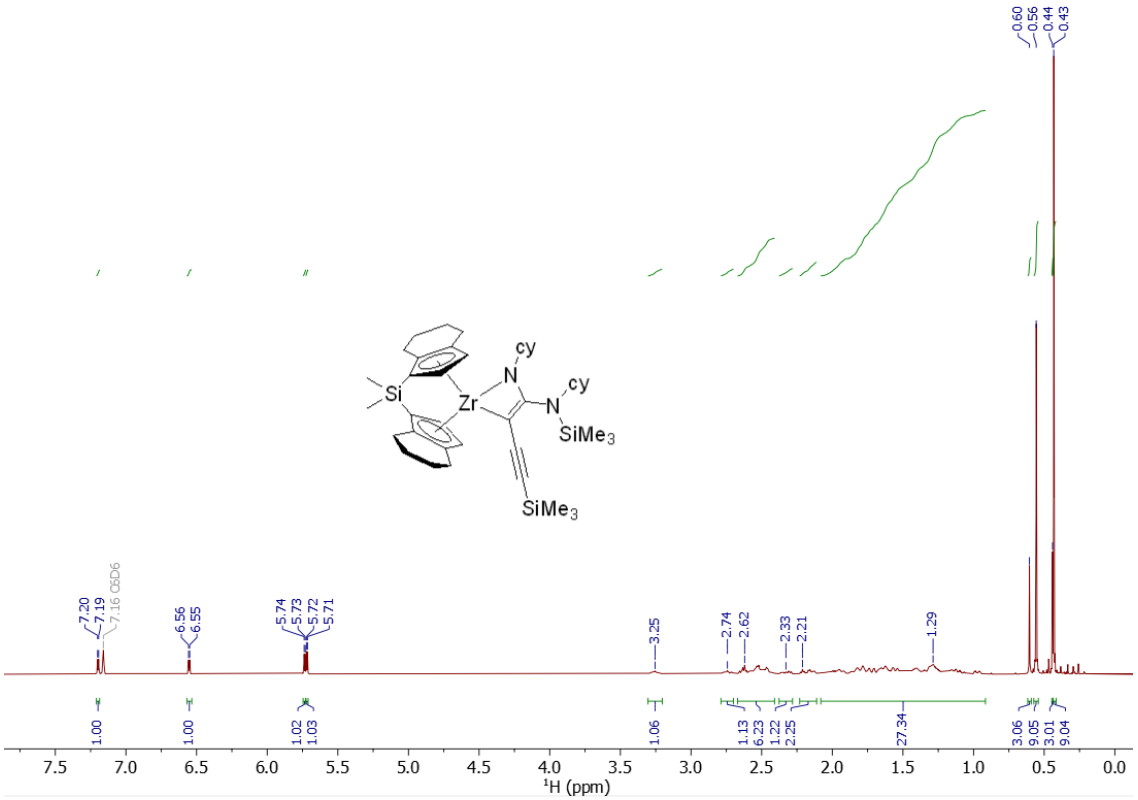

Figure S83. ^{1}H NMR spectrum of **$P_{2b\text{-}Cy}$** (25 °C, benzene-*d*6, 400.1 MHz).

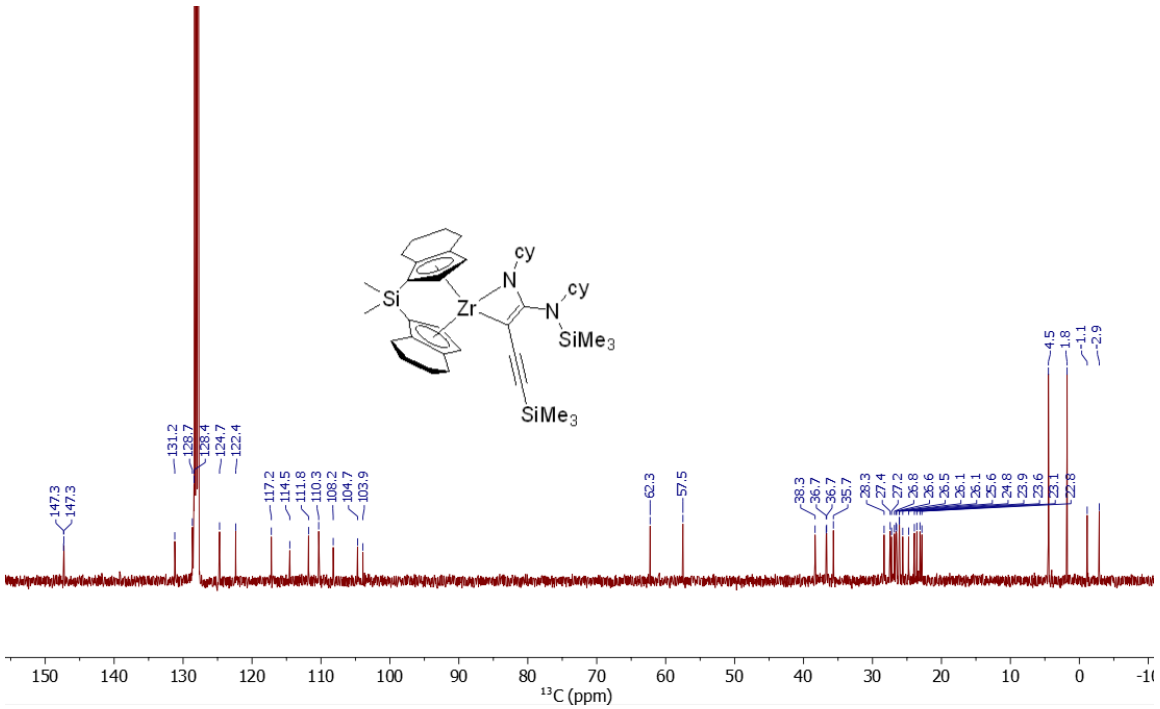

Figure S84. $^{13}C\{^{1}H\}$ NMR spectrum of **$P_{2b\text{-}Cy}$** (25 °C, benzene-*d*6, 100.6 MHz).

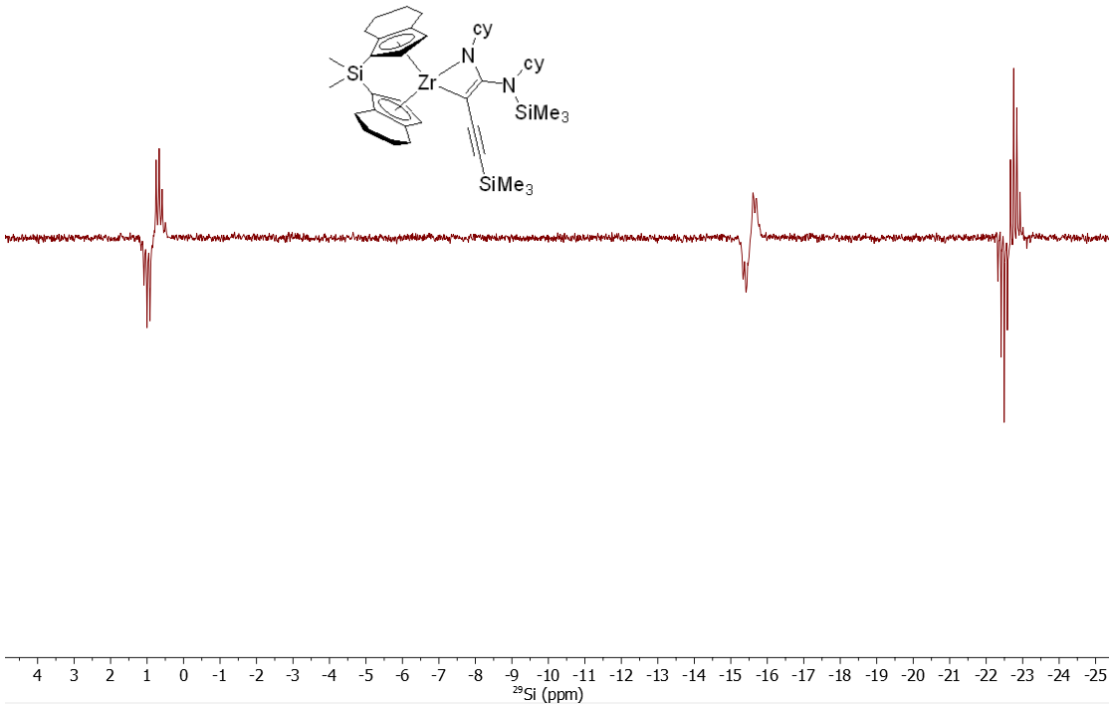

Figure S85. ^{29}Si INEPT NMR spectrum of **P2b-Cy** (25 °C, benzene-*d*6, 79.5 MHz).

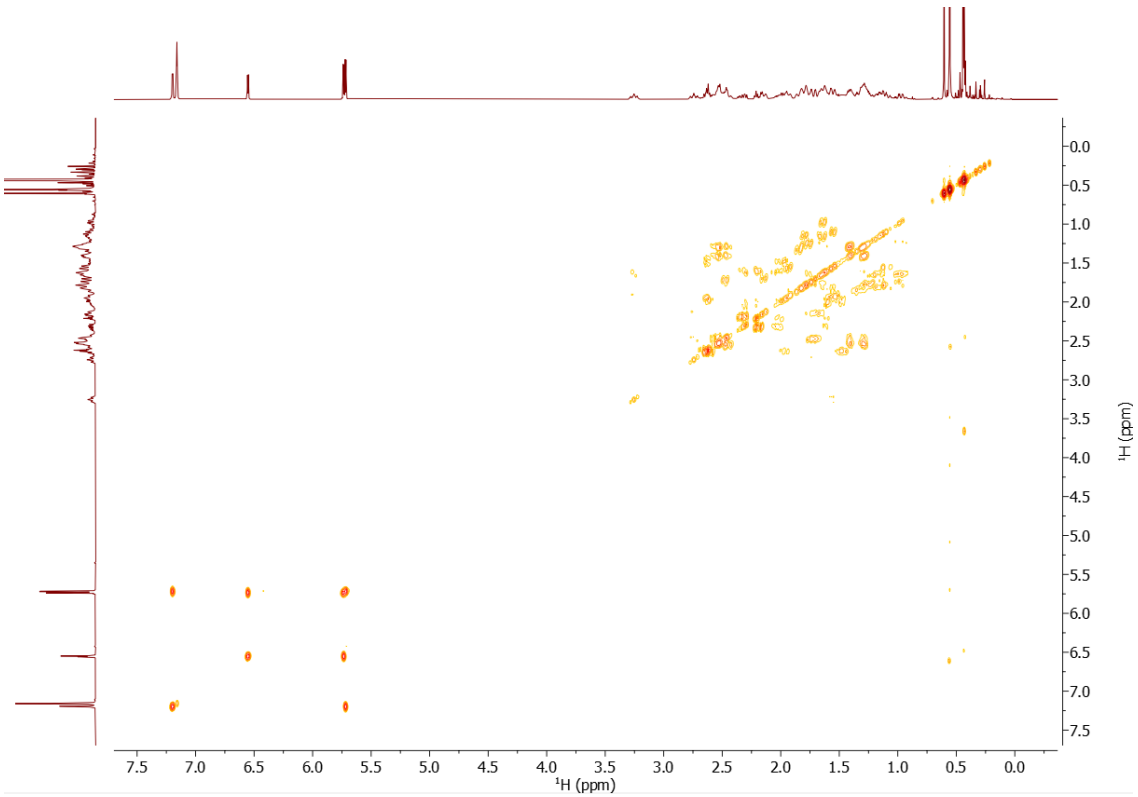

Figure S86. ^{1}H-^{1}H COSY NMR spectrum of **P2b-Cy** (25 °C, benzene-*d*6, 400.1, 400.1 MHz).

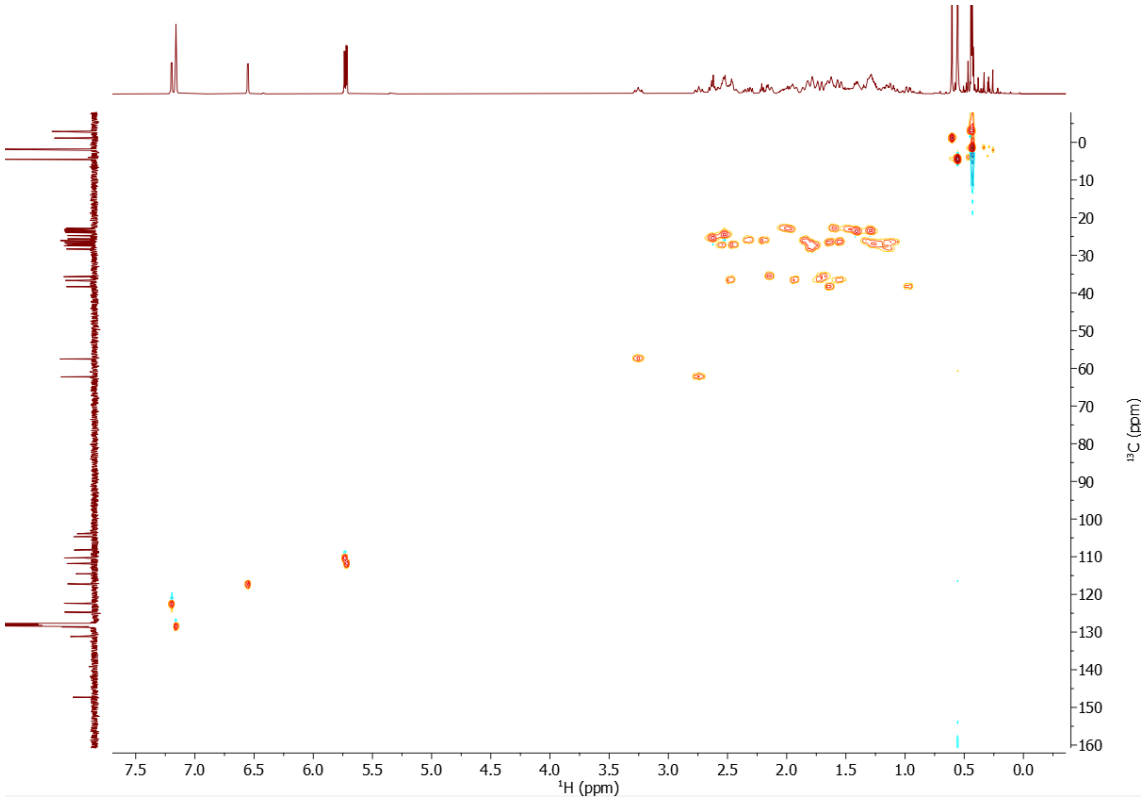

Figure S87. ^{1}H-^{13}C HSQC NMR spectrum of **P2b-Cy** (25 °C, benzene-*d*6, 400.1, 100.6 MHz).

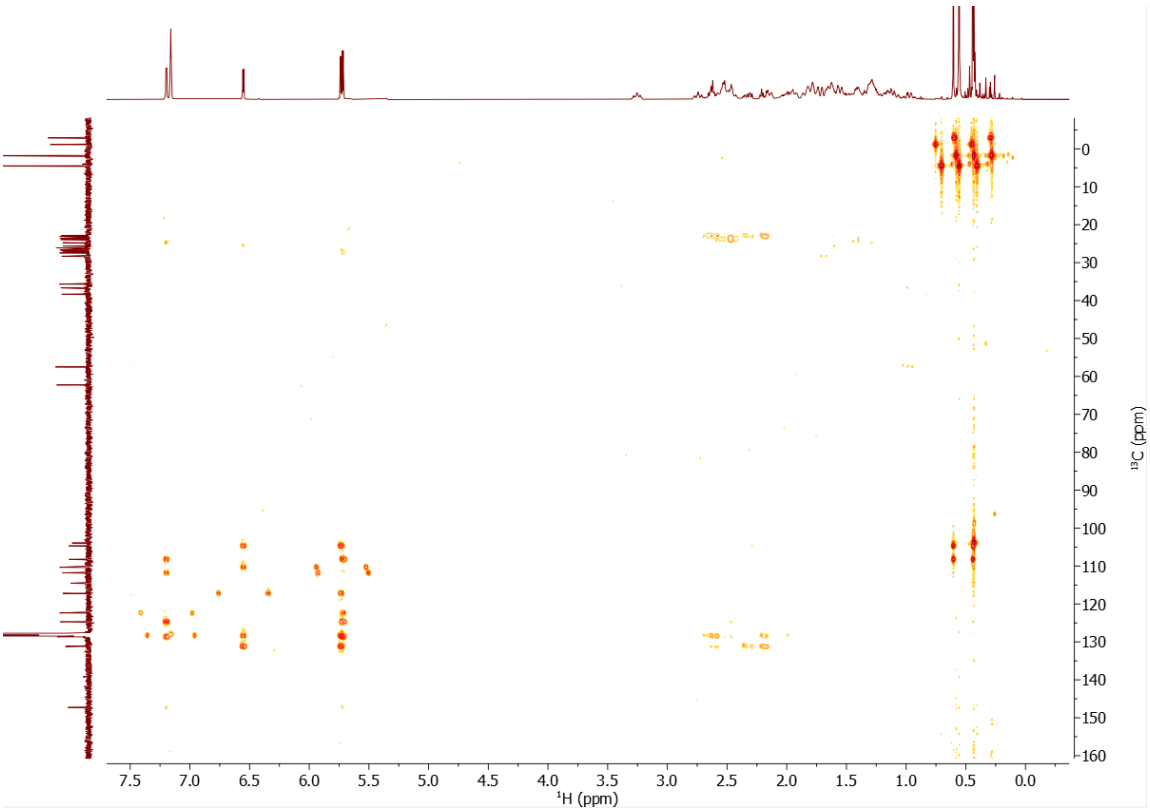

Figure S88. ^{1}H-^{13}C HMBC NMR spectrum of **P2b-Cy** (25 °C, benzene-*d*6, 400.1, 100.6 MHz).

7.13 NMR spectra of $P_{2c\text{-}Cy}$

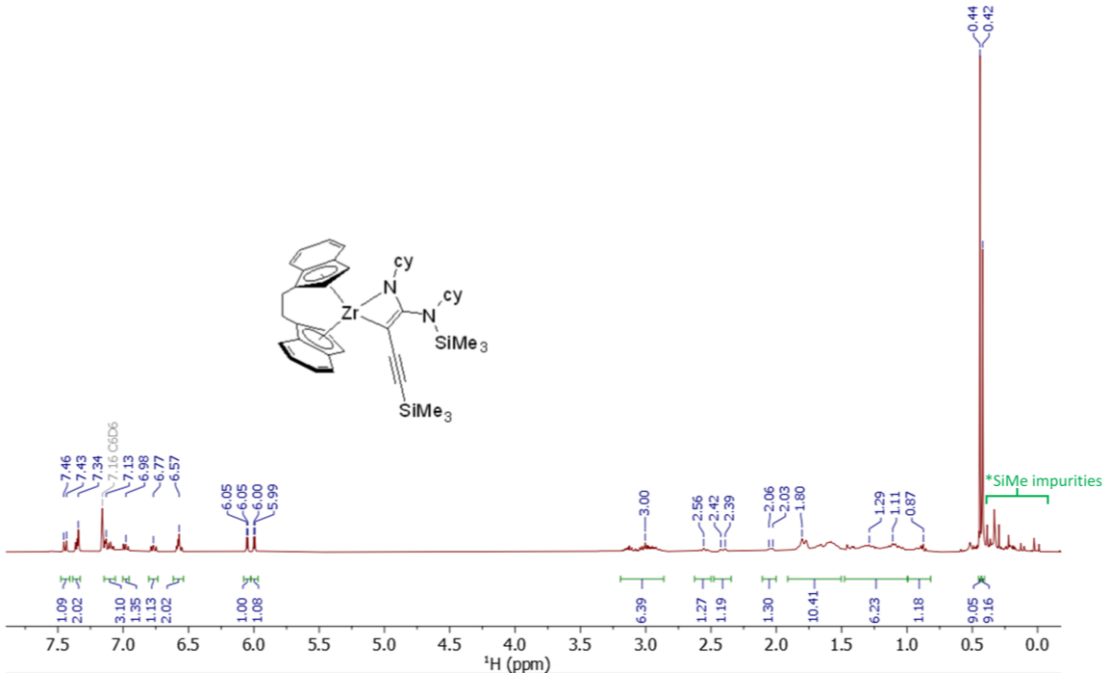

Figure S89. ^{1}H NMR spectrum of **$P_{2c\text{-}Cy}$** (25 °C, benzene-*d*6, 400.1 MHz).

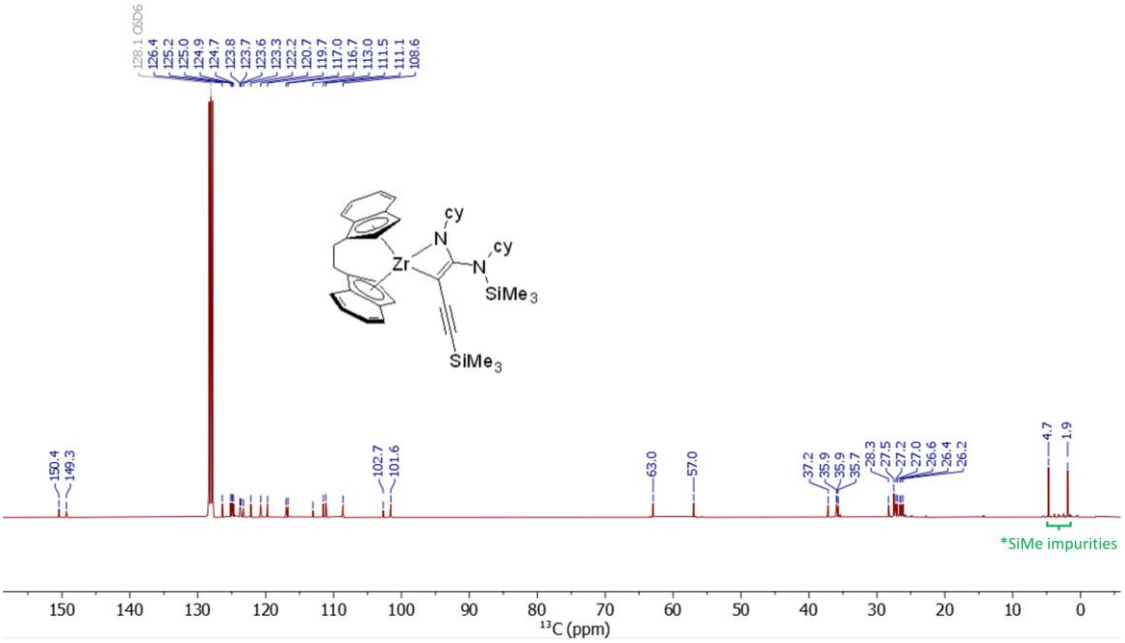

Figure S90. $^{13}C\{^{1}H\}$ NMR spectrum of **$P_{2c\text{-}Cy}$** (25 °C, benzene-*d*6, 100.6 MHz).

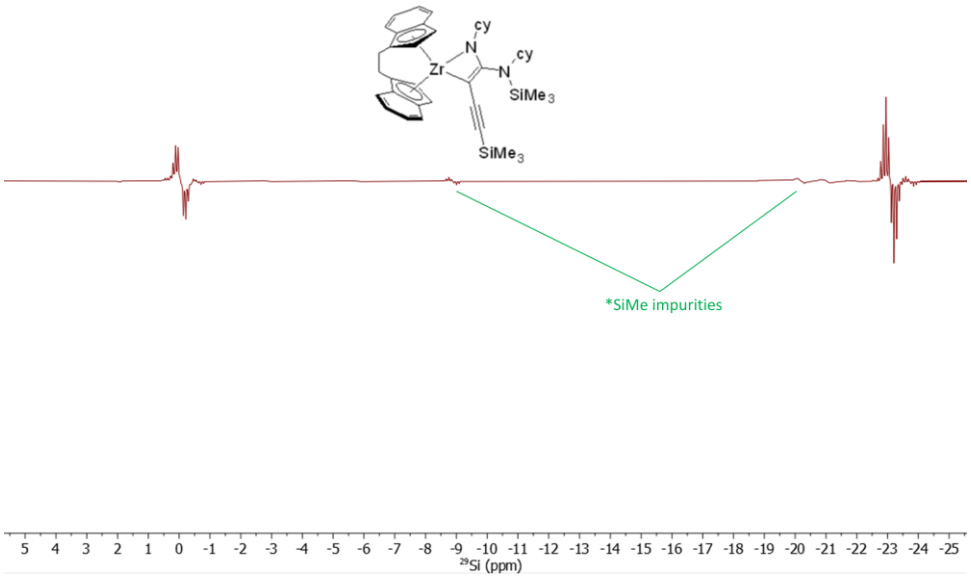

Figure S91. ^{29}Si INEPT NMR spectrum of **P2c-Cy** (25 °C, benzene-*d*6, 79.5 MHz).

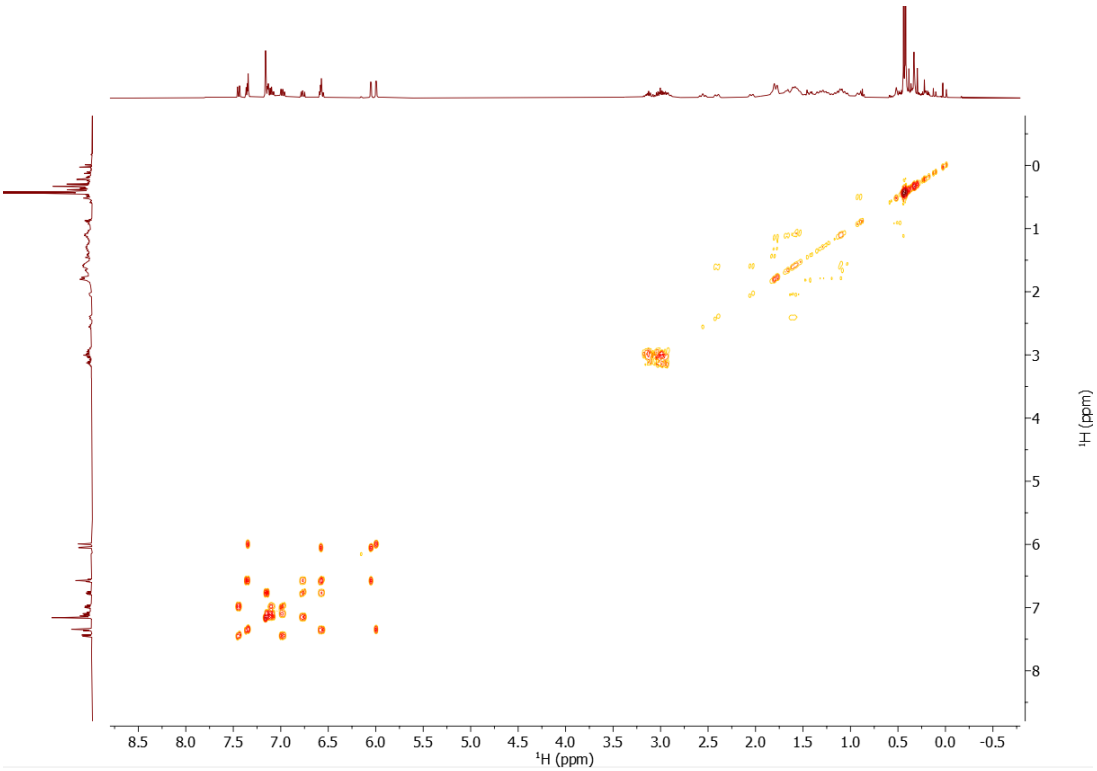

Figure S92. ^{1}H-^{1}H COSY NMR spectrum of **P2c-Cy** (25 °C, benzene-*d*6, 400.1, 400.1 MHz).

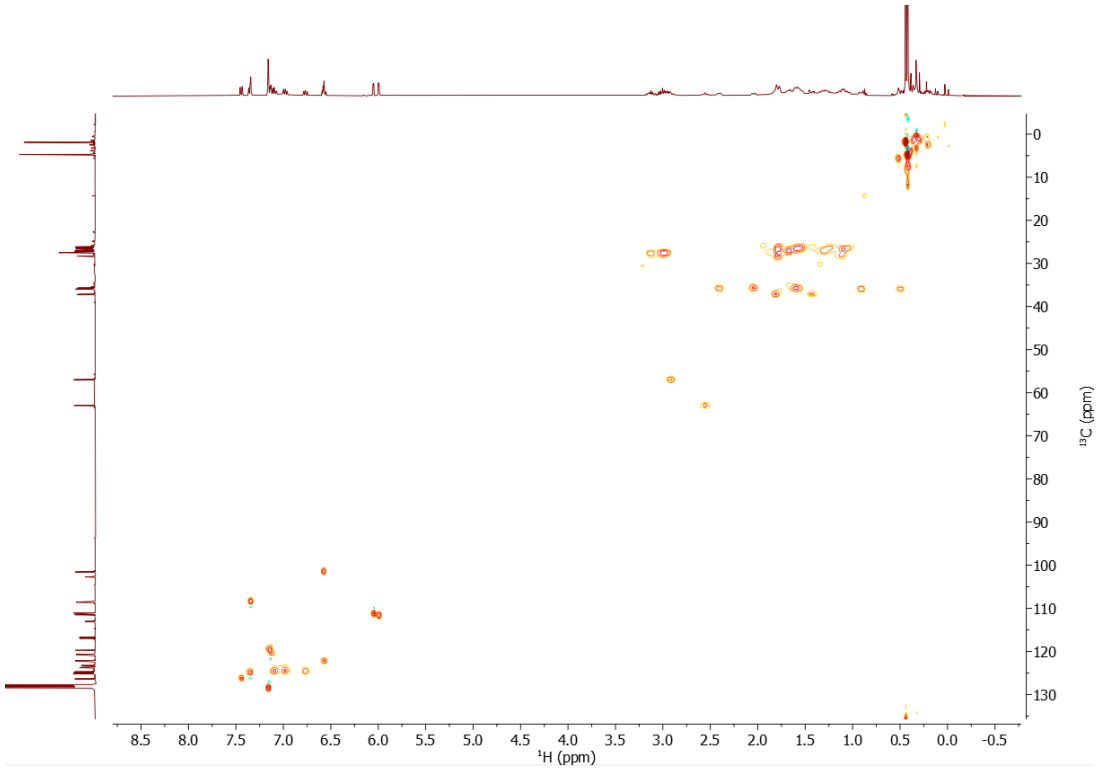

Figure S93. ^{1}H-^{13}C HSQC NMR spectrum of **P2c-Cy** (25 °C, benzene-*d*6, 400.1, 100.6 MHz).

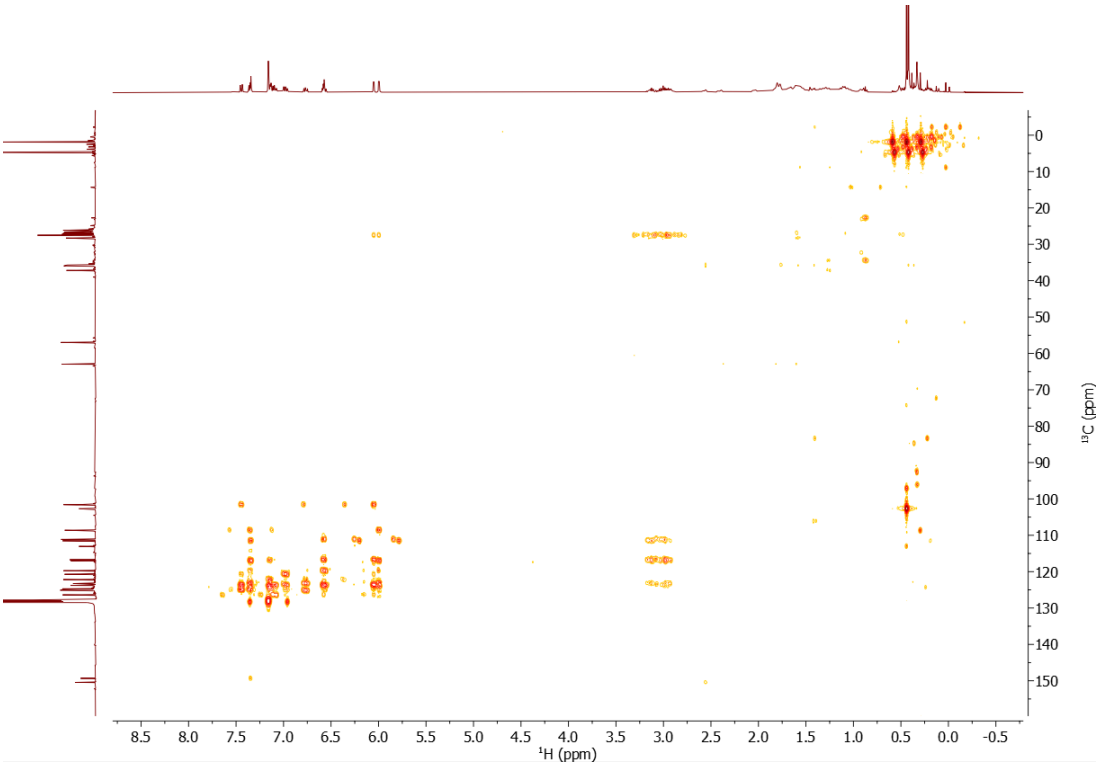

Figure S94. ^{1}H-^{13}C HMBC NMR spectrum of **P2c-Cy** (25 °C, benzene-*d*6, 400.1, 100.6 MHz).

7.14 NMR spectra of $P_{2d\text{-}Cy}$

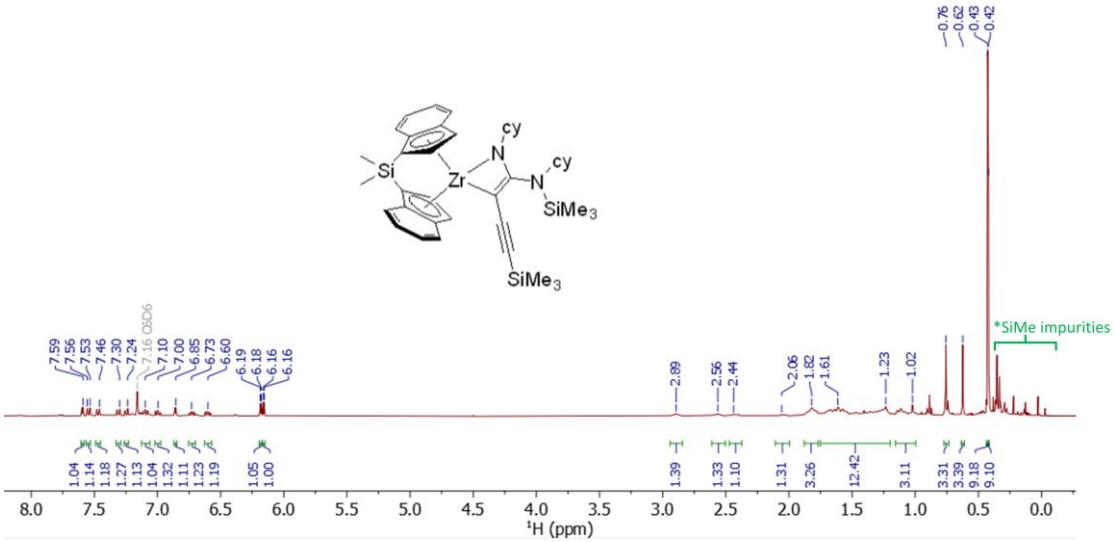

Figure S95. ^{1}H NMR spectrum of **$P_{2d\text{-}Cy}$** (25 °C, benzene-d_6, 400.1 MHz).

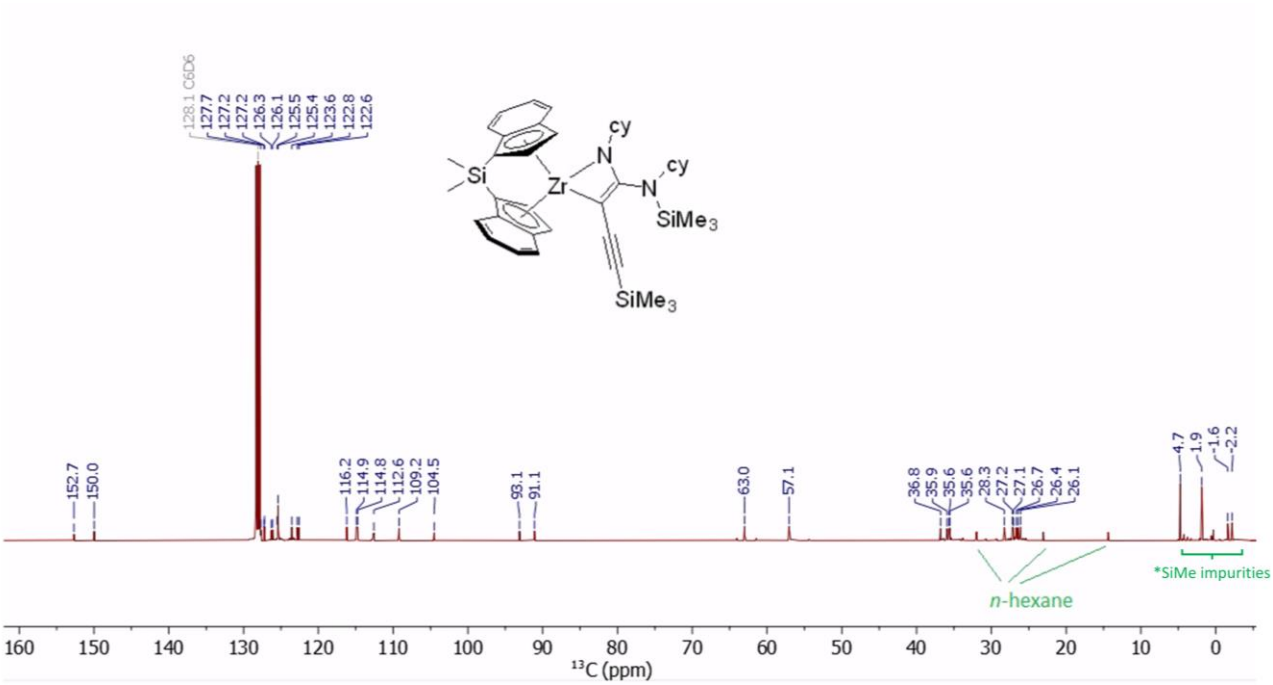

Figure S96. $^{13}C\{^{1}H\}$ NMR spectrum of **$P_{2d\text{-}Cy}$** (25 °C, benzene-d_6, 100.6 MHz).

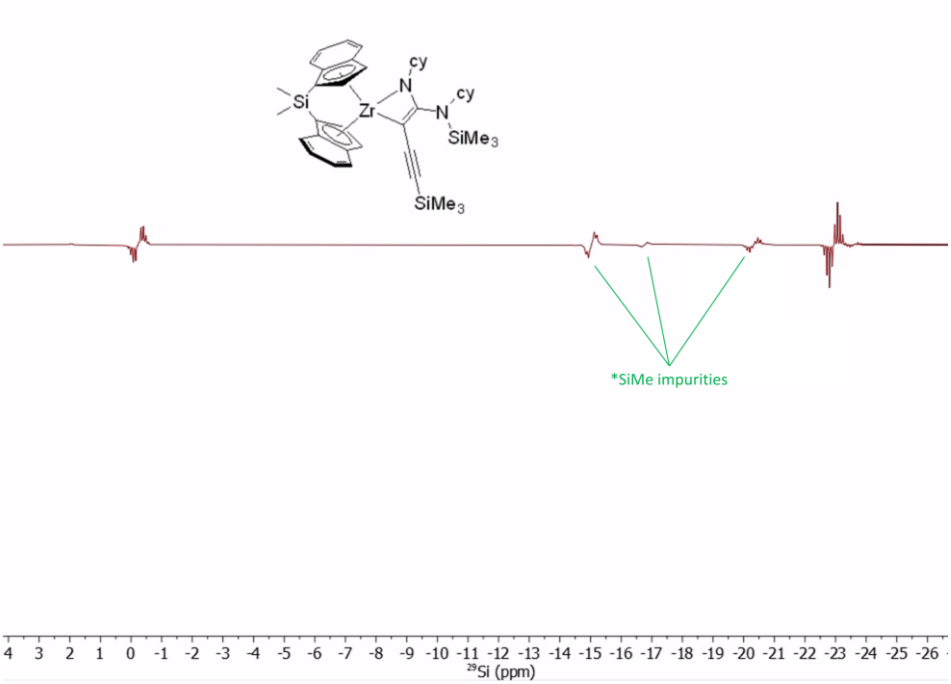

Figure S97. ^{29}Si INEPT NMR spectrum of **P2d-Cy** (25 °C, benzene-*d*6, 79.5 MHz).

7.15 NMR spectra of $P_{1a\text{-}p\text{-}Tol}$

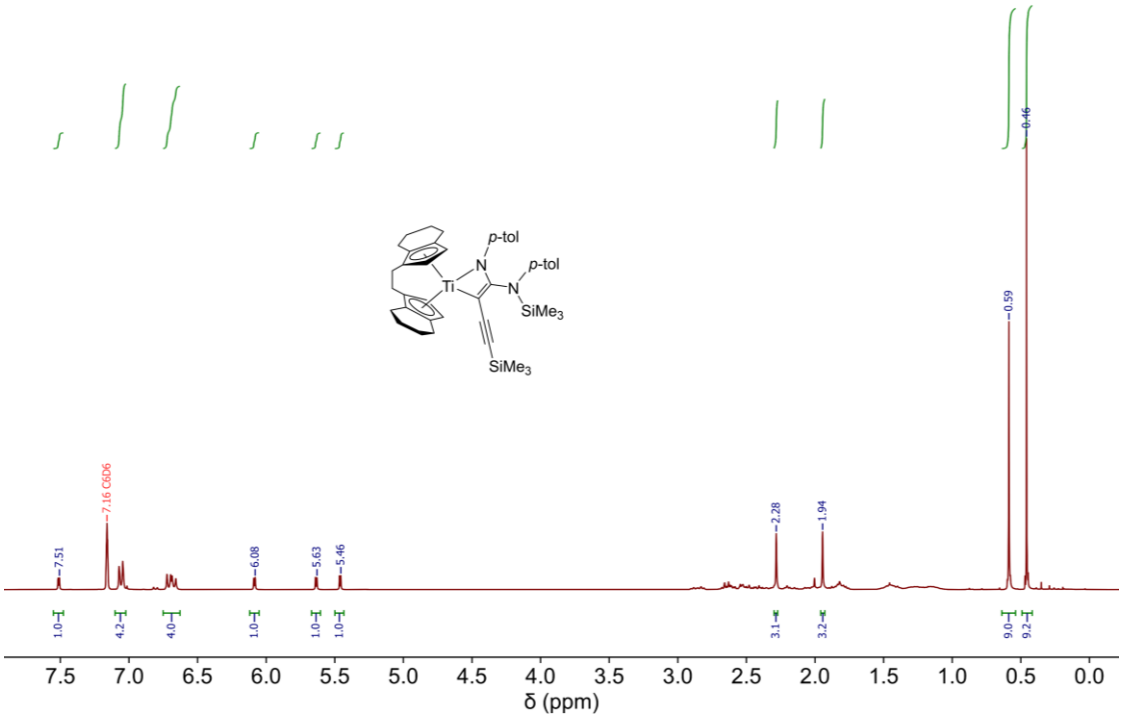

Figure S98. ^{1}H NMR spectrum of **$P_{1a\text{-}p\text{-}Tol}$** (25 °C, benzene-$d_6$, 400.1 MHz).

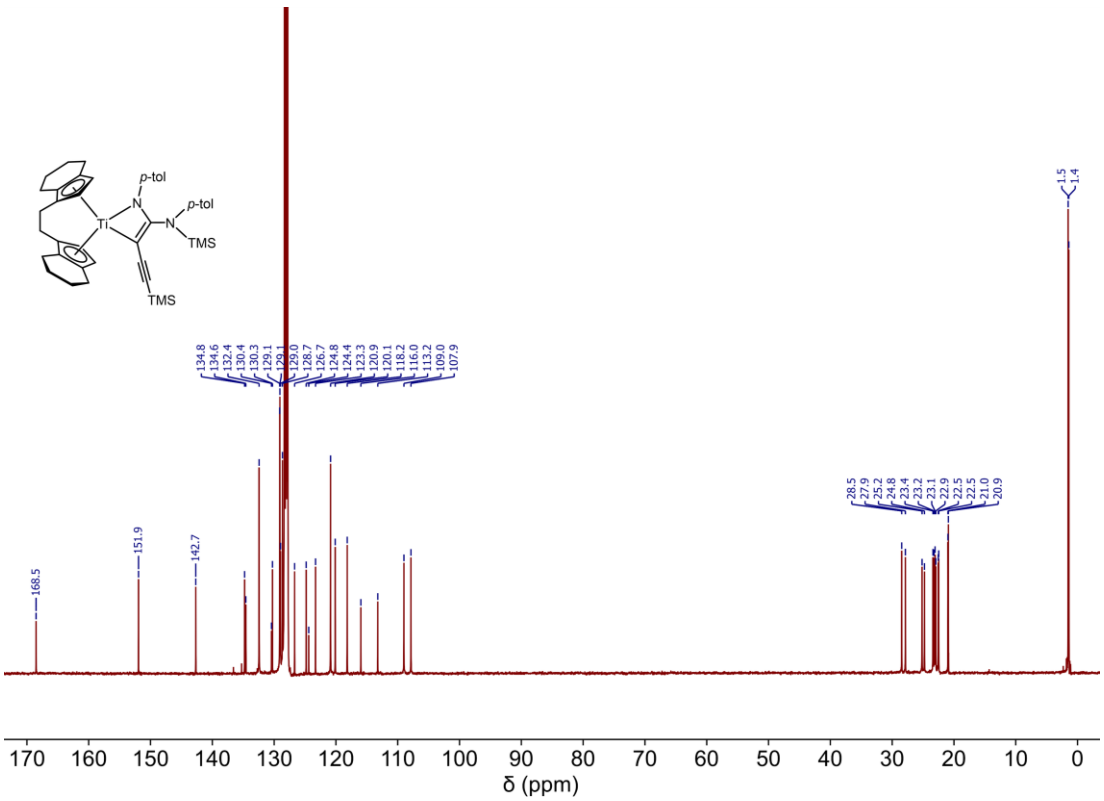

Figure S99. $^{13}C\{^{1}H\}$ NMR spectrum of **$P_{1a\text{-}p\text{-}Tol}$** (25 °C, benzene-$d_6$, 100.6 MHz).

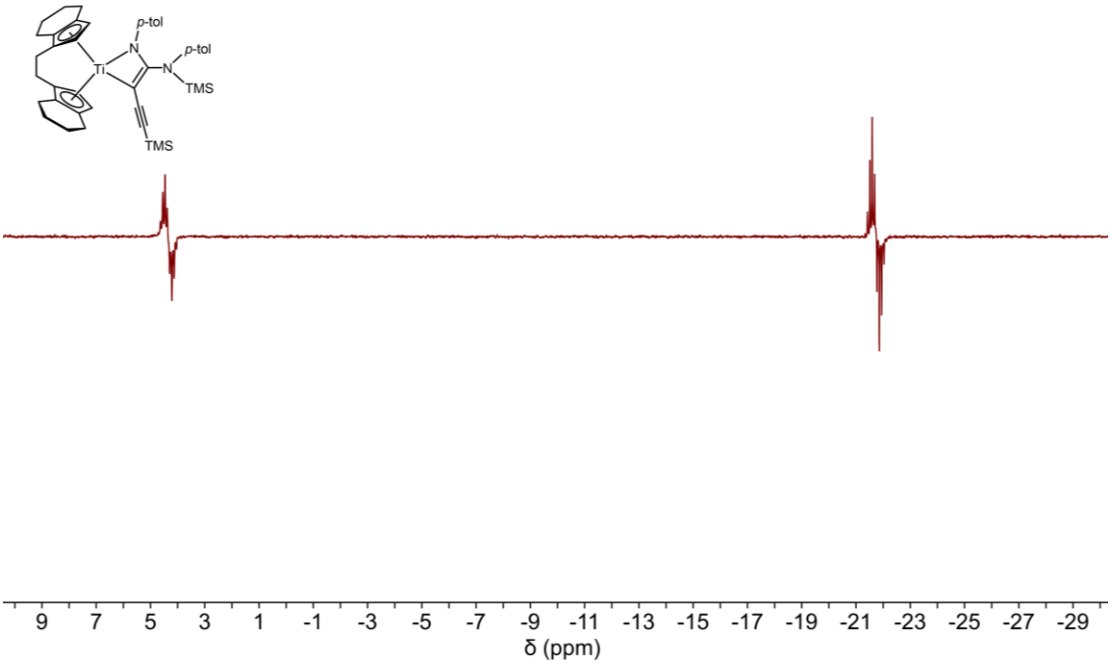

Figure S100. ^{29}Si INEPT NMR spectrum of **P1a-*p*-Tol** (25 °C, benzene-*d*6, 79.5 MHz).

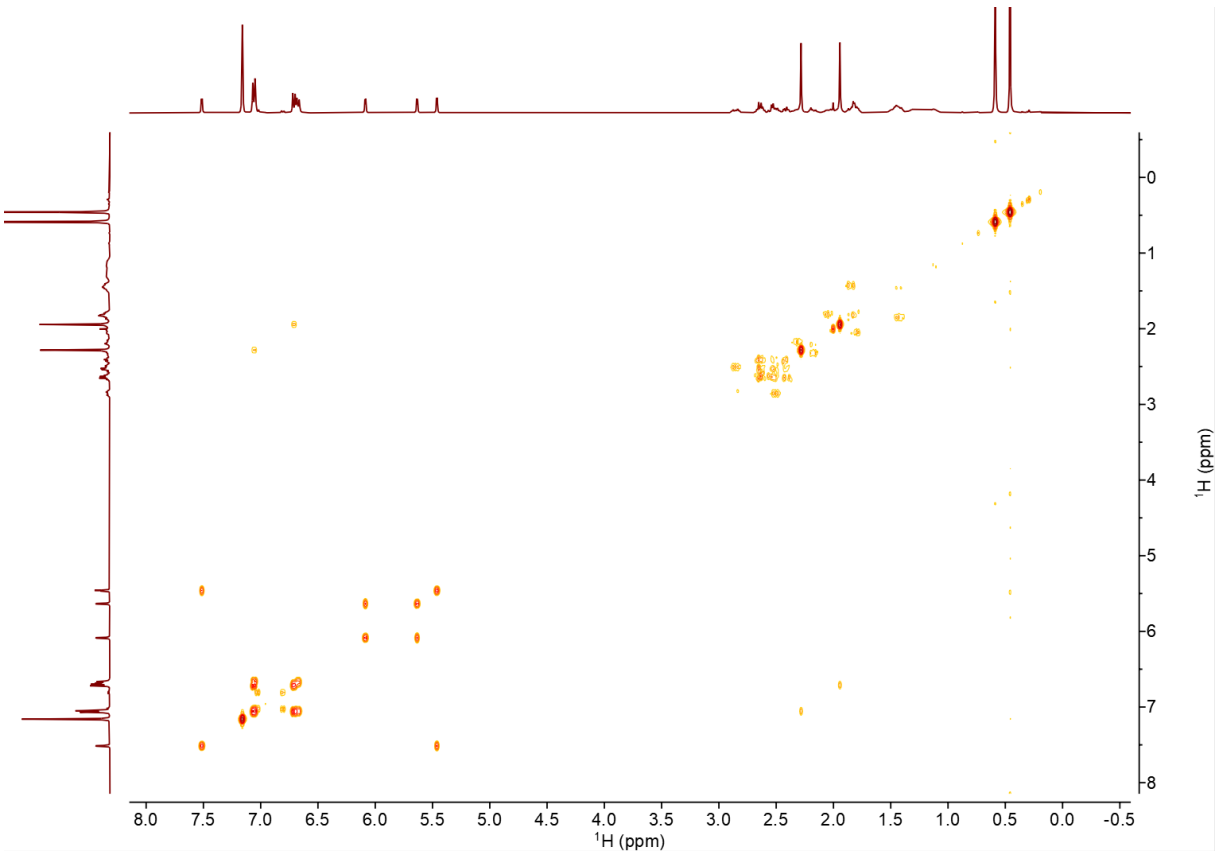

Figure S101. ^{1}H-^{1}H COSY NMR spectrum of **P1a-*p*-Tol** (25 °C, benzene-*d*6, 400.1, 400.1 MHz).

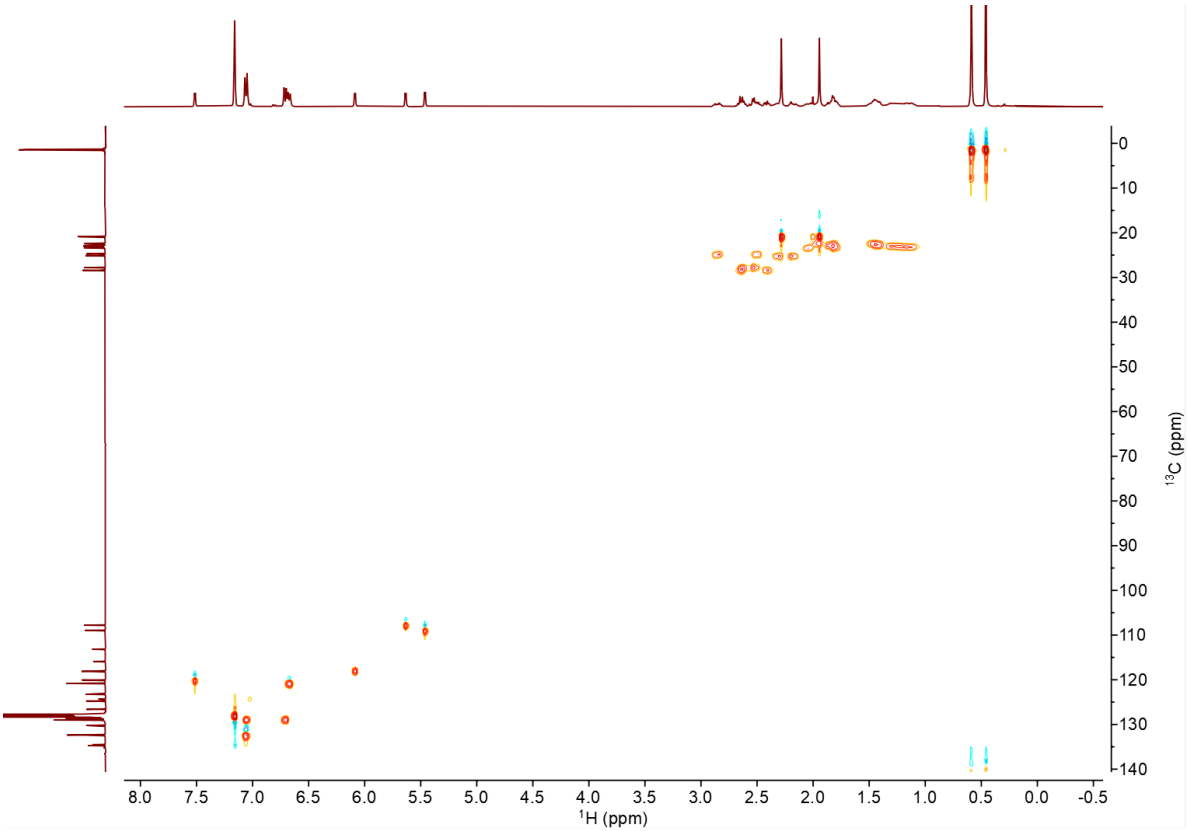

Figure S102. ^{1}H-^{13}C HSQC NMR spectrum of **P1a-*p*-Tol** (25 °C, benzene-*d*6, 400.1, 100.6 MHz).

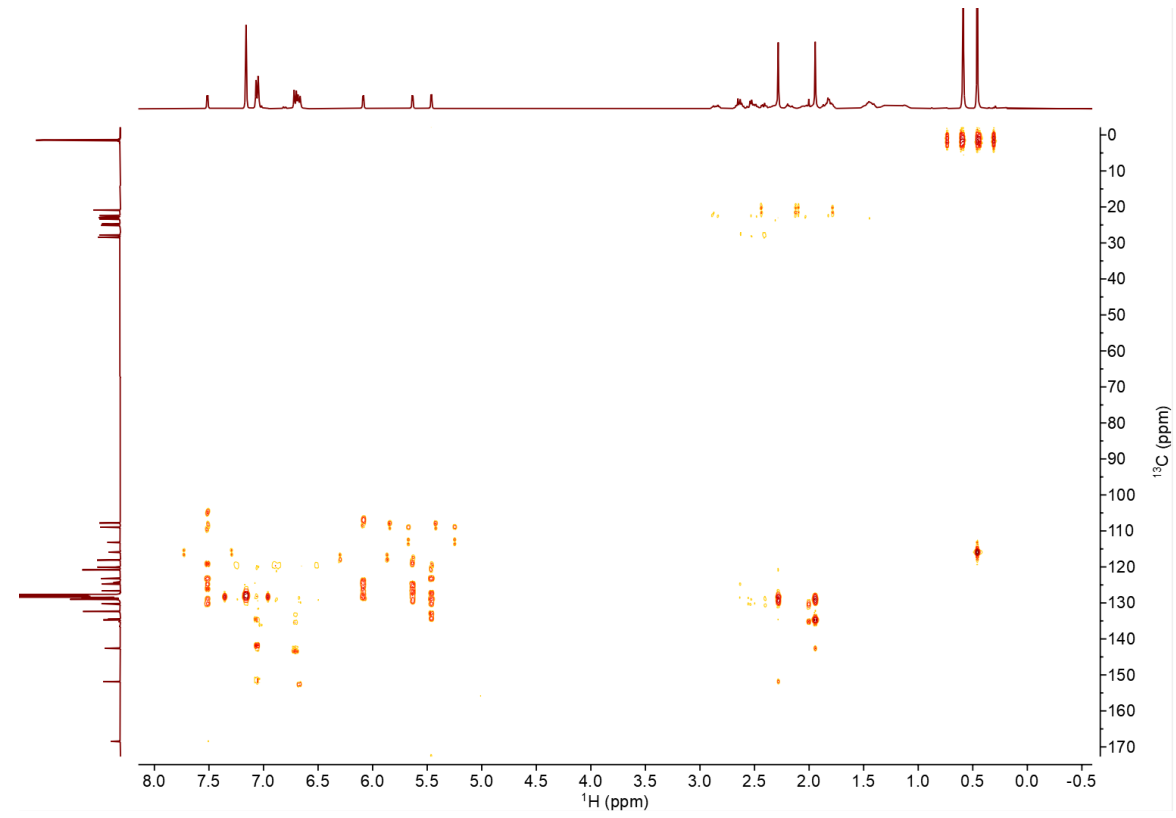

Figure S103. ^{1}H-^{13}C HMBC NMR spectrum of **P1a-*p*-Tol** (25 °C, benzene-*d*6, 400.1, 100.6 MHz).

7.16 NMR spectra of $P_{2a\text{-}p\text{-}Tol}$

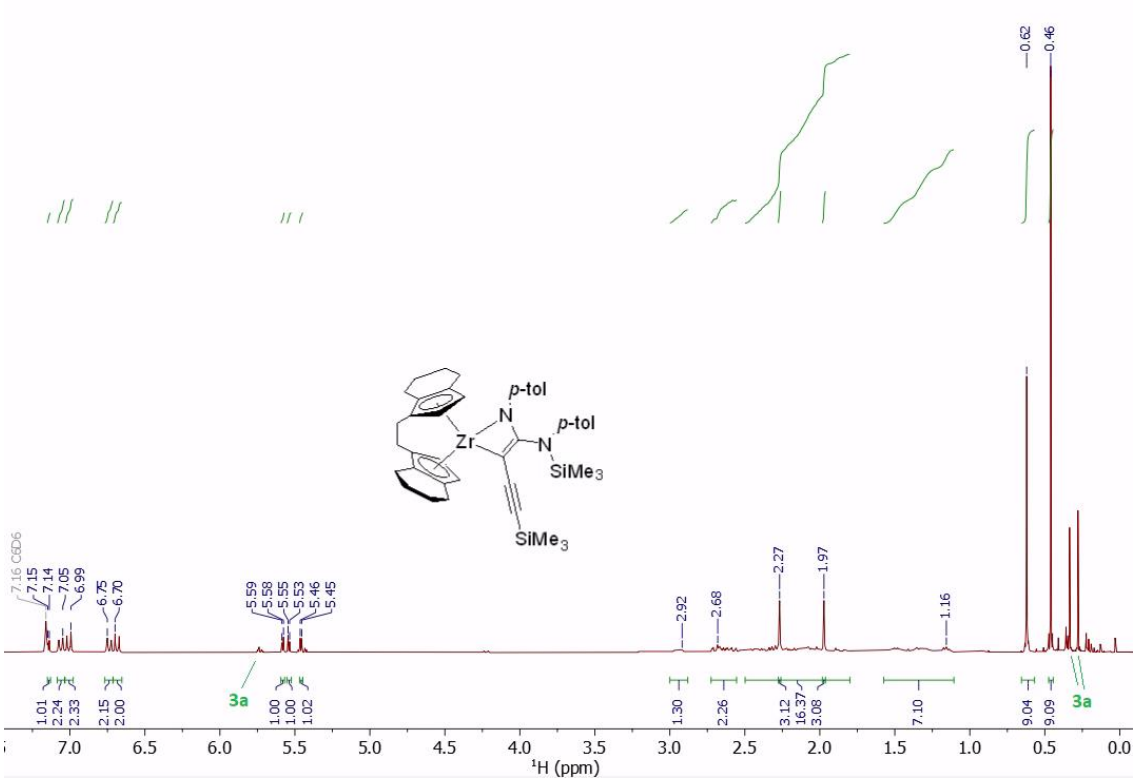

Figure S104. ^{1}H NMR spectrum of **$P_{2a\text{-}p\text{-}Tol}$** (Minor impurity of the propargyl complex **3a** was observed due to the slow conversion of **2a** to **3a** at room temperature; 25 °C, benzene-d_6, 400.1 MHz).

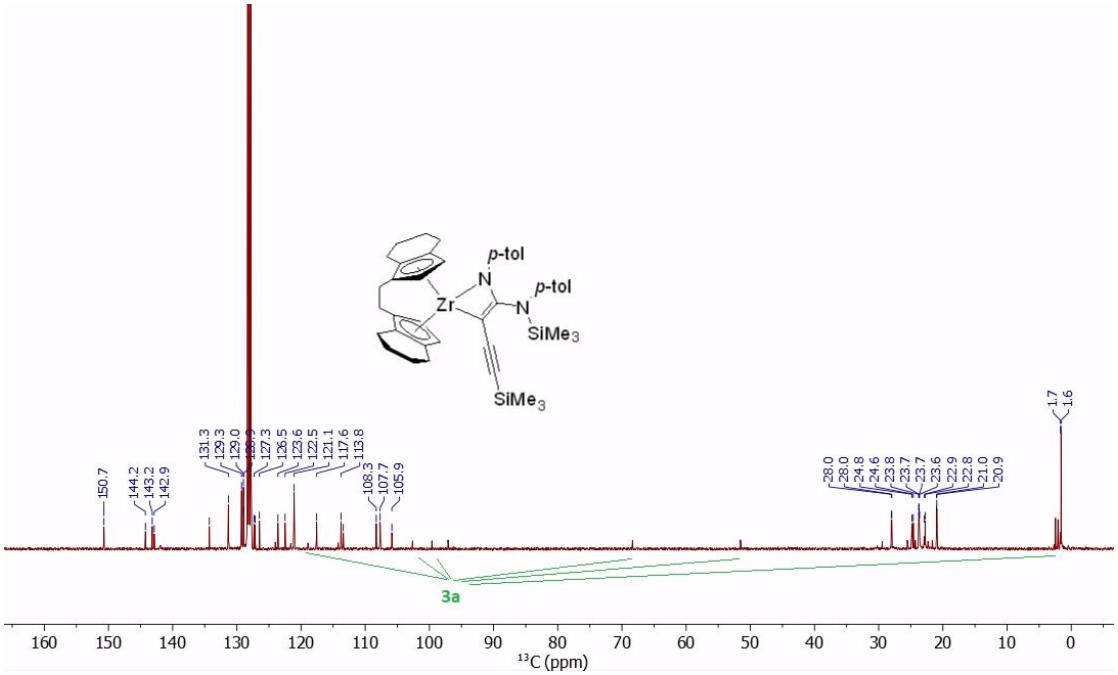

Figure S105. $^{13}C\{^{1}H\}$ NMR spectrum of **$P_{2a\text{-}p\text{-}Tol}$** (Minor impurity of the propargyl complex **3a** was observed due to the slow conversion of **2a** to **3a** at room temperature; 25 °C, benzene-d_6, 100.6 MHz).

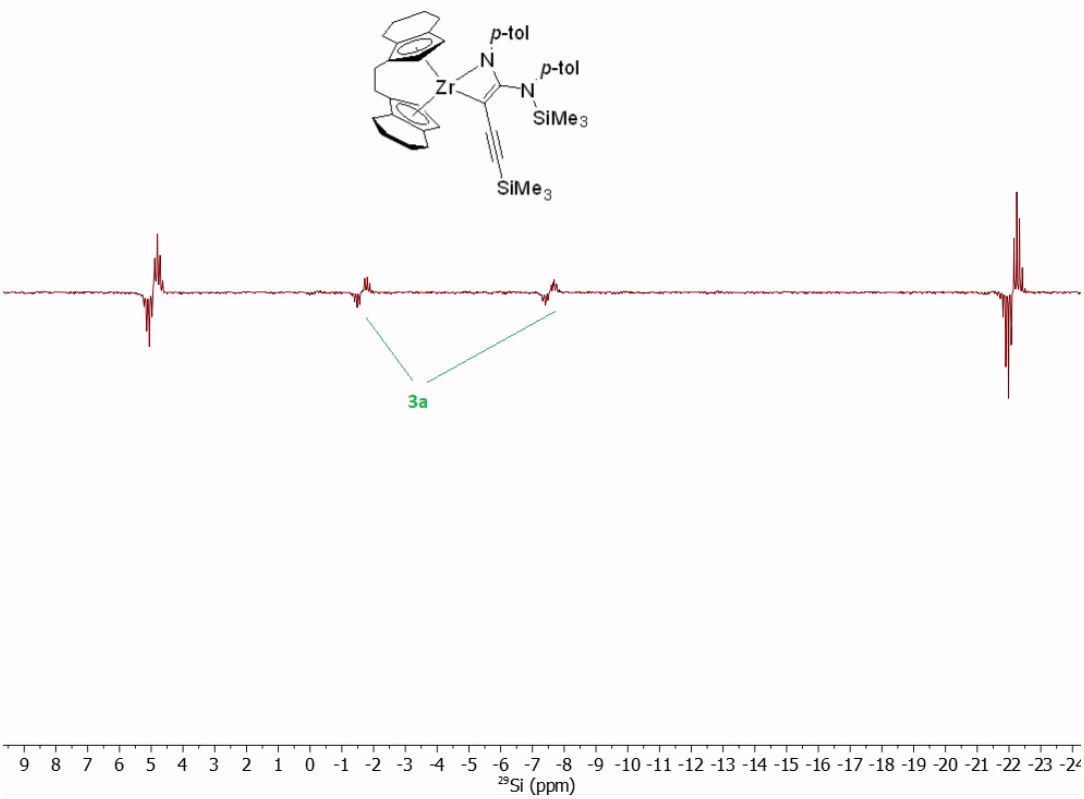

Figure S106. ^{29}Si INEPT NMR spectrum of **P2a-*p*-Tol** (Minor impurity of the propargyl complex **3a** was observed due to the slow conversion of **2a** to **3a** at room temperature; 25 °C, benzene-*d*6, 79.5 MHz).

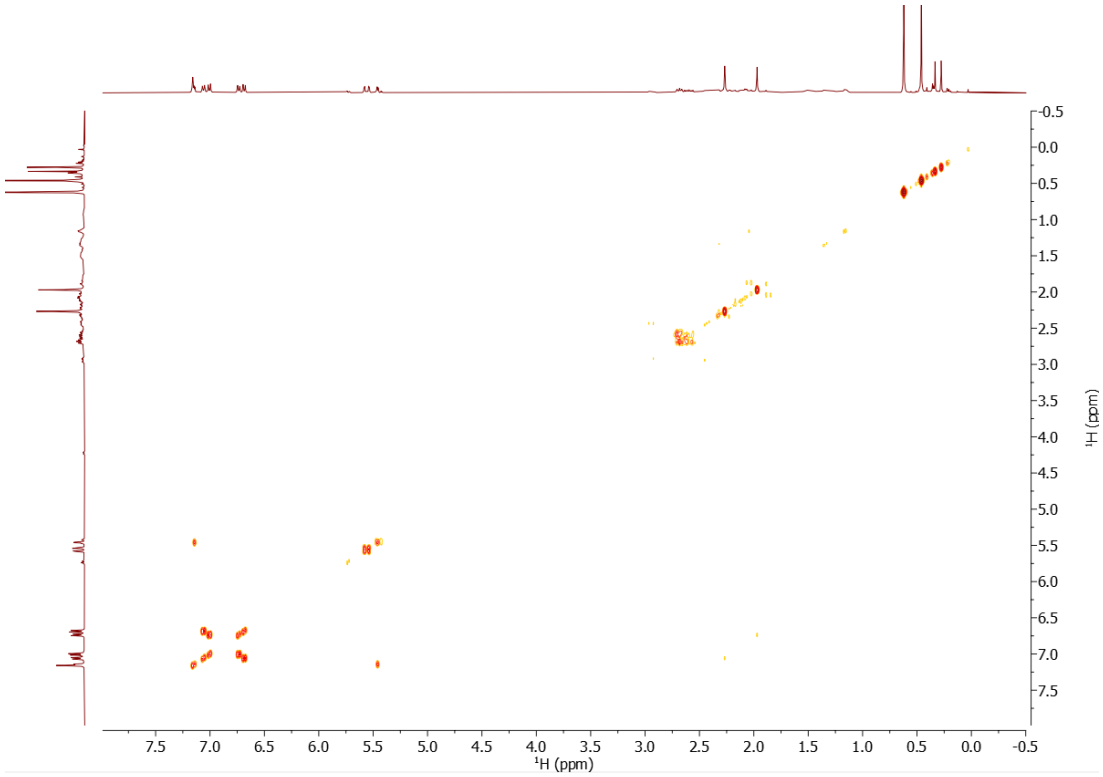

Figure S107. ^{1}H-^{1}H COSY NMR spectrum of **P2a-*p*-Tol** (25 °C, benzene-*d*6, 400.1, 400.1 MHz).

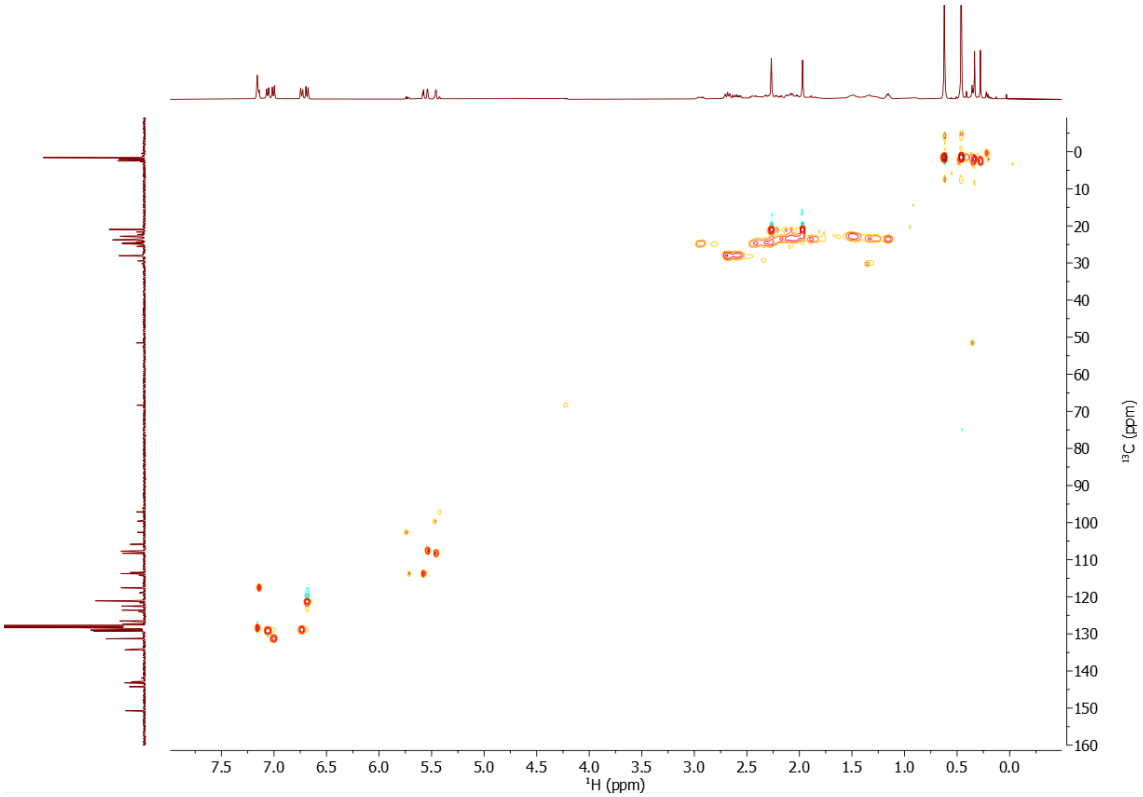

Figure S108. ^{1}H-^{13}C HSQC NMR spectrum of **P2a-*p*-Tol** (25 °C, benzene-*d*6, 400.1, 100.6 MHz).

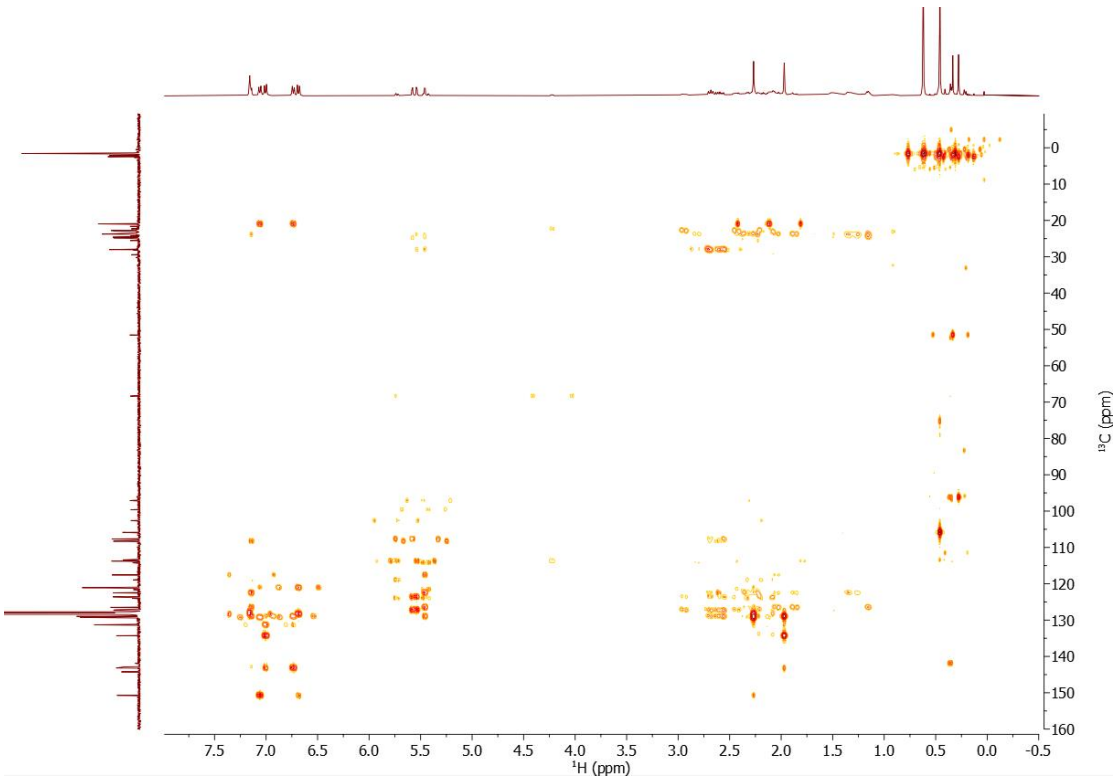

Figure S109. ^{1}H-^{13}C HMBC NMR spectrum of **P2a-*p*-Tol** (25 °C, benzene-*d*6, 400.1, 100.6 MHz).

7.17 NMR spectra of $P_{2b\text{-}p\text{-}Tol}$

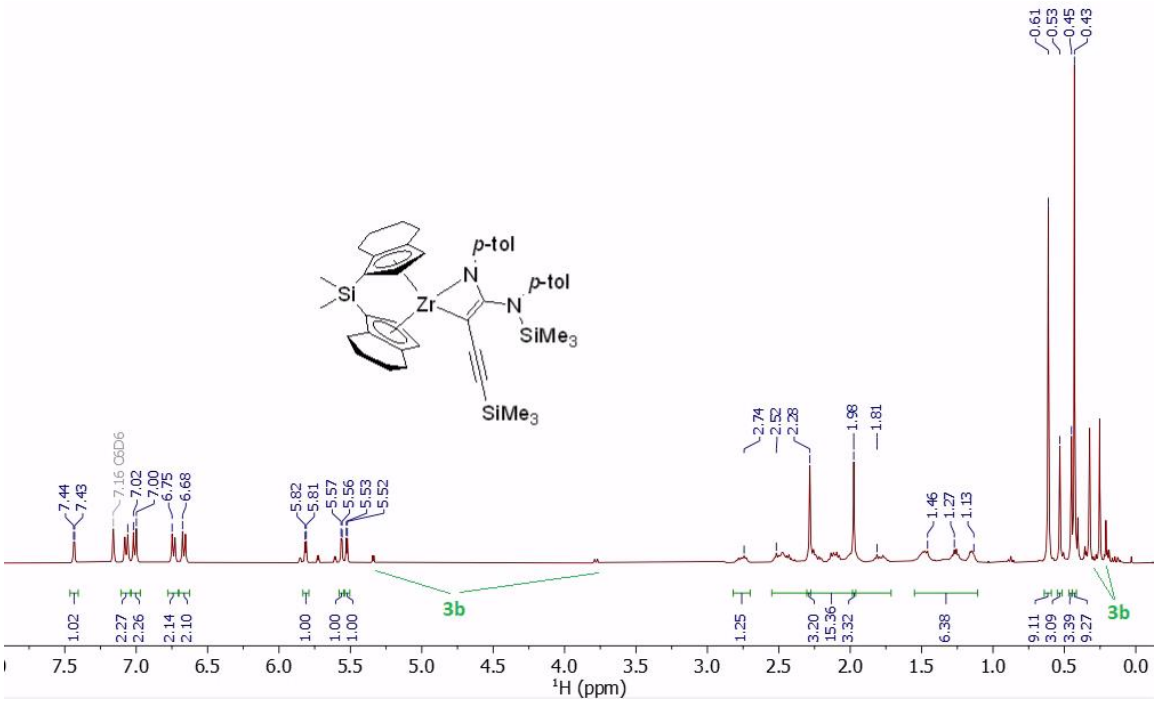

Figure S110. ^{1}H NMR spectrum of **$P_{2b\text{-}p\text{-}Tol}$** (Minor impurity of the propargyl complex **3b** was observed due to the slow conversion of **2b** to **3b** at room temperature; 25 °C, benzene-*d*6, 400.1 MHz).

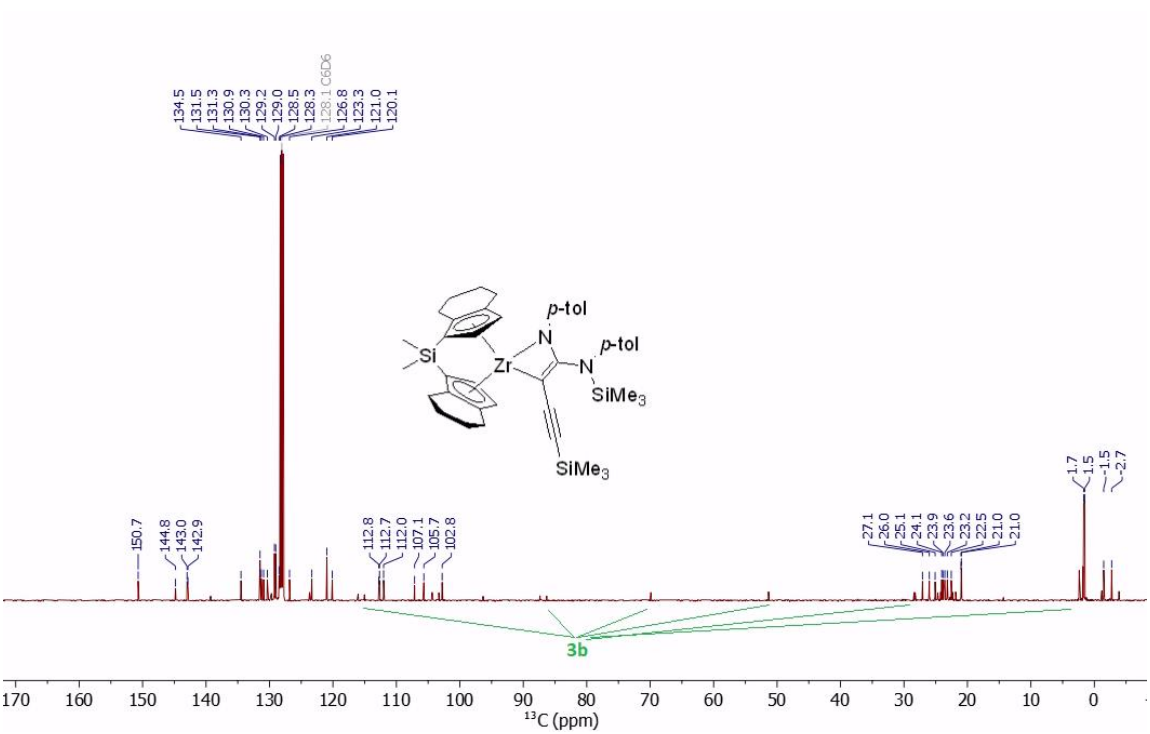

Figure S111. $^{13}C\{^{1}H\}$ NMR spectrum of **$P_{2b\text{-}p\text{-}Tol}$** (Minor impurity of the propargyl complex **3b** was observed due to the slow conversion of **2b** to **3b** at room temperature; 25 °C, benzene-*d*6, 100.6 MHz).

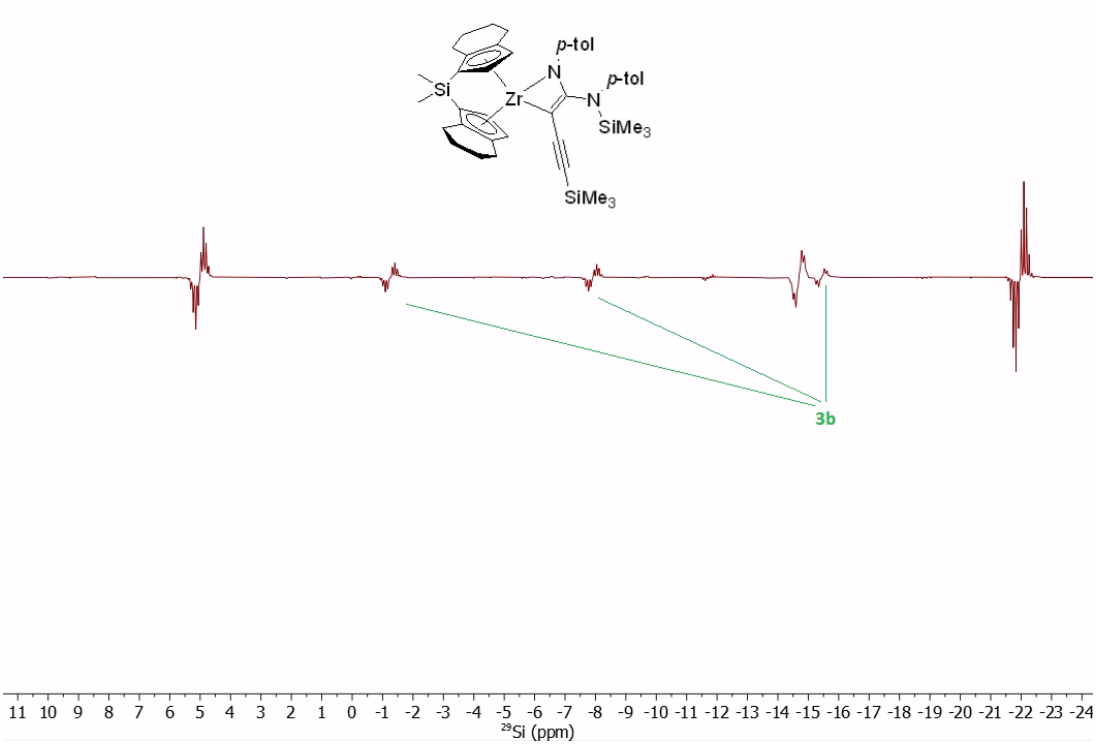

Figure S112. ^{29}Si INEPT NMR spectrum of **P2b-*p*-Tol** (Minor impurity of the propargyl complex **3b** was observed due to the slow conversion of **2b** to **3b** at room temperature; 25 °C, benzene-*d*6, 79.5 MHz).

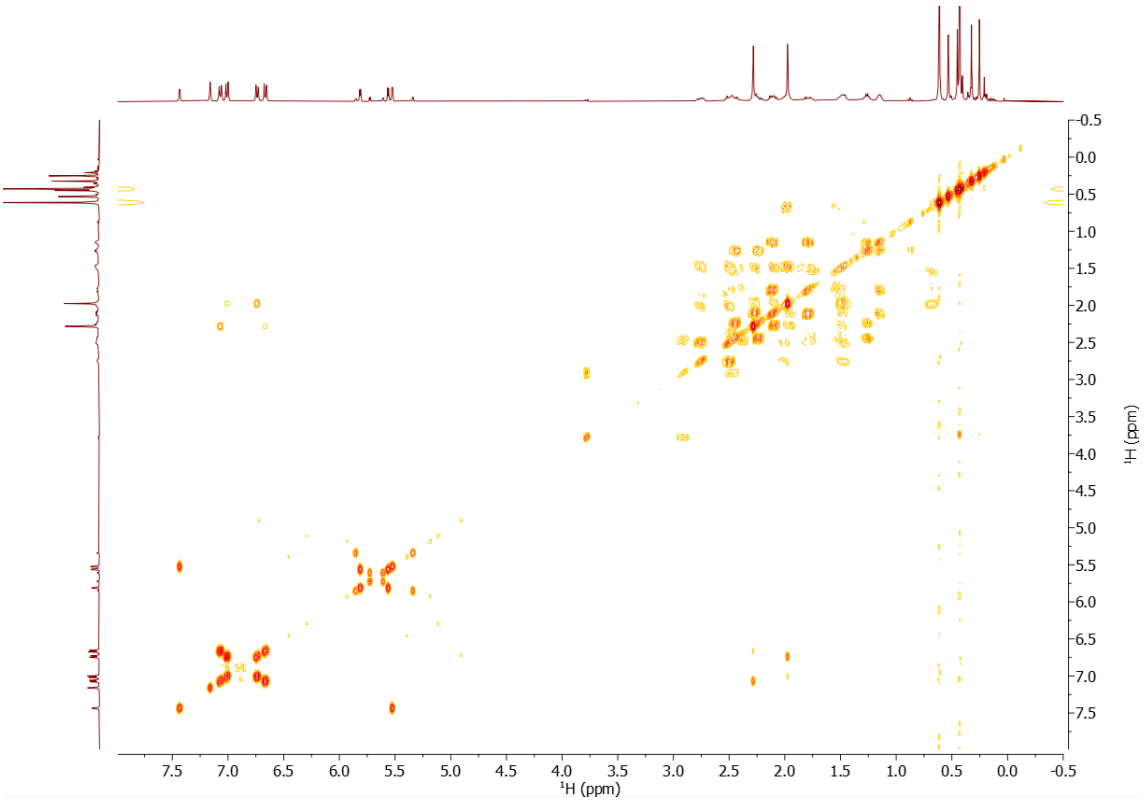

Figure S113. ^{1}H-^{1}H COSY NMR spectrum of **P2b-*p*-Tol** (Minor impurity of the propargyl complex **3b** was observed due to the slow conversion of **2b** to **3b** at room temperature; 25 °C, benzene-*d*6, 400.1, 400.1 MHz).

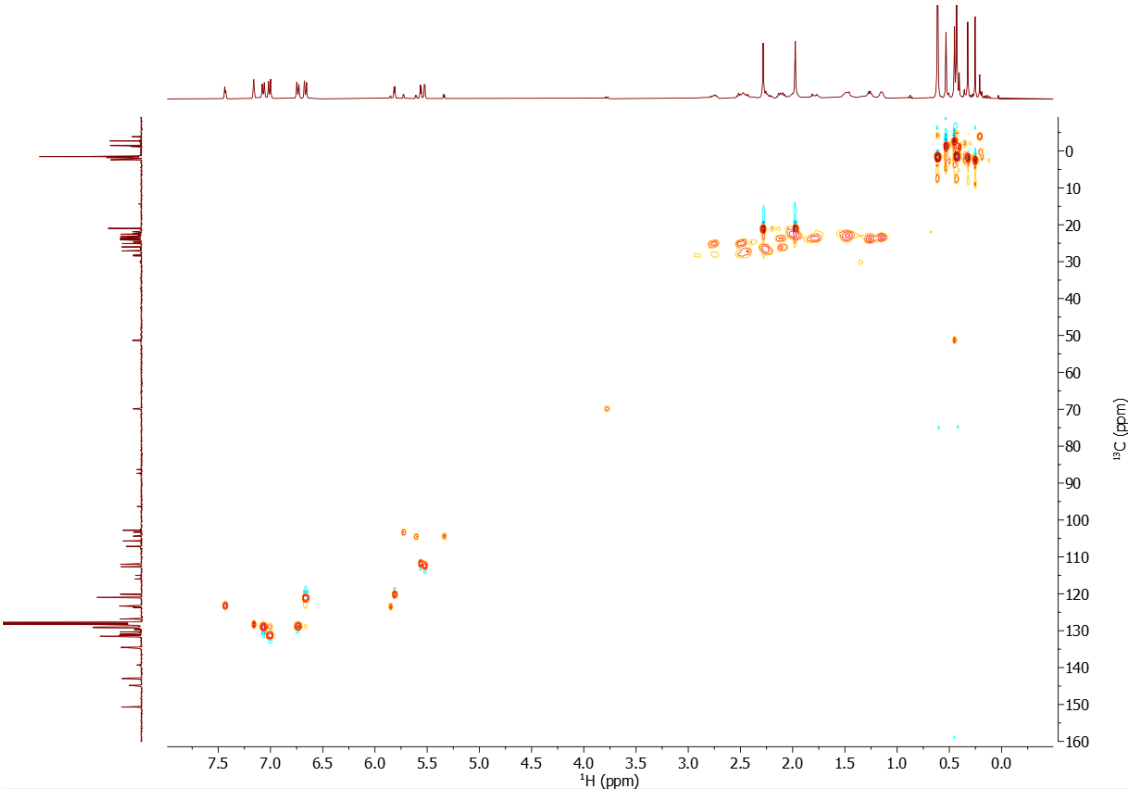

Figure S114. ^{1}H-^{13}C HSQC NMR spectrum of **P2b-*p*-Tol** (Minor impurity of the propargyl complex **3b** was observed due to the slow conversion of **2b** to **3b** at room temperature; 25 °C, benzene-*d*6, 400.1, 100.6 MHz).

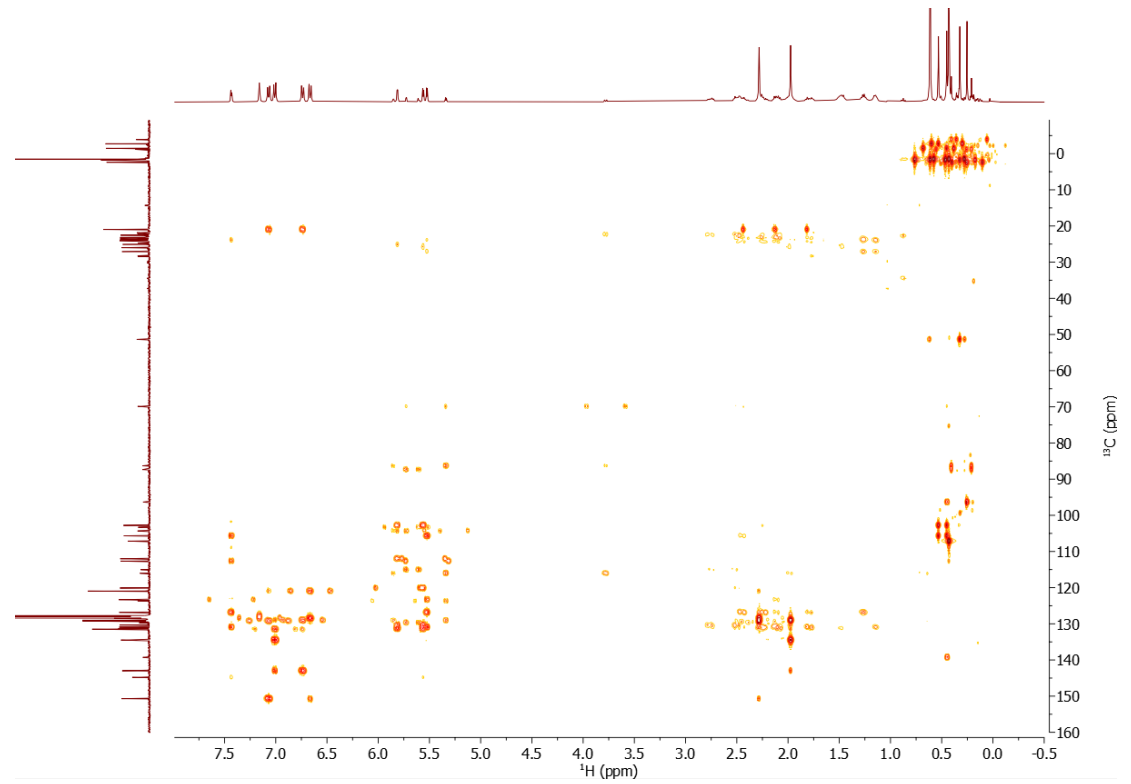

Figure S115. ^{1}H-^{13}C HMBC NMR spectrum of **P2b-*p*-Tol** (Minor impurity of the propargyl complex **3b** was observed due to the slow conversion of **2b** to **3b** at room temperature; 25 °C, benzene-*d*6, 400.1, 100.6 MHz).

7.18 NMR spectra of $P_{2c\text{-}p\text{-}Tol}$

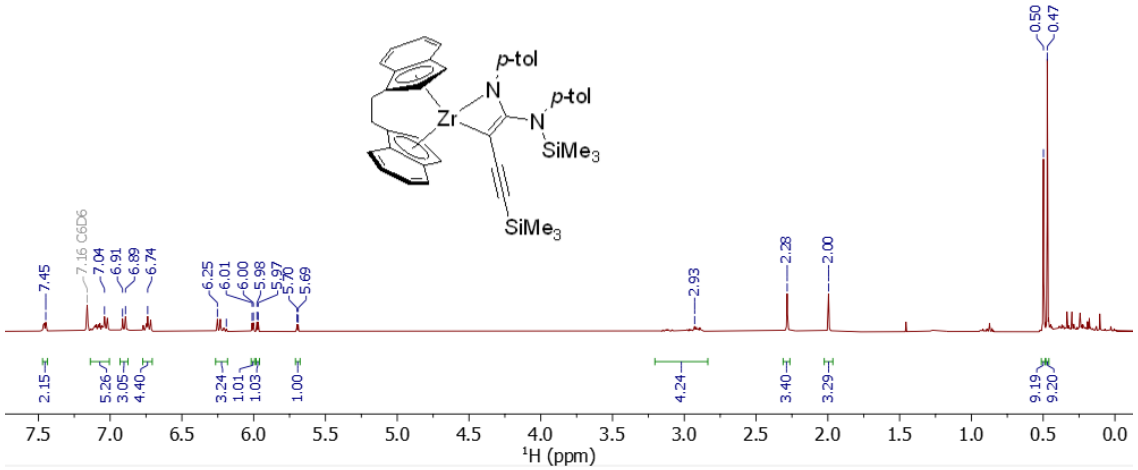

Figure S116. ^{1}H NMR spectrum of **$P_{2c\text{-}p\text{-}Tol}$** (25 °C, benzene-$d_6$, 400.1 MHz).

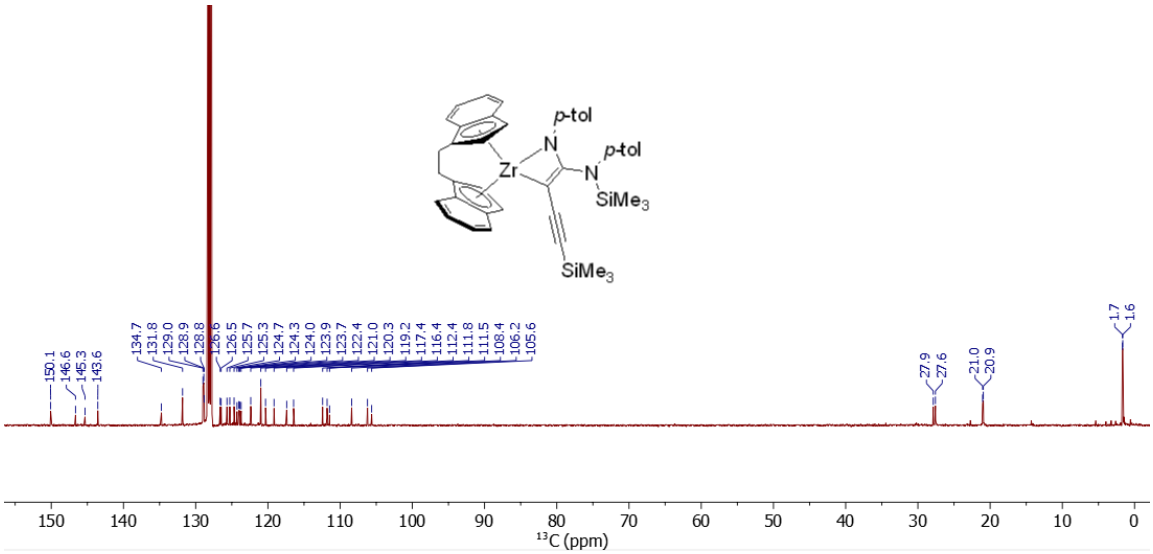

Figure S117. $^{13}C\{^{1}H\}$ NMR spectrum of **$P_{2c\text{-}p\text{-}Tol}$** (25 °C, benzene-$d_6$, 100.6 MHz).

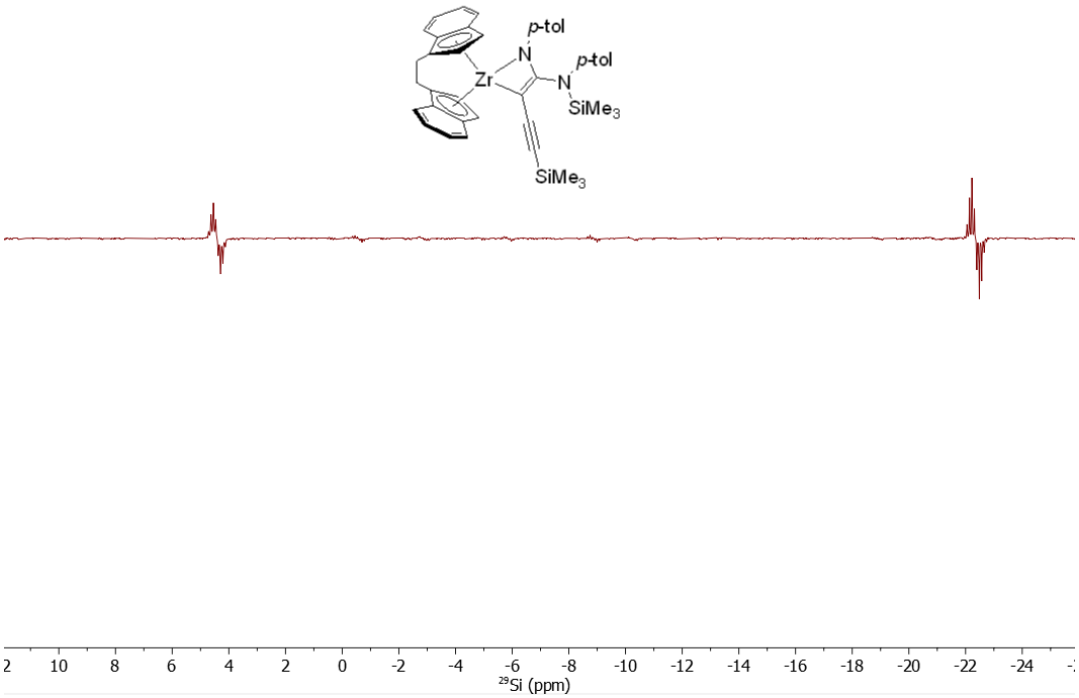

Figure S118. ^{29}Si INEPT NMR spectrum of **P2c-*p*-Tol** (25 °C, benzene-*d*6, 79.5 MHz).

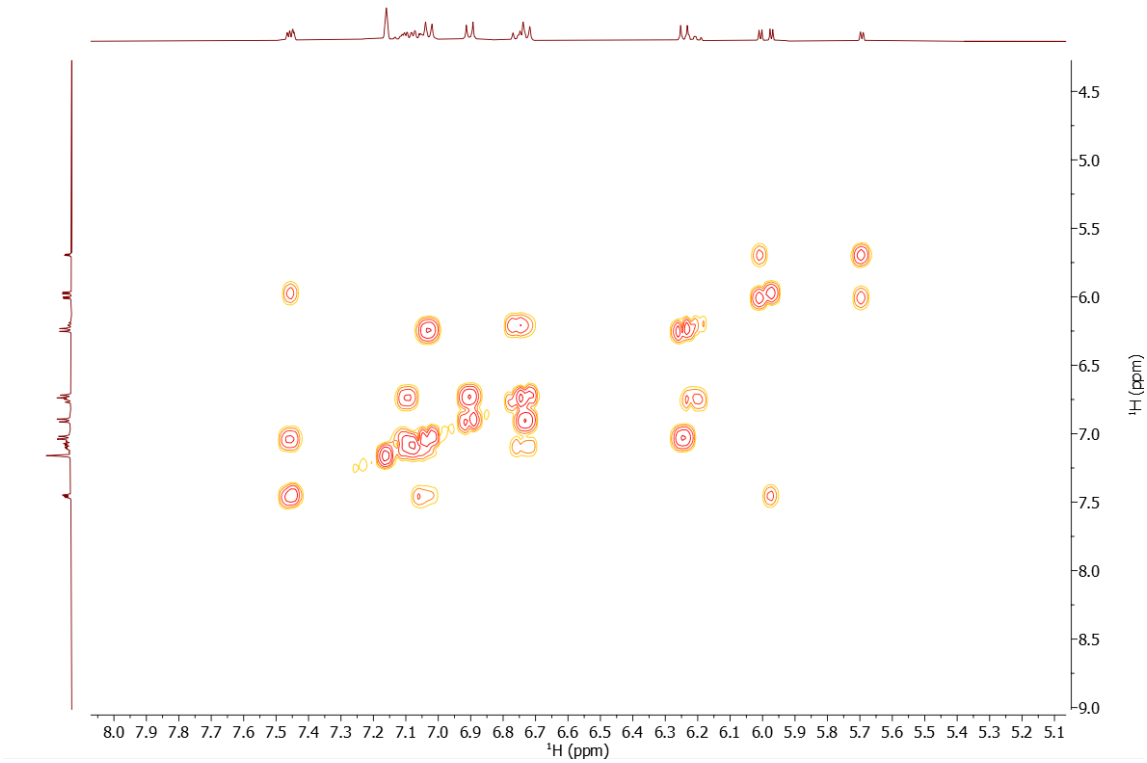

Figure S119. ^{1}H-^{1}H COSY NMR spectrum of **P2c-*p*-Tol** (25 °C, benzene-*d*6, 400.1, 400.1 MHz). For clarity only the low-field region is shown.

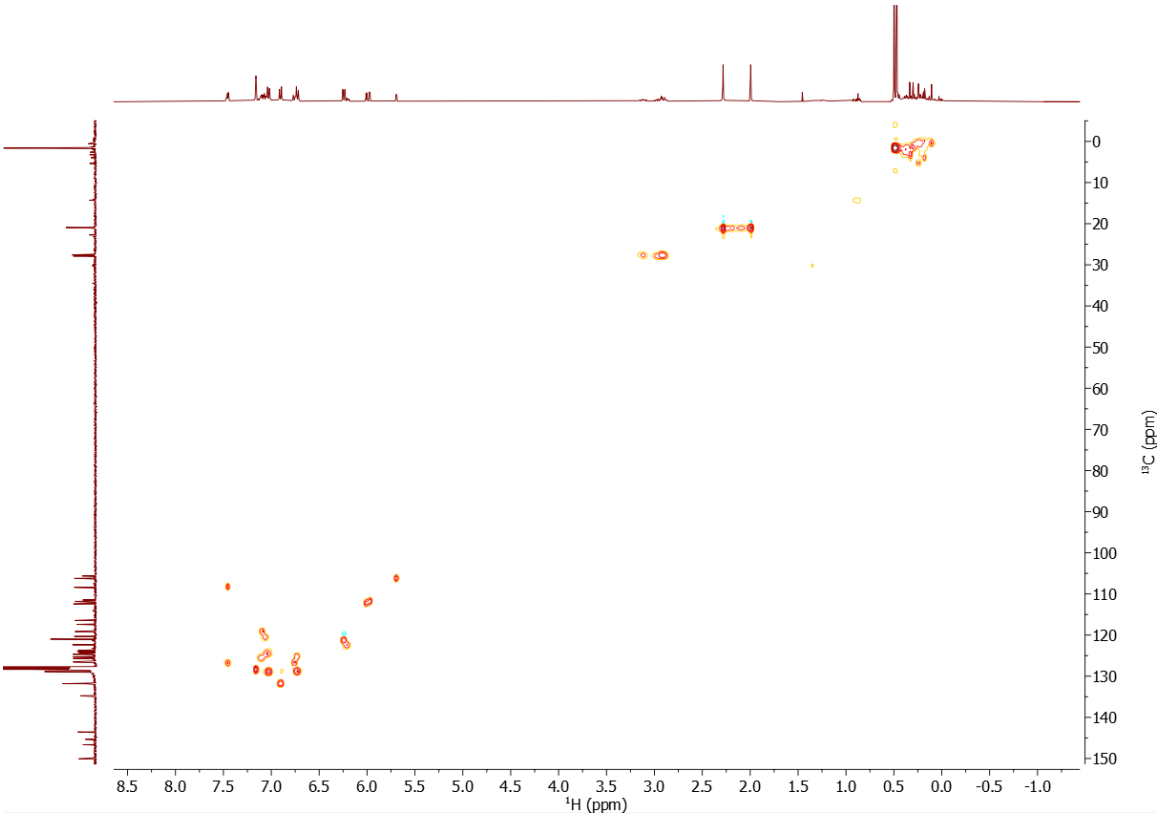

Figure S120. ^{1}H-^{13}C HSQC NMR spectrum of **P2c-*p*-Tol** (25 °C, benzene-*d*6, 400.1, 100.6 MHz).

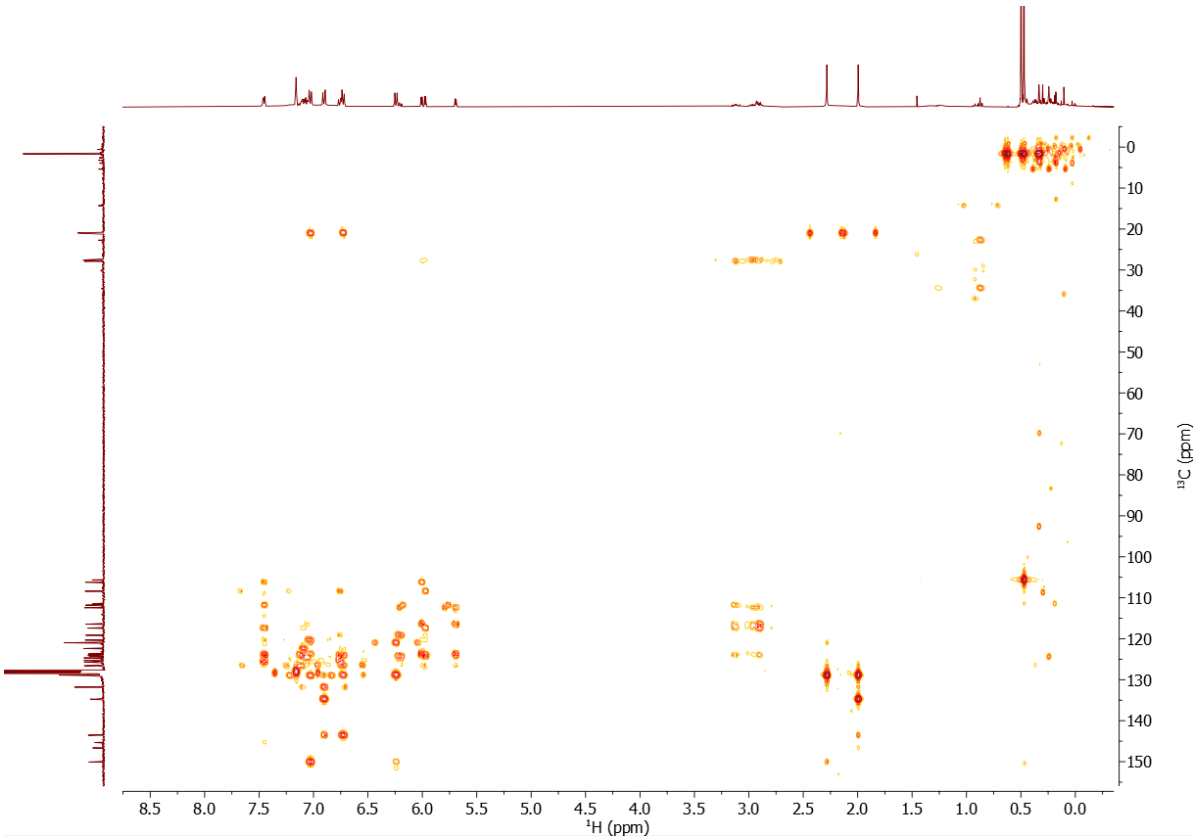

Figure S121. ^{1}H-^{13}C HMBC NMR spectrum of **P2c-*p*-Tol** (25 °C, benzene-*d*6, 400.1, 100.6 MHz).

7.19 NMR spectra of $P_{2d\text{-}p\text{-}Tol}$

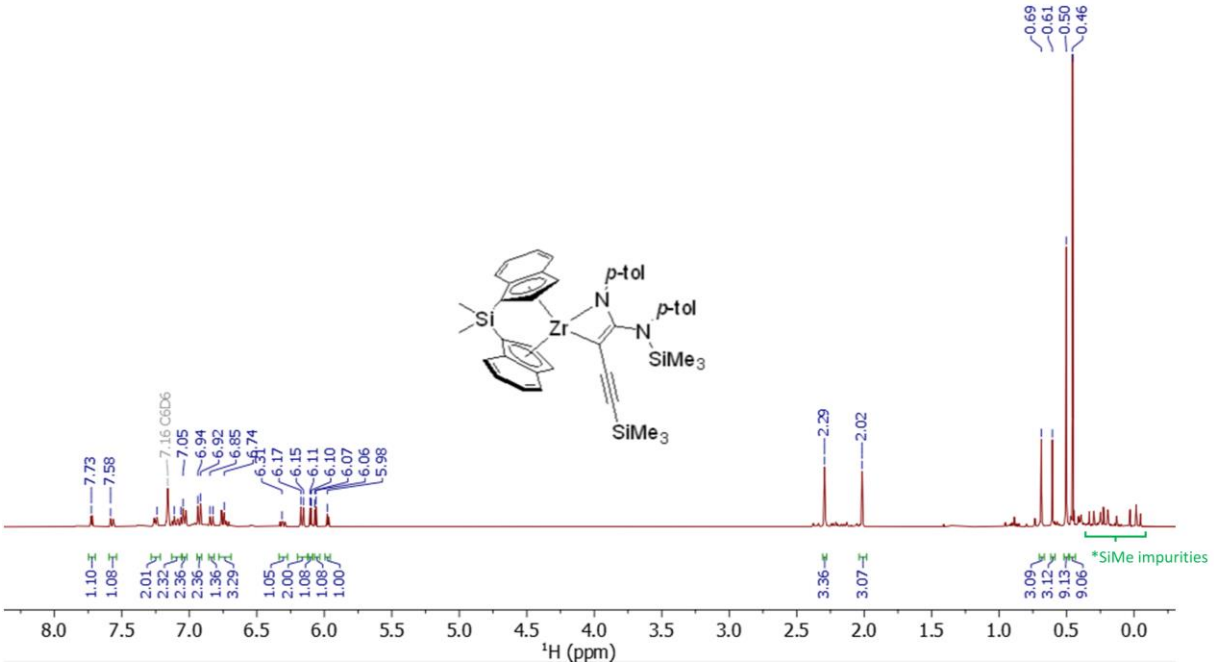

Figure S122. ^{1}H NMR spectrum of **$P_{2d\text{-}p\text{-}Tol}$** (25 °C, benzene-$d_6$, 400.1 MHz).

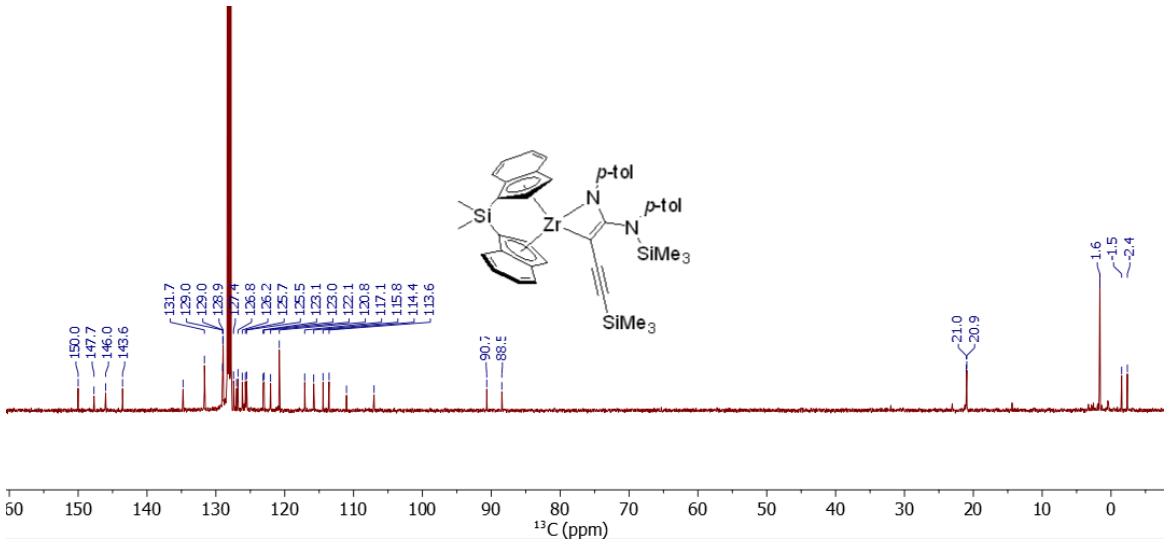

Figure S123. $^{13}C\{^{1}H\}$ NMR spectrum of **$P_{2d\text{-}p\text{-}Tol}$** (25 °C, benzene-$d_6$, 100.6 MHz).

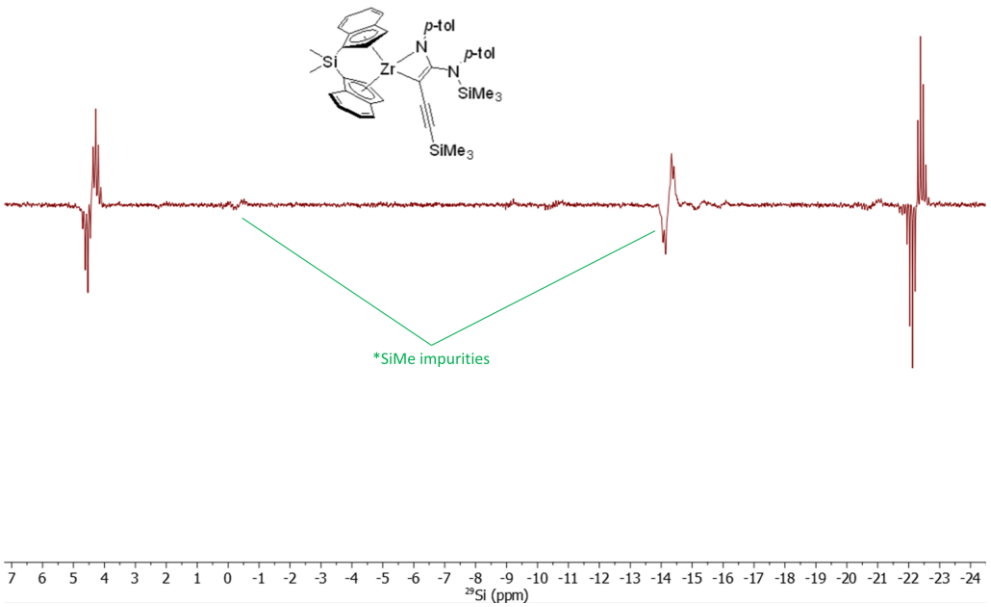

Figure S124. ^{29}Si INEPT NMR spectrum of **P2d-*p*-Tol** (25 °C, benzene-*d*6, 79.5 MHz).

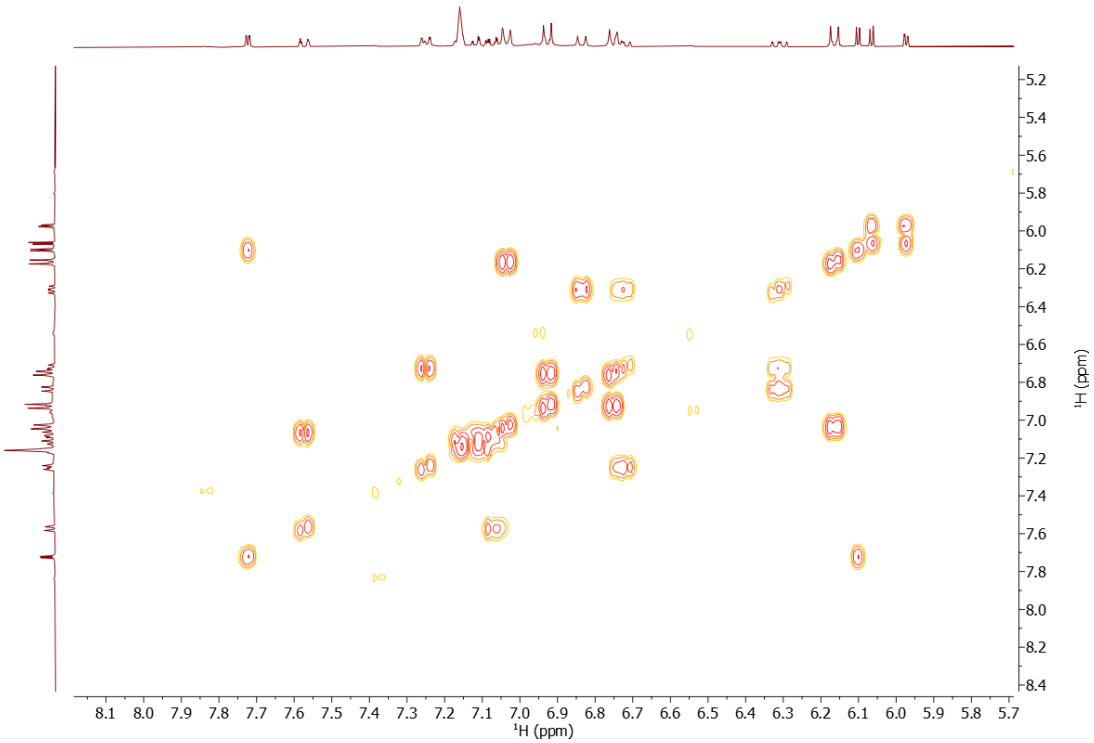

Figure S125. ^{1}H-^{1}H COSY NMR spectrum of **P2d-*p*-Tol** (25 °C, benzene-*d*6, 400.1, 400.1 MHz). For clarity only the low-field region is shown.

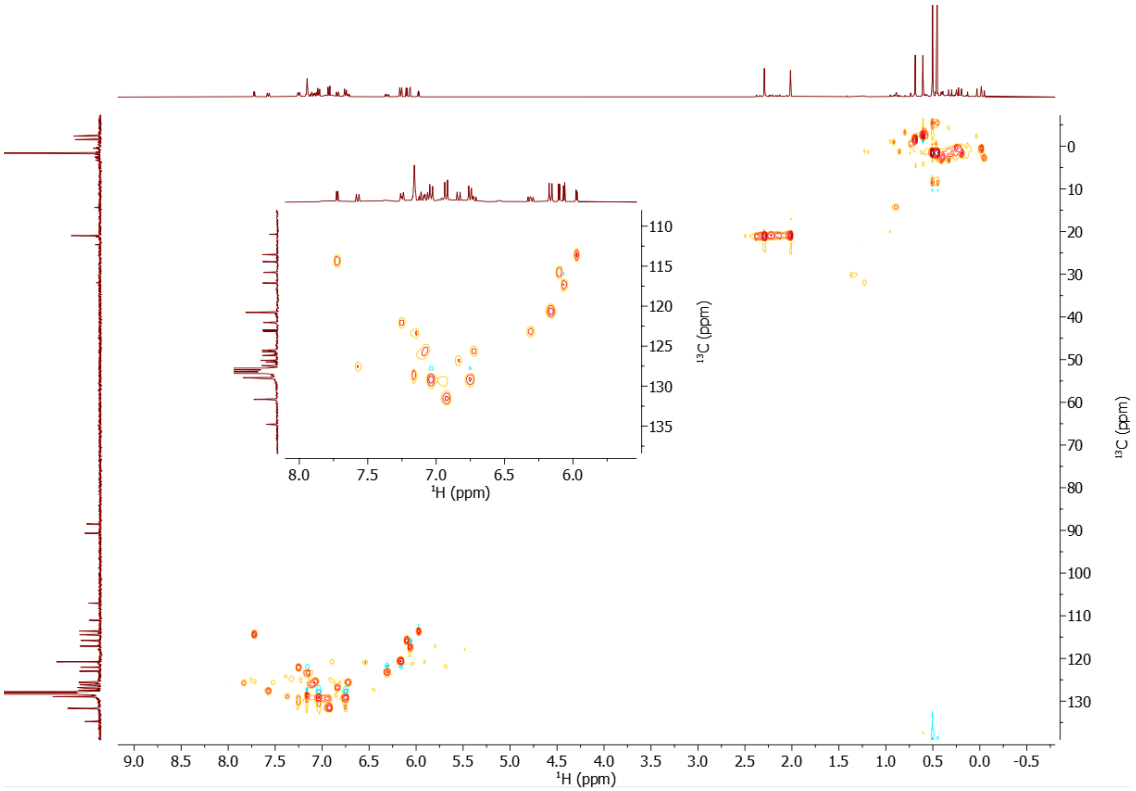

Figure S126. ^{1}H-^{13}C HSQC NMR spectrum of **P2d-*p*-Tol** (25 °C, benzene-*d*6, 400.1, 100.6 MHz).

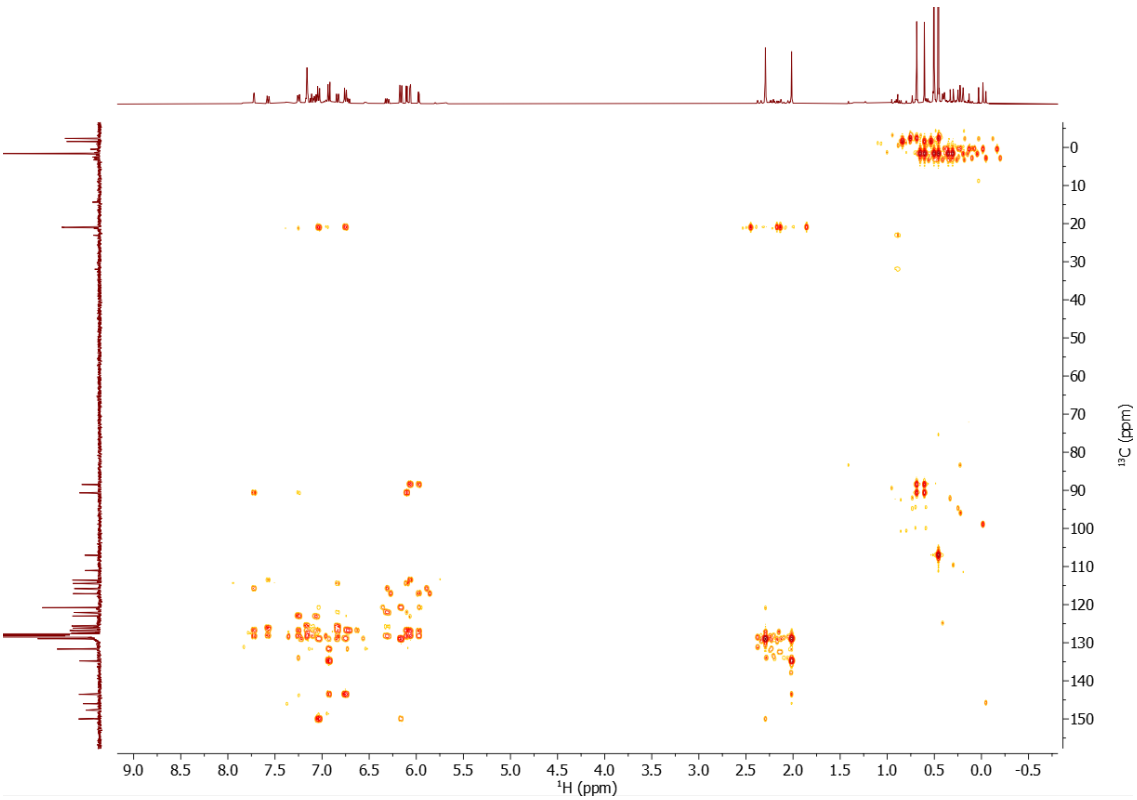

Figure S127. ^{1}H-^{13}C HMBC NMR spectrum of **P2d-*p*-Tol** (25 °C, benzene-*d*6, 400.1, 100.6 MHz).

7.20 NMR spectra of $P_{2c\text{-}SiMe3}$

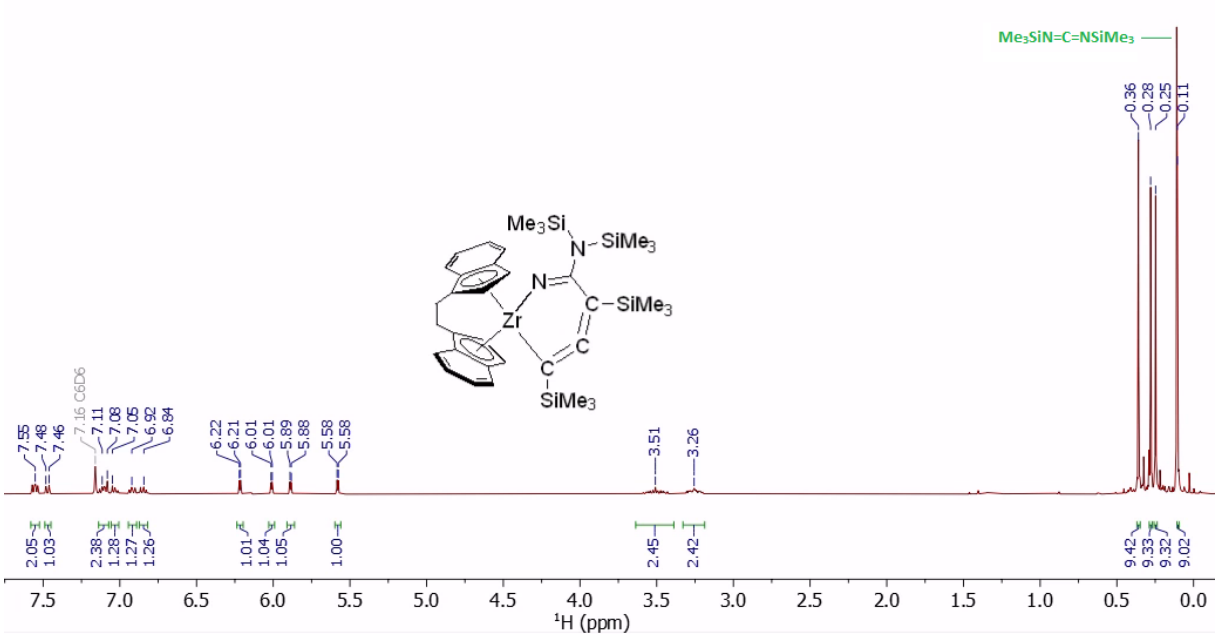

Figure S128. ^{1}H NMR spectrum of **$P_{2c\text{-}SiMe3}$** (Minor impurity of $Me_3SiN{=}C{=}NSiMe_3$ was generally observed as it was used to stabilise **$P_{2c\text{-}SiMe3}$**; 25 °C, benzene-d_6, 400.1 MHz).

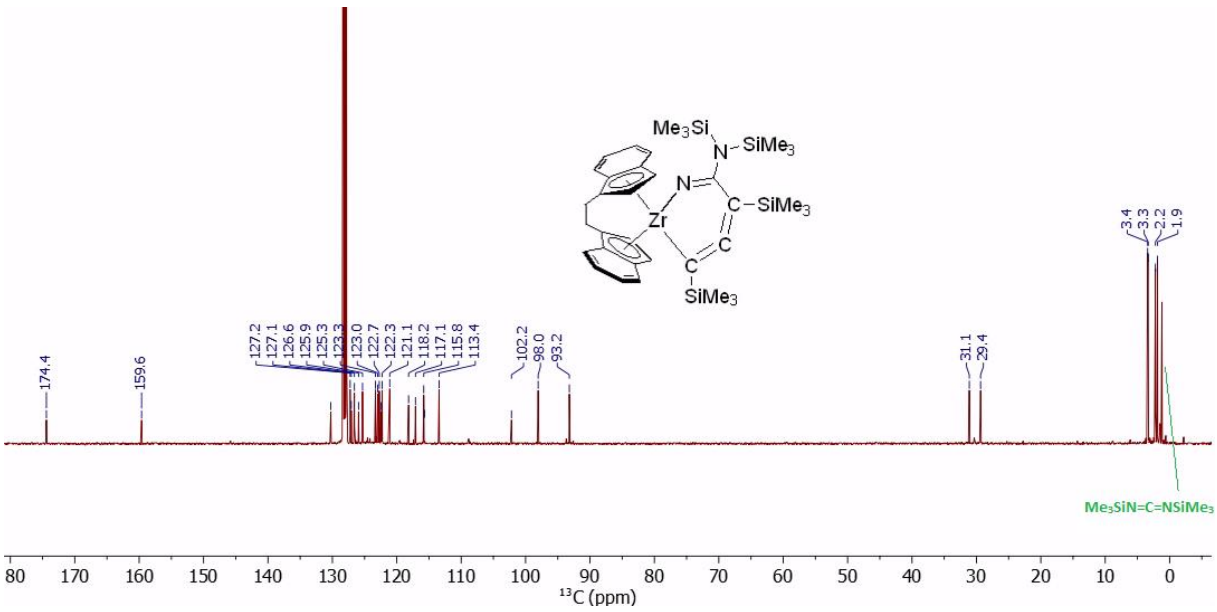

Figure S129. $^{13}C\{^{1}H\}$ NMR spectrum of **$P_{2c\text{-}SiMe3}$** (Minor impurity of $Me_3SiN{=}C{=}NSiMe_3$ was generally observed as it was used to stabilise **$P_{2c\text{-}SiMe3}$**; 25 °C, benzene-d_6, 100.6 MHz).

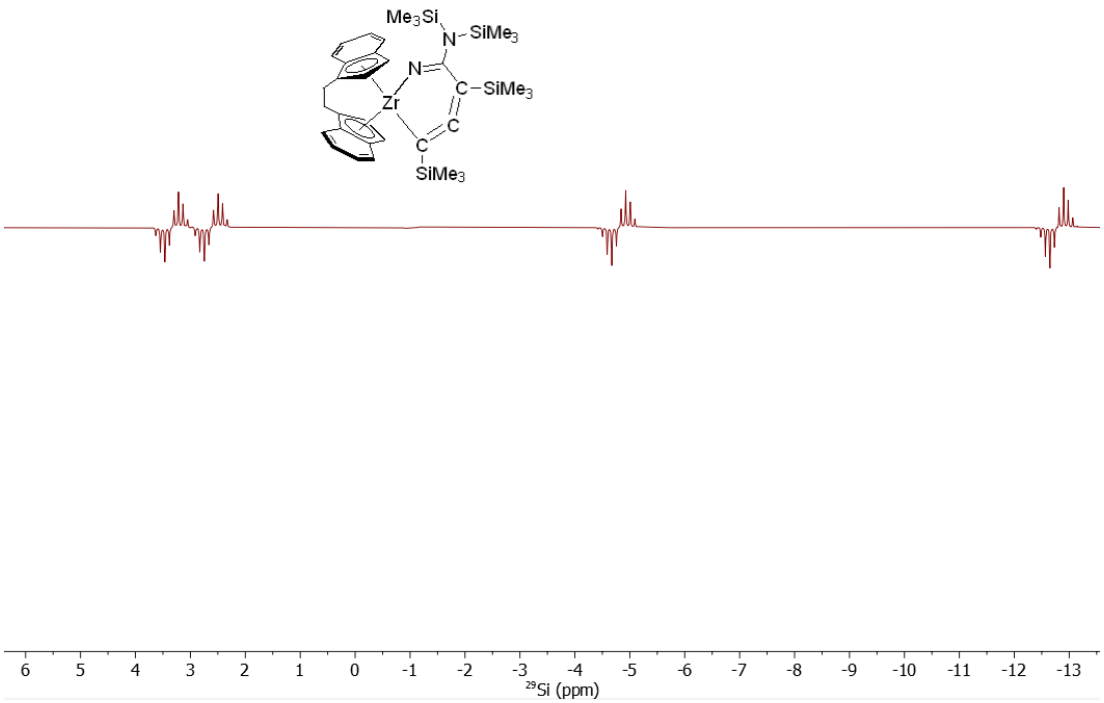

Figure S130. ^{29}Si INEPT NMR spectrum of **P2c-SiMe3** (25 °C, benzene-*d*6, 79.5 MHz).

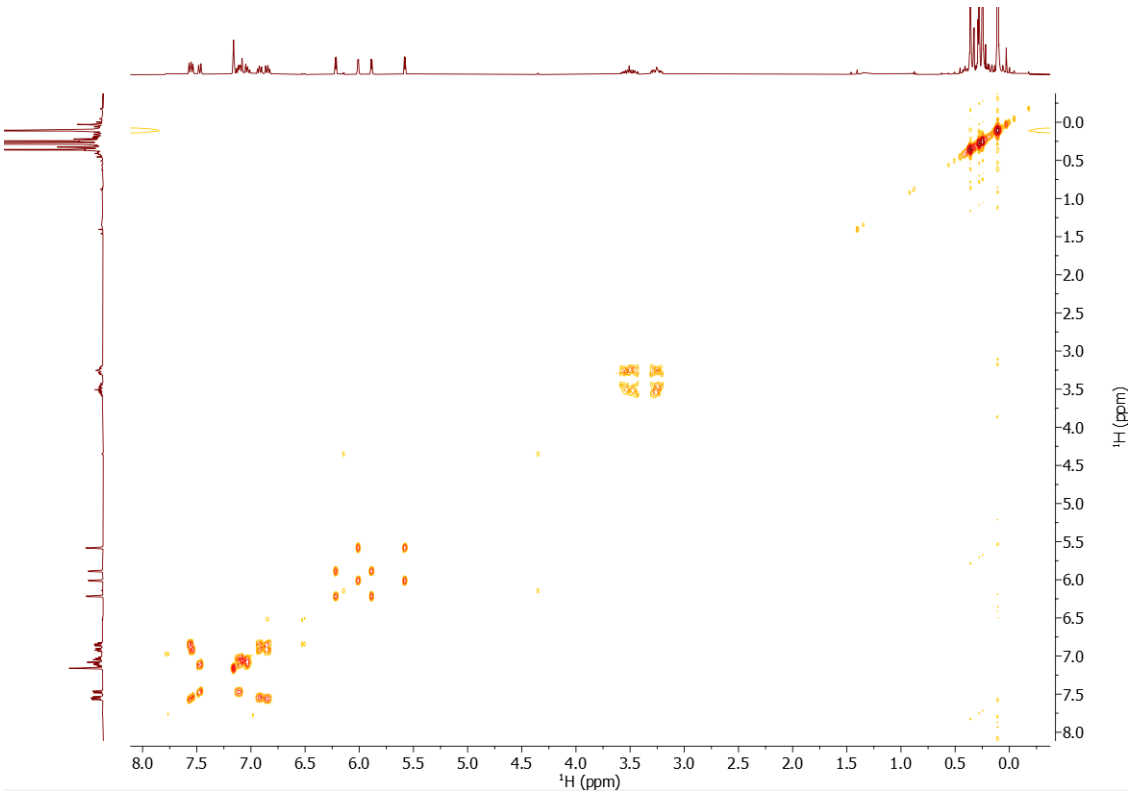

Figure S131. ^{1}H-^{1}H COSY NMR spectrum of **P2c-SiMe3** (25 °C, benzene-*d*6, 400.1, 400.1 MHz).

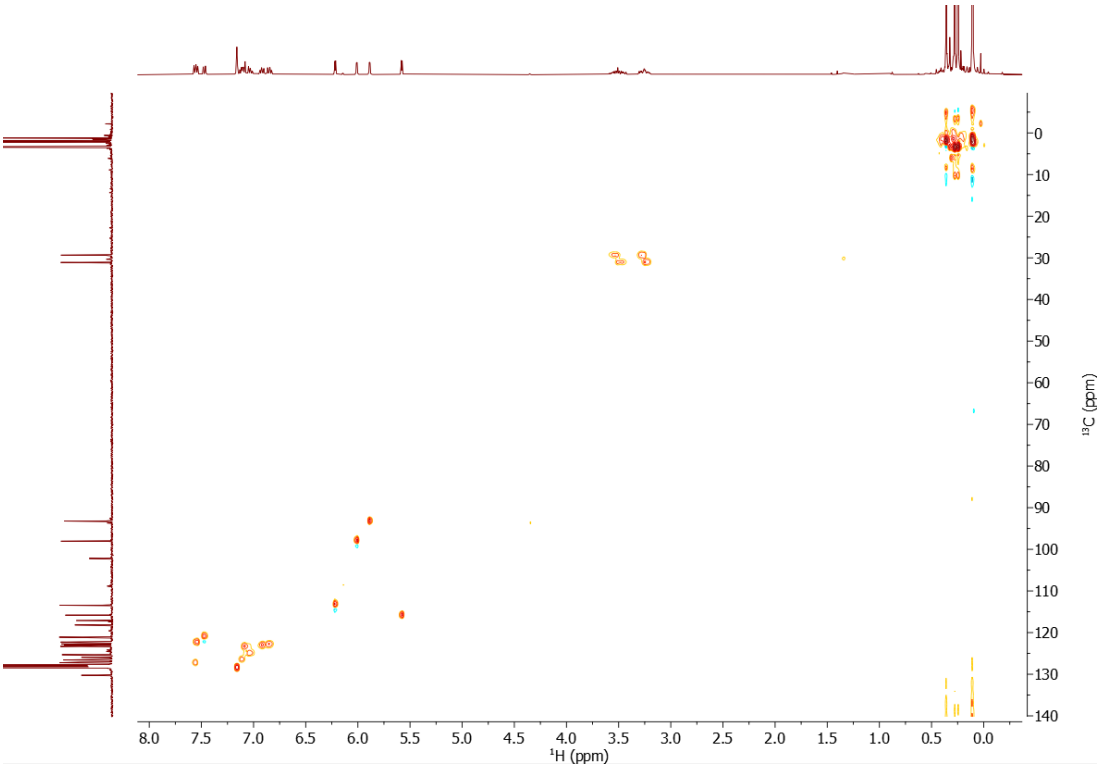

Figure S132. ^{1}H-^{13}C HSQC NMR spectrum of **P2c-SiMe3** (25 °C, benzene-*d*6, 400.1, 100.6 MHz).

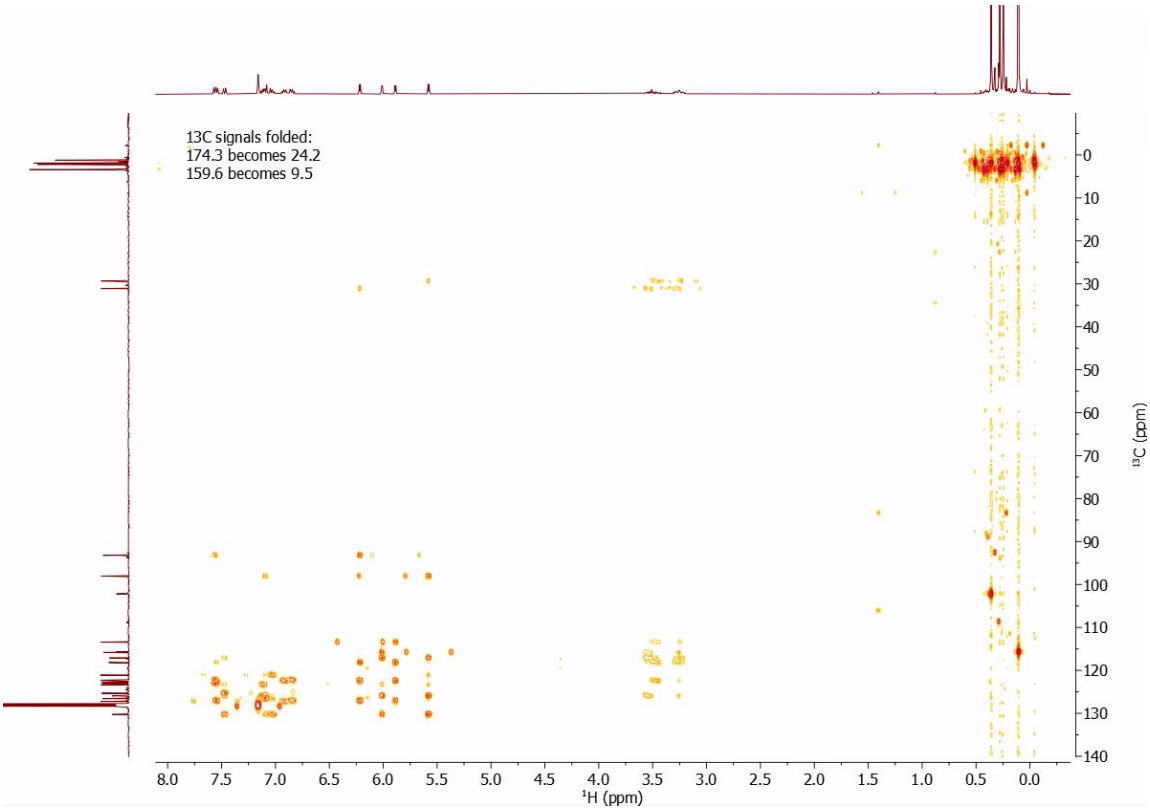

Figure S133. ^{1}H-^{13}C HMBC NMR spectrum of **P2c-SiMe3** (25 °C, benzene-*d*6, 400.1, 100.6 MHz).

7.21 NMR spectra of $P_{2d\text{-}SiMe3}$

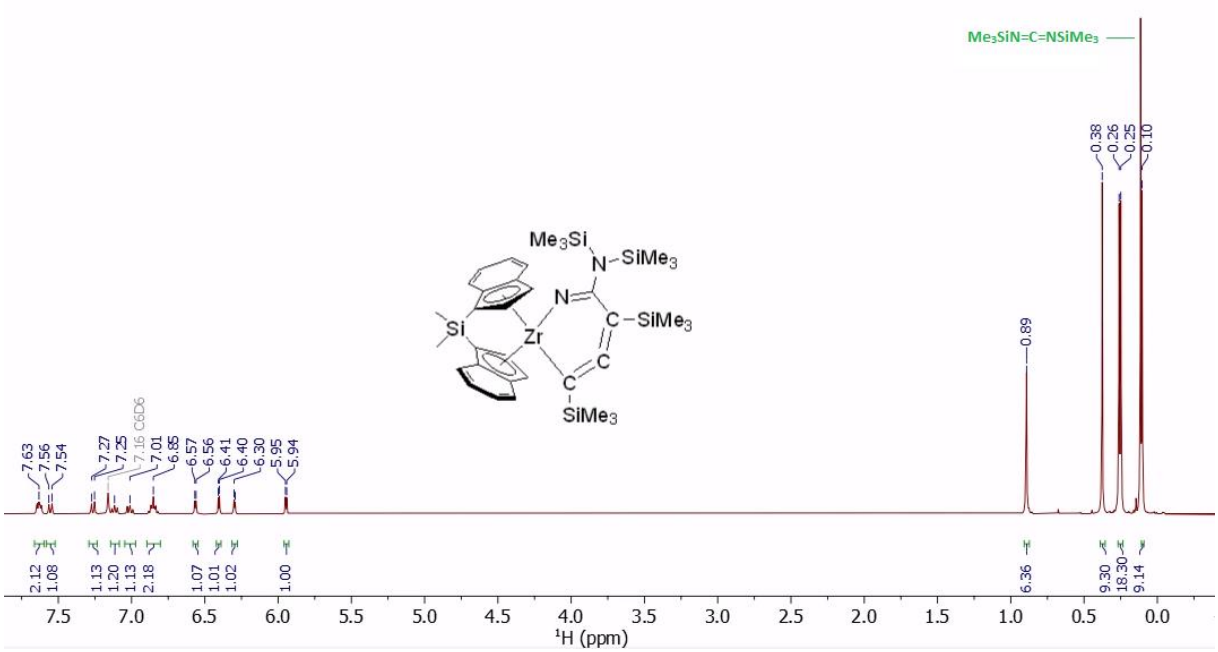

Figure S134. ^{1}H NMR spectrum of **$P_{2d\text{-}SiMe3}$** (Minor impurity of $Me_3SiN{=}C{=}NSiMe_3$ was generally observed as it was used to stabilise **$P_{2d\text{-}SiMe3}$**; 25 °C, benzene-d_6, 400.1 MHz).

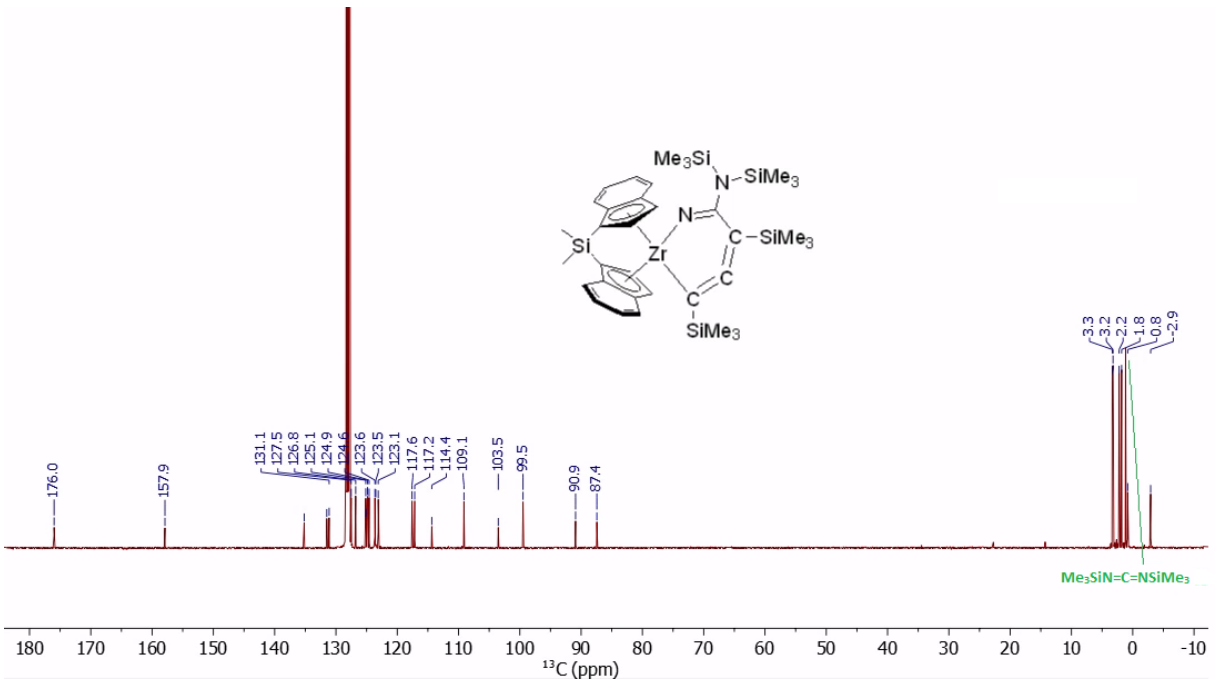

Figure S135. $^{13}C\{^{1}H\}$ NMR spectrum of **$P_{2d\text{-}SiMe3}$** (Minor impurity of $Me_3SiN{=}C{=}NSiMe_3$ was generally observed as it was used to stabilise **$P_{2d\text{-}SiMe3}$**; 25 °C, benzene-d_6, 100.6 MHz).

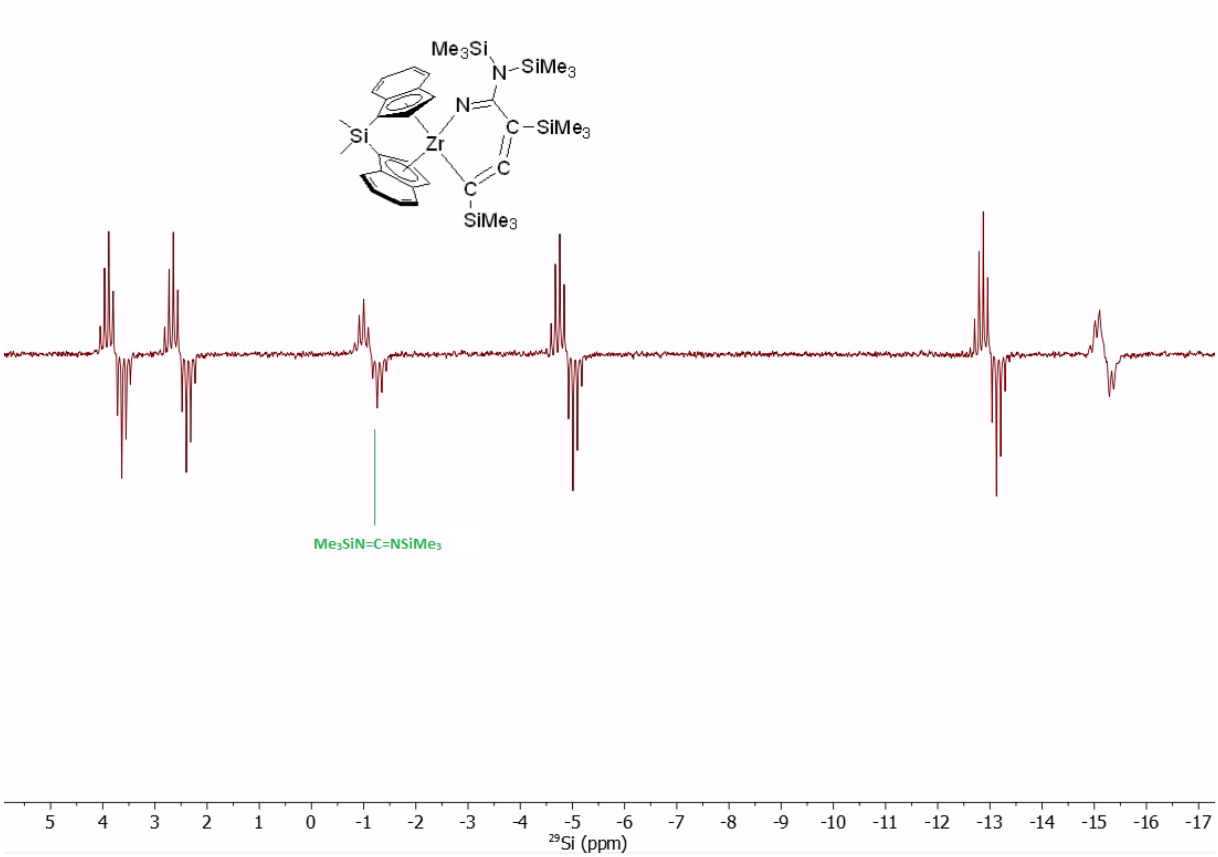

Figure S136. ^{29}Si INEPT NMR spectrum of **P2d-SiMe3** (25 °C, benzene-*d*6, 79.5 MHz).

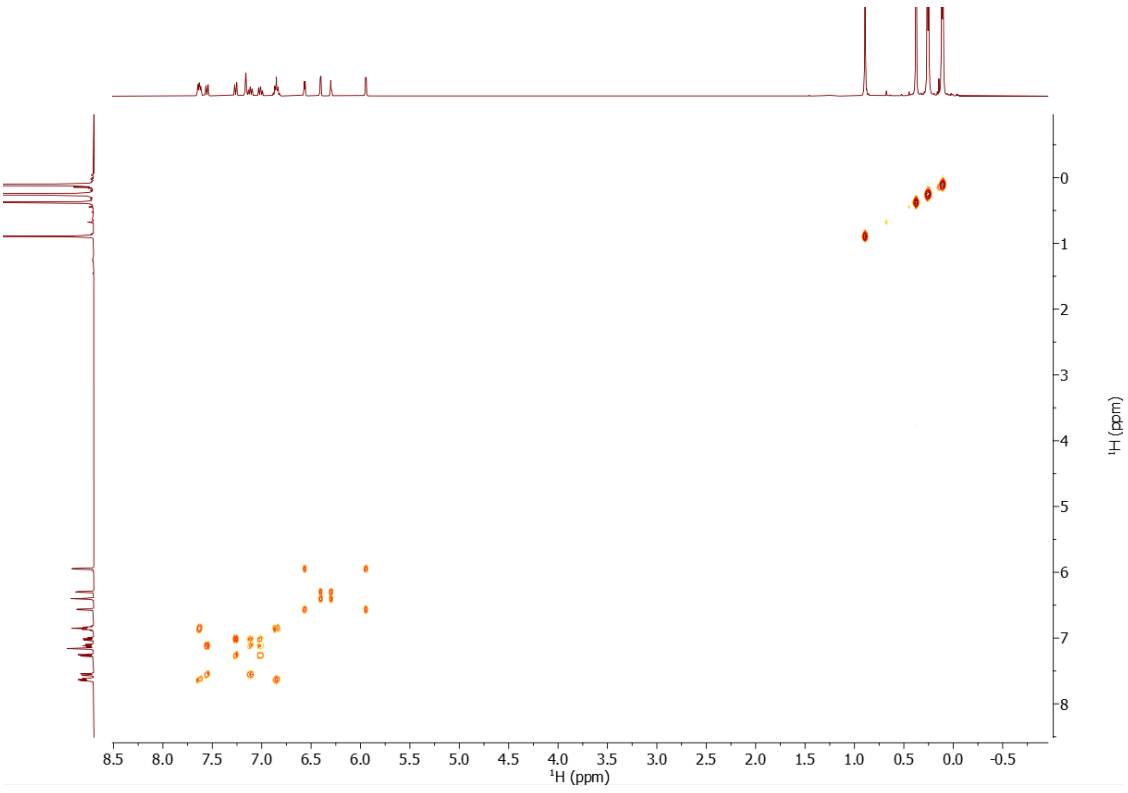

Figure S137. ^{1}H-^{1}H COSY NMR spectrum of **P2d-SiMe3** (25 °C, benzene-*d*6, 400.1, 400.1 MHz).

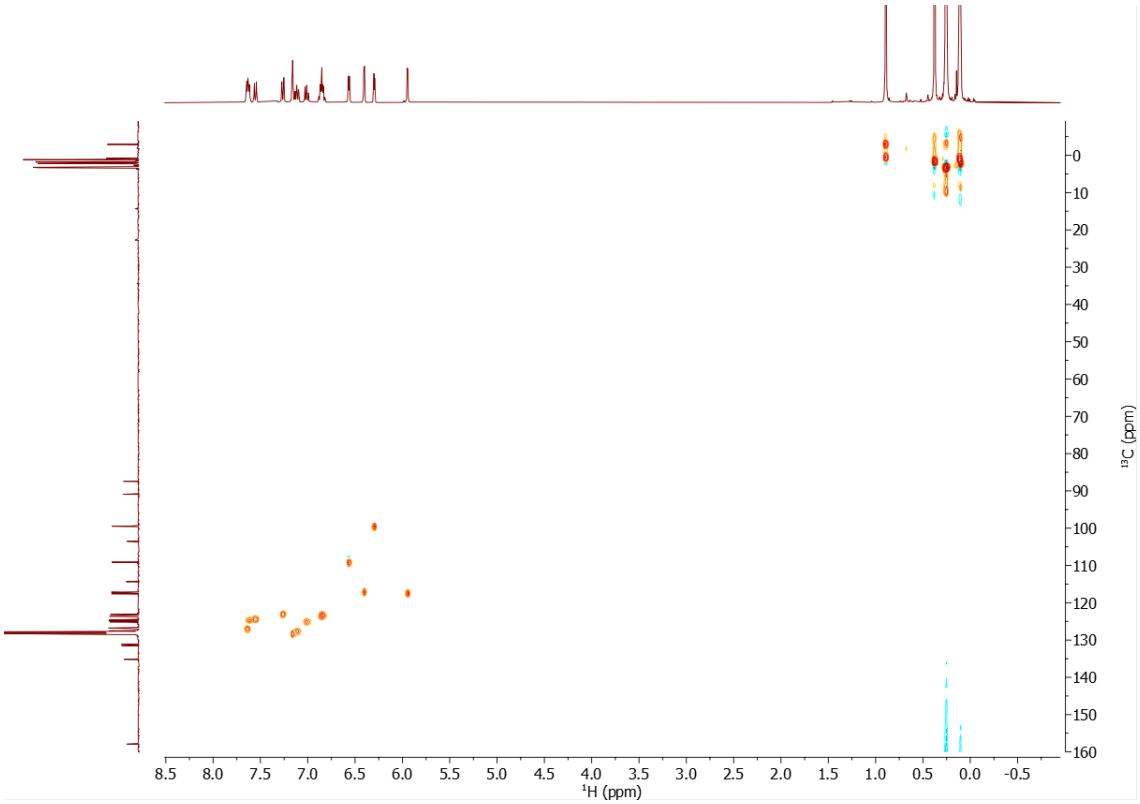

Figure S138. ^{1}H-^{13}C HSQC NMR spectrum of **P2d-SiMe3** (25 °C, benzene-*d*6, 400.1, 100.6 MHz).

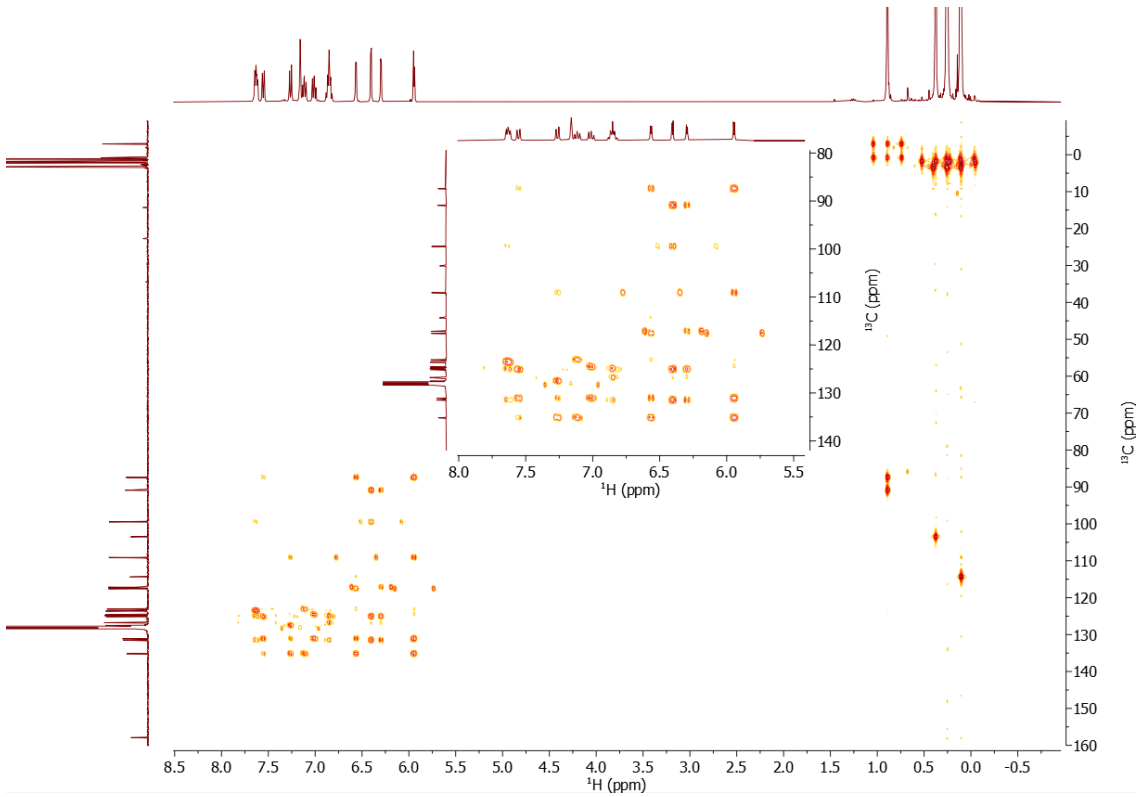

Figure S139. ^{1}H-^{13}C HMBC NMR spectrum of **P2d-SiMe3** (25 °C, benzene-*d*6, 400.1, 100.6 MHz).

8. Vibrational spectra

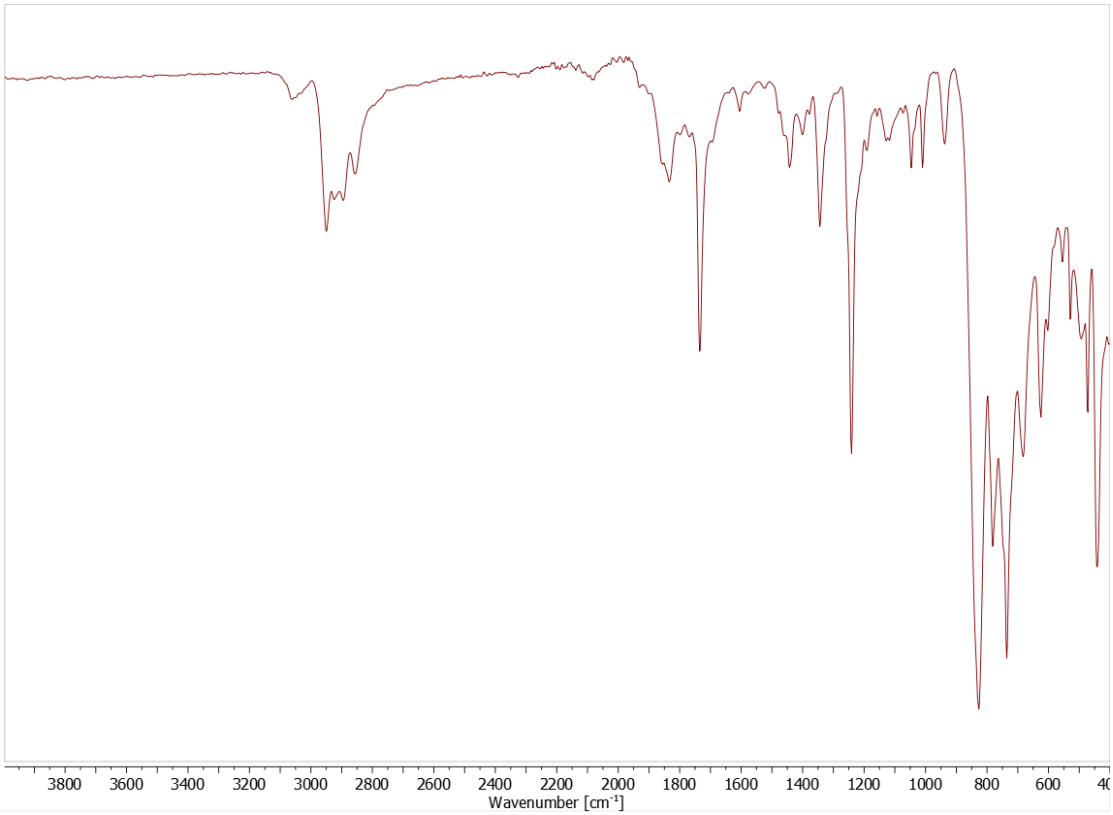

Figure S140. IR spectrum of **2c**.

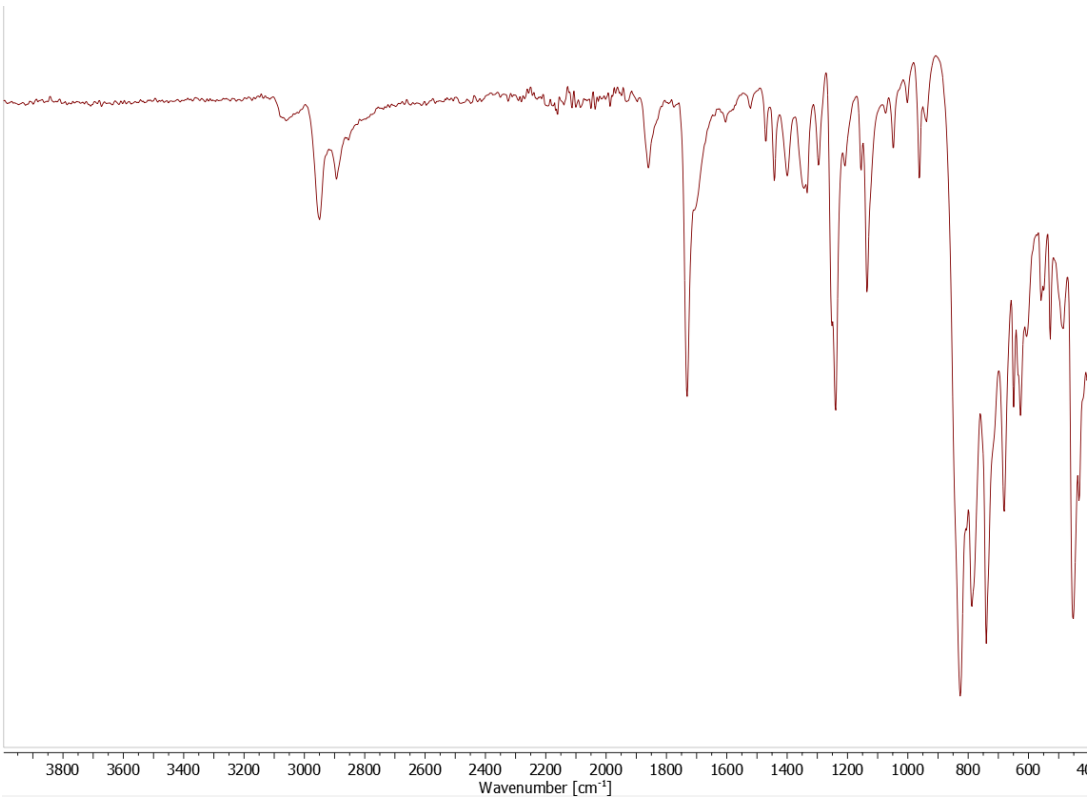

Figure S141. IR spectrum of **2d**.

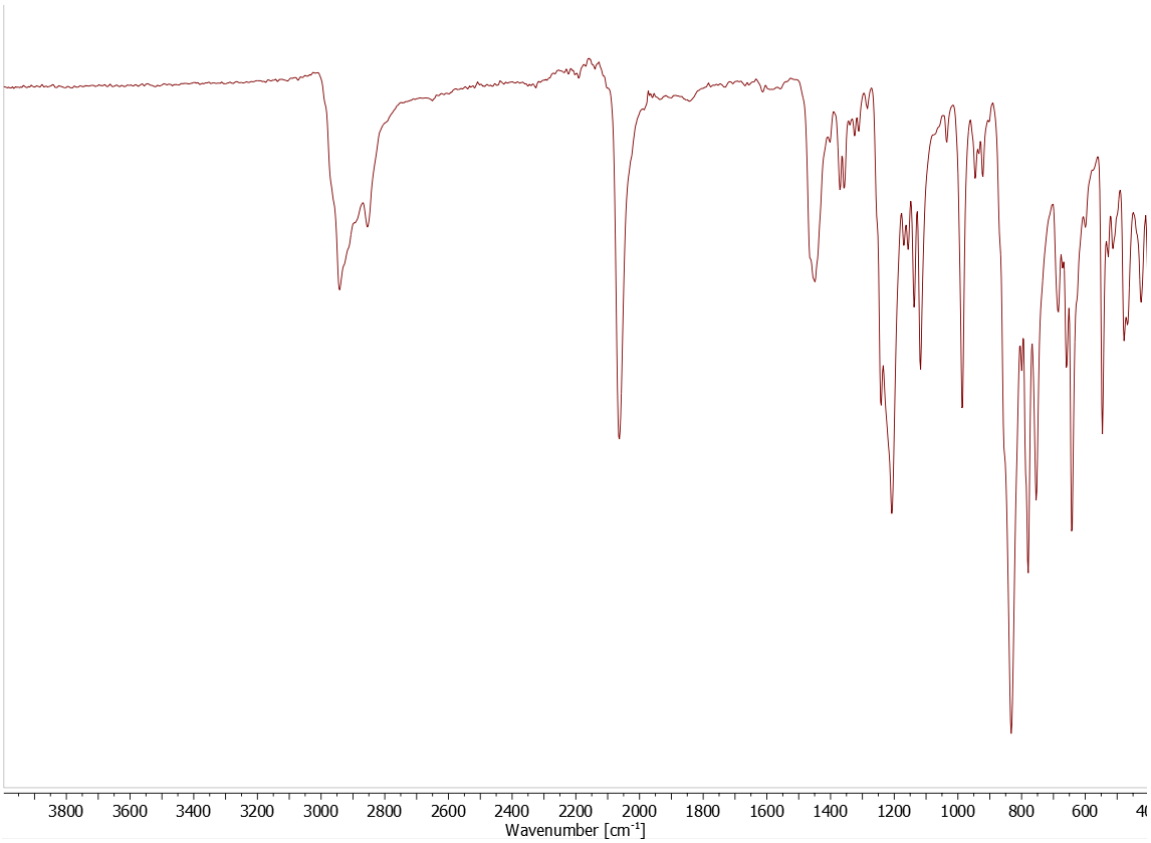

Figure S142. IR spectrum of **P2a-*i*Pr**.

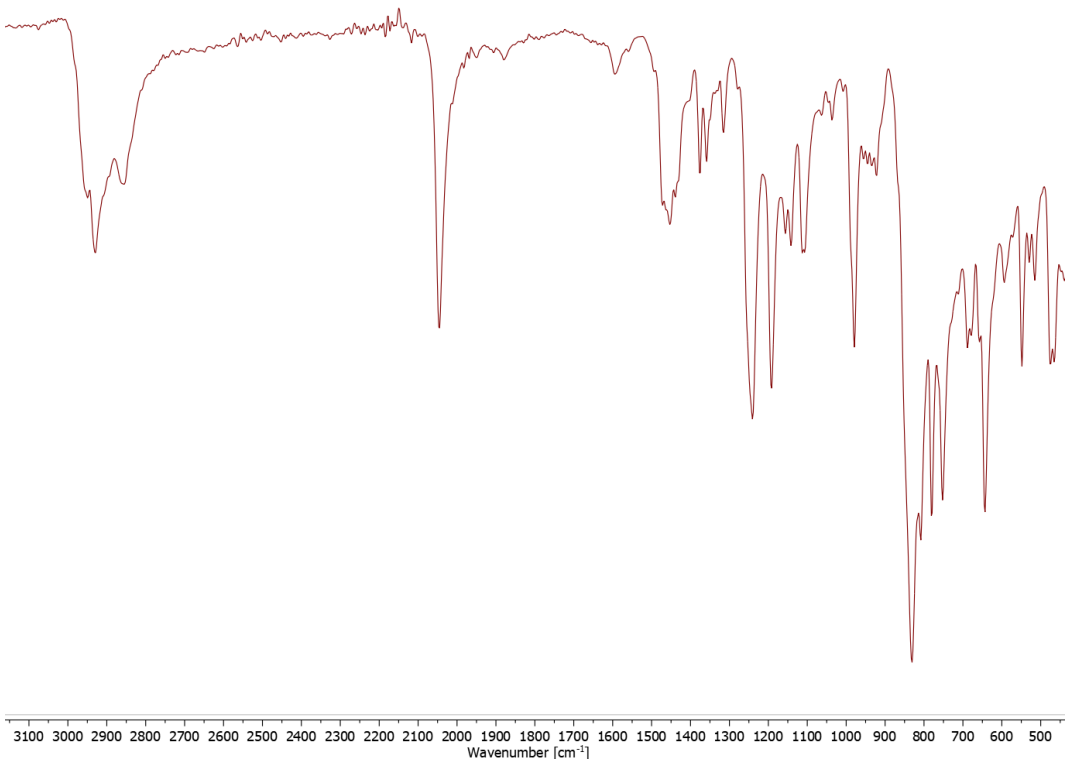

Figure S143. IR spectrum of **P1a-*i*Pr**.

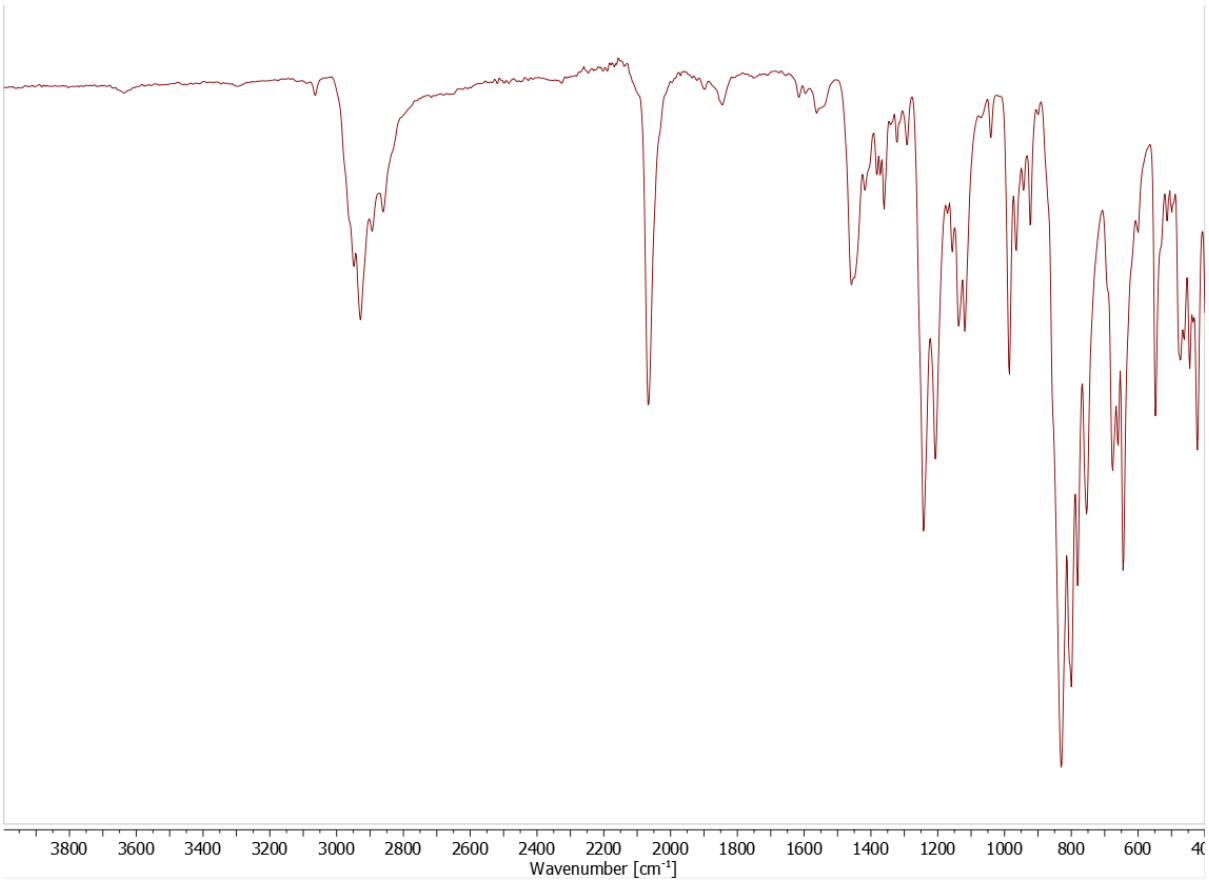

Figure S144. IR spectrum of **P2b-*i*Pr**.

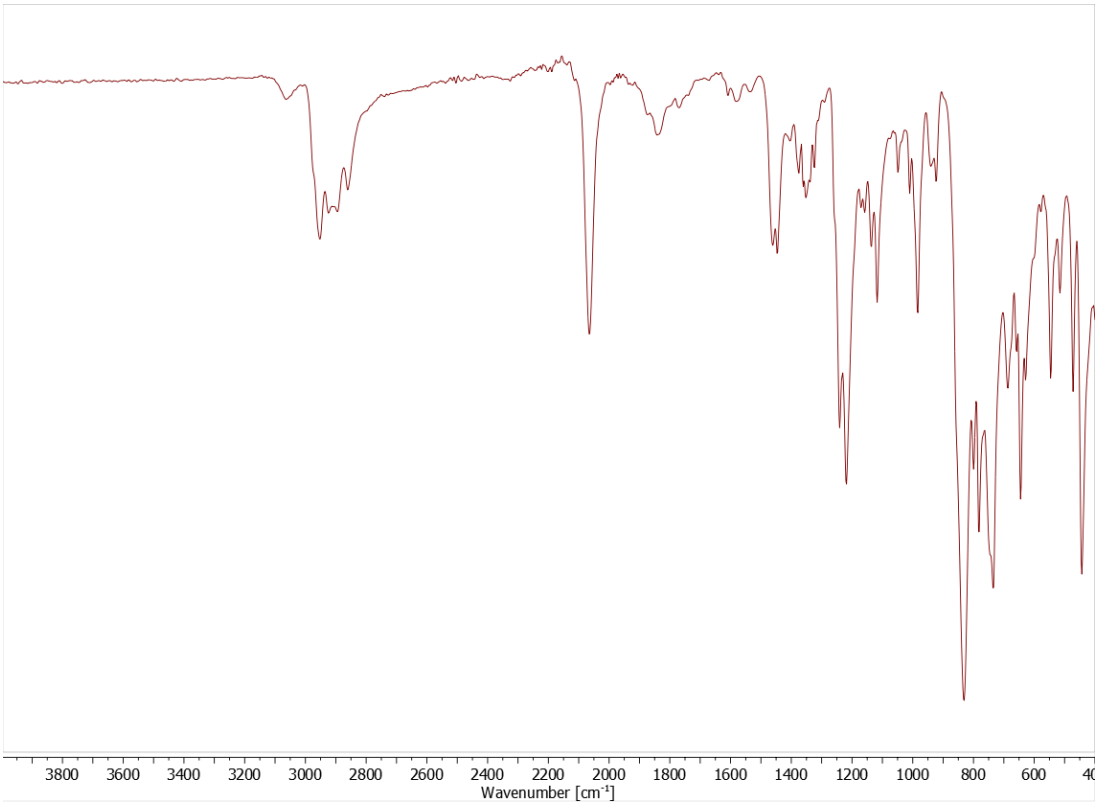

Figure S145. IR spectrum of **P2c-*i*Pr**.

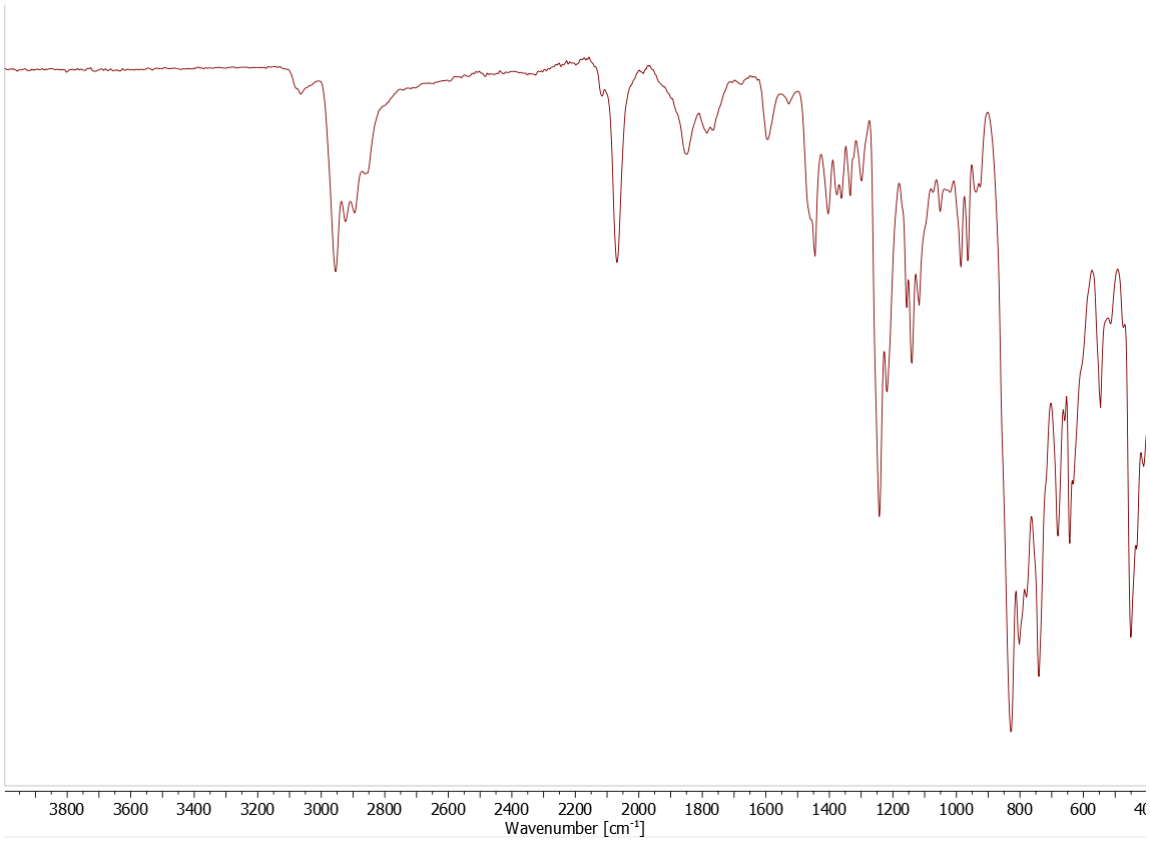

Figure S146. IR spectrum of **P2d-*i*Pr**.

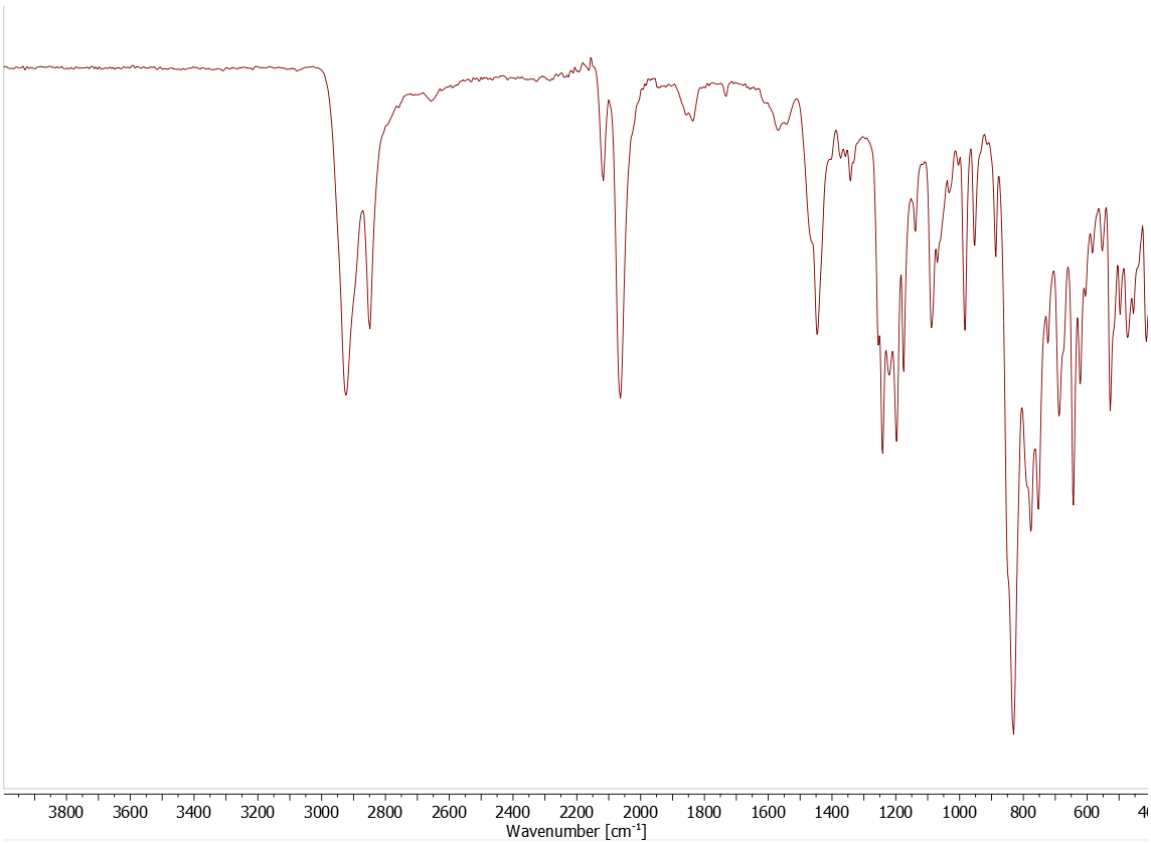

Figure S147. IR spectrum of **P2a-Cy**.

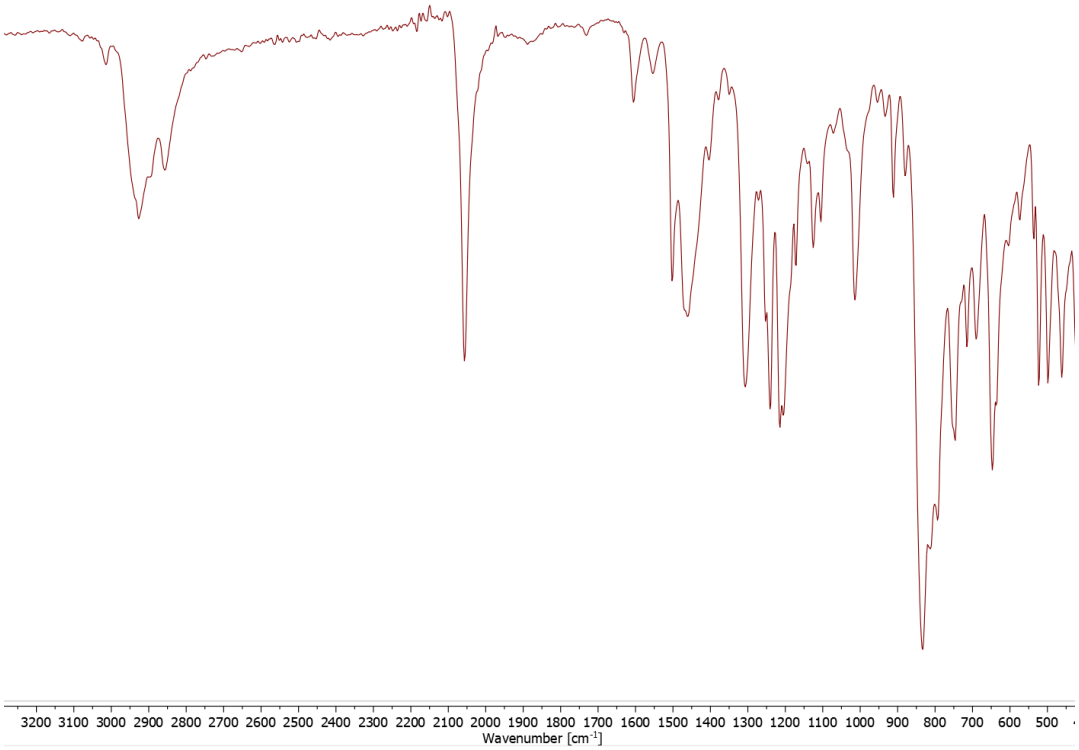

Figure S148. IR spectrum of **P1a-Cy**.

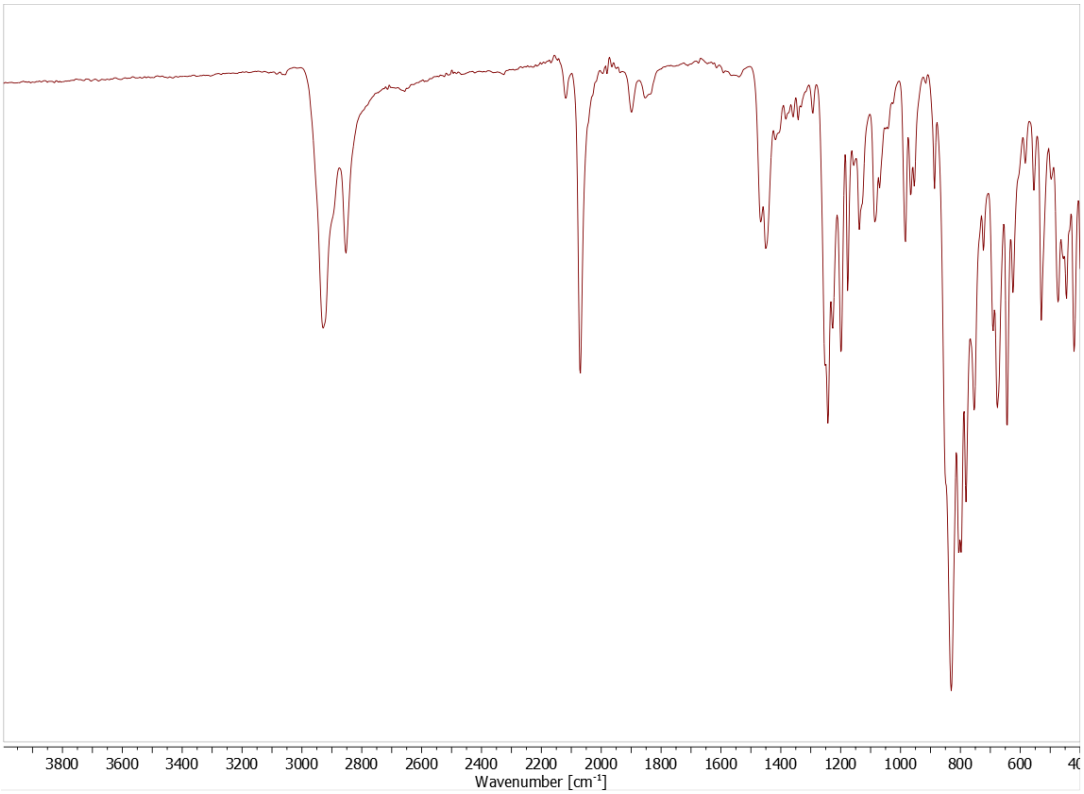

Figure S149. IR spectrum of **P2b-Cy**.

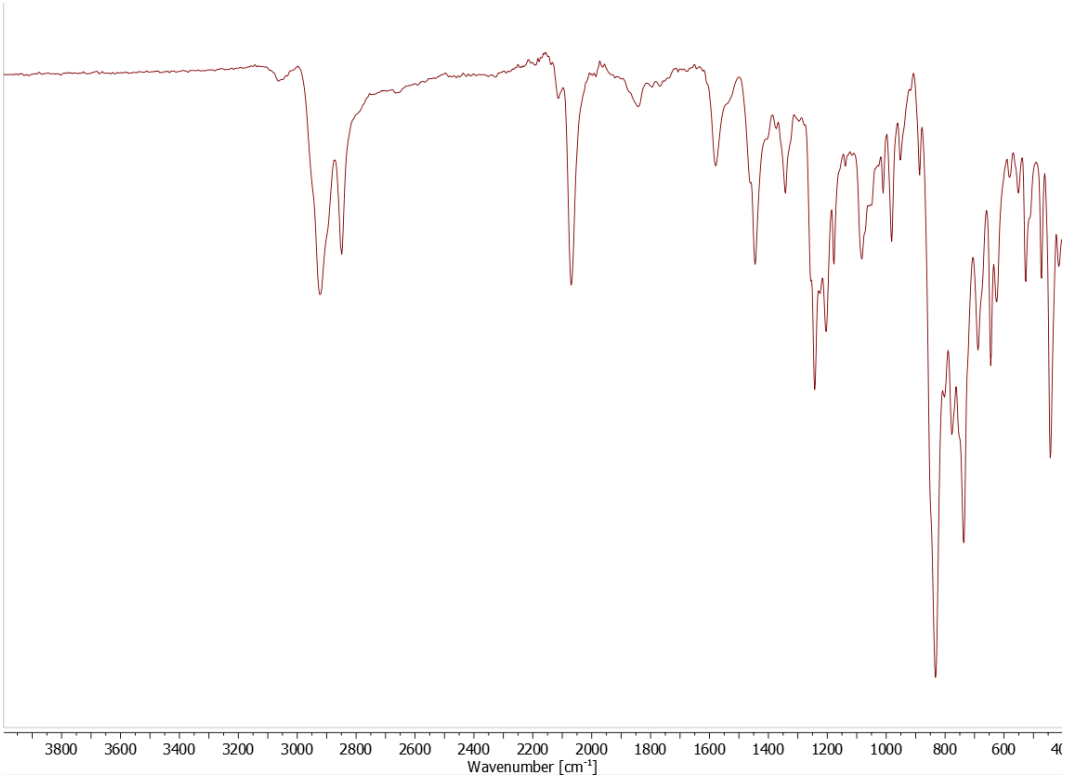

Figure S150. IR spectrum of **P2c-Cy**.

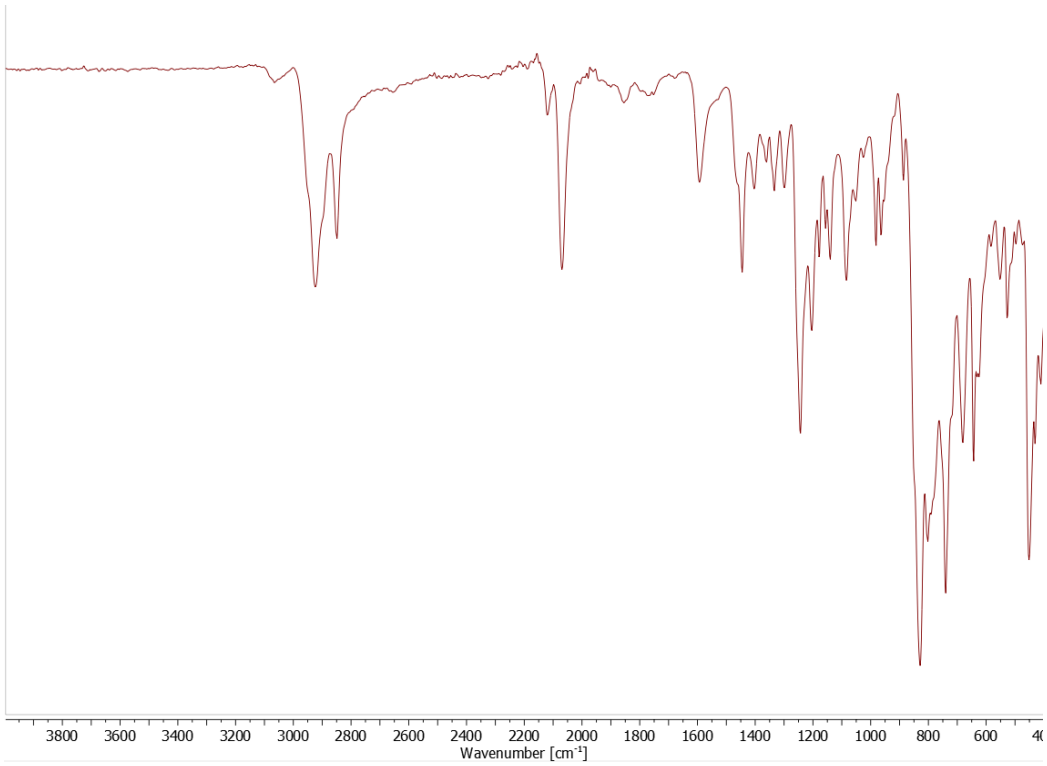

Figure S151. IR spectrum of **P2d-Cy**.

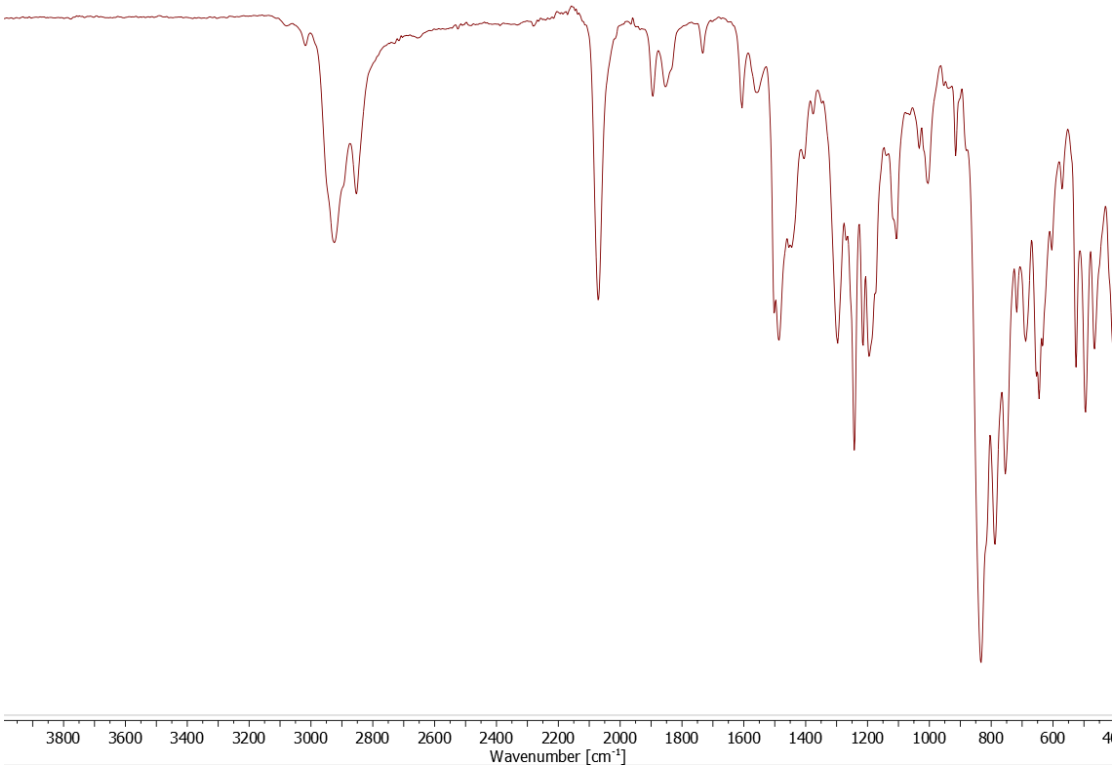

Figure S152. IR spectrum of **P2a-*p*-Tol**.

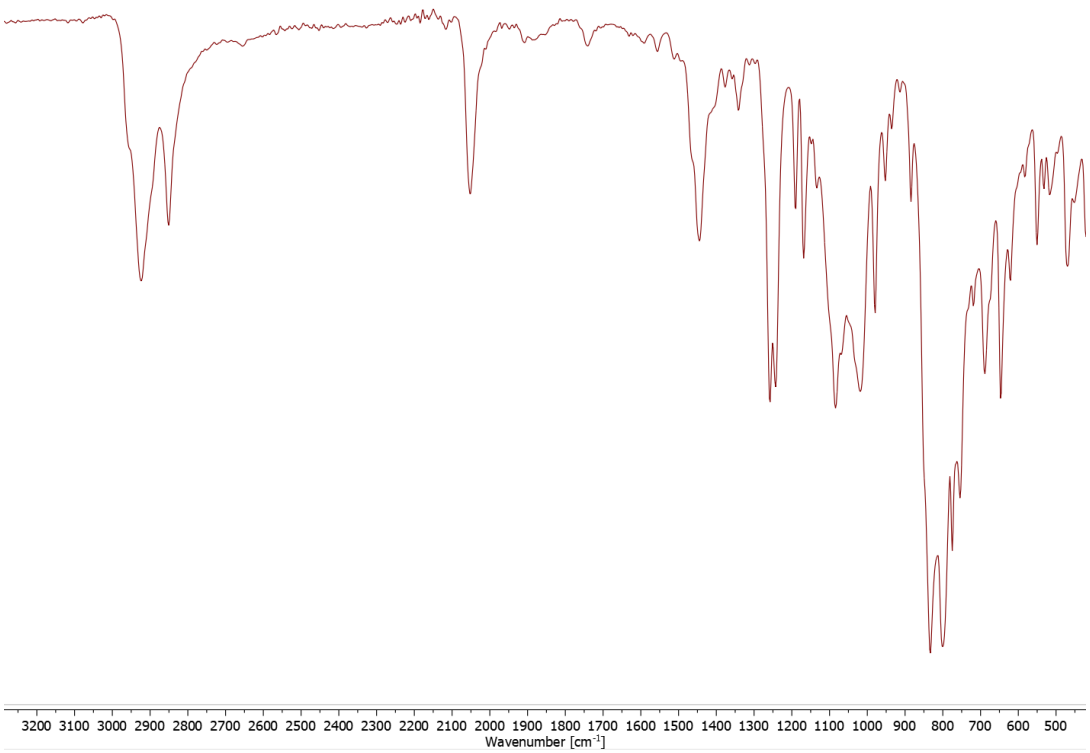

Figure S153. IR spectrum of **P1a-*p*-Tol**.

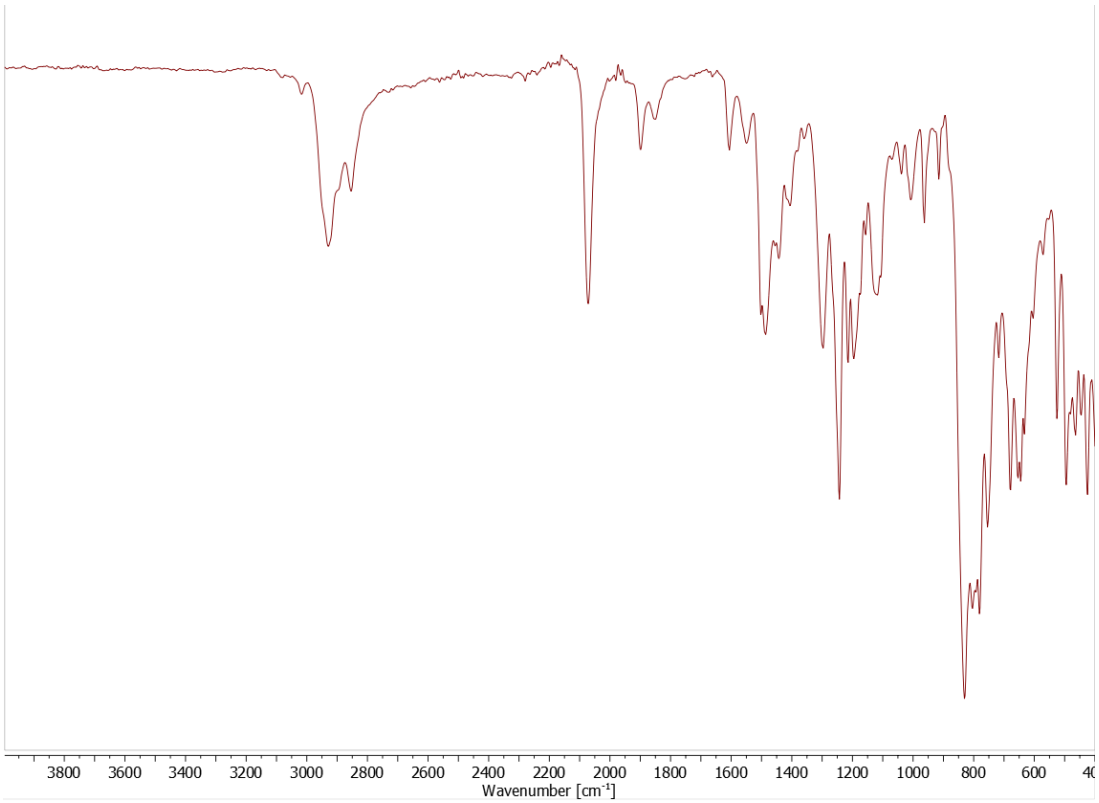

Figure S154. IR spectrum of **P2b-*p*-Tol**.

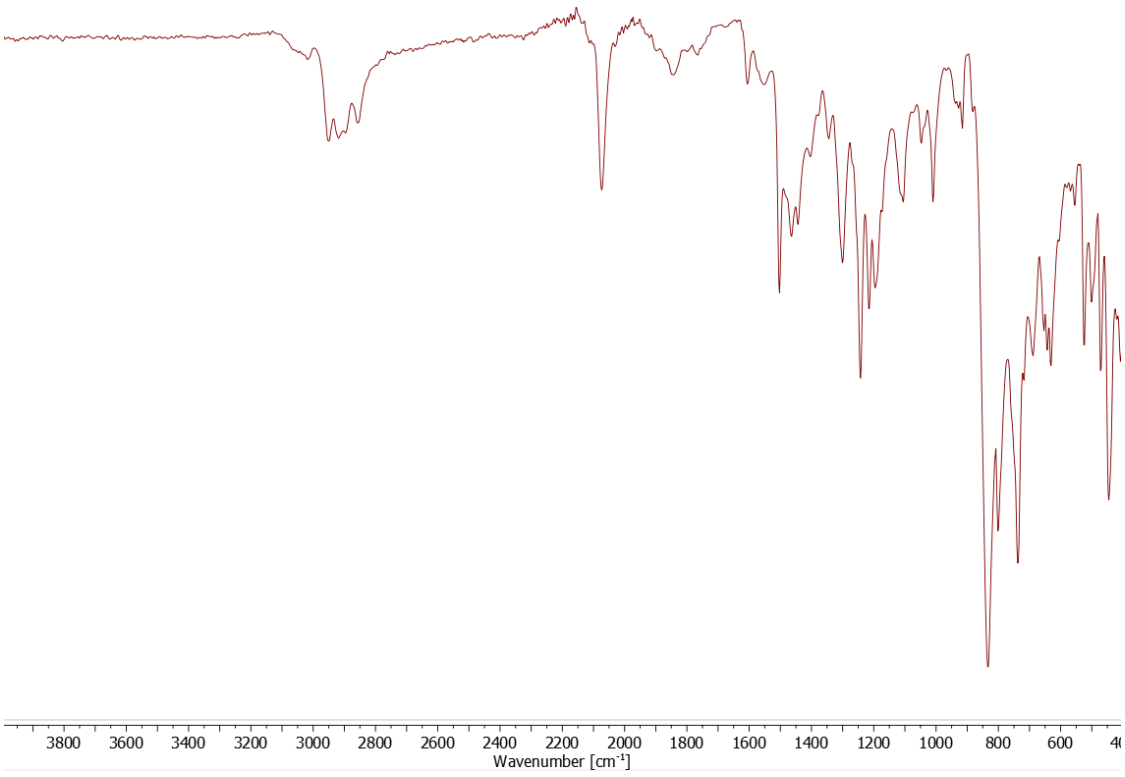

Figure S155. IR spectrum of **P2c-*p*-Tol**.

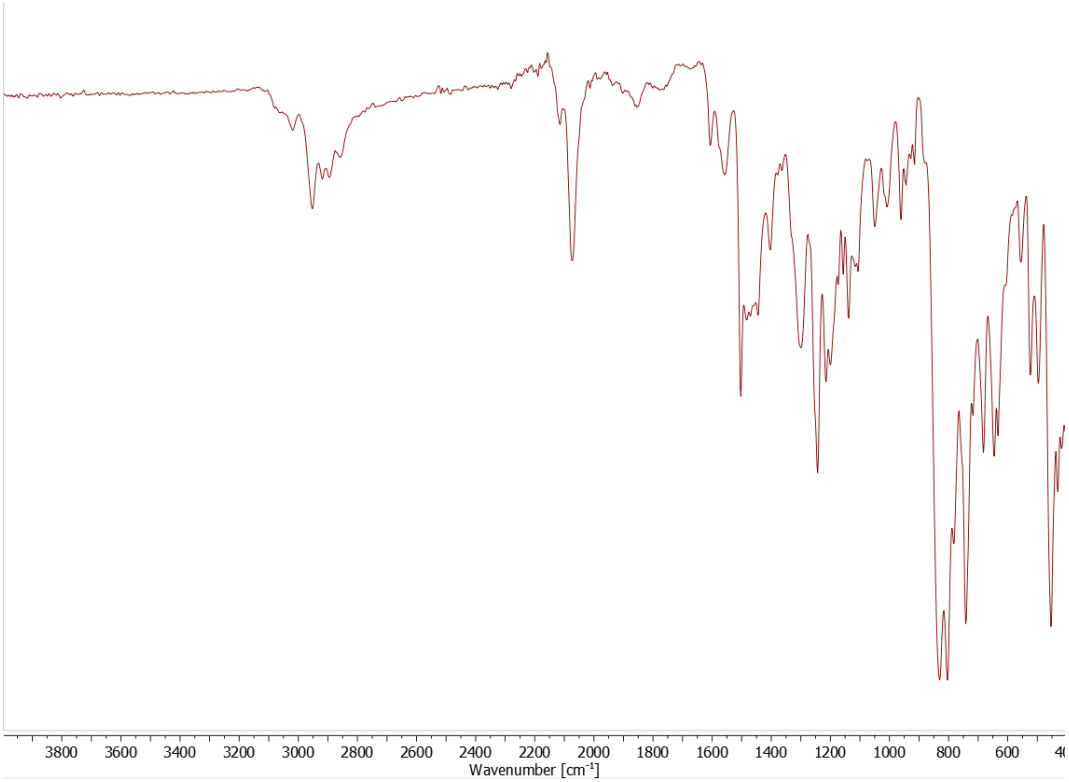

Figure S156. IR spectrum of **P2d-*p*-Tol**.

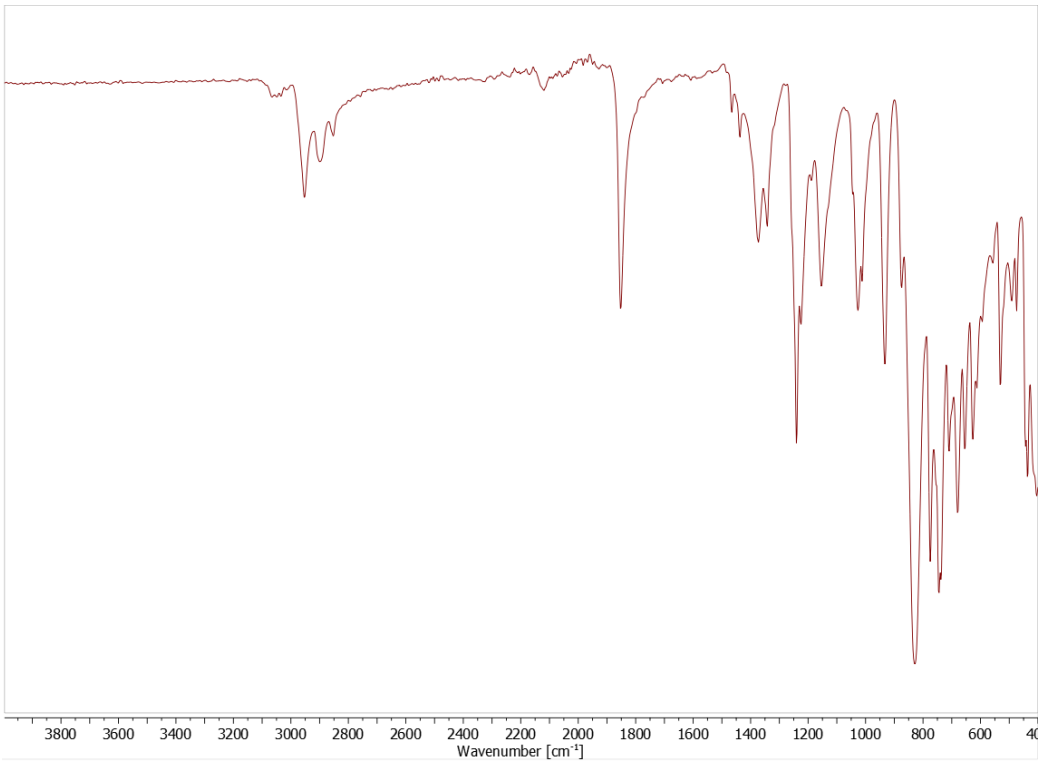

Figure S157. IR spectrum of **P2c-SiMe3**.

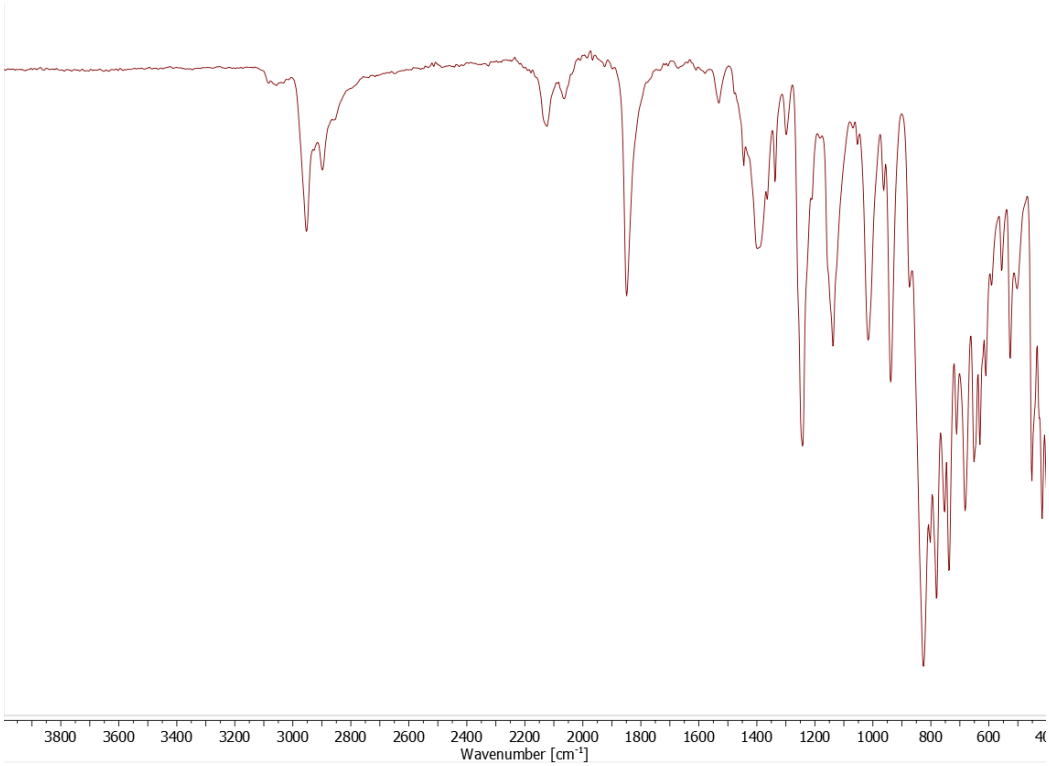

Figure S158. IR spectrum of **P2d-SiMe3**.

9. Computational details

9.1 General remarks

Computations were carried out using *Gaussian16*[11] and the standalone version of *NBO 6.0*.[12] In this section, we have compiled the main and secondary findings of a detailed DFT study to support the main findings discussed in the manuscript as well as to provide further detailed information. The focus of this study was on four central questions that arose during the experimental study.

1. Why does the Dipp carbodiimide not react with any of the 1-metallacyclobuta-2,3-dienes?
2. Why is a completely different reactivity found for the Me_3Si substituted carbodiimide leading to 2-aza-1-metallacyclohexa-2,4,5-trienes?
3. Why is only one conformer formed for this product class?
4. Why is this reactivity restricted to the indenyl substituted zirconocenes?

First, thermodynamic calculations were performed on the triple-ζ level of theory to approach the answer to these questions. Therefore, we have optimised the real-size molecules using the hybrid density functional method B3LYP,[13,14] in combination with the basis set def2tzvp,[15] and the empirical dispersion correction GD3BJ [16] (notation: B3LYP/GD3BJ/def2tzvp). Vibrational frequencies were also computed, to include zero-point vibrational energies in thermodynamic parameters and to characterise all structures as minima on the potential energy surface. To confirm the accuracy of the calculated transition states (TS), we performed intrinsic reaction coordinate (IRC) analysis on these structures. The results are summarised in chapter 9.2.1. Furthermore, chapter 9.2.2 contains figures of the Interaction Region Indicator (IRI)[17] analyses on the hypothetic complexes $\mathbf{P_{1a\text{-}Dipp}}$ and $\mathbf{P_{2a\text{-}Dipp}}$ which were also structurally optimised on this level. In the sections 9.2.3 - 9.2.6 we summarised the main results of a detailed mechanistic study. Therefore, about 90 structures were optimised at double-ζ level, followed by single point calculations at triple-ζ level (notation: B3LYP/GD3BJ/def2svpp//def2tzvp). Chapter 9.3 contains the main results of a series of binding analyses carried out on selected examples of the compounds presented here. QT-AIM, ELF, IRI and Wiberg bond index calculations/visualisation were performed using MultiWfn 3.5 employing *Gaussian16* formatted checkpoint files.[18] For the visualisation of 3D-quantum chemical results we used GaussView 6.1.1.[19]

In addition to the Supporting Information, we provide a multi-structure xyz file with all calculated molecules. For a better understanding and a more intuitive view of the calculated 3D structures, we strongly recommend using this file, e.g., with the free program MERCURY.[20]

Please note that all computations were carried out for single, isolated molecules in the gas phase (ideal gas approximation). There may well be significant differences between gas phase and condensed phase.

9.2 Thermochemistry & mechanistic aspects

In this chapter we summarise the results of our thermodynamic calculations, which were performed on the B3LYP/GD3BJ/def2tzvp level of theory. The purpose of these thermodynamic calculations was to substantiate the observed reactivities or lack thereof, so only selected representatives were considered.

9.2.1 Formation of 1-metalla-2-aza-but-3-enes

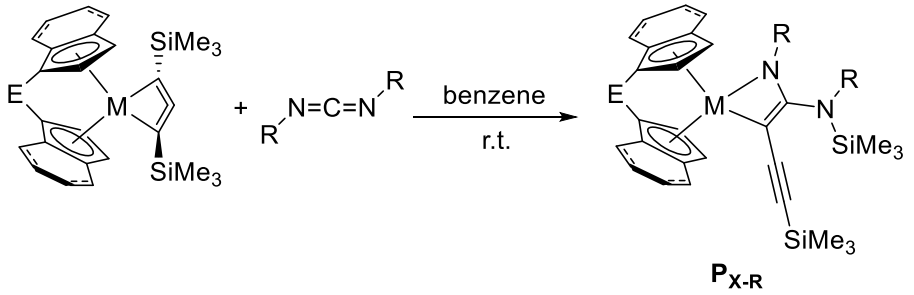

$\mathbf{P_{X\text{-}R}}$

tetrahydroindenyl complexes
1a: M = Ti, E = C_2H_4
2a: M = Zr, E = C_2H_4
2b: M = Zr, E = Me_2Si
indenyl complexes
2c: M = Zr, E = C_2H_4
2d: M = Zr, E = Me_2Si

tetrahydroindenyl complexes
$\mathbf{P_{1a\text{-}iPr}}$: M = Ti, E = C_2H_4, R = *i*Pr
$\mathbf{P_{1a\text{-}Me3Si}}$: M = Ti, E = C_2H_4, R = Me_3Si
$\mathbf{P_{1a\text{-}Dipp}}$: M = Ti, E = C_2H_4, R = Dipp
$\mathbf{P_{2a\text{-}iPr}}$: M = Zr, E = C_2H_4, R = *i*Pr
$\mathbf{P_{2a\text{-}Me3Si}}$: M = Zr, E = C_2H_4, R = Me_3Si
$\mathbf{P_{2a\text{-}Dipp}}$: M = Zr, E = C_2H_4, R = Dipp
$\mathbf{P_{2b\text{-}iPr}}$: M = Zr, E = Me_2Si, R = *i*Pr
$\mathbf{P_{2b\text{-}Me3Si}}$: M = Zr, E = Me_2Si, R = Me_3Si
indenyl complexes
$\mathbf{P_{2c\text{-}iPr}}$: M = Zr, E = C_2H_4, R = *i*Pr
$\mathbf{P_{2c\text{-}Me3Si}}$: M = Zr, E = C_2H_4, R = Me_3Si
$\mathbf{P_{2d\text{-}iPr}}$: M = Zr, E = Me_2Si, R = *i*Pr
$\mathbf{P_{2d\text{-}Me3Si}}$: M = Zr, E = Me_2Si, R = Me_3Si

Scheme S1. Considered examples of 2-aza-1-metallacyclobut-3-ene complexes for thermodynamic calculations B3LYP/GD3BJ/def2tzvp level of theory.

Table S4. Calculated reaction enthalpies and Gibbs free energies of the considered examples of 2-aza-1-metallacyclobut-3-ene complexes for thermodynamic calculations B3LYP/GD3BJ/def2tzvp level of theory.

Main Product	Δ_RH [kJ/mol]	Δ_RG [kJ/mol]	Δ_RH [kcal/mol]	Δ_RG [kcal/mol]
racEBTHI_Ti_iPr P1-iPr	-143.1	-70.6	-34.2	-16.9
racEBTHI_Ti_TMS P1-Me3Si	-91.0	1.8	-21.8	0.4
racEBTHI_Ti_TMS P1-Dipp	-17.9	77.2	-4.3	18.4
racEBTHI_Zr_iPr P2a-iPr	-155.9	-85.3	-37.3	-20.4
racEBTHI_Zr_TMS P2a-Me3Si	-110.1	-17.3	-26.3	-4.1
racEBTHI_Zr_Dipp P2a-Dipp	-45.6	51.2	-10.9	12.2
racMe2SiBTHI_Zr_iPr P2b-iPr	-157.3	-88.0	-37.6	-21.0
racMe2SiBTHI_Zr_TMS P2b-Me3Si	-118.5	-27.9	-28.3	-6.7
racEBI_Zr_iPr P2c-iPr	-159.6	-85.8	-38.2	-20.5
racEBI_Zr_TMS P2c-Me3Si 2-aza-1-metallacyclobut-3-ene	-104.8	-15.9	-25.1	-3.8
racEBIZr_NCNTMS2TMSCCCTMS P2c-Me3Si 2-aza-1metallacyclohexa-2,4,5-triene	-117.4	-20.0	-28.1	-4.8
racMe2SiBI_Zr_iPr P2d-iPr	-159.9	-89.7	-38.2	-21.4
racMe2SiBI_Zr_TMS P2d-Me3Si 2-aza-1-metallacyclobut-3-ene	-115.1	-27.2	-27.5	-6.5
racMe2BIZr_NCNTMS2TMSCCCTMS P2d-Me3Si 2-aza-1metallacyclohexa-2,4,5-triene	-117.1	-23.8	-28.0	-5.7

9.2.2 IRI – Analysis of P1a-Dipp and P2a-Dipp

To obtain a better understanding of the absence of the reactions of **1a** and **2a** with DippNCNDipp, in addition to the thermodynamic calculation, an interaction region identifier analysis[17] was carried out on the basis of the calculated structures. This analysis clearly shows multiple repulsive interactions (orange – red surfaces; **Table S5**) of the *rac*-(ebthi) ligand, Dipp and Me_3Si substituents in both cases, which is simply due to steric overloading of the Dipp ligand.

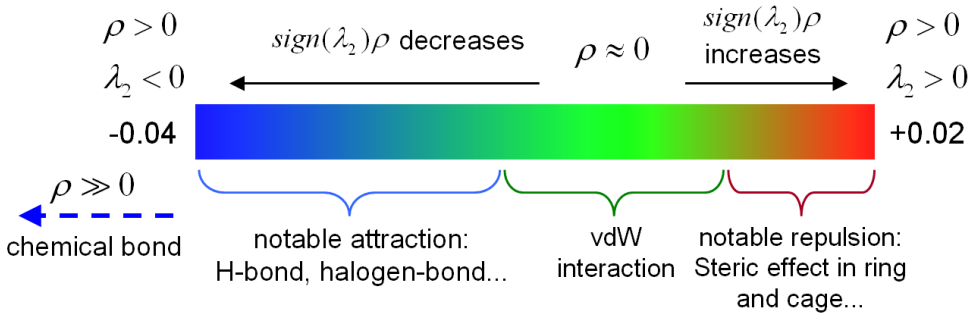

Table S5. Comparison of Interaction Region Indicator analyses of the calculated **P1a-Dipp** (left) and **P2a-Dipp** (right).

P1a-Dipp front	**P2a-Dipp** front
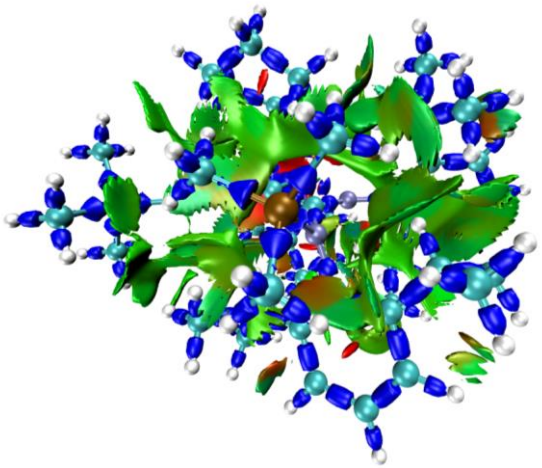	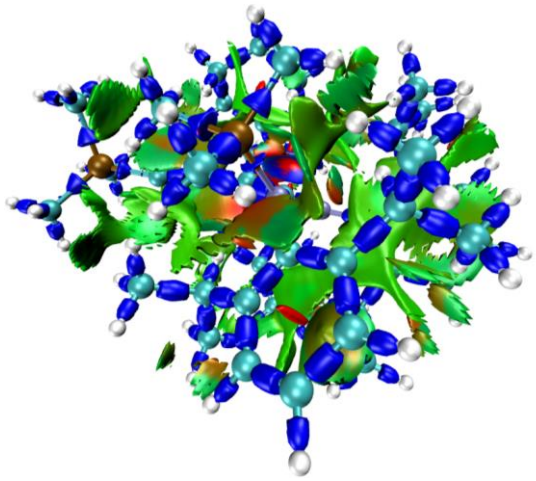

$P_{1a\text{-}Dipp}$ side 1	**$P_{2a\text{-}Dipp}$** side 1
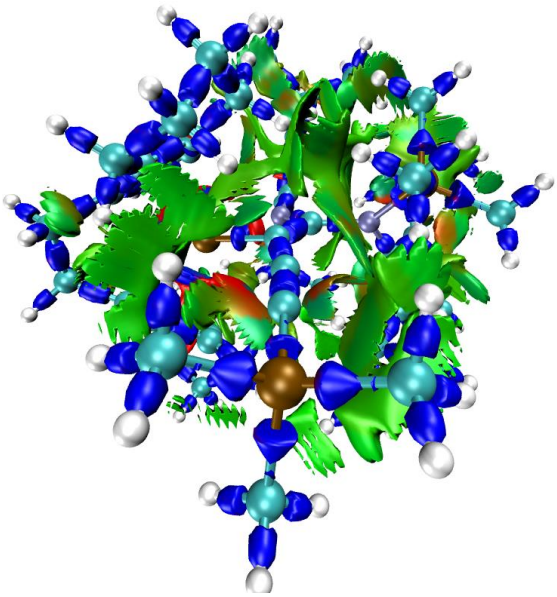	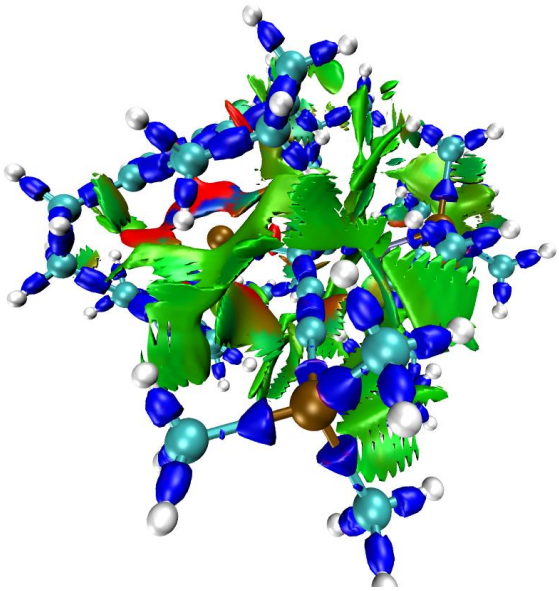
$P_{1a\text{-}Dipp}$ back	**$P_{2a\text{-}Dipp}$** back
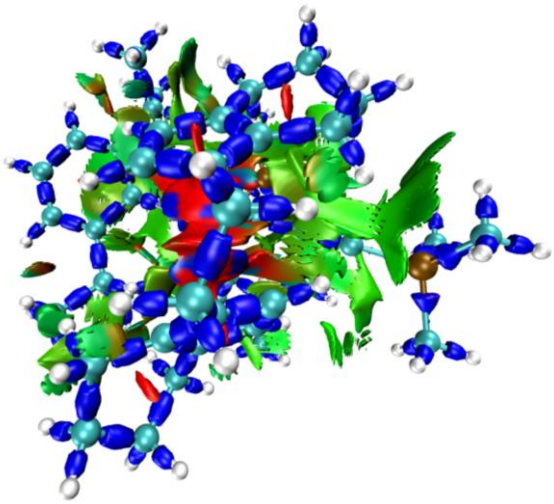	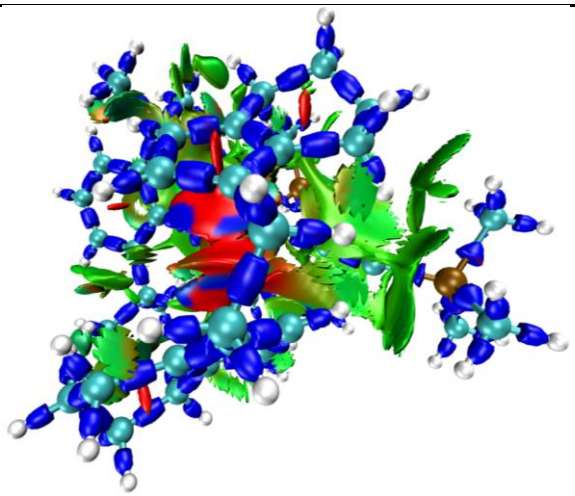
$P_{1a\text{-}Dipp}$ side 2	**$P_{2a\text{-}Dipp}$** side2
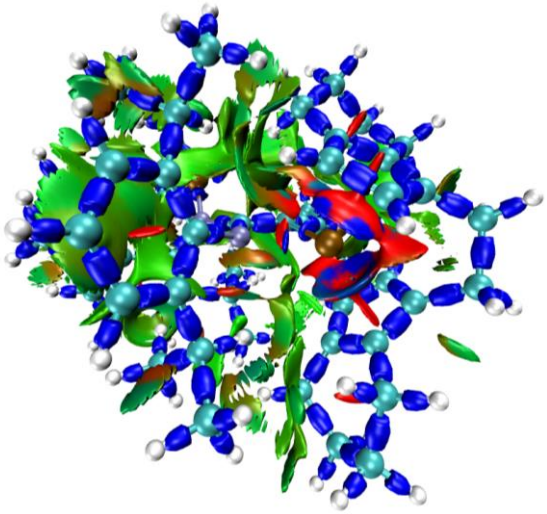	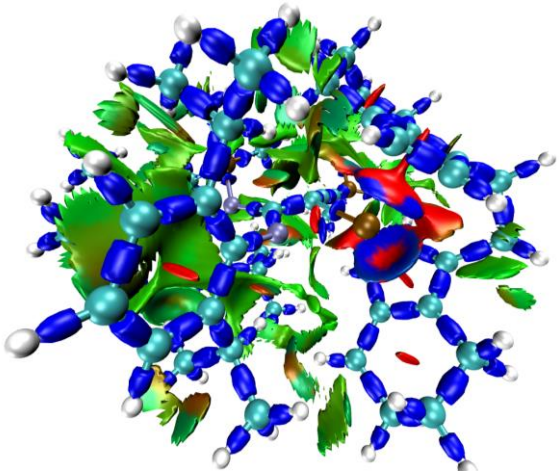

9.2.3 Investigation of the first reaction step between 1-zirconacyclobuta-2,3-dienes and selected carbodiimides.

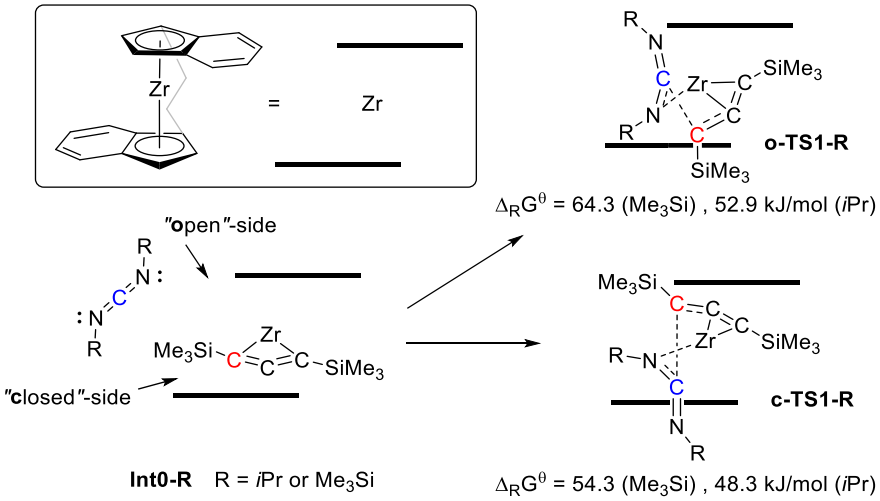

Scheme S2. Illustration of the two different pathways studied for the approach of the carbodiimide to the 1-zirconacyclobuta-2,3-diene.

Table S6. Calculated reaction enthalpies and Gibbs free energies of the two different pathways studied for the approach of the carbodiimide to the 1-zirconacyclobuta-2,3-diene (B3LYP/GD3BJ/def2svpp//def2tzvp) level of theory).

Calculated complex	Δ_RH [kJ/mol]	Δ_RG [kJ/mol]	Δ_RH [kcal/mol]	Δ_RG [kcal/mol]
EBIZr_TMS_int0_sp_tzvp **Int0-Me3Si**	0.0	0.0	0.0	0.0
EBIZr_TMS_TS3_sp_tzvp **o-TS1-Me3Si**	35.8	64.3	8.6	15.4
EBIZr_TMS_TS13_sp_tzvp **c-TS1-Me3Si**	23.8	54.3	5.7	13.0
EBIZr_iPr_int0_sp_tzvp **Int0-iPr**	0.0	0.0	0.0	0.0
o_TS1_iPr_sp_tzvp **o-TS1-iPr**	27.5	52.9	6.6	12.6
EBIZr_iPr_TS1_sp_tzvp **c-TS1-iPr**	20.2	48.3	4.8	11.6
EBTHIZr_TMS_Int0_sp_tzvp **Int0-Me3Si EBTHI**	0.0	0.0	0.0	0.0
EBTHIZr_TMS_TS3_sp_tzvp **o-TS1-Me3Si EBTHI**	59.2	85.9	14.1	20.5
EBTHIZr_TMS_TS23_sp_tzvp **c-TS1-Me3Si EBTHI**	37.0	67.9	8.8	16.2

Table S7. Comparison of Interaction Region Indicator analyses of the calculated **o/c-TS1-Me3Si** transition state structures of EBI complexes.

o-TS1-iPr front 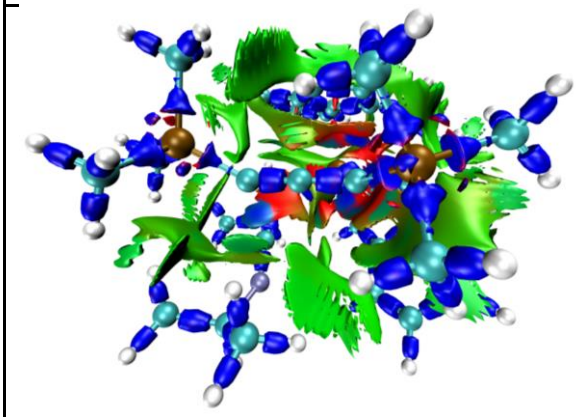	**c-TS1- iPr** front 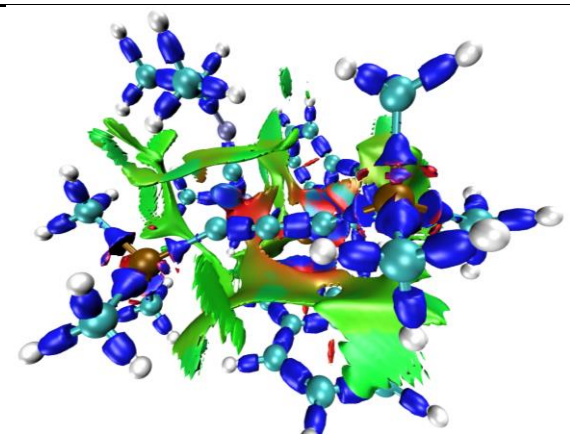
o-TS1- iPr side1 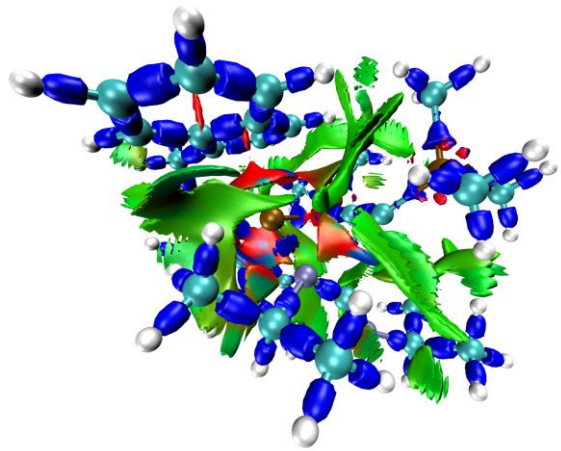	**c-TS1- iPr** side1 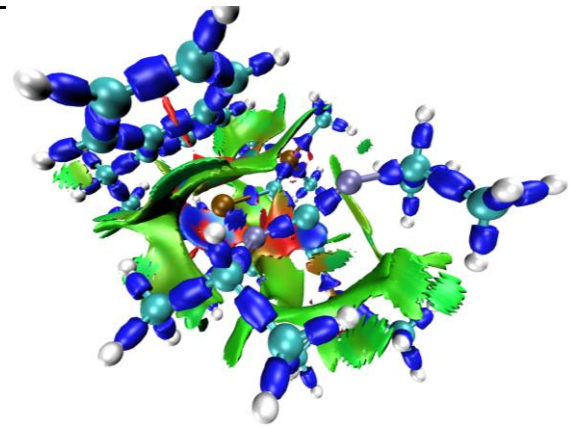
o-TS1- iPr back 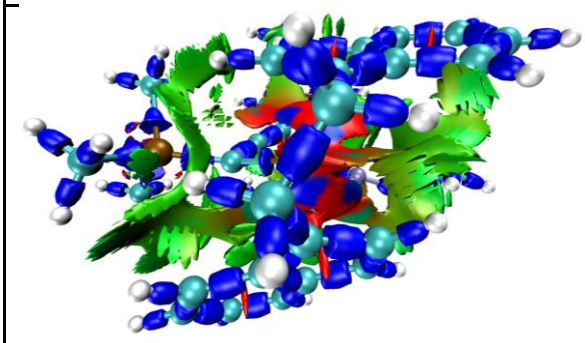	**c-TS1- iPr** back 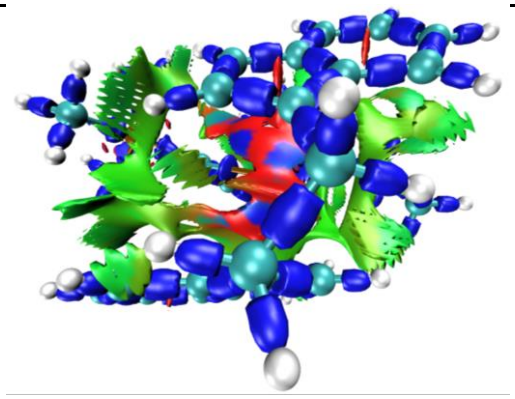

o-TS1- iPr side2	**c-TS1- iPr** side2
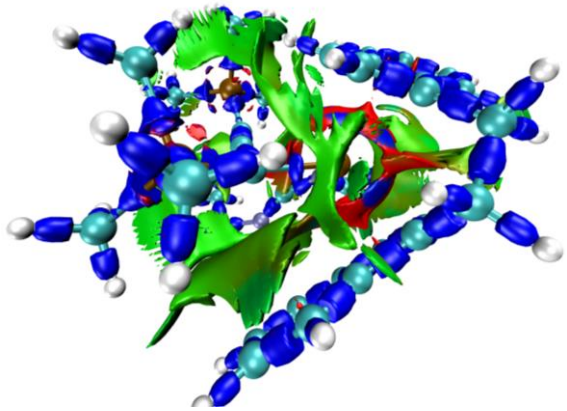	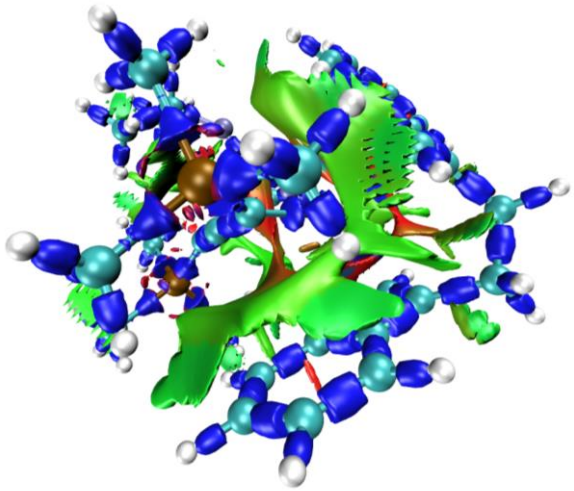
o-TS1- iPr IRI scattering graph	**c-TS1- iPr** IRI scattering graph
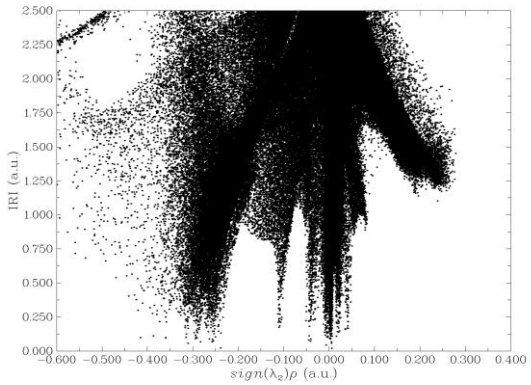	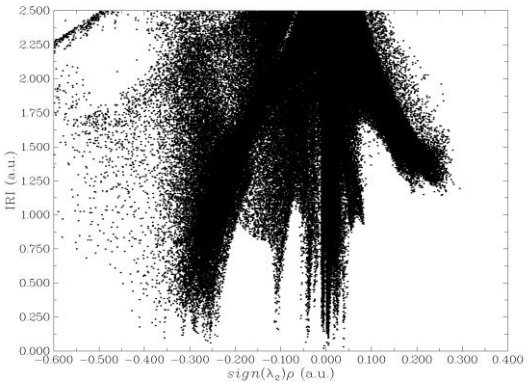

Table S8. Comparison of Interaction Region Indicator analyses of the calculated **o/c-TS1-Me3Si** transition state structures of EBI complexes.

o-TS1-Me3Si front	**c-TS1-Me3Si** front
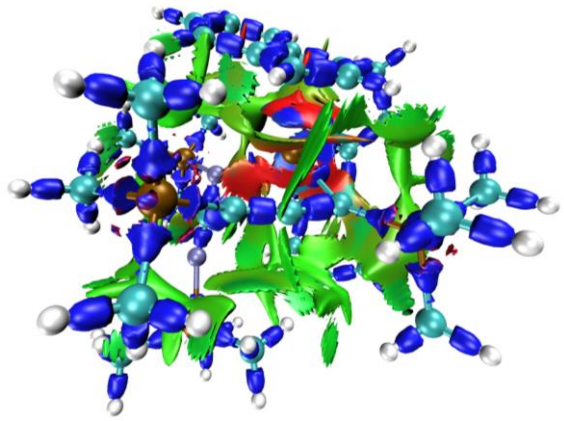	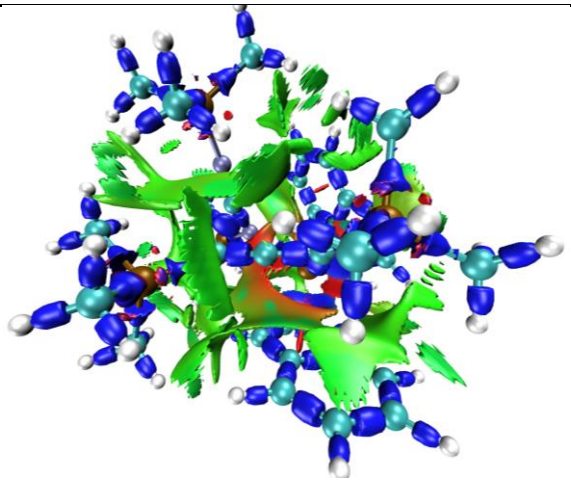
o-TS1-Me3Si side1	**c-TS1-Me3Si** side1
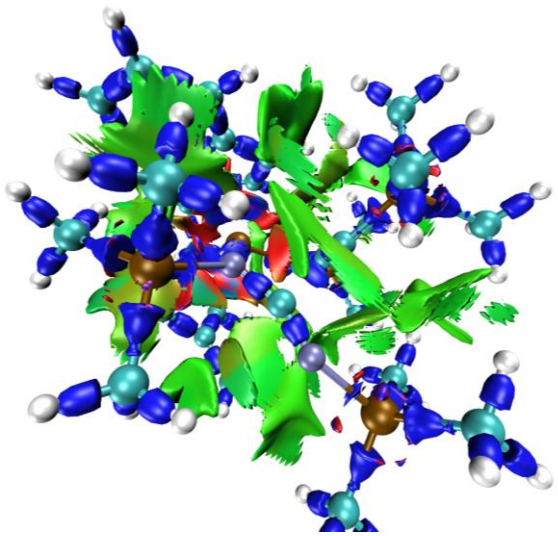	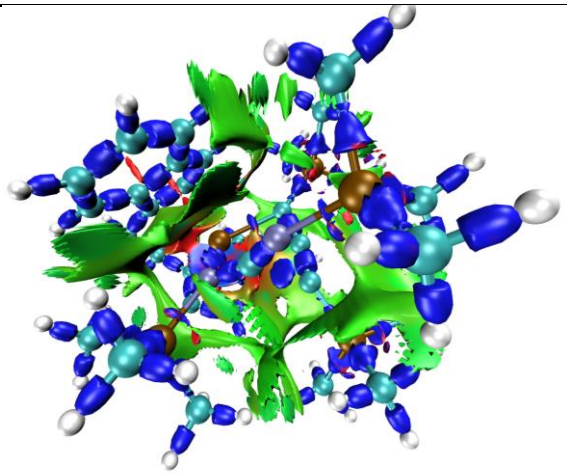
o-TS1-Me3Si back	**c-TS1-Me3Si** back
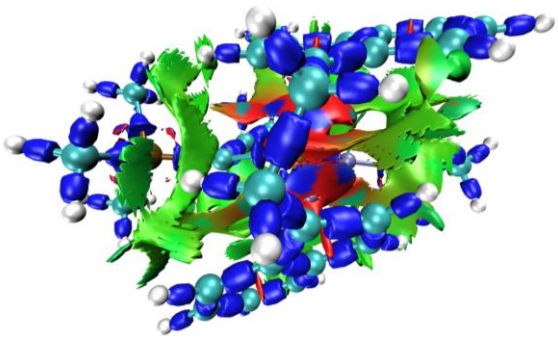	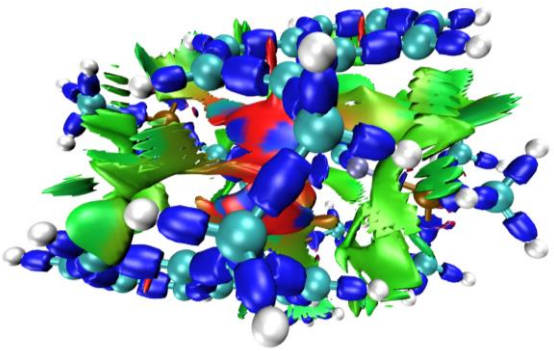

o-TS1-Me3Si side2	**c-TS1-Me3Si** side2
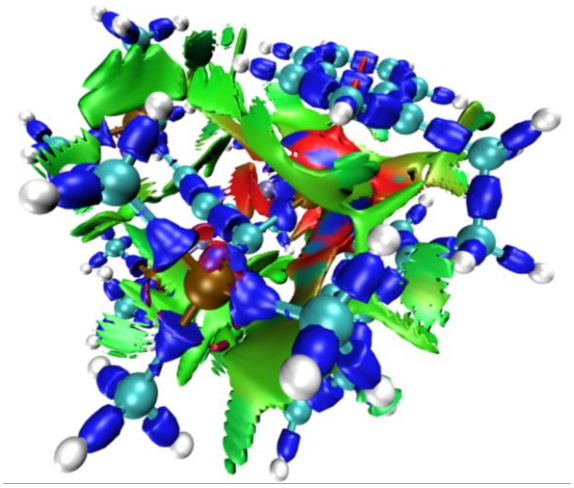	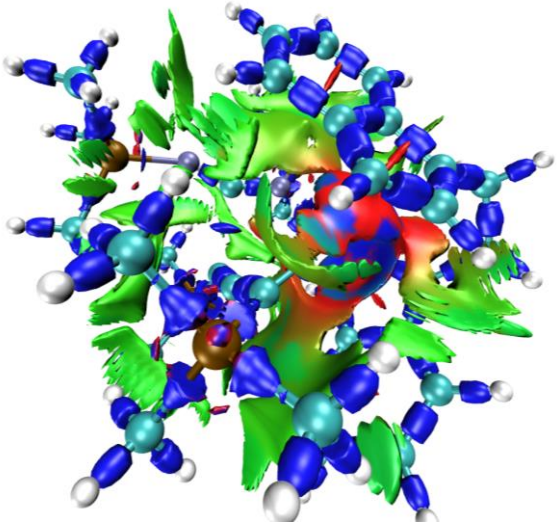
o-TS1-Me3Si IRI scattering graph	**c-TS1-Me3Si** IRI scattering graph
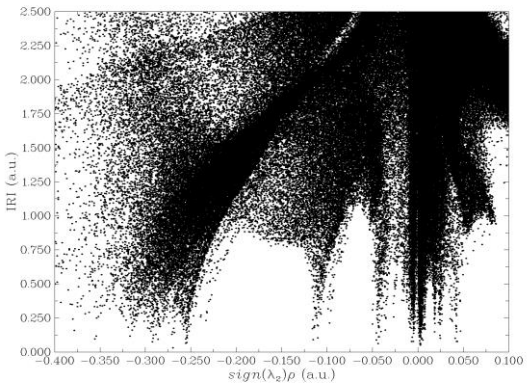	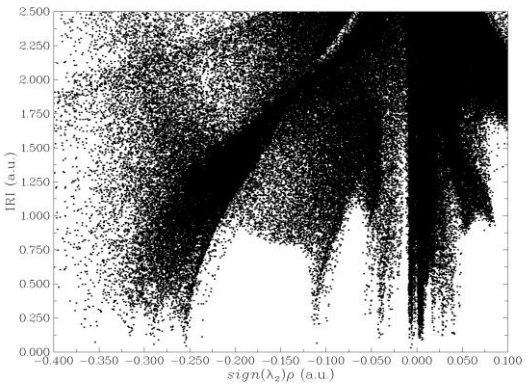

9.2.4 Investigation of a reaction sequence to form 2-aza-1-metallacyclobut-3-ene complexes via a six membered metallacycle pathway.

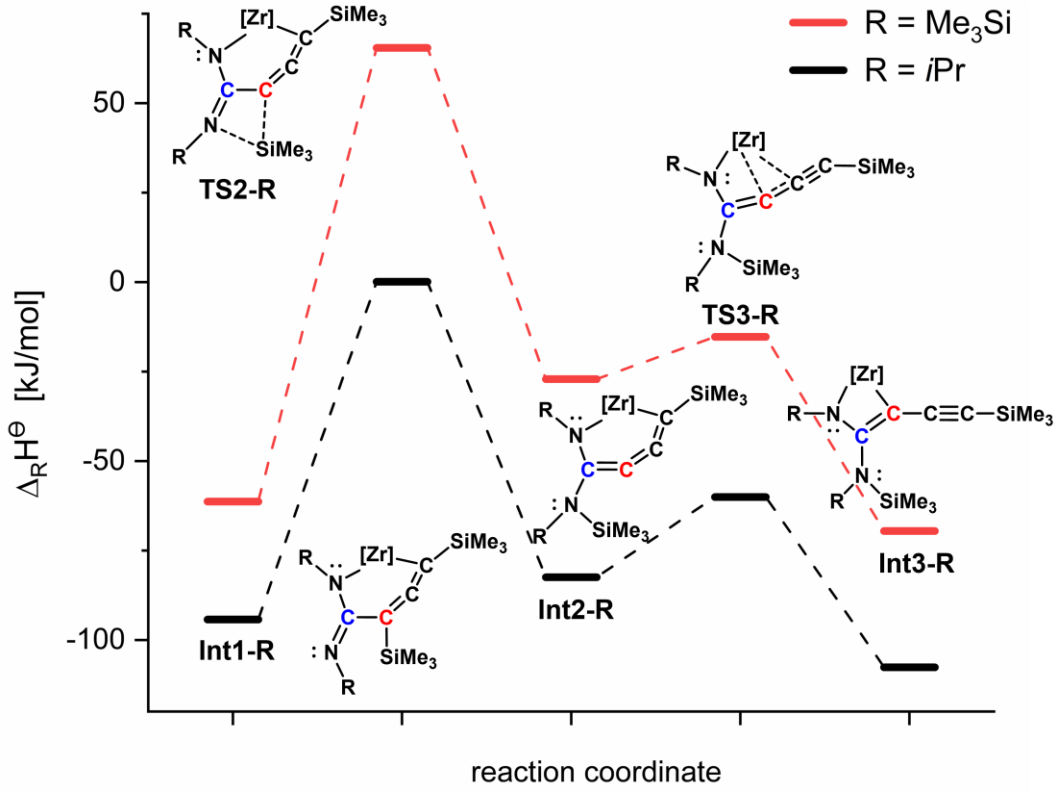

Scheme S3. Comparison of the standard reaction enthalpy profiles of two differently substituted carbodiimides (R = Me_3Si and *i*Pr) via a six membered metallacycle pathway to form 2-aza-1-metallacyclobut-3-ene complexes. Energies were referenced to their corresponding **Int0-R** structures; [Zr] = *rac*-(ebi)Zr; B3LYP/GD3BJ/def2svpp//def2tzvp level of theory.

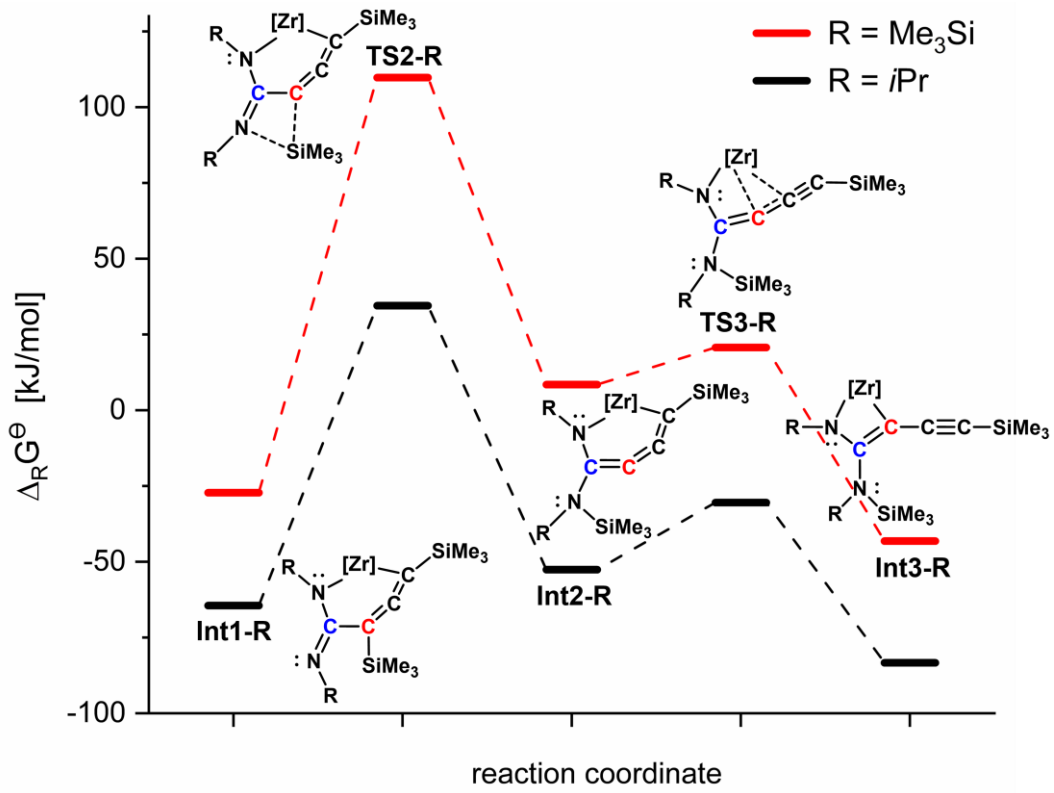

Scheme S4. Comparison of the standard Gibbs free energy profiles of two differently substituted carbodiimides (R = Me_3Si and *i*Pr) via a six membered metallacycle pathway to form 2-aza-1-metallacyclobut-3-ene complexes. Energies were referenced to their corresponding **Int0-R** structures; [Zr] = *rac*-(ebi)Zr; B3LYP/GD3BJ/def2svpp//def2tzvp level of theory.

Table S9. Calculated Gibbs free energies and reaction enthalpies for the considered six membered metallacycle pathway to form 2-aza-1-metallacyclobut-3-ene (**P2c-iPr** = **Int3-iPr**).

Calculated complex	Δ_RH [kJ/mol]	Δ_RG [kJ/mol]	Δ_RH [kcal/mol]	Δ_RG [kcal/mol]
EBIZr_iPr_int0_sp_tzvp **Int0-iPr**	0.00	0.00	0.00	0.00
EBIZr_iPr_Int1_sp_tzvp **c-Int1-iPr**	-94.29	-64.45	-22.54	-15.40
EBIZr_iPr_Int1_TMSshift_TS2_sp_tzvp **c-TS2-iPr-6m**	0.09	34.53	0.02	8.25
EBIZr_iPr_Int1_TMSshift_Int2_sp_tzvp **c-Int2-iPr-6m**	-82.45	-52.59	-19.71	-12.57
EBIZr_iPr_Int1Int2TS_sp_tzvp **c-TS3-iPr-6m**	-60.04	-30.48	-14.35	-7.29
EBIZr_iPrNCNiPrTMSCCCTMS_sp_tzvp **Int3-iPr**	-107.64	-83.34	-25.73	-19.92

Table S10. Calculated Gibbs free energies and reaction enthalpies for the considered six membered metallacycle pathway to form 2-aza-1-metallacyclobut-3-ene (**Int3-Me3Si**).

Calculated complex	Δ_RH [kJ/mol]	Δ_RG [kJ/mol]	Δ_RH [kcal/mol]	Δ_RG [kcal/mol]
EBIZr_TMS_int0_sp_tzvp **Int0-Me3Si**	0.00	0.00	0.00	0.00
EBIZr_TMS_Int13_sp_tzvp **c-Int1-Me3Si**	-61.34	-27.20	-14.66	-6.50
EBIZr_TMS_TS23_TCshift_sp_tzvp **c-TS2-Me3Si-6m**	65.44	109.77	15.64	26.24
EBIZr_TMS_Int23_TCshift_sp_tzvp **c-Int2-Me3Si-6m**	-27.08	8.43	-6.47	2.01
EBIZr_TMS_Int3Int1TS_sp_tzvp **o/c-TS3-Me3Si-6m**	-15.31	20.68	-3.66	4.94
EBIZr_TMSNCNTMSTMSCCCTMS_sp_tzvp_empi **Int3-Me3Si**	-69.57	-43.20	-16.63	-10.32

Table S11. Comparison of structural features of different calculated **o/c-Int1-R** structures data were measured with Mercury from the structures optimised on B3LYP/GD3BJ/def2svpp level of theory.

o-Int1-iPr	**c-Int1-iPr**
"open"-Pathway was not considered for this species.	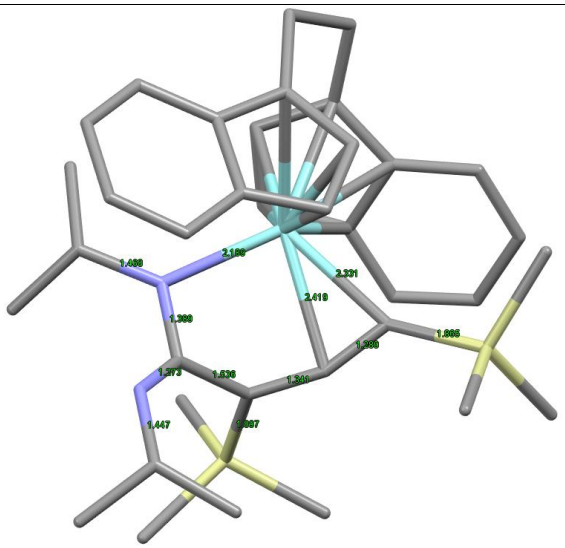
o-Int1-Me3Si	**c-Int1-Me3Si**
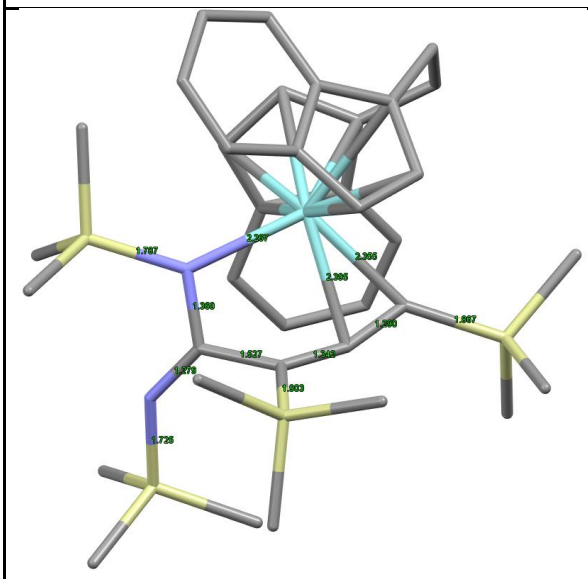	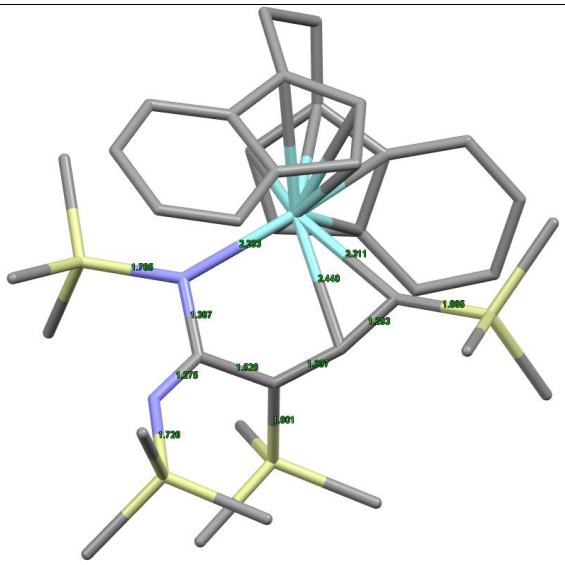

o-Int1-Me3Si EBTHI	c-Int1-Me3Si EBTHI
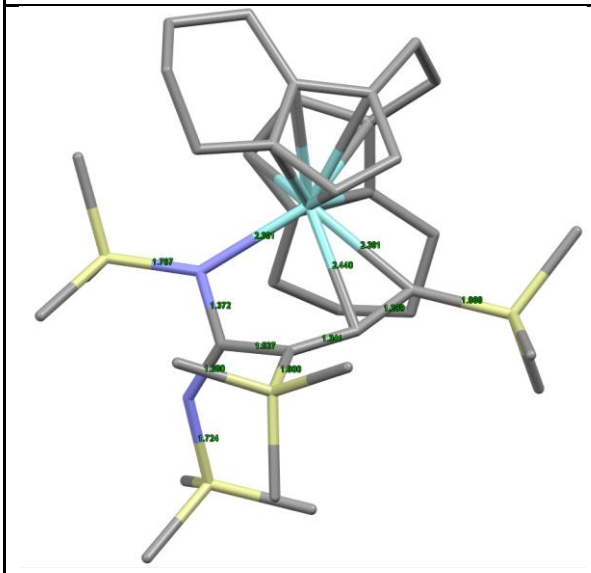	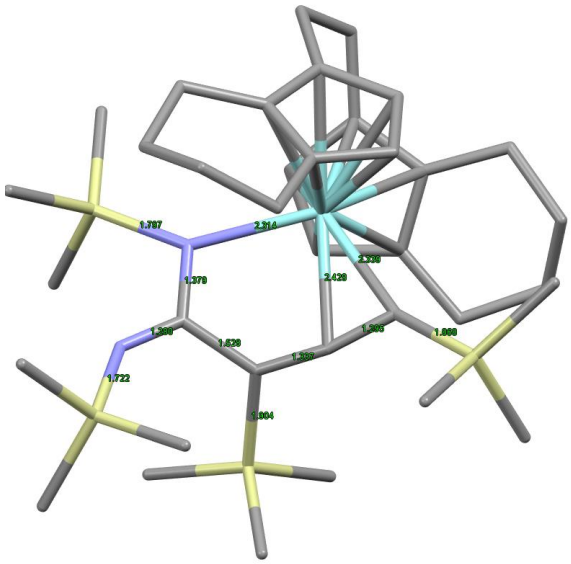

9.2.5 Investigation of a R Group shift to form 1-metalla-2-aza-cyclohexa-2,4,5-triene complexes.

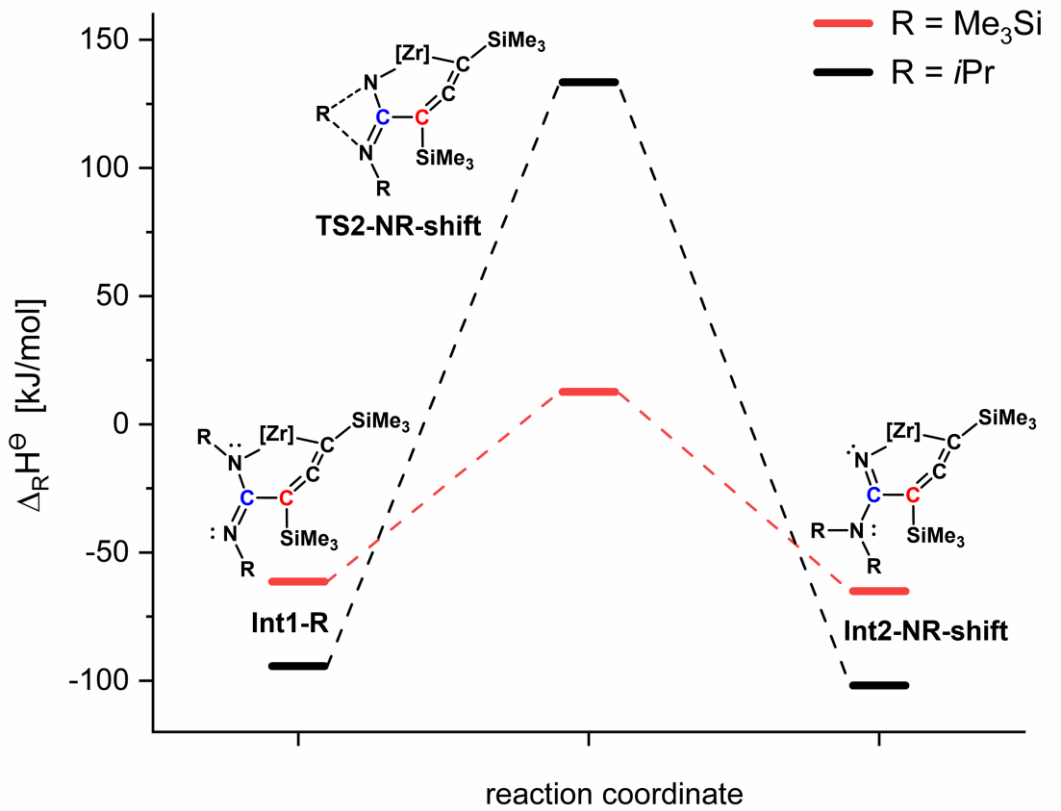

Scheme S5. Comparison of the standard reaction enthalpy profiles of two differently substituted carbodiimides (R = Me_3Si and iPr) via a R group shift from the metal-bound nitrogen to the second nitrogen atom of the former carbodiimide to form 2-aza-1-metallacyclohexa-2,4,5-triene complexes. Energies were referenced to their corresponding **Int0-R** structures; [Zr] = *rac*-(ebi)Zr; B3LYP/GD3BJ/def2svpp//def2tzvp level of theory.

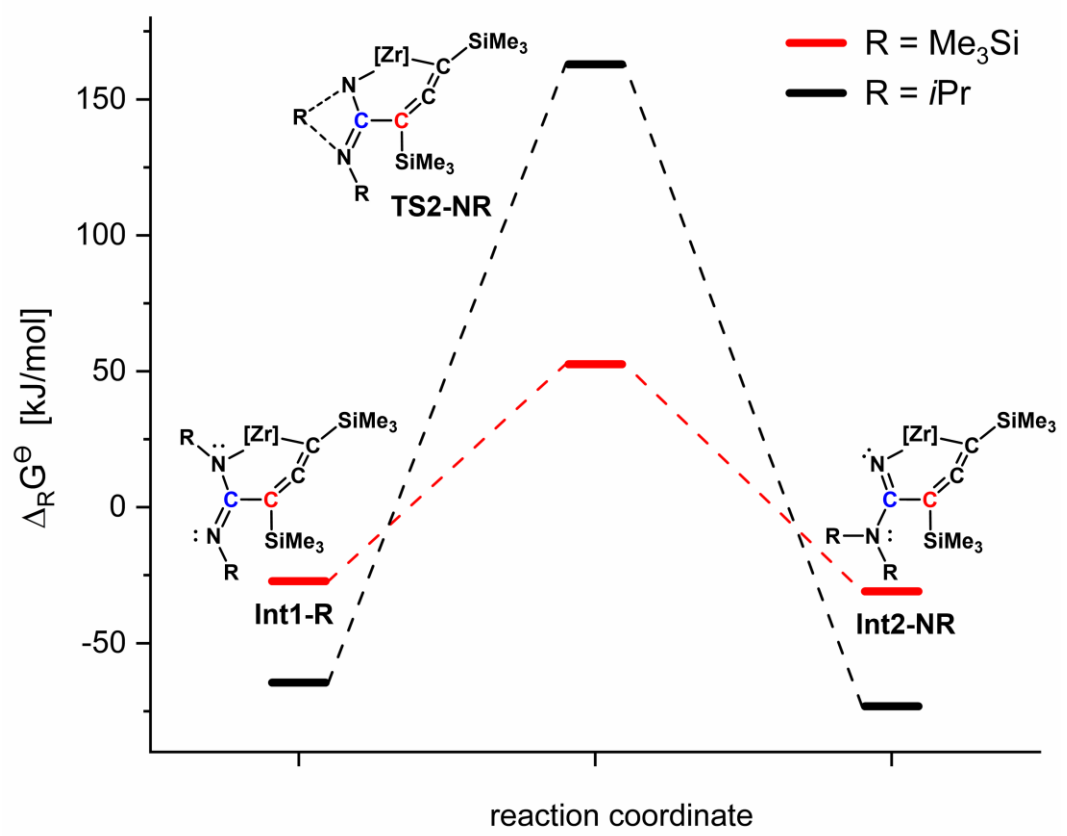

Scheme S6. Comparison of Gibbs free energy profiles of two differently substituted carbodiimides (R = Me_3Si and *i*Pr) via a R group shift from the metal-bound nitrogen to the second nitrogen atom of the former carbodiimide to form 2-aza-1-metalla-cyclohexa-2,4,5-triene complexes. Energies were referenced to their corresponding **Int0-R** structures; [Zr] = *rac*-(ebi)Zr; B3LYP/GD3BJ/def2svpp//def2tzvp level of theory.

Table S12. Calculated Gibbs free energies and reaction enthalpies for the considered R group shift to form 2-aza-1-metalla-cyclohexa-2,4,5-triene complexes (**c-Int2-NR-shift**).

Calculated complex	Δ_RH [kJ/mol]	Δ_RG [kJ/mol]	Δ_RH [kcal/mol]	Δ_RG [kcal/mol]
EBIZr_iPr_int0_sp_tzvp **Int0-iPr**	0.00	0.00	0.00	0.00
EBIZr_iPr_Int1_iPrshift_TS1_sp_tzvp **c-TS2-NiPr-shift**	133.44	162.86	31.89	38.92
EBIZr_iPr_Int1_iPrshift_Int1_sp_tzvp **c-Int2-NiPr-shift**	-101.88	-73.15	-24.35	-17.48
EBIZr_TMS_int0_sp_tzvp **Int0-Me3Si**	0.00	0.00	0.00	0.00
EBIZr_TMS_TS23_TNshift_sp_tzvp **c-TS2-NMe3Si-shift**	12.69	52.60	3.03	12.57
EBIZr_TMS_Int23_TNshift_sp_tzvp **c-Int2-NMe3Si-shift**	-65.07	-30.91	-15.55	-7.39

9.2.6 Investigation of ethylene bridge flip in 1-metallacyclobuta-2,3-dienes.

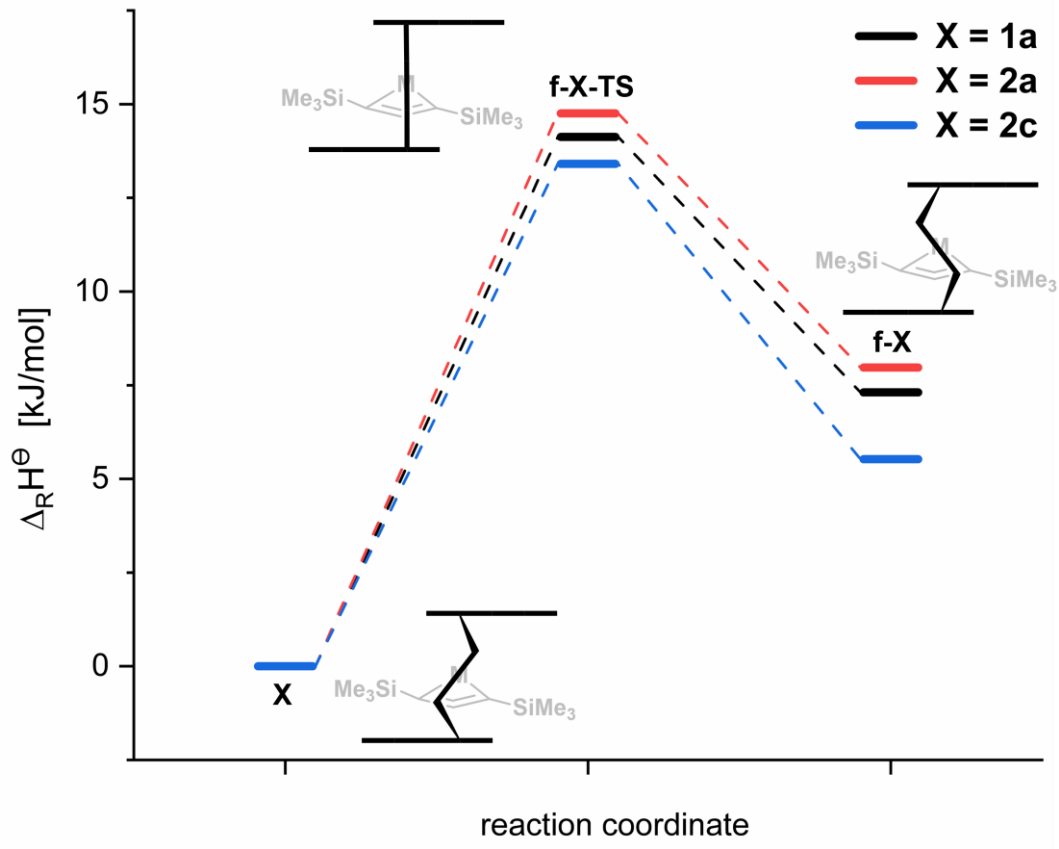

Scheme S7. Comparison of the standard reaction enthalpy profiles for the ethylene bridge flip in three 1-metallacyclobuta-2,3-dienes. Energies were referenced to their corresponding structures **X** which are lower in energy and in line with SC-XRD measurements. B3LYP/GD3BJ/def2svpp//def2tzvp level of theory.

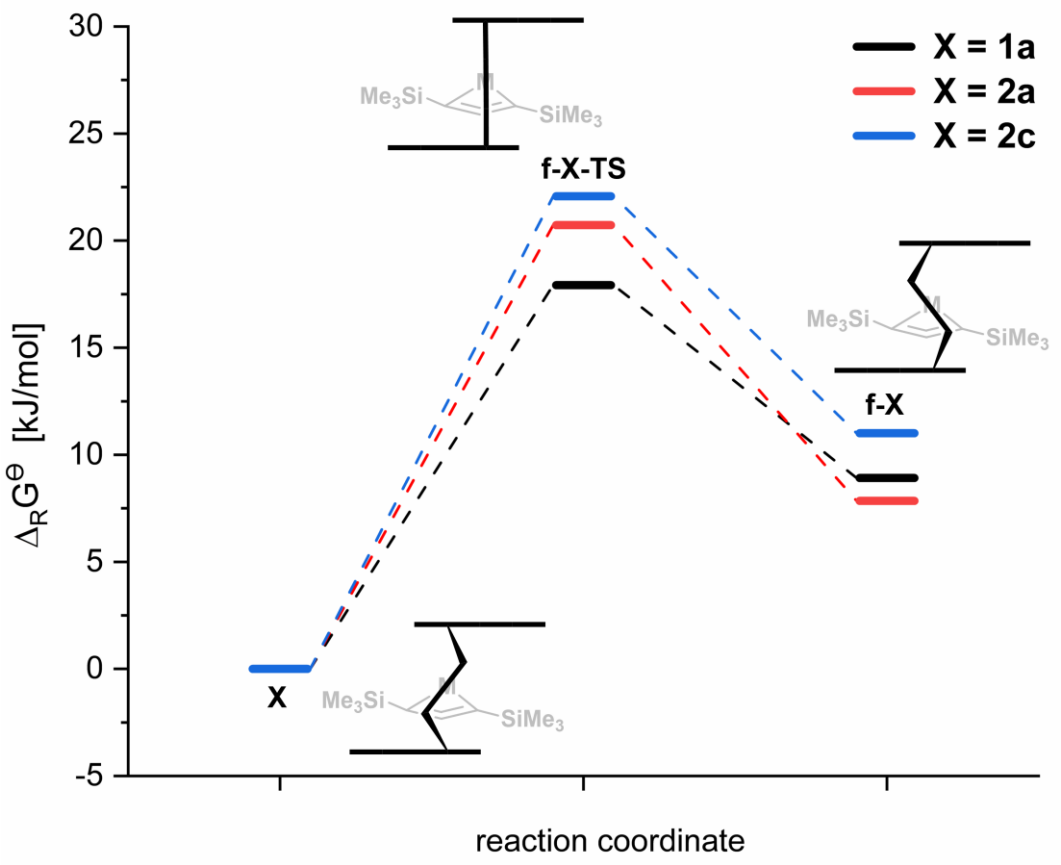

Scheme S8. Comparison of the Gibbs free energy profiles for the ethylene bridge flip in three 1-metallacyclobuta-2,3-dienes. Energies were referenced to their corresponding structures **X** which are lower in energy and in line with SC-XRD measurements. B3LYP/GD3BJ/def2svpp//def2tzvp level of theory.

Table S13. Calculated Gibbs free energies and reaction enthalpies for the ethylene bridge flip to form the corresponding flipped isomers/conformers **f-X**.

Calculated complex	Δ_RH [kJ/mol]	Δ_RG [kJ/mol]	Δ_RH [kcal/mol]	Δ_RG [kcal/mol]
EBTHITi_TMS2C3_sp_tzvp **1a**	0.00	0.00	0.00	0.00
EBTHITi_TMSC3_TS_EBTHIflip_sp_tzvp **f-1a-TS**	14.13	17.93	3.38	4.28
EBTHITi_TMSC3_Int_EBTHIflip_sp_tzvp **f-1a**	7.31	8.92	1.75	2.13
EBTHIZr_TMS2C3_sp_tzvp **2a**	0.00	0.00	0.00	0.00
EBTHIZr_TMSC3_TS_EBTHIflip_sp_tzvp **f-2a-TS**	14.75	20.72	3.53	4.95
EBTHIZr_TMSC3_Int_EBTHIflip_sp_tzvp **f-2a**	7.97	7.84	1.91	1.87
EBIZr_TMS2C3_sp_tzvp **2c**	0.00	0.00	0.00	0.00
EBIZr_TMSC3_TSEBIflip_sp_tzvp **f-2c-TS**	13.41	22.08	3.20	5.28
EBIZr_TMSC3_IntEBIflip_sp_tzvp **f-2c**	5.53	11.01	1.32	2.63

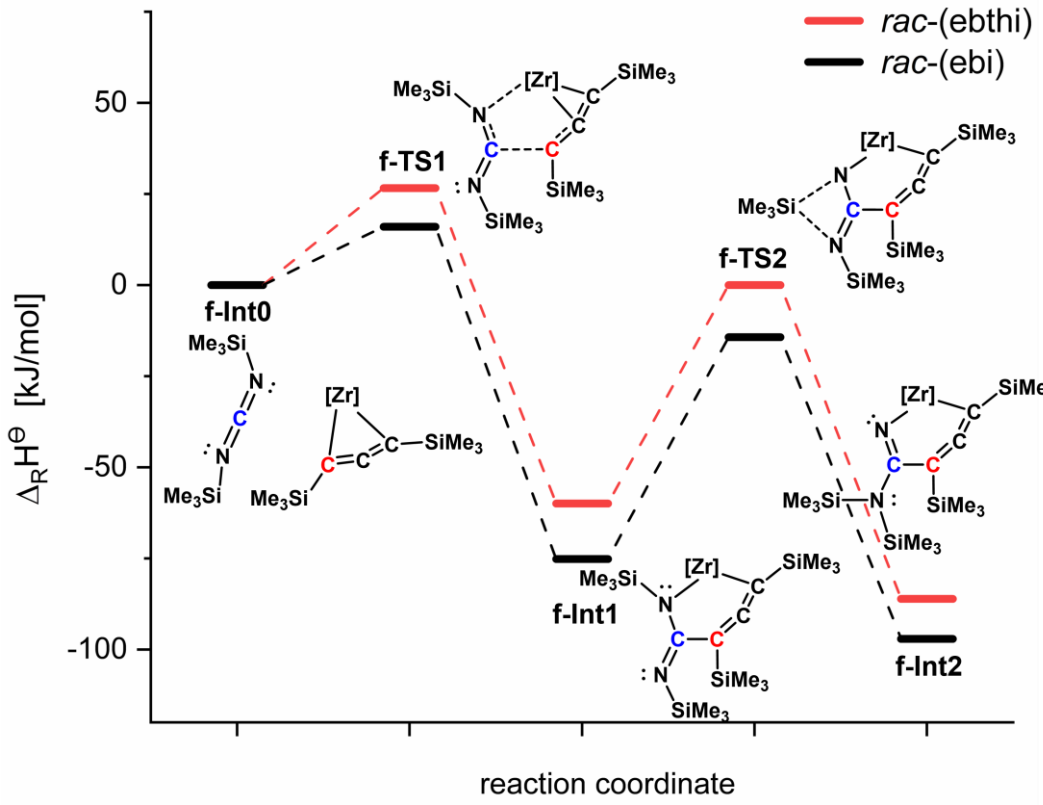

Scheme S9. Comparison of the standard reaction enthalpy profiles for the ethylene bridge flipped 1-metallacyclobuta-2,3-dienes *rac*-(ebthi)Zr (red) and *rac*-(ebi)Zr (black) in the reaction with $Me_3SiNCNSiMe_3$ to form the 2-aza-1-metalla-cyclohexa-2,4,5-triene complex which was only experimentally observed in case of *rac*-(ebi)Zr. B3LYP/GD3BJ/def2svpp//def2tzvp level of theory.

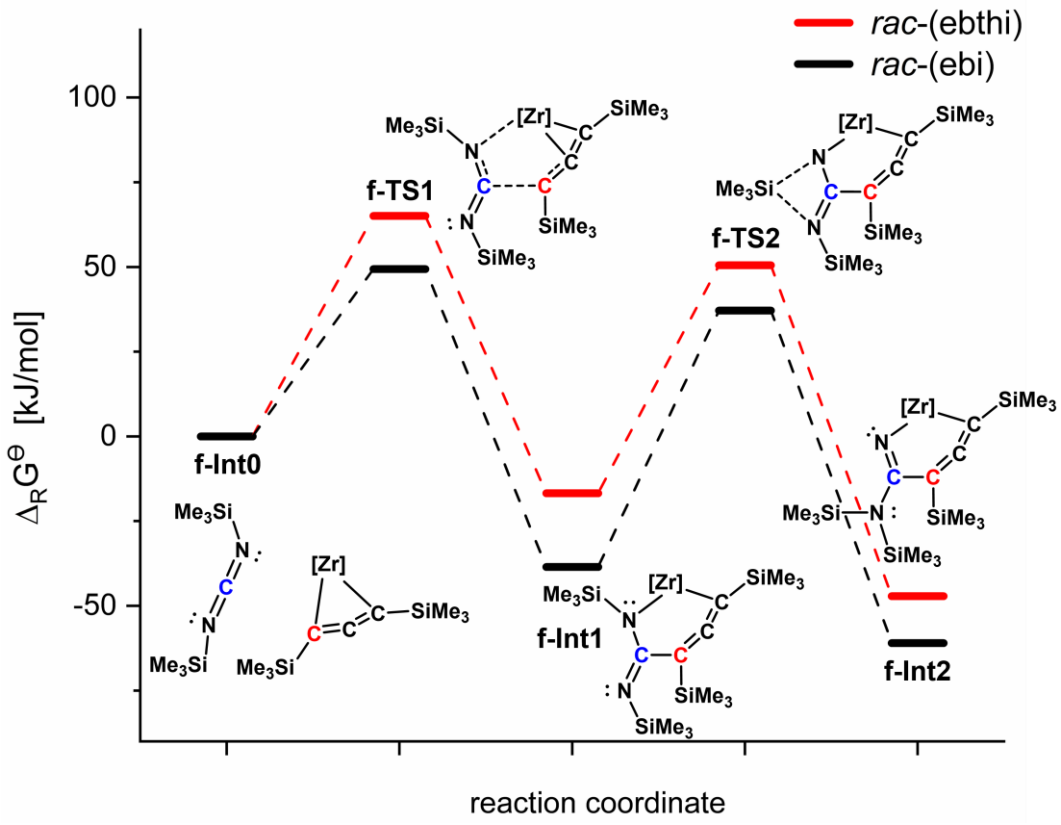

Scheme S10. Comparison of the Gibbs free energy profiles for the ethylene bridge flipped 1-metallacyclobuta-2,3-dienes *rac*-(ebthi)Zr (red) and *rac*-(ebi)Zr (black) in the reaction with $Me_3SiNCNSiMe_3$ to form the -2-aza 1-metalla-cyclohexa-2,4,5-triene complex which was only experimentally observed in case of *rac*-(ebi)Zr. B3LYP/GD3BJ/def2svpp//def2tzvp level of theory.

Table S14. Calculated Gibbs free energies and reaction enthalpies for the reaction of ethylene bridge flipped 1-metallacyclobuta-2,3-dienes and with $Me_3SiNCNSiMe_3$. B3LYP/GD3BJ/def2svpp//def2tzvp level of theory.

Calculated complex	$\Delta_R H$ [kJ/mol]	$\Delta_R G$ [kJ/mol]	$\Delta_R H$ [kcal/mol]	$\Delta_R G$ [kcal/mol]
EBIZr_TMS_Int04_sp_tzvp **f-Int0**	0.00	0.00	0.00	0.00
EBIZr_TMS_TS14_sp_tzvp **f-TS1**	15.97	49.36	3.82	11.80
EBIZr_TMS_Int14_sp_tzvp **f-Int1**	-75.16	-38.54	-17.96	-9.21
EBIZr_TMS_TS24_sp_tzvp **f-TS2**	-14.33	37.16	-3.42	8.88
EBIZr_TMS_Int24_sp_tzvp **f-Int2**	-97.10	-60.97	-23.21	-14.57
EBTHIZr_TMS_Int05_sp_tzvp **f-Int0**	0.00	0.00	0.00	0.00
EBTHIZr_TMS_TS15_sp_tzvp **f-TS1**	26.62	65.09	6.36	15.56
EBTHIZr_TMS_Int15_sp_tzvp **f-Int1**	-59.97	-16.75	-14.33	-4.00
EBTHIZr_TMS_TS25_sp_tzvp **f-TS2**	-0.03	50.51	-0.01	12.07
EBTHIZr_TMS_Int25_sp_tzvp **f-Int2**	-86.13	-47.15	-20.59	-11.27

9.2.7 Total enthalpies and energies for all calculated molecules

Table S15. Summary of thermodynamic data of all calculated compounds level of theory B3LYP/GD3BJ/def2tzvp

Compound	Nimag	HF	ZPE [kcal/mol]	H_{tot} [a.u.]	G_{tot} [a.u.]	Method	Basis set
Me3SiCl	0	-869.6592458	70.42432	-869.537476	-869.579564	B3LYP/GD3BJ	def2tzvp
Me3SiOSiMe3	0	-894.1117432	141.98261	-893.868131	-893.929022	B3LYP/GD3BJ	def2tzvp
Ethane	0	-79.8694016	46.708110	-79.790541	-79.816384	B3LYP/GD3BJ	def2tzvp
Acetone	0	-193.2481561	52.24638	-193.15849	-193.194179	B3LYP/GD3BJ	def2tzvp
Acetophenone	0	-385.0743385	86.34292	-384.927953	-384.969597	B3LYP/GD3BJ	def2tzvp
Benzophenone	0	-576.8981672	119.97312	-576.695283	-576.744654	B3LYP/GD3BJ	def2tzvp
iPrNCNiPr	0	-384.8472261	127.25376	-384.632026	-384.683452	B3LYP/GD3BJ	def2tzvp
Me3SiNCNSiMe3	0	-966.4872614	148.6919	-966.230598	-966.302690	B3LYP/GD3BJ	def2tzvp
DippNCNDipp	0	-1083.177807	334.74369	-1082.6143	-1082.705644	B3LYP/GD3BJ	def2tzvp
rac(EBTHI)ZCl2	0	-1744.767621	247.71914	-1744.350654	-1744.422075	B3LYP/GD3BJ	def2tzvp
rac(EBTHI)ZrMe2	0	-903.9987739	289.39662	-903.513891	-903.586976	B3LYP/GD3BJ	def2tzvp
rac(Me2SiBTHI)ZrMe2	0	-1194.770949	300.29944	-1194.264846	-1194.345954	B3LYP/GD3BJ	def2tzvp
rac(EBI)ZrMe2	0	-899.1501255	230.88838	-898.760405	-898.829056	B3LYP/GD3BJ	def2tzvp
racEBTHIZrO sing.	0	-899.4229762	246.43767	-899.009718	-899.079015	B3LYP/GD3BJ	def2tzvp
racEBTHIZrO trip.	0	-899.3439768	245.66399	-898.931736	-899.001353	B3LYP/GD3BJ	def2tzvp
racMe2SiBTHIZrO sing.	0	-1190.192674	257.57811	-1189.758004	-1189.833592	B3LYP/GD3BJ	def2tzvp
Cp2Ti(Me3SiCCCSiMe3) sing	0	-2169.864576	255.86548	-2169.427444	-2169.513708	B3LYP/GD3BJ	def2tzvp
Cp2Ti(Me3SiCCCSiMe3) sp trip	0	-2169.855337	255.50882	-2169.418719	-2169.506762	B3LYP/GD3BJ	def2tzvp
Cp*2Ti(Me3SiCCCSiMe3) sing	0	-2563.224056	429.90121	-2562.492906	-2562.611974	B3LYP/GD3BJ	def2tzvp
Cp*2Ti(Me3SiCCCSiMe3) sp trip	0	-2563.227809	429.80239	-2562.496839	-2562.616917	B3LYP/GD3BJ	def2tzvp
rac(EBTHI)Ti(Me3SiCCCSiMe3) sing	0	-2559.611824	395.88384	-2558.943125	-2559.04643	B3LYP/GD3BJ	def2tzvp
rac(EBTHI)Ti(Me3SiCCCSiMe3) sp trip	0	-2559.59604	395.5044	-2558.927845	-2559.033934	B3LYP/GD3BJ	def2tzvp
rac(EBI)Ti(Me3SiCCCSiMe3) sing	0	-2554.758579	337.20292	-2554.18525	-2554.285628	B3LYP/GD3BJ	def2tzvp

rac(EBI)Ti(Me3SiCCCSiMe3) sp trip	1	-2554.748994	336.9513	-2554.176976	-2554.274748	B3LYP/GD3BJ	def2tzvp
rac(EBTHI)Zr(Me3SiCCCSiMe3) sing	0	-1757.232947	395.319800	-1756.564802	-1756.669563	B3LYP/GD3BJ	def2tzvp
rac(EBTHI)Zr(Me3SiCCCSiMe3) sp trip	1	-1757.194949	394.55129	-1756.528695	-1756.632130	B3LYP/GD3BJ	def2tzvp
racMe2SiBTHIZr(Me3SiCCCSiMe3) sing	0	-2048.004523	406.34419	-2047.315153	-2047.427473	B3LYP/GD3BJ	def2tzvp
racMe2SiBTHIZr(Me3SiCCCSiMe3) sp trip	1	-2047.967599	405.63397	-2047.280058	-2047.390984	B3LYP/GD3BJ	def2tzvp
rac(EBI)Zr(Me3SiCCCSiMe3) sing	0	-1752.380268	336.44402	-1751.807689	-1751.910082	B3LYP/GD3BJ	def2tzvp
rac(EBI)Zr(Me3SiCCCSiMe3) sp trip	1	-1752.34918	335.79638	-1751.778345	-1751.879087	B3LYP/GD3BJ	def2tzvp
racMe2SiBI(Me3SiCCCSiMe3) sing	0	-2043.154902	347.63158	-2042.560911	-2042.670022	B3LYP/GD3BJ	def2tzvp
racMe2SiBI(Me3SiCCCSiMe3) sp trip	1	-2043.124938	346.97125	-2042.532708	-2042.640383	B3LYP/GD3BJ	def2tzvp
racEBTHI_Ti_iPr P1a-iPr	0	-2944.517742	526.5755	-2943.629638	-2943.756778	B3LYP/GD3BJ	def2tzvp
racEBTHI_Ti_TMS P1a-TMS	0	-3526.138332	548.74108	-3525.2084	-3525.348426	B3LYP/GD3BJ	def2tzvp
racEBTHI_Ti_TMS P1a-Dipp	0	-3642.803287	736.39355	-3641.564225	-3641.722675	B3LYP/GD3BJ	def2tzvp
racEBTHI_Zr_iPr P2a-iPr	0	-2142.143172	525.56046	-2141.256198	-2141.385486	B3LYP/GD3BJ	def2tzvp
racEBTHI_Zr_TMS P2a-TMS	0	-2723.766193	547.7582	-2722.83733	-2722.97885	B3LYP/GD3BJ	def2tzvp
racEBTHI_Zr_Dipp P2a-Dipp	0	-2840.434643	735.78041	-2839.196452	-2839.355705	B3LYP/GD3BJ	def2tzvp
racMe2SiBTHI_Zr_iPr P2b-iPr	0	-2432.915346	536.53757	-2432.007102	-2432.144456	B3LYP/GD3BJ	def2tzvp
racMe2SiBTHI_Zr_TMS P2a-TMS	0	-3014.54083	558.5886	-3013.590893	-3013.740802	B3LYP/GD3BJ	def2tzvp
racEBI_Zr_iPr P2c-iPr	0	-2137.292259	466.97801	-2136.500522	-2136.626226	B3LYP/GD3BJ	def2tzvp
racEBI_Zr_TMS P2c-TMS	0	-2718.911477	488.59975	-2718.078222	-2718.218814	B3LYP/GD3BJ	def2tzvp
racMe2SiBI_Zr_iPr P2d-iPr	0	-2428.066782	477.88674	-2427.25384	-2427.387632	B3LYP/GD3BJ	def2tzvp
racMe2SiBI_Zr_TMS P2d-TMS	0	-3009.689859	499.73096	-3008.83534	-3008.983068	B3LYP/GD3BJ	def2tzvp
racEBIZr_NCNTMS2TMSCCCTMS	0	-2718.915597	488.48934	-2718.083003	-2718.220407	B3LYP/GD3BJ	def2tzvp
racMe2BIZr_NCNTMS2TMSCCCTMS	0	-3009.689997	499.45084	-3008.83611	-3008.981765	B3LYP/GD3BJ	def2tzvp
racEBTHIZr_NCNTMS2TMSCCCTMS	0	-2723.767436	547.38582	-2722.839307	-2722.979352	B3LYP/GD3BJ	def2tzvp

Table S16. Summary of thermodynamic data of all calculated compounds level of theory B3LYP/GD3BJ/def2svpp.

File-Name	Nimag	HF	ZPE [kcal/mol]	Th. Corr. H	Th. Corr. G	H_{tot} [a.u.]	G_{tot} [a.u.]
EBIZr_TMS2C3 **2c**	0	-1750.8497315	336.27351	0.572252	0.469811	-1750.277480	-1750.379921
EBIZr_TMSC3_TSEBIflip **f-2c-TS**	1	-1750.844035	336.32377	0.571503	0.472363	-1750.272532	-1750.371672
EBIZr_TMSC3_IntEBIflip **f-2c**	0	-1750.847953	336.54143	0.572409	0.472054	-1750.275544	-1750.375899
EBTHIZr_TMS2C3 **2a**	0	-1755.681117	394.90885	0.667411	0.562446	-1755.013706	-1755.118671
EBTHIZr_TMSC3_TS_EBTHIflip_opt_freq **f-2a-TS**	1	-1755.6748999	394.87727	0.666594	0.563902	-1755.008306	-1755.110998
EBTHIZr_TMSC3_Int_EBTHIflip_opt_freq **f-2a**	0	-1755.678023	394.88671	0.667348	0.562334	-1755.010675	-1755.115689
EBTHITi_TMS2C3 **1a**	0	-2557.970342	395.53716	0.667987	0.565519	-2557.302355	-2557.404822
EBTHITi_TMSC3_TS_EBTHIflip **f-1a-TS**	1	-2557.964761	395.54729	0.667227	0.566206	-2557.297533	-2557.398555
EBTHITi_TMSC3_Int_EBTHIflip **f-1a**	0	-2557.968315	395.77519	0.668111	0.566256	-2557.300203	-2557.402058
EBIZr_TMS_int0_opt_freq_svp_empi_2 **Int0-Me3Si**	0	-2716.655084	485.81977	0.831059	0.681705	-2715.824025	-2715.973378
EBIZr_TMS_TS2_svp_opt_freq	1	-2716.648816	485.81312	0.829997	0.6837	-2715.818818	-2715.965116
EBIZr_TMS_Int1_svp_opt_freq	1	-2716.653207	486.11344	0.830256	0.685328	-2715.822952	-2715.967879
EBIZr_TMS_Int02_opt_freq_svp	0	-2716.642867	486.60837	0.831756	0.686937	-2715.811111	-2715.95593
EBIZr_TMS_TS12_opt_freq_svp	1	-2716.639773	486.81151	0.830813	0.690492	-2715.808961	-2715.949281
EBIZr_TMS_Int2_svp_opt_freq	0	-2716.655314	487.01939	0.831632	0.690758	-2715.823681	-2715.964555
EBIZr_TMS_TS3_svp_opt_freq **o-TS1-Me3Si**	1	-2716.6460013	486.724650	0.830176	0.691661	-2715.815826	-2715.954340
EBIZr_TMS_int3_svp_opt_freq **o-Int1-Me3Si**	0	-2716.687017	488.86934	0.83298	0.696261	-2715.854037	-2715.990757
EBIZr_TMS_Int3_CTMS_TS1 **o-TS2-Me3Si-6m**	1	-2716.639776	488.78096	0.831616	0.698184	-2715.80816	-2715.941592
EBIZr_TMS_Int3_CTMS_Int1 **o-Int2-Me3Si-6m**	0	-2716.678992	489.12775	0.833126	0.697770	-2715.845866	-2715.981222
EBIZr_TMS_Int3_NTMS_TS1_2 **o-TS2-NMe3Si-shift**	1	-2716.65943	488.96137	0.831847	0.698916	-2715.827584	-2715.960514
EBIZr_TMS_Int3_NTMS_Int1 **o-Int2-NMe3Si-shift**	0	-2716.678811	488.80325	0.832543	0.697094	-2715.846268	-2715.981717
EBIZr_TMS_Int3Int1TS_svp **o/c-TS3-Me3Si-6m**	1	-2716.667682	488.27499	0.831429	0.695783	-2715.836253	-2715.971899
EBIZr_TMS_Int3TS1_p2_svp.chk **o-TS2-Me3Si-4m**	1	-2716.664499	487.67183	0.831059	0.694774	-2715.83344	-2715.969725
EBIZr_TMS_Int3Int1_p2_svp **o-Int2-Me3Si-4m**	0	-2716.669495	487.69707	0.831978	0.692664	-2715.837517	-2715.976832
EBIZr_TMS_Int3Int1p2_TMS_TS **o-TS3-Me3Si-4m**	1	-2716.618925	487.72449	0.830828	0.694876	-2715.788097	-2715.924049

EBIZr_NCNTMS2CTMSCCTMS_opt_freq_svp	0	-2716.695864	488.04519	0.831769	0.694816	-2715.864095	-2716.001048
EBIZr_TMSNCNTMSTMSCCCTMS_opt_freq_empi_svp **Int3-Me3Si**	0	-2716.689380	488.20052	0.832350	0.693042	-2715.85703	-2715.996339
EBIZr_TMS_Int3_NTMS_Int1_Tsflip	1	-2716.66963	487.86527	0.830700	0.695247	-2715.838930	-2715.974383
EBIZr_TMS_Int3_NTMS_Int1_Int1flip	0	-2716.686095	488.00430	0.831740	0.694820	-2715.854355	-2715.991275
EBIZr_TMS_Int3_NTMS_Int1_Int1flip_TSEBIflip	1	-2716.681545	487.73643	0.830752	0.695008	-2715.850793	-2715.986537
EBIZr_TMS_Int3_NTMS_Int1_Int1flip_IntEBIflip	0	-2716.695864	488.04175	0.831770	0.694715	-2715.864094	-2716.001148
EBIZr_TMS_Int03_opt_freq_svp	0	-2716.652475	486.80771	0.831712	0.686759	-2715.820763	-2715.965717
EBIZr_TMS_TS13_opt_freq_svp **c-TS1-Me3Si**	1	-2716.651083	486.77414	0.830196	0.692463	-2715.820886	-2715.958619
EBIZr_TMS_Int13_opt_freq_svp **c-Int1-Me3Si**	0	-2716.689181	488.79644	0.832835	0.696482	-2715.856346	-2715.992699
EBIZr_TMS_TS23_Tcshift_opt_freq_svp **c-TS2-Me3Si-6m**	1	-2716.638783	488.83392	0.831652	0.699182	-2715.807131	-2715.939602
EBIZr_TMS_Int23_TCshift_opt_freq_svp2 **c-Int2-Me3Si-6m**	0	-2716.675062	489.43442	0.833346	0.697517	-2715.841715	-2715.977545
EBIZr_TMS_TS23_TNshift_opt_freq_svp3 **c-TS2-NMe3Si-shift**	1	-2716.659873	488.58366	0.831632	0.697479	-2715.82824	-2715.962393
EBIZr_TMS_Int23_TNshift_opt_freq_svp **c-Int2-NMe3Si-shift**	0	-2716.69004	488.40485	0.832068	0.695726	-2715.857972	-2715.994314
EBIZr_TMS_Int33_TNshift_opt_freq_svp	0	-2716.692236	488.46717	0.832180	0.696233	-2715.860056	-2715.996003
EBIZr_TMS_TS33_opt_freq_svp	1	-2716.686912	488.2631	0.831258	0.696108	-2715.855654	-2715.990804
EBIZr_TMS_Int43_opt_freq	0	-2716.693622	488.47814	0.832078	0.696367	-2715.861543	-2715.997255
EBIZr_TMS_Int04_opt_freq_svp2 **f-Int0**	0	-2716.6494377	485.88394	0.831182	0.680479	-2715.818256	-2715.968959
EBIZr_TMS_TS14_opt_freq **f-TS1**	1	-2716.6467002	486.98505	0.830532	0.692546	-2715.816168	-2715.954154
EBIZr_TMS_Int14_opt_freq **f-Int1**	0	-2716.6884737	488.77303	0.832790	0.696035	-2715.855684	-2715.992439
EBIZr_TMS_TS24_opt_freq **f-TS2**	1	-2716.6651133	489.30166	0.832005	0.700911	-2715.833108	-2715.964202
EBIZr_TMS_Int24_opt_freq **f-Int2**	0	-2716.6958636	488.0452	0.831767	0.694828	-2715.864097	-2716.001035
EBIZr_iPr_int0_opt_freq_svp_empi	0	-2135.2537	464.684790	0.790080	0.656386	-2134.463620	-2134.597314
EBIZr_iPr_Int02_opt_freq_svp	0	-2135.232807	464.64886	0.790025	0.656201	-2134.442782	-2134.576606
EBIZr_iPr_Int2_opt_freq_svp	0	-2135.260084	465.39706	0.790600	0.662265	-2134.469484	-2134.597819
EBIZr_iPr_TS1_svp_opt_freq2 **c-TS1-iPr**	1	-2135.251632	465.71467	0.789482	0.666513	-2134.46215	-2134.585119

EBIZr_iPr_TS12_opt_freq_svp	1	-2135.234448	465.57735	0.789996	0.664182	-2134.444452	-2134.570266
o_TS1_iPr_svp_opt_freq **o-TS1-iPr**	1	-2135.247877	465.49607	0.789491	0.665448	-2134.458386	-2134.582429
EBIZr_iPr_Int1_svp_opt_freq **c-Int1-iPr**	0	-2135.300502	467.14868	0.791482	0.669155	-2134.50902	-2134.631347
EBIZr_iPr_Int1_TMSshift_TS1	1	-2135.277368	465.79734	0.789428	0.665309	-2134.48794	-2134.61206
EBIZr_iPr_Int1_TMSshift_Int1	0	-2135.303234	467.27624	0.791791	0.668722	-2134.511443	-2134.634512
EBIZr_iPr_Int1_TMSshift_TS2 **c-TS2-iPr-6m**	1	-2135.26299	466.98665	0.790556	0.669978	-2134.472435	-2134.593012
EBIZr_iPr_Int1_TMSshift_Int2 **c-Int2-iPr-6m**	0	-2135.294213	467.63549	0.792287	0.669968	-2134.501926	-2134.624245
EBIZr_iPr_Int1_iPrshift_TS1 **c-TS2-NiPr-shift**	1	-2135.206215	465.33547	0.788475	0.665987	-2134.41774	-2134.540228
EBIZr_iPr_Int1_iPrshift_Int1 **c-Int2-NiPr-shift**	0	-2135.302785	467.09155	0.791343	0.668592	-2134.511442	-2134.634193
EBIZr_iPr_Int1Int2TS_svp **c-TS3-iPr-6m**	1	-2135.284057	466.87517	0.790661	0.668225	-2134.493396	-2134.615831
EBIZr_iPr_Int1Int1_p2_svp2 **c-Int2-iPr-4m**	0	-2135.277968	467.11545	0.791552	0.667237	-2134.486416	-2134.610731
EBIZr_iPr_Int1Int1p2_TS1_qst3_svp	1	-2135.264894	465.7437	0.789513	0.664779	-2134.475381	-2134.600115
EBIZr_iPr_Int1Int1p2_Int1_svp	0	-2135.281112	466.89706	0.791530	0.666084	-2134.489582	-2134.615028
EBIZr_iPr_Int1Int1p2_TS2_svp **c-TS3-iPr-4m**	1	-2135.25224	466.6949	0.790385	0.667329	-2134.461855	-2134.584911
EBIZr_iPrNCNiPrTMSCCCTMS_opt_freq_empi_svp **c-Int3-iPr**	0	-2135.318702	467.08189	0.791583	0.667146	-2134.519287	-2134.643724
EBTHIZr_TMS_Int02_opt_freq_svp	0	-2721.464	545.20968	0.926771	0.778145	-2720.537467	-2720.686093
EBTHIZr_TMS_TS02_opt_freq_svp	1	-2721.463353	545.38165	0.925910	0.781370	-2720.537443	-2720.681983
EBTHIZr_TMS_Int2_opt_freq	0	-2721.470692	545.69581	0.926801	0.783155	-2720.543891	-2720.687537
EBTHIZr_TMS_TS3_opt_freq	1	-2721.468181	545.3222	0.925414	0.784194	-2720.542767	-2720.683986
EBTHIZr_TMS_Int3_opt_freq_svp **o-Int1-Me3Si EBTHI**	0	-2721.510772	547.65026	0.928284	0.789460	-2720.582488	-2720.721311
EBTHIZr_TMS_Int3_NTMS_TS1_opt_freq_svp	1	-2721.486385	547.84518	0.927292	0.791824	-2720.559093	-2720.694561
EBTHIZr_NCNTMS2CTMSCCTMS_opt_freq_svp	0	-2721.527033	546.82216	0.926999	0.787859	-2720.600034	-2720.739174
EBTHIZr_TMS_Int0_opt_freq_svp	0	-2721.487572	544.59334	0.926344	0.774944	-2720.561228	-2720.712628
EBTHIZr_TMS_TS13_opt_freq4	1	-2721.47713	545.96666	0.926313	0.784768	-2720.550817	-2720.692361
EBTHIZr_TMS_Int13_opt_freq_svp	0	-2721.485568	544.87441	0.926370	0.775909	-2720.559198	-2720.70966
EBTHIZr_TMS_Int23_opt_freq	0	-2721.480542	546.21585	0.927365	0.784283	-2720.553177	-2720.69626
EBTHIZr_TMS_TS23_opt_freq	1	-2721.476444	545.98994	0.926003	0.786372	-2720.550441	-2720.690072

EBTHIZr_TMS_Int43_opt_freq **c-Int1-Me3Si EBTHI**	0	-2721.512571	547.62344	0.928022	0.789567	-2720.584549	-2720.723004
EBTHIZr_TMS_TS43_opt_freq_svp	1	-2721.487202	548.11887	0.927354	0.792822	-2720.559848	-2720.69438
EBTHIZr_TMS_Int53_opt_freq_svp	0	-2721.524738	547.04646	0.927217	0.788684	-2720.597521	-2720.736054
EBTHIZr_TMS_TS53_opt_freq	1	-2721.519852	546.81030	0.926328	0.788652	-2720.593523	-2720.7312
EBTHIZr_TMS_Int63_opt_freq	0	-2721.524041	546.75355	0.926944	0.787006	-2720.597096	-2720.737034
EBTHIZr_TMS_Int05_freq **f-Int0**	0	-2721.481389	544.24667	0.926133	0.771337	-2720.555255	-2720.710052
EBTHIZr_TMS_TS15_opt_freq **f-TS1**	1	-2721.474465	545.86767	0.925939	0.785795	-2720.548526	-2720.68867
EBTHIZr_TMS_Int15_opt_freq **f-Int1**	0	-2721.513647	547.5457	0.927912	0.78958	-2720.585735	-2720.724067
EBTHIZr_TMS_TS25_opt_freq **f-TS2**	1	-2721.490797	547.78454	0.927067	0.791521	-2720.56373	-2720.699276
EBTHIZr_TMS_Int25_opt_freq **f-Int2**	0	-2721.524041	546.75261	0.926945	0.786996	-2720.597096	-2720.737045

Table S17. Summary of thermodynamic data of all calculated compounds level of theory B3LYP/GD3BJ/def2svpp//def2tzvp.

File-Name	Nimag	HF	ZPE [kcal/mol]	Th. Corr. H	Th. Corr. G	H_{tot} [a.u.]	G_{tot} [a.u.]
EBIZr_TMS2C3_sp_tzvp **2c**	-	-1752.375121	taken from def2svpp opt freq calc.			-1751.802869	-1751.90531
EBIZr_TMSC3_TSEBIflip_sp_tzvp **f-2c-TS**		-1752.369265	taken from def2svpp opt freq calc.			-1751.797762	-1751.896902
EBIZr_TMSC3_IntEBIflip_sp_tzvp **f-2c**	-	-1752.373172	taken from def2svpp opt freq calc.			-1751.800763	-1751.901118
EBTHIZr_TMS2C3_sp_tzvp **2a**	-	-1757.227555	taken from def2svpp opt freq calc.			-1756.560144	-1756.665109
EBTHIZr_TMSC3_TS_EBTHIflip_sp_tzvp **f-2a-TS**	-	-1757.221118	taken from def2svpp opt freq calc.			-1756.554524	-1756.657216
EBTHIZr_TMSC3_Int_EBTHIflip_sp_tzvp **f-2a**	-	-1757.224455	taken from def2svpp opt freq calc.			-1756.557107	-1756.662121
EBTHITi_TMS2C3_sp_tzvp **1a**	-	-2559.606456	taken from def2svpp opt freq calc.			-2558.938469	-2559.040937
EBTHITi_TMSC3_TS_EBTHIflip_sp_tzvp **f-1a-TS**	-	-2559.600315	taken from def2svpp opt freq calc.			-2558.933088	-2559.034109
EBTHITi_TMSC3_Int_EBTHIflip_sp_tzvp **f-1a**	-	-2559.603795	taken from def2svpp opt freq calc.			-2558.935684	-2559.037539
	-						
EBIZr_TMS_int0_sp_tzvp **Int0-Me3Si**	-	-2718.876095	taken from def2svpp opt freq calc.			-2718.045036	-2718.19439
EBIZr_TMS_TS2_sp_tzvp	-	-2718.870294	taken from def2svpp opt freq calc.			-2718.040297	-2718.186594

EBIZr_TMS_Int1_sp_tzvp	-	-2718.874323	taken from def2svpp opt freq calc.	-2718.044067	-2718.188995
EBIZr_TMS_Int02_sp_tzvp	-	-2718.861283	taken from def2svpp opt freq calc.	-2718.029527	-2718.174346
EBIZr_TMS_TS12_sp_tzvp	-	-2718.858651	taken from def2svpp opt freq calc.	-2718.027838	-2718.168159
EBIZr_TMS_Int2_sp_opt_freq	-	-2718.870837	taken from def2svpp opt freq calc.	-2718.039205	-2718.180079
EBIZr_TMS_TS3_sp_tzvp **o-TS1-Me3Si**	-	-2718.861558	taken from def2svpp opt freq calc.	-2718.031382	-2718.169897
EBIZr_TMS_int3_sp_tzvp **o-Int1-Me3Si**	-	-2718.898728	taken from def2svpp opt freq calc.	-2718.065748	-2718.202467
EBIZr_TMS_Int3_CTMS_TS1_sp_tzvp **o-TS2-Me3Si-6m**	-	-2718.852236	taken from def2svpp opt freq calc.	-2718.02062	-2718.154052
EBIZr_TMS_Int3_CTMS_Int1_sp_tzvp **o-Int2-Me3Si-6m**	-	-2718.892497	taken from def2svpp opt freq calc.	-2718.059371	-2718.194727
EBIZr_TMS_Int3_NTMS_TS1_2 **o-TS2-NMe3Si-shift**	-	-2718.870875	taken from def2svpp opt freq calc.	-2718.039028	-2718.171959
EBIZr_TMS_Int3_NTMS_Int1_sp_tzvp **o-Int2-NMe3Si-shift**	-	-2718.890304	taken from def2svpp opt freq calc.	-2718.057761	-2718.19321
EBIZr_TMS_Int3Int1TS_sp_tzvp **o/c-TS3-Me3Si-6m**	-	-2718.882295	taken from def2svpp opt freq calc.	-2718.050866	-2718.186512
EBIZr_TMS_Int3TS1_p2_sp_tzvp **o-TS2-Me3Si-4m**	-	-2718.877031	taken from def2svpp opt freq calc.	-2718.045972	-2718.182257
EBIZr_TMS_Int3Int1_p2_sp_tzvp **o-Int2-Me3Si-4m**	-	-2718.881425	taken from def2svpp opt freq calc.	-2718.049447	-2718.188761
EBIZr_TMS_Int3Int1p2_TMS_TS_sp_tzvp **o-TS3-Me3Si-4m**	-	-2718.831928	taken from def2svpp opt freq calc.	-2718.0011	-2718.137052
EBIZr_NCNTMS2CTMSCCTMS_sp_tzvp	-	-2718.907775	taken from def2svpp opt freq calc.	-2718.076006	-2718.212959
EBIZr_TMSNCNTMSTMSCCCTMS_sp_tzvp_empi **Int3-Me3Si**	-	-2718.903885	taken from def2svpp opt freq calc.	-2718.071535	-2718.210843
EBIZr_TMS_Int3_NTMS_Int1_TSflip_sp_tzvp	-	-2718.882008	taken from def2svpp opt freq calc.	-2718.051308	-2718.186761
EBIZr_TMS_Int3_NTMS_Int1_Int1flip_sp_tzvp	-	-2718.898520	taken from def2svpp opt freq calc.	-2718.06678	-2718.2037
EBIZr_TMS_Int3_NTMS_Int1_Int1flip_TSEBIflip_sp_tzvp	-	-2718.893964	taken from def2svpp opt freq calc.	-2718.063212	-2718.198956
EBIZr_TMS_Int3_NTMS_Int1_Int1flip_IntEBIflip_sp_tzvp	-	-2718.907782	taken from def2svpp opt freq calc.	-2718.076012	-2718.213067
EBIZr_TMS_Int03_sp_tzvp	-	-2718.872501	taken from def2svpp opt freq calc.	-2718.040789	-2718.185742
EBIZr_TMS_TS13_sp_tzvp **c-TS1-Me3Si**	-	-2718.866178	taken from def2svpp opt freq calc.	-2718.035982	-2718.173715
EBIZr_TMS_Int13_sp_tzvp **c-Int1-Me3Si**	-	-2718.901232	taken from def2svpp opt freq calc.	-2718.068397	-2718.20475
EBIZr_TMS_TS23_TCshift_sp_tzvp **c-TS2-Me3Si-6m**	-	-2718.851761	taken from def2svpp opt freq calc.	-2718.020109	-2718.152579
EBIZr_TMS_Int23_TCshift_sp_tzvp **c-Int2-Me3Si-6m**		-2718.888696	taken from def2svpp opt freq calc.	-2718.05535	-2718.191179
EBIZr_TMS_TS23_TNshift_sp_tzvp **c-TS2-NMe3Si-shift**		-2718.871836	taken from def2svpp opt freq calc.	-2718.040204	-2718.174357
EBIZr_TMS_Int23_TNshift_sp_tzvp **c-Int2-NMe3Si-shift**	-	-2718.9018869	taken from def2svpp opt freq calc.	-2718.069819	-2718.206161

EBIZr_TMS_Int33_TNshift_sp_tzvp		-2718.9044569	taken from def2svpp opt freq calc.	-2718.072277	-2718.208224
EBIZr_TMS_TS33_sp_tzvp **f-c-TS3-NMe3Si-shift**		-2718.8990103	taken from def2svpp opt freq calc.	-2718.067752	-2718.202902
EBIZr_TMS_Int43_sp_tzvp **c-Int3-NMe3Si-shift**		-2718.9055586	taken from def2svpp opt freq calc.	-2718.073481	-2718.209192
EBIZr_TMS_Int04_sp_tzvp **f-Int0**	-	-2718.8702064	taken from def2svpp opt freq calc.	-2718.039024	-2718.189727
EBIZr_TMS_TS14_sp_tzvp **f-TS1**	-	-2718.863473	taken from def2svpp opt freq calc.	-2718.032941	-2718.170927
EBIZr_TMS_Int14_sp_tzvp **f-Int1**	-	-2718.9004404	taken from def2svpp opt freq calc.	-2718.06765	-2718.204405
EBIZr_TMS_TS24_sp_tzvp **f-TS2**	-	-2718.8764868	taken from def2svpp opt freq calc.	-2718.044482	-2718.175576
EBIZr_TMS_Int24_sp_tzvp **f-Int2**	-	-2718.9077763	taken from def2svpp opt freq calc.	-2718.076009	-2718.212948
EBIZr_iPr_int0_sp_tzvp	-	-2137.235748	taken from def2svpp opt freq calc.	-2136.445668	-2136.579362
EBIZr_iPr_Int02_sp_tzvp	-	-2137.213949	taken from def2svpp opt freq calc.	-2136.423924	-2136.557748
EBIZr_iPr_Int2_sp_tzvp	-	-2137.237233	taken from def2svpp opt freq calc.	-2136.446633	-2136.574968
EBIZr_iPr_TS1_sp_tzvp **c-TS1-iPr**	-	-2137.227466	taken from def2svpp opt freq calc.	-2136.437984	-2136.560953
EBIZr_iPr_TS12_sp_tzvp	-	-2137.213903	taken from def2svpp opt freq calc.	-2136.423907	-2136.549721
o_TS1_iPr_sp_tzvp **o-TS1-iPr**	-	-2137.224671	taken from def2svpp opt freq calc.	-2136.43518	-2136.559223
EBIZr_iPr_Int1_sp_tzvp **c-Int1-iPr**	-	-2137.273064	taken from def2svpp opt freq calc.	-2136.481582	-2136.603909
EBIZr_iPr_Int1_TMSshift_TS1_sp_tzvp	-	-2137.248531	taken from def2svpp opt freq calc.	-2136.459103	-2136.583222
EBIZr_iPr_Int1_TMSshift_Int1_sp_tzvp	-	-2137.276847	taken from def2svpp opt freq calc.	-2136.485056	-2136.608125
EBIZr_iPr_Int1_TMSshift_TS2_sp_tzvp **c-TS2-iPr-6m**	-	-2137.236189	taken from def2svpp opt freq calc.	-2136.445633	-2136.566211
EBIZr_iPr_Int1_TMSshift_Int2_sp_tzvp **c-TS2-iPr-6m**	-	-2137.269359	taken from def2svpp opt freq calc.	-2136.477072	-2136.599391
EBIZr_iPr_Int1_iPrshift_TS1_sp_tzvp **c-TS2-NiPr-shift**	-	-2137.183318	taken from def2svpp opt freq calc.	-2136.394843	-2136.517331
EBIZr_iPr_Int1_iPrshift_Int1_sp_tzvp **c-Int2-NiPr-shift**	-	-2137.275815	taken from def2svpp opt freq calc.	-2136.484472	-2136.607223
EBIZr_iPr_Int1Int2TS_sp_tzvp **c-TS3-iPr-6m**	-	-2137.259198	taken from def2svpp opt freq calc.	-2136.468537	-2136.590973
EBIZr_iPr_Int1Int1_p2_sp_tzvp **c-Int2-iPr-4m**	-	-2137.249983	taken from def2svpp opt freq calc.	-2136.458431	-2136.582746
EBIZr_iPr_Int1Int1p2_TS1_sp_tzvp	-	-2137.235593	taken from def2svpp opt freq calc.	-2136.44608	-2136.570814
EBIZr_iPr_Int1Int1p2_Int1_sp_tzvp	-	-2137.25513	taken from def2svpp opt freq calc.	-2136.4636	-2136.589046
EBIZr_iPr_Int1Int1p2_TS2_sp_tzvp **c-TS3-iPr-4m**	-	-2137.226437	taken from def2svpp opt freq calc.	-2136.436052	-2136.559108
EBIZr_iPrNCNiPrTMSCCCTMS_sp_tzvp **c-Int3-iPr**	-	-2137.278249	taken from def2svpp opt freq calc.	-2136.486666	-2136.611103

EBTHIZr_TMS_Int02_sp_tzvp	-	-2723.705358	taken from def2svpp opt freq calc.	-2722.778587	-2722.927213
EBTHIZr_TMS_TS02_sp_tzvp	-	-2723.704359	taken from def2svpp opt freq calc.	-2722.778449	-2722.922989
EBTHIZr_TMS_Int2_sp_tzvp	-	-2723.708634	taken from def2svpp opt freq calc.	-2722.781833	-2722.925479
EBTHIZr_TMS_TS3_sp_tzvp	-	-2723.705011	taken from def2svpp opt freq calc.	-2722.779597	-2722.920817
EBTHIZr_TMS_Int3_sp_tzvp **o-Int1-Me3Si EBTHI**	-	-2723.743764	taken from def2svpp opt freq calc.	-2722.81548	-2722.954304
EBTHIZr_TMS_Int3_NTMS_TS1_sp_tzvp	-	-2723.718817	taken from def2svpp opt freq calc.	-2722.791525	-2722.926993
EBTHIZr_NCNTMS2CTMSCCTMS_sp_tzvp	-	-2723.75935	taken from def2svpp opt freq calc.	-2722.832351	-2722.971491
EBTHIZr_TMS_Int0_sp_tzvp.out	-	-2723.728477	taken from def2svpp opt freq calc.	-2722.802133	-2722.953533
EBTHIZr_TMS_TS13_4_sp_tzvp.out	-	-2723.716952	taken from def2svpp opt freq calc.	-2722.790639	-2722.932184
EBTHIZr_TMS_Int13_sp_tzvp	-	-2723.726969	taken from def2svpp opt freq calc.	-2722.800599	-2722.95106
EBTHIZr_TMS_Int23_sp_tzvp	-	-2723.719352	taken from def2svpp opt freq calc.	-2722.791987	-2722.935069
EBTHIZr_TMS_TS23_sp_tzvp	-	-2723.714035	taken from def2svpp opt freq calc.	-2722.788032	-2722.927663
EBTHIZr_TMS_Int43_sp_tzvp **c-Int1-Me3Si EBTHI**	-	-2723.745222	taken from def2svpp opt freq calc.	-2722.8172	-2722.955655
EBTHIZr_TMS_TS43_sp_tzvp	-	-2723.719269	taken from def2svpp opt freq calc.	-2722.791915	-2722.926447
EBTHIZr_TMS_Int53_sp_tzvp.out	-	-2723.756914	taken from def2svpp opt freq calc.	-2722.829697	-2722.96823
EBTHIZr_TMS_TS53_sp_tzvp	-	-2723.752098	taken from def2svpp opt freq calc.	-2722.82577	-2722.963446
EBTHIZr_TMS_Int63_sp_tzvp	-	-2723.756214	taken from def2svpp opt freq calc.	-2722.82927	-2722.969208
EBTHIZr_TMS_Int05_sp_tzvp **f-Int0**	-	-2723.722595	taken from def2svpp opt freq calc.	-2722.796462	-2722.951258
EBTHIZr_TMS_TS15_sp_tzvp **f-TS1**	-	-2723.712263	taken from def2svpp opt freq calc.	-2722.786324	-2722.926468
EBTHIZr_TMS_Int15_sp_tzvp **f-Int1**	-	-2723.747216	taken from def2svpp opt freq calc.	-2722.819304	-2722.957636
EBTHIZr_TMS_TS25_sp_tzvp **f-TS2**	-	-2723.723542	taken from def2svpp opt freq calc.	-2722.796475	-2722.932021
EBTHIZr_TMS_Int25_sp_tzvp **f-Int2**	-	-2723.756212	taken from def2svpp opt freq calc.	-2722.829267	-2722.969216

9.3 Bond analysis of selected complexes

9.3.1 Summary of NBO/NLMO Analysis of 2c and 2d

NBO6.0 analyses of the B3LYP/GD3BJ/def2tzvp optimised structures of **2c** and **2d** were performed to analyse the natural localised molecular orbitals (NLMO). The NBO routine found two double bonds along the central CCC unit (**2c**: Table S18; **2d**: Table S20). As expected, these bonds can be described as one σ bond type with sp^2-sp hybrid orbitals, and one π type bond formed from a pure p-type orbital at the central carbon atom (β-C) and one p type orbital with minor s character at the α carbon atoms. These findings are corroborated by the corresponding NLMO analysis of the central CCC unit (**2c**: Table S19; **2d**: Table S21). Furthermore, this analysis reveals for the CC π-type orbitals minor contributions (7.4 – 6.8%) of a d orbital at the Zr centre, which are absent for the corresponding CC σ type orbitals.

While this NBO/NLMO routine works well for the bond description of the allene unit, it cannot be adapted for the Zr-C bond description. The NBO analysis of **2c** and **2d** found a pair of a π bonding and π* antibonding orbitals between the two α carbon atoms, with low occupancies (π: 1.1; π^* 1.5 e^-) and the NLMO analysis of these can be best interpreted as the Zr-C bond orbitals, with main contributions (π: 13; π^* 19 %) of a d type orbital from Zr. In particular, these π NLMOs have just 50% of their parent NBO left. This, together with the low occupation numbers of the π NB orbitals, gives an indication of a delocalised electronic situation in these complexes.

9.3.2 NBO/NLMO analysis of 2c

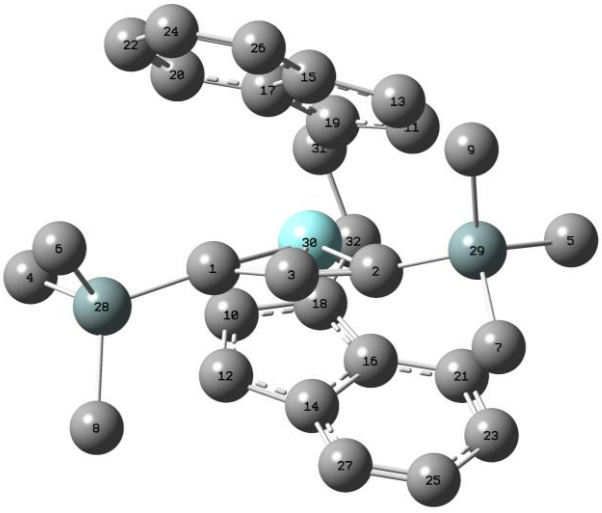

Figure S159. Labeling scheme of the NBO/NLMO analysis of complex **2c**.

Table S18. Summary of selected NBO analysis of **2c**.

46. (1.09298) BD (1) C 1- C 2 (49.99%) 0.7071* C 1 s(8.75%)p10.41(91.10%)d 0.01(0.08%) f 0.01(0.06%) (50.01%) 0.7071* C 2 s(8.75%)p10.41(91.10%)d 0.01(0.08%) f 0.01(0.06%)	47. (1.95625) BD (1) C 1- C 3 (47.67%) 0.6904* C 1 s(31.87%)p 2.13(67.83%)d 0.01(0.25%) f 0.00(0.04%) (52.33%) 0.7234* C 3 s(49.75%)p 1.01(50.06%)d 0.00(0.11%) f 0.00(0.08%)
48. (1.77203) BD (2) C 1- C 3 (57.69%) 0.7595* C 1 s(9.27%)p 9.78(90.58%)d 0.01(0.11%) f 0.00(0.04%) (42.31%) 0.6505* C 3 s(0.17%)p99.99(99.36%)d 2.20(0.38%) f 0.49(0.08%)	50. (1.95625) BD (1) C 2- C 3 47.67%) 0.6904* C 2 s(31.87%)p 2.13(67.83%)d 0.01(0.25%) f 0.00(0.04%) (52.33%) 0.7234* C 3 s(49.75%)p 1.01(50.06%)d 0.00(0.11%) f 0.00(0.08%)
51. (1.77199) BD (2) C 2- C 3 (57.69%) 0.7595* C 2 s(9.27%)p 9.77(90.58%)d 0.01(0.11%) f 0.00(0.04%) (42.31%) 0.6505* C 3 s(0.17%)p99.99(99.36%)d 2.20(0.38%) f 0.49(0.08%)	124. (1.52448) BD*(1) C 1- C 2 (50.01%) 0.7071* C 1 s(8.75%)p10.41(91.10%)d 0.01(0.08%) f 0.01(0.06%) (49.99%) -0.7071* C 2 s(8.75%)p10.41(91.10%)d 0.01(0.08%) f 0.01(0.06%)

Table S19. Summary of selected NLMOs of **2c**.

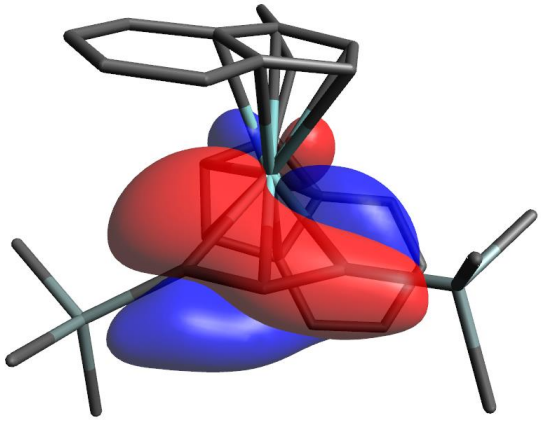	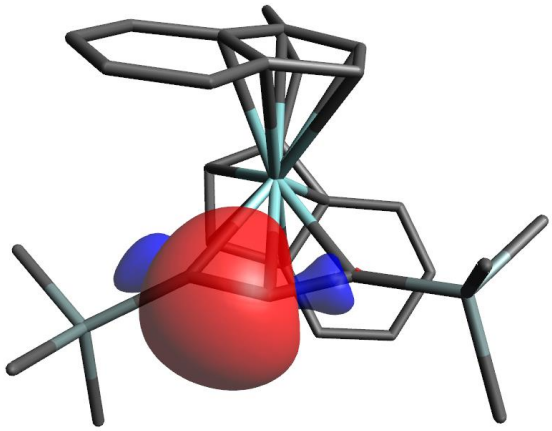
Shortened NLMO 46 Analysis of C(1)-C(3)-C(2) π-bond as well as C(1) and C(2) binding contribution to one d orbital at the Zr(30) centre (threshold > 1.3%) 46. (2.00000) 50.6529% BD (1) C 1- C 2 32.225% C 1 s(12.46%)p 7.01(87.39%)d 0.01(0.12%) f 0.00(0.03%) 32.233% C 2 s(12.45%)p 7.02(87.39%)d 0.01(0.12%) f 0.00(0.03%) 19.966% C 3 s(0.00%)p 1.00(99.55%)d 0.00(0.35%) f 0.00(0.10%) 13.327% Zr 30 s(0.00%)p 1.00(0.05%)d99.99(99.85%) f 2.00(0.10%)	Shortened NLMO 47 Analysis C(1)-C(3) σ-bond (threshold > 1.3%) 47. (2.00000) 97.7816% BD (1) C 1- C 3 46.771% C 1 s(29.70%)p 2.36(70.00%)d 0.01(0.25%) f 0.00(0.04%) 51.481% C 3 s(44.38%)p 1.25(55.43%)d 0.00(0.11%) f 0.00(0.08%)
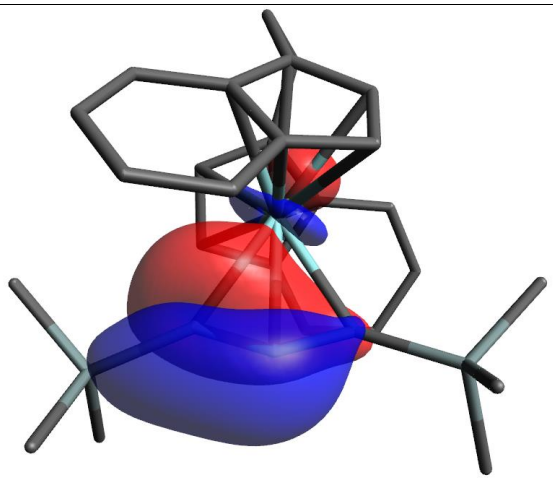	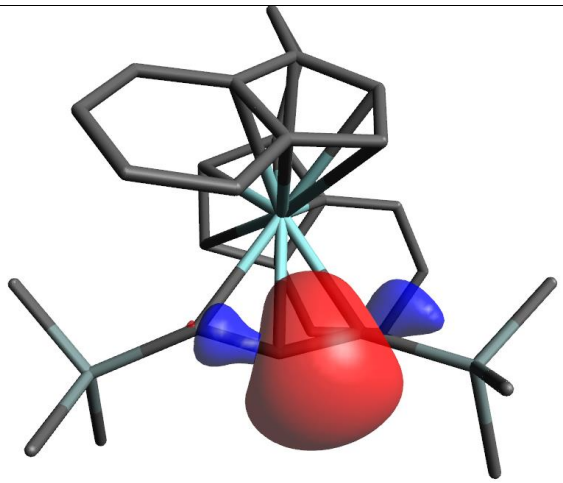

Shortened NLMO 48 Analysis of of C(1)-C(3) π-bond (threshold > 1.3%) 48. (2.00000) 87.9907% BD (2) C 1- C 3 51.395% C 1 s(7.61%)p12.12(92.24%)d 0.01(0.11%) f 0.01(0.05%) 1.765% C 2 s(0.58%)p99.99(98.88%)d 0.84(0.49%) f 0.10(0.06%) 37.709% C 3 s(0.10%)p99.99(99.45%)d 3.54(0.36%) f 0.77(0.08%) 7.235% Zr 30 s(1.39%)p 0.22(0.31%)d70.40(98.10%) f 0.14(0.20%)	Shortened NLMO 50 Analysis of of C(2)-C(3) σ -bond (threshold > 1.3%) 50. (2.00000) 97.7815% BD (1) C 2- C 3 46.771% C 2 s(29.70%)p 2.36(70.00%)d 0.01(0.25%) f 0.00(0.04%) 51.480% C 3 s(44.38%)p 1.25(55.42%)d 0.00(0.11%) f 0.00(0.08%)
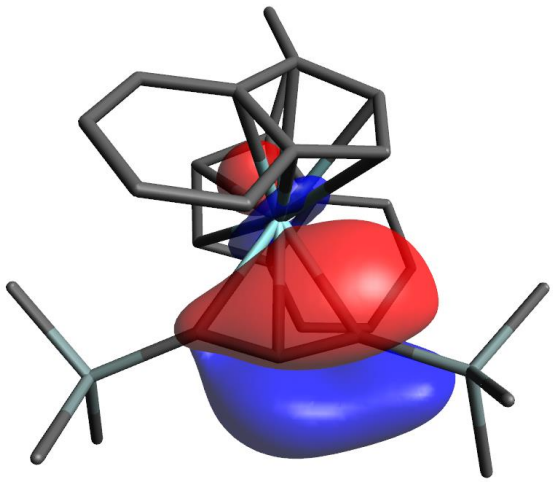	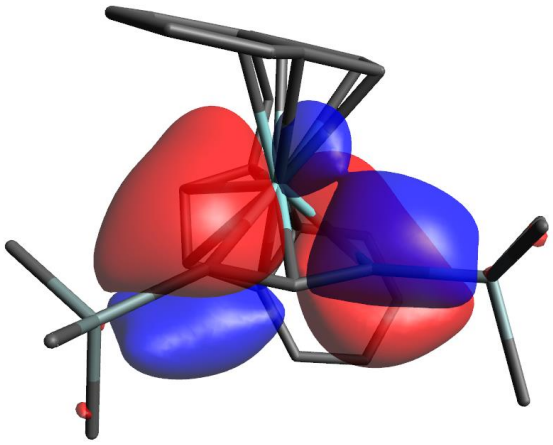
Shortened NLMO 51 Analysis of of C(1)-C(2) π -bond (threshold > 1.3%) 51. (2.00000) 87.9890% BD (2) C 2- C 3 1.766% C 1 s(0.58%)p99.99(98.88%)d 0.84(0.48%) f 0.10(0.06%) 51.394% C 2 s(7.61%)p12.11(92.24%)d 0.01(0.11%) f 0.01(0.05%) 7.234% Zr 30 s(1.40%)p 0.22(0.31%)d70.30(98.10%) f 0.14(0.20%)	Shortened NLMO 124 Analysis of of C(1)-C(2) π*-bond (threshold > 1.3%) 124. (2.00000) 74.8846% BD*(1) C 1- C 2 37.703% C 1 s(8.11%)p11.31(91.75%)d 0.01(0.08%) f 0.01(0.07%) 37.695% C 2 s(8.10%)p11.32(91.75%)d 0.01(0.08%) f 0.01(0.07%) 18.749% Zr 30 s(14.27%)p 0.00(0.07%)d 5.99(85.54%) f 0.01(0.12%)

9.3.3 NBO/NLMO analysis of 2d

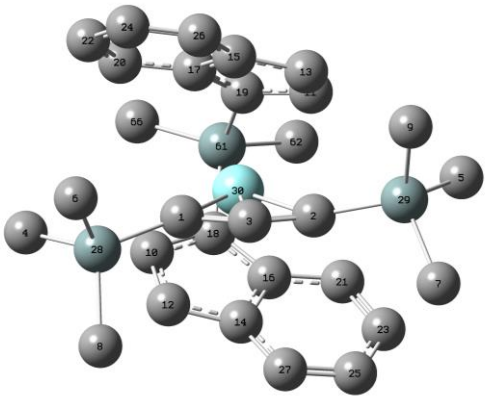

Figure S160. Labelling scheme of the NBO/NLMO analysis of complex **2d**.

Table S20. Summary of selected NBO analysis of **2d**.

51. (1.08809) BD (1) C 1- C 2 (50.14%) 0.7081* C 1 s(8.09%)p11.35(91.77%)d 0.01(0.08%) f 0.01(0.06%) (49.86%) 0.7061* C 2 s(8.10%)p11.32(91.75%)d 0.01(0.08%) f 0.01(0.06%)	52. (1.95724) BD (1) C 1- C 3 (47.75%) 0.6910* C 1 s(31.82%)p 2.13(67.90%)d 0.01(0.24%) f 0.00(0.04%) (52.25%) 0.7229* C 3 s(49.74%)p 1.01(50.07%)d 0.00(0.11%) f 0.00(0.08%)
53. (1.77007) BD (2) C 1- C 3 57.82%) 0.7604* C 1 s(9.64%)p 9.36(90.21%)d 0.01(0.11%) f 0.00(0.04%) (42.18%) 0.6495* C 3 s(0.17%)p99.99(99.36%)d 2.24(0.38%) f 0.50(0.09%)	55. (1.95689) BD (1) C 2- C 3 (47.70%) 0.6906* C 2 s(31.86%)p 2.13(67.84%)d 0.01(0.26%) f 0.00(0.04%) (52.30%) 0.7232* C 3 s(49.76%)p 1.01(50.06%)d 0.00(0.10%) f 0.00(0.08%)
56. (1.77163) BD (2) C 2- C 3 (57.71%) 0.7597* C 2 s(9.46%)p 9.55(90.39%)d 0.01(0.11%) f 0.00(0.04%) (42.29%) 0.6503* C 3 s(0.18%)p99.99(99.36%)d 2.05(0.37%) f 0.47(0.09%)	132. (1.50045) BD*(1) C 1- C 2 (49.86%) 0.7061* C 1 s(8.09%)p11.35(91.77%)d 0.01(0.08%) f 0.01(0.06%) (50.14%) -0.7081* C 2 s(8.10%)p11.32(91.75%)d 0.01(0.08%) f 0.01(0.06%)

Table S21. Summary of selected NLMOs of **2d**.

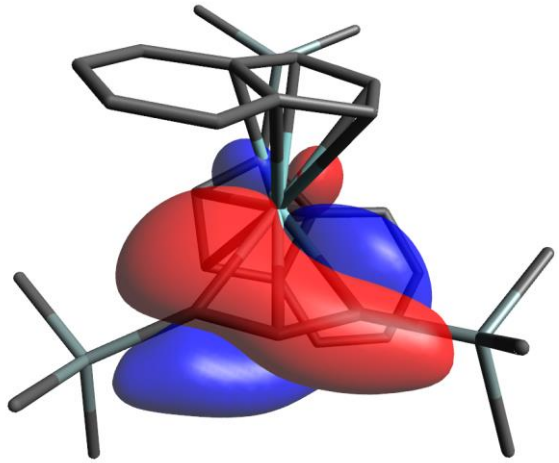	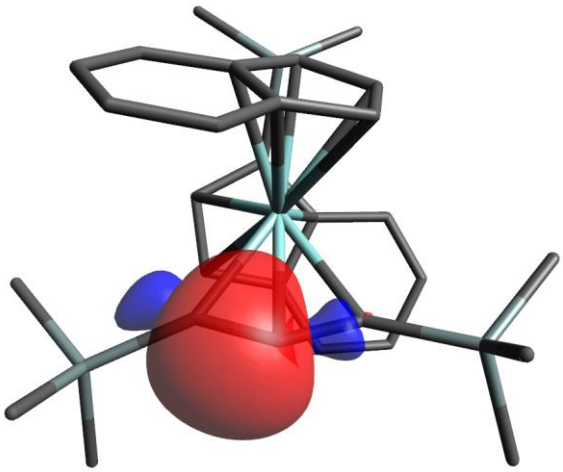
Shortened NLMO 51 Analysis of C(1)-C(3)-C(2) π-bond as well as C(1) and C(2) binding contribution to one d orbital at the Zr(30) centre (threshold > 1.3%) 51. (2.00000) 50.0856% BD (1) C 1- C 2 32.068% C 1 s(12.04%)p 7.29(87.81%)d 0.01(0.11%) f 0.00(0.03%) 32.023% C 2 s(11.96%)p 7.35(87.89%)d 0.01(0.12%) f 0.00(0.03%) 20.384% C 3 s(0.00%)p 1.00(99.54%)d 0.00(0.36%) f 0.00(0.10%) 13.356% Zr 30 s(0.00%)p 1.00(0.04%)d99.99(99.85%) f 2.43(0.11%)	Shortened NLMO 52 Analysis C(1)-C(3) σ-bond (threshold > 1.3%) 52. (2.00000) 97.8324% BD (1) C 1- C 3 46.881% C 1 s(29.75%)p 2.35(69.97%)d 0.01(0.24%) f 0.00(0.04%) 51.417% C 3 s(44.46%)p 1.24(55.35%)d 0.00(0.11%) f 0.00(0.08%)

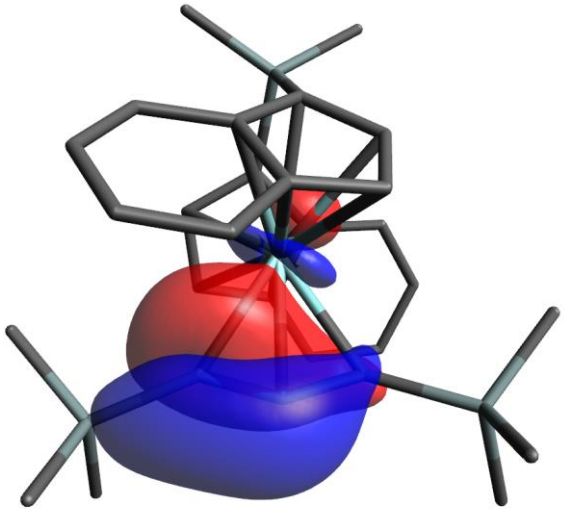

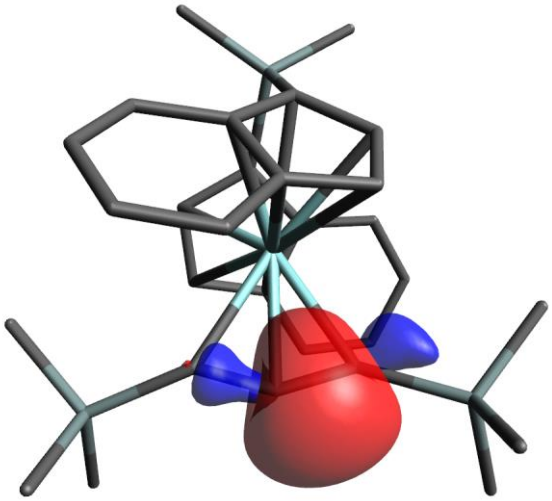

Shortened NLMO 53 Analysis C(1)-C(3) π -bond (threshold > 1.3%)

53. (2.00000) 87.6876% BD (2) C 1- C 3

51.791% C 1 s(7.92%)p11.60(91.93%)d 0.01(0.10%) f 0.01(0.04%)

2.165% C 2 s(0.34%)p99.99(99.20%)d 1.17(0.40%) f 0.17(0.06%)

36.811% C 3 s(0.08%)p99.99(99.47%)d 4.47(0.37%) f 0.98(0.08%)

7.368% Zr 30 s(1.43%)p 0.21(0.30%)d68.80(98.07%) f 0.14(0.20%)

Shortened NLMO 55 Analysis C(2)-C(3) σ-bond (threshold > 1.3%)

55. (2.00000) 97.8158% BD (1) C 2- C 3

46.827% C 2 s(29.81%)p 2.34(69.89%)d 0.01(0.26%) f 0.00(0.04%)

51.470% C 3 s(44.41%)p 1.25(55.40%)d 0.00(0.11%) f 0.00(0.09%)

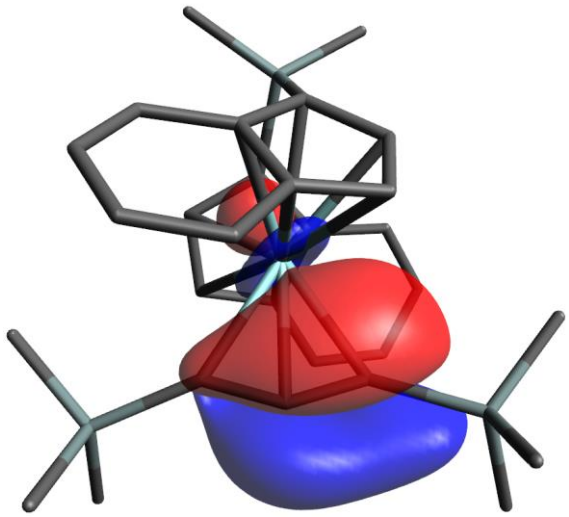

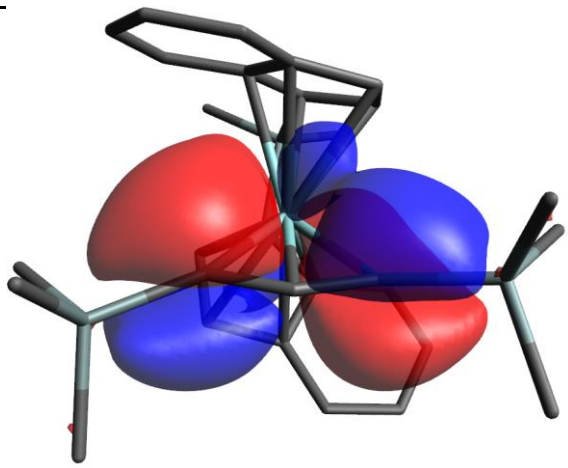

Shortened NLMO Analysis of of C(2)-C(3) π -bond (threshold > 1.3%)	Shortened NLMO Analysis of of C(1)-C(2) π*-bond (threshold > 1.3%)
56. (2.00000) 88.1595% BD (2) C 2- C 3 1.668% C 1 s(1.39%)p70.43(98.06%)d 0.35(0.49%) f 0.04(0.06%) 51.141% C 2 s(7.97%)p11.52(91.88%)d 0.01(0.10%) f 0.01(0.05%) 38.541% C 3 s(0.09%)p99.99(99.48%)d 3.89(0.35%) f 0.86(0.08%) 6.861% Zr 30 s(1.89%)p 0.16(0.30%)d51.74(97.62%) f 0.11(0.20%)	132. (2.00000) 73.6303% BD*(1) C 1- C 2 36.946% C 1 s(7.35%)p12.59(92.51%)d 0.01(0.07%) f 0.01(0.07%) 37.084% C 2 s(7.44%)p12.42(92.41%)d 0.01(0.08%) f 0.01(0.07%) 6.253% Zr 30 s(1.06%)p 0.37(0.40%)d92.44(98.31%) f 0.21(0.23%) 19.388% Zr 30 s(13.75%)p 0.00(0.05%)d 6.26(86.09%) f 0.01(0.11%)

9.3.4 Comparison of natural charges from NBO analysis in the formal allenediide unit in complexes 2a, 2b, and A.

To evaluate the differences in the bond situation of group 4 1-metallacyclobuta-2,3-dienes we calculated the sum of the natural charges in the formal allenediide units in these complexes (Table S22). The higher negative charge in the zirconocene complexes suggest a higher polarity of the M-C interaction in the metallacycles which is well in line with the greater biradicaloid character of the Ti complexes **A**, **B**, **1a** and **1c** leading to a formal Ti(III) centre which is antiferromagnetically coupled to the delocalised electron in the allene unit (**A** = $Cp_2Ti(Me_3SiCCCSiMe_3)$, **B** = $Cp^*_2Ti(Me_3SiCCCSiMe_3)$). Based on this calculation, the formal oxidation state of Zr is greater than Zr(III), so the interaction in **2a** and **2b** is best described as a Zr(IV) centre coordinated with an allenediide ligand. The new η^5-indenyl complexes **1c**, **2c** and **2d** show significantly lower charges compared to their corresponding η^5-tetrahydroindenyl complexes which reveals on this level of theory a slightly higher degree of biradicaloid character.

Table S22. Calculation of the sum of natural charges in the formal allenediide/allenide units from NBO analysis (B3LYP/GD3BJ/def2tzvp).

A		B singlett		B triplett		1a		1c		2a		2b		2c		2d	
A	Nat Charge	Atom	Nat Charge	Atom	Nat Charge	Atom	Nat Charge	Atom	Nat Charge	Atom	Nat Charge	Atom	Nat Charge	Atom	Nat Charge	Atom	Nat Charge
C 22	-0.68576	C 12	-0.905270	C 12	-0.65136	C 1	-0.76858	C 1	-0.721950	C 1	-0.89502	C 1	-0.885	C 1	-0.87592	C 1	-0.8672
C 23	-0.68576	C 13	-0.823620	C 13	-0.65108	C 2	-0.76858	C 2	-0.721850	C 2	-0.89502	C 2	-0.88348	C 2	-0.87591	C 2	-0.86636
C 24	-0.01899	C 14	-0.059370	C 14	-0.16398	C 3	-0.08284	C 3	-0.073990	C 3	-0.06522	C 3	-0.06565	C 3	-0.04851	C 3	-0.04987
Si 25	1.6638	Si 15	1.689720	Si 15	1.66344	C 4	-1.09218	C 4	-1.092460	C 4	-1.09072	C 4	-1.09131	C 4	-1.08978	C 4	-1.09126
Si 26	1.6638	Si 16	1.677930	Si 16	1.66343	C 5	-1.09218	C 5	-1.092450	C 5	-1.09072	C 5	-1.09217	C 5	-1.08978	C 5	-1.09103
C 27	-1.08198	C 17	-1.079770	C 17	-1.08731	C 6	-1.08335	C 6	-1.080850	C 6	-1.0835	C 6	-1.08324	C 6	-1.0812	C 6	-1.08083
H 28	0.22408	H 18	0.220610	H 18	0.22577	C 7	-1.08335	C 7	-1.080840	C 7	-1.0835	C 7	-1.08392	C 7	-1.0812	C 7	-1.08058
H 29	0.2297	H 19	0.224070	H 19	0.22823	C 8	-1.09268	C 8	-1.090000	C 8	-1.09285	C 8	-1.09248	C 8	-1.09046	C 8	-1.08937
H 30	0.22968	H 20	0.226970	H 20	0.22893	C 9	-1.09268	C 9	-1.089980	C 9	-1.09285	C 9	-1.09142	C 9	-1.09045	C 9	-1.08893
C 31	-1.08776	C 21	-1.093310	C 21	-1.09631	Si 28	1.67321	Si 28	1.672720	Si 28	1.67753	Si 28	1.67659	Si 28	1.67788	Si 28	1.67751
H 32	0.22615	H 22	0.22768	H 22	0.2295	Si 29	1.67321	Si 29	1.67271	Si 29	1.67753	Si 29	1.67925	Si 29	1.67788	Si 29	1.67714
H 33	0.2205	H 23	0.22304	H 23	0.22977	H 33	0.2288	H 32	0.22743	H 33	0.22759	H 31	0.2291	H 33	0.22651	H 31	0.22773
H 34	0.2271	H 24	0.22125	H 24	0.22472	H 34	0.2288	H 33	0.22743	H 34	0.22759	H 32	0.22787	H 34	0.22651	H 32	0.22767
C 35	-1.09708	C 25	-1.09738	C 25	-1.08808	H 35	0.22771	H 34	0.23439	H 35	0.22711	H 33	0.22619	H 35	0.23264	H 33	0.23322
H 36	0.22974	H 26	0.22559	H 26	0.22809	H 36	0.22771	H 35	0.23441	H 36	0.22711	H 34	0.22689	H 36	0.23264	H 34	0.23319
H 37	0.228	H 27	0.22898	H 27	0.23039	H 37	0.22178	H 36	0.22061	H 37	0.22027	H 35	0.22253	H 37	0.21872	H 35	0.21958
H 38	0.22422	H 28	0.21715	H 28	0.22401	H 38	0.22178	H 37	0.22061	H 38	0.22027	H 36	0.22102	H 38	0.21872	H 36	0.21956
C 39	-1.09708	C 29	-1.09491	C 29	-1.08733	H 39	0.22603	H 38	0.22684	H 39	0.22559	H 37	0.22585	H 39	0.2259	H 37	0.22584
H 40	0.22422	H 30	0.22257	H 30	0.22823	H 40	0.22603	H 39	0.22684	H 40	0.22559	H 38	0.22588	H 40	0.22591	H 38	0.22585
H 41	0.22974	H 31	0.22318	H 31	0.22578	H 41	0.22189	H 40	0.2192	H 41	0.22035	H 39	0.22112	H 41	0.21785	H 39	0.21876
H 42	0.228	H 32	0.22768	H 32	0.22893	H 42	0.22189	H 41	0.2192	H 42	0.22035	H 40	0.22002	H 42	0.21785	H 40	0.21871
C 43	-1.08776	C 33	-1.09515	C 33	-1.09629	H 43	0.23047	H 42	0.22973	H 43	0.23032	H 41	0.23085	H 43	0.22958	H 41	0.23007
H 44	0.2205	H 34	0.21889	H 34	0.22471	H 44	0.23047	H 43	0.22972	H 44	0.23032	H 42	0.23012	H 44	0.22957	H 42	0.23005
H 45	0.2271	H 35	0.22279	H 35	0.22976	H 45	0.22347	H 44	0.22255	H 45	0.22277	H 43	0.22314	H 45	0.2219	H 43	0.22204
H 46	0.22615	H 36	0.22924	H 36	0.2295	H 46	0.22347	H 45	0.22255	H 46	0.22277	H 44	0.22292	H 46	0.22191	H 44	0.22202
C 47	-1.08198	C 37	-1.08352	C 37	-1.08807	H 47	0.22923	H 46	0.22906	H 47	0.22849	H 45	0.229	H 47	0.22846	H 45	0.22871
H 48	0.22968	H 38	0.22624	H 38	0.23038	H 48	0.22923	H 47	0.22905	H 48	0.22849	H 46	0.22854	H 48	0.22846	H 46	0.22869
H 49	0.22408	H 39	0.22083	H 39	0.22809	H 49	0.22631	H 48	0.22869	H 49	0.22684	H 47	0.22616	H 49	0.22804	H 47	0.22802
H 50	0.2297	H 40	0.21786	H 40	0.22401	H 50	0.22631	H 49	0.22869	H 50	0.22684	H 48	0.22715	H 50	0.22804	H 48	0.22799
Sum	-0.52	Sum	-0.94	Sum	-0.58	Sum	-0.74	Sum	-0.62	Sum	-0.98	Sum	-0.95	Sum	-0.91	Sum	-0.88

9.3.5 QT-AIM analysis of complexes 1c, 2c, 2d, $P_{2c\text{-}iPr}$ and $P_{2c\text{-}SiMe3}$

QT-AIM analysis[21] for group 4 1-metallacyclobuta-2,3-diene complexes **1c**, **2c** and **2d** revealed two M–C bond paths in the metallacycles in between the metal centre and the α-carbon atoms (Figure S162 - Figure S163). Furthermore, this analysis shows in all cases a ring critical point between the metal centre and the β-carbon atom. These findings point to the absence of a bond between the central carbon atom and the metal centre, which was considered when drawing the Lewis representations of these complexes. In addition to the contour plot of the Laplacian of the electron density $\nabla^2 r$ of the investigated complexes we added the Wiberg bond indices (WBI) next to the bond critical points in italic numbers. The lower WBI between the central carbon atom and the metal centre compared to the α-C-M bonds supports the result of the QT-AIM analysis. Furthermore, the WBI of 1.94 for the C-C bonds in the allene units in **2c** and **2d** clearly indicate double bonds based on this theory (*c.f.* 1.93 in **1a**, 1.92 in **1c**, 1.95 in **2a** and **2b**).

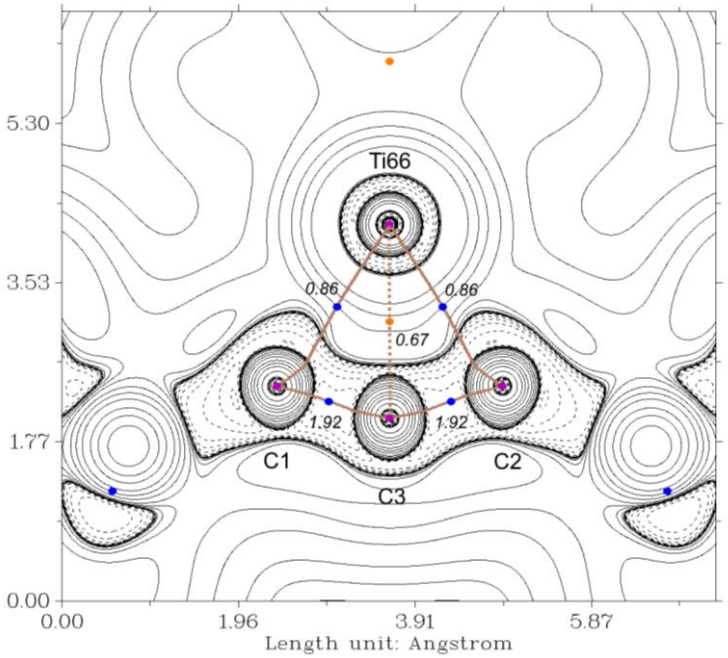

Figure S161. Contour plot of the Laplacian of the electron density $\nabla^2 r$ of complex **1c** in the C-Ti-C plane. Dashed lines indicate negative (local charge concentration), solid lines indicate positive values (local charge depletion). The Laplacian plot is overlaid with the molecular graph from QT-AIM analysis and Wiberg bond indices (italic small numbers). Brown lines indicate bond paths, brown dashed lines are hypothetical bonds, blue dots correspond to bond critical points, light brown dots indicate ring critical points. Density from B3LYP/GD3BJ/def2tzvp calculation.

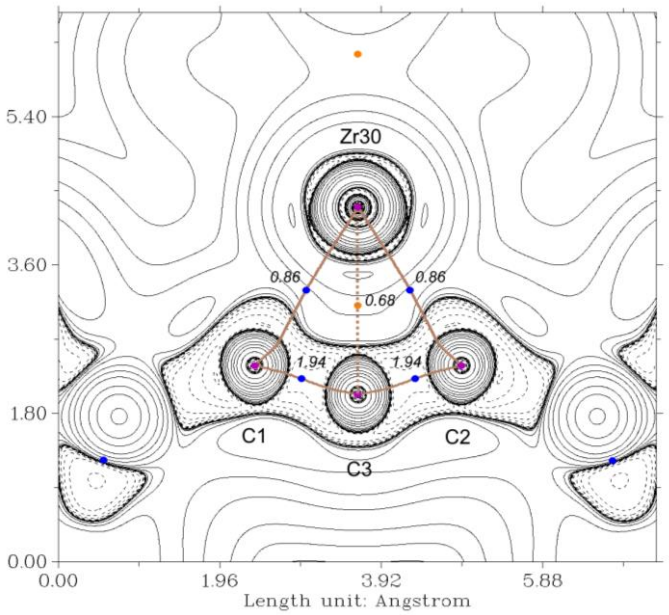

Figure S162. Contour plot of the Laplacian of the electron density $\nabla^2 r$ of complex **2c** in the C-Zr-C plane. Dashed lines indicate negative (local charge concentration), solid lines indicate positive values (local charge depletion). The Laplacian plot is overlaid with the molecular graph from QT-AIM analysis and Wiberg bond indices (italic small numbers). Brown lines indicate bond paths, brown dashed lines are hypothetical bonds, blue dots correspond to bond critical points, light brown dots indicate ring critical points. Density from B3LYP/GD3BJ/def2tzvp calculation.

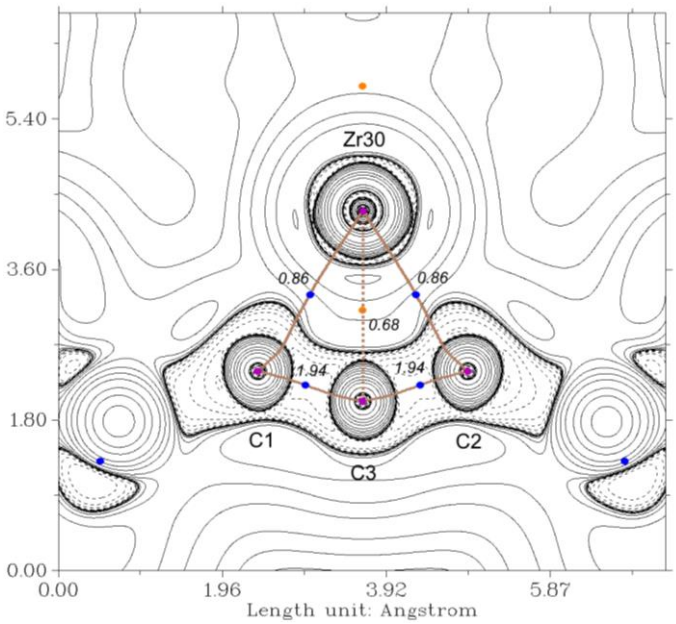

Figure S163. Contour plot of the Laplacian of the electron density $\nabla^2 r$ of complex **2d** in the C-Zr-C plane. Dashed lines indicate negative (local charge concentration), solid lines indicate positive values (local charge depletion). The Laplacian plot is overlaid with the molecular graph from QT-AIM analysis and Wiberg bond indices (italic small numbers). Brown lines indicate bond paths, brown dashed lines are hypothetical bonds, blue dots correspond to bond critical points, light brown dots indicate ring critical points. Density from B3LYP/GD3BJ/def2tzvp calculation.

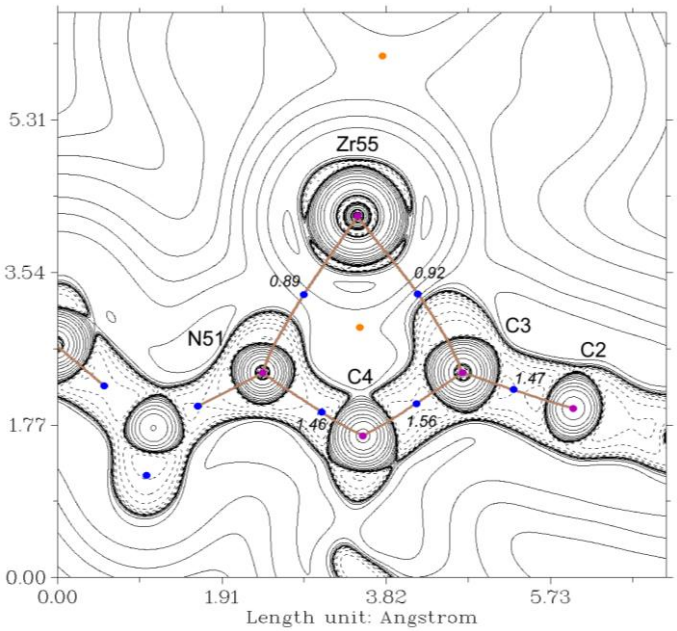

Figure S164. Contour plot of the Laplacian of the electron density $\nabla^2 r$ of complex **P2c-iPr** in the N51-Zr55-C3 plane. Dashed lines indicate negative (local charge concentration), solid lines indicate positive values (local charge depletion). The Laplacian plot is overlaid with the molecular graph from QT-AIM analysis and Wiberg bond indices (italic small numbers). Brown lines indicate bond paths, blue dots correspond to bond critical points, light brown dots indicate ring critical points. Density from B3LYP/GD3BJ/def2tzvp calculation.

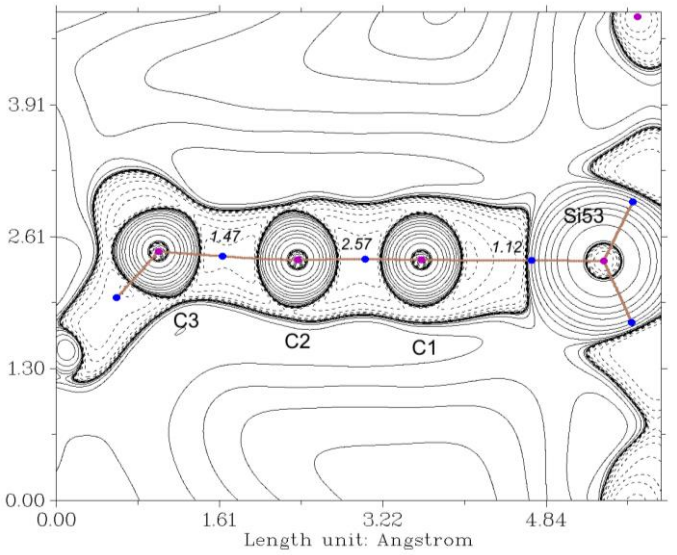

Figure S165. Contour plot of the Laplacian of the electron density $\nabla^2 r$ of complex **P2c-iPr** in the C1-C2-C3 plane. Dashed lines indicate negative (local charge concentration), solid lines indicate positive values (local charge depletion). The Laplacian plot is overlaid with the molecular graph from QT-AIM analysis and Wiberg bond indices (italic small numbers). Brown lines indicate bond paths, blue dots correspond to bond critical points, light brown dots indicate ring critical points. Density from B3LYP/GD3BJ/def2tzvp calculation.

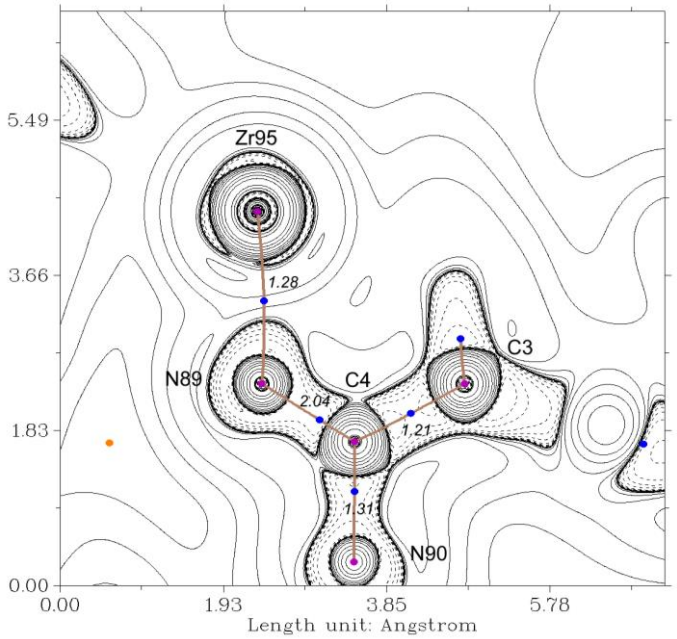

Figure S166. Contour plot of the Laplacian of the electron density $\nabla^2 r$ of complex **P2c-SiMe3** in the N89-Zr95-C3 plane. Dashed lines indicate negative (local charge concentration), solid lines indicate positive values (local charge depletion). The Laplacian plot is overlaid with the molecular graph from QT-AIM analysis and Wiberg bond indices (italic small numbers). Brown lines indicate bond paths, blue dots correspond to bond critical points, light brown dots indicate ring critical points. Density from B3LYP/GD3BJ/def2tzvp calculation.

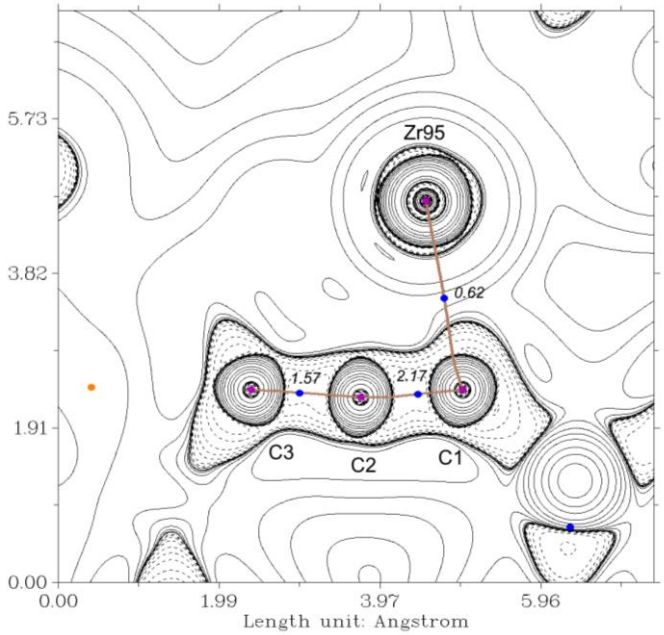

Figure S167. Contour plot of the Laplacian of the electron density $\nabla^2 r$ of complex **P2c-SiMe3** in the C1-Zr95-C3 plane. Dashed lines indicate negative (local charge concentration), solid lines indicate positive values (local charge depletion). The Laplacian plot is overlaid with the molecular graph from QT-AIM analysis and Wiberg bond indices (italic small numbers). Brown lines indicate bond paths, blue dots correspond to bond critical points, light brown dots indicate ring critical points. Density from B3LYP/GD3BJ/def2tzvp calculation.

9.3.6 Biradical character of 1-zirconacyclobuta-2,3dienes 2c & 2d

Since the electronic situation in the 1-titanacylobuta-2,3-diene complex **1a** is best described as a biradicaloid bearing a Ti(III) fragment which is antiferromagnetically coupled to a delocalised electron at the C_3 unit, we analysed the stability of the Kohn-Sham wavefunction from B3LYP calculation. This was found to be stable, but the Hartree-Fock wavefunction shows an RHF/UHF instability for the three complexes **1c**, **2c** and **2d**. To further evaluate the electronic situation of these as open-shell singlet we next performed Complete Active Space (CAS) calculations. The "broken-symmetry" solution is not a true eigenfunction of the S^2 operator. In fact, it may be considered as a 50:50 mixture of the singlet and triplet state, if the overlap between the singly occupied orbitals and spin polarisation are small.[22] The actual singlet wave function can then be expressed in terms of a linear combination of *two* "broken-symmetry" wave functions

$$^1\Psi = \frac{1}{\sqrt{2}}(|\cdots \chi_+\overline{\chi_-}\rangle - |\cdots \overline{\chi_+}\chi_-\rangle)$$

where χ_+, χ_- are the singly occupied orbitals and the overline indicates β spin. Therefore, the open-shell singlet must be described by a multi-reference wave function.

In the "broken-symmetry" picture, the singly occupied orbitals χ_+ and χ_- are, in principle, localised orbitals formed by linear combinations of the (delocalised) canonical HOMO ϕ_{H} and LUMO ϕ_{L}:

$$\chi_\pm = \frac{1}{\sqrt{2}}(\phi_H \pm \phi_{\mathrm{L}})$$

Hence, the multi-reference wave function expressed in terms of the canonical MOs is given by

$$^1\Psi = c_1|\cdots \phi_{\mathrm{H}}^2\rangle + c_2|\cdots \phi_{\mathrm{L}}^2\rangle$$

where the expansion coefficients c_i are the square roots of the relative weight of each determinant. This type of multi-determinant open-shell singlet wave function can be obtained by the CAS SCF method and gives a qualitatively correct description of the electronic structure of a biradical. The biradical character can be evaluated as

$$\beta = \frac{2c_2^2}{c_1^2 + c_2^2}$$

where a value of β = 1 indicates a "perfect" biradical with two electrons in two degenerate orbitals.[23] Smaller values indicate an increasing energy gap between HOMO and LUMO, and $\beta \rightarrow 0$ indicates a closed-shell species.

Consequently, the smallest active space to properly describe a biradical is a CAS(2,2) calculation (*i.e.* two electrons in two orbitals). In case of compound **2c** & **2d**, in analogy to the calculations on **1a**, we chose to include eight electrons in nine orbitals in the active space (CAS(8,9), comprising the formal π orbitals at the ligand and d orbitals at Zr, *vide infra*), as these orbitals are energetically relatively closely spaced.

In complex **1a** the largest contributions to the multi-determinant wave function are the two determinants placing two electrons either in the formal HOMO (ϕ_4) or LUMO (ϕ_5; β = 24 %), which show an occupancy of the formal LUMO with 0.30 electrons. For the Zr analog **2a** only a low coefficient for this determinant and a neglectable occupation of the formal LUMO ϕ_5 with only 0.08 electrons could be found. Based on this calculation compound **2a** show a negligible biradicaloid character and we abstain from further discussions. This is well in line with previous calculations of group 4 metallocene phosphinidenes, where the Zr derivative also showed significantly lower biradicaloid character compared to the Ti complex.[24] Nevertheless, the ligand influence is clearly seen when we look from the tetrahydroindenyl metallocenes (**1a**, **2a**, **2b**) to the indenyl metallocenes (**1c**, **2c**, **2d**). Here, in all three complexes investigated, significantly higher biradicaloid fractions are found. Furthermore, it becomes clear that the more rigid Me_2Si bridging unit will increase the b value as well compared to the flexible C_2H_4 bridge.

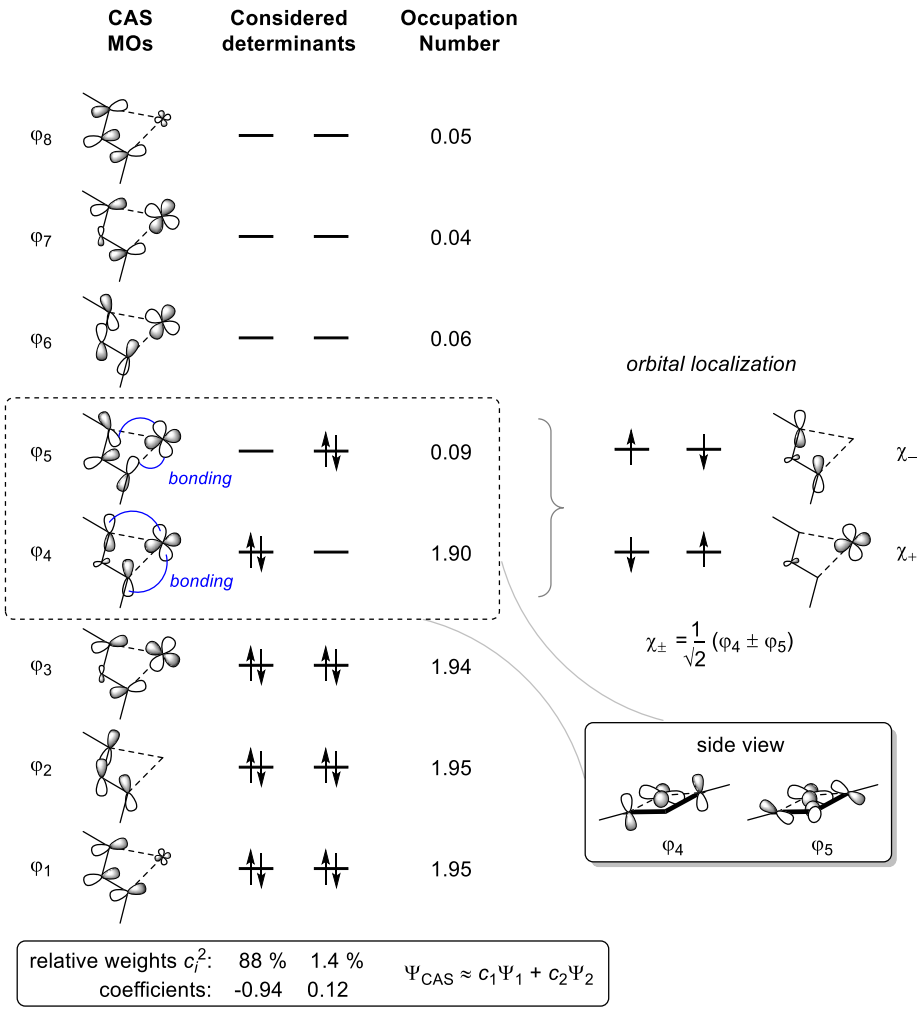

Figure S168. Schematic depiction of the important active orbitals of a CAS(8,9)/def2tzvp calculation of **2c**. The low occupation of ϕ_5 and the small coefficient c_2 reveal a negligible biradicaloid character in this molecule.

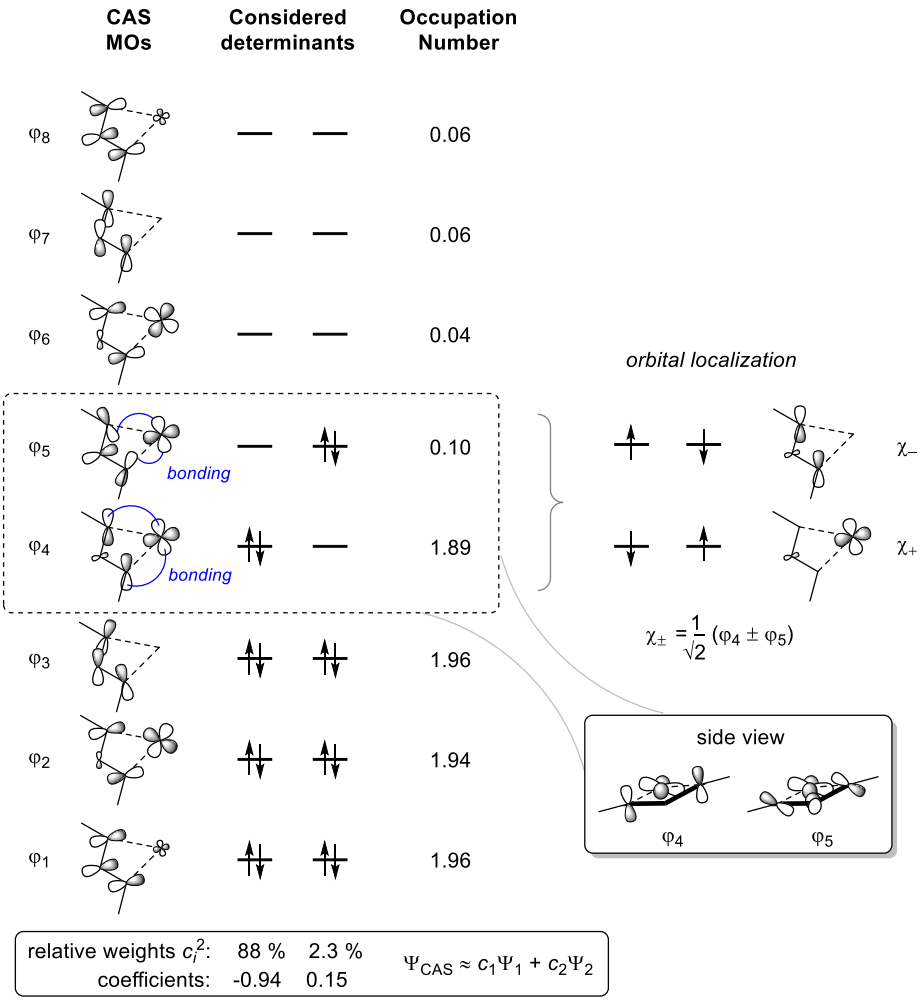

Figure S169. Schematic depiction of the important active orbitals of a CAS(8,9)/def2tzvp calculation of **2d**. The low occupation of ϕ_5 and the small coefficient c_2 reveal a negligible biradicaloid character in this molecule.

Table S23. Representation of the most important CAS(8,9) molecular orbitals of **2c** (isovalue = 0.03).

LUMO+3	LUMO+2
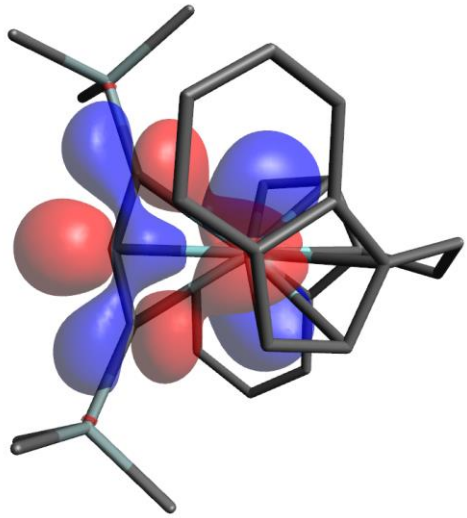	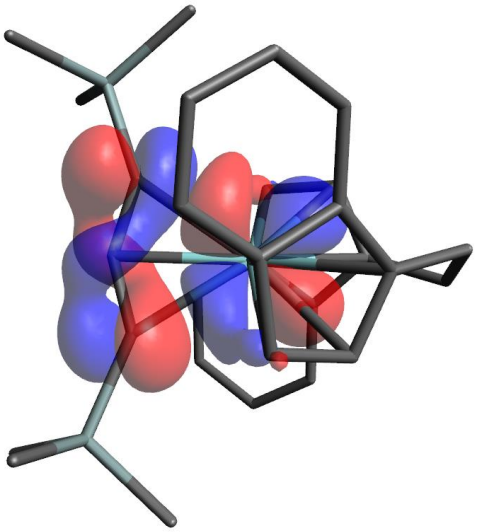
LUMO+1	LUMO
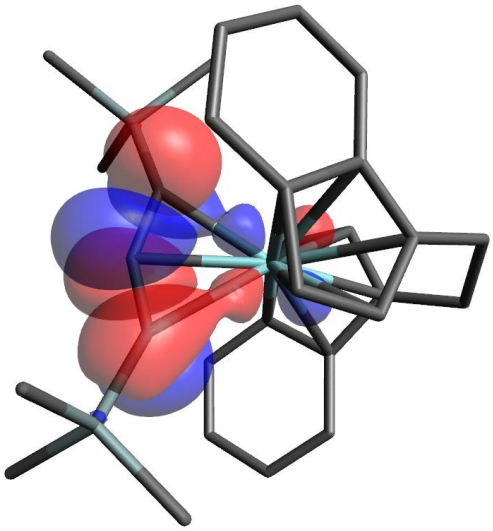	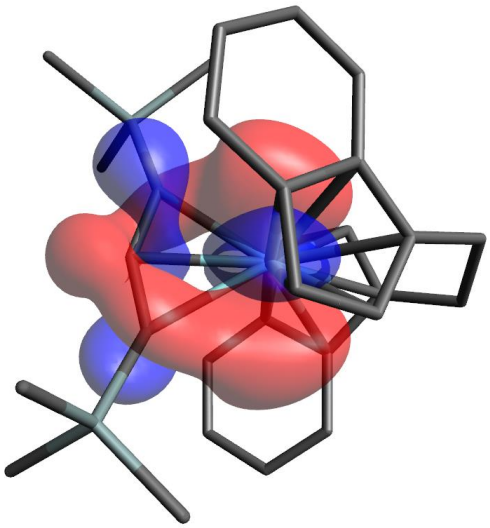

HOMO	HOMO-1
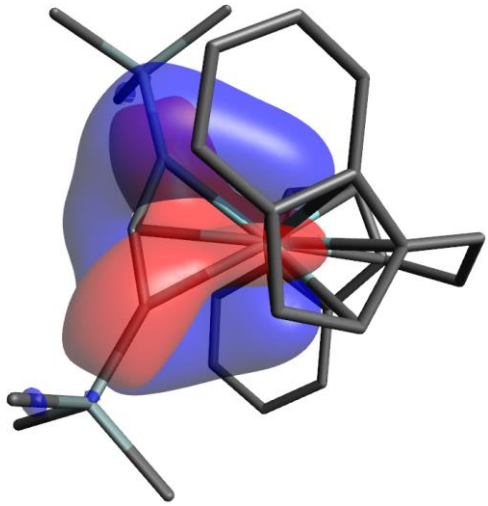	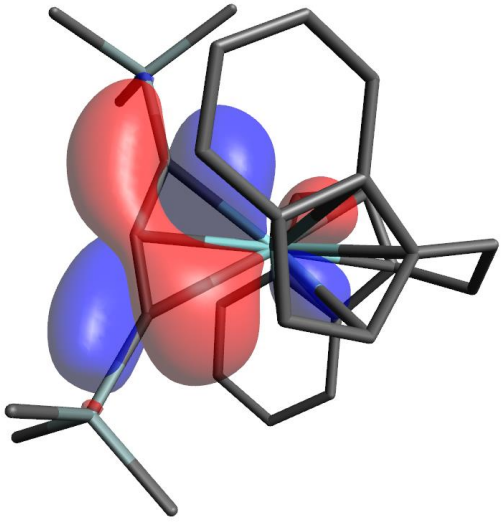
HOMO-2	HOMO-3
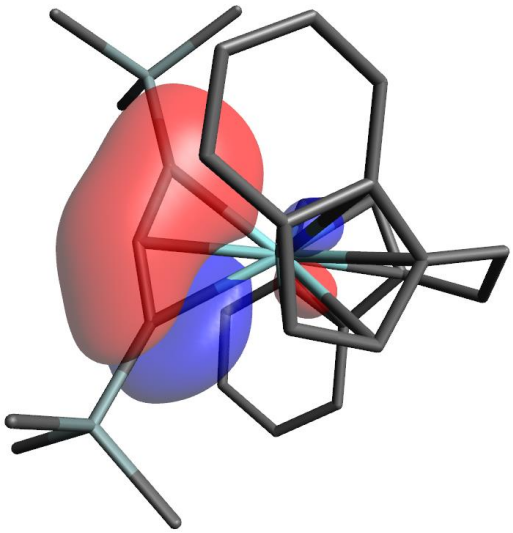	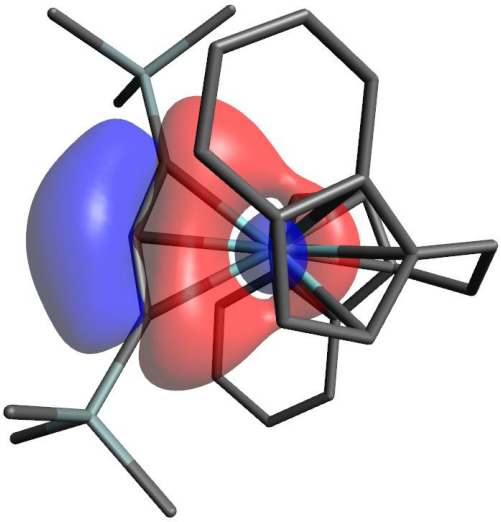

Table S24. Representation of the most important CAS(8,9) molecular orbitals of **2d** (isovalue = 0.03).

LUMO+3	LUMO+2
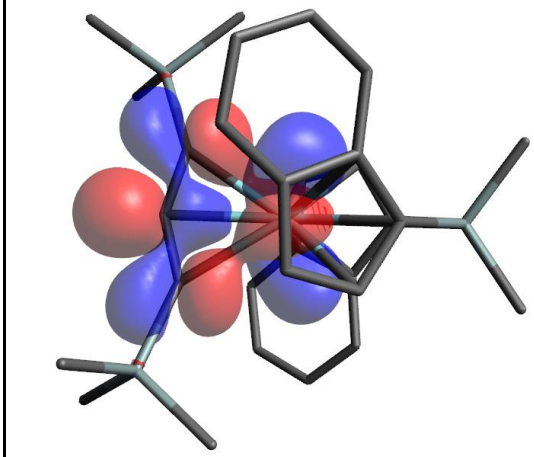	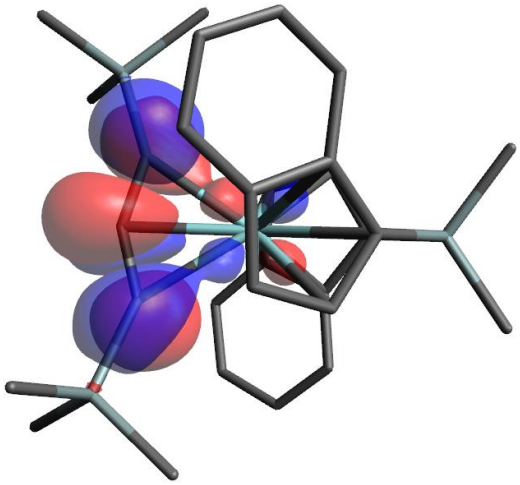
LUMO+1	LUMO
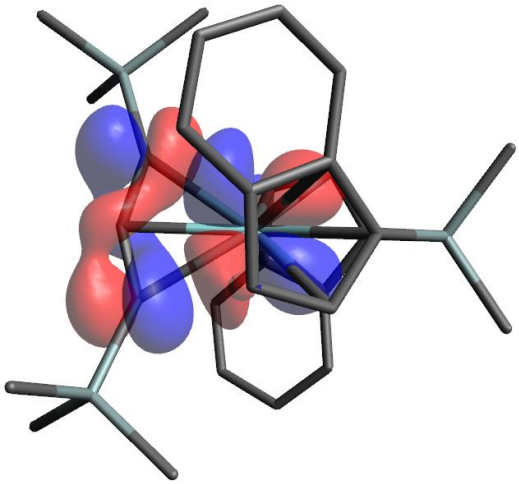	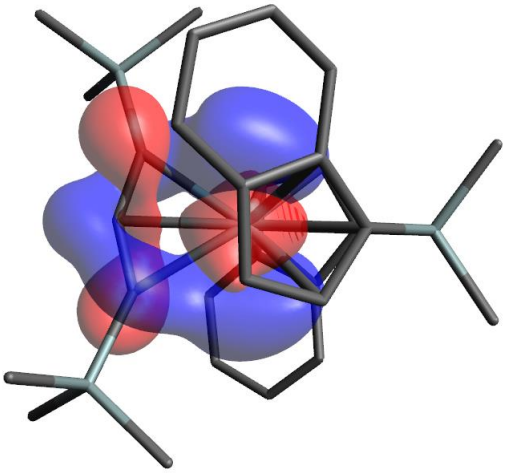
HOMO	HOMO-1
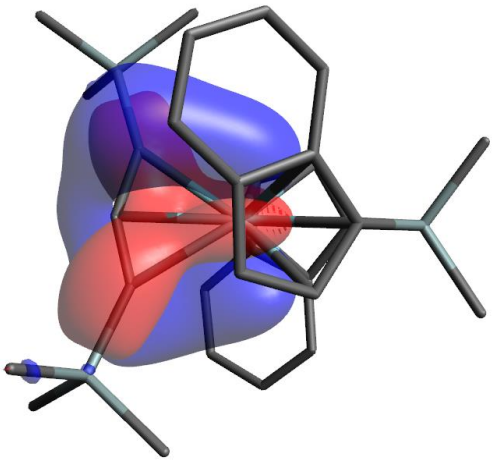	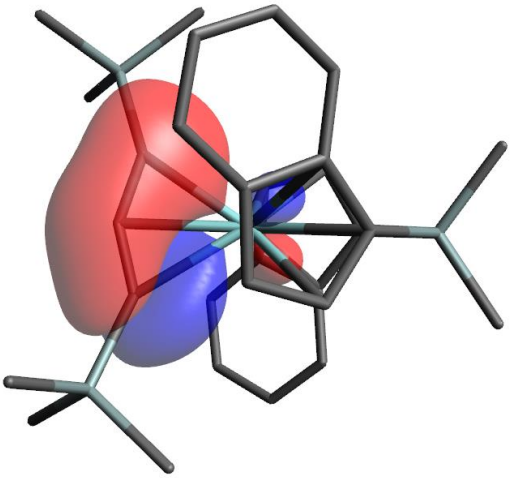

HOMO-2	HOMO-3
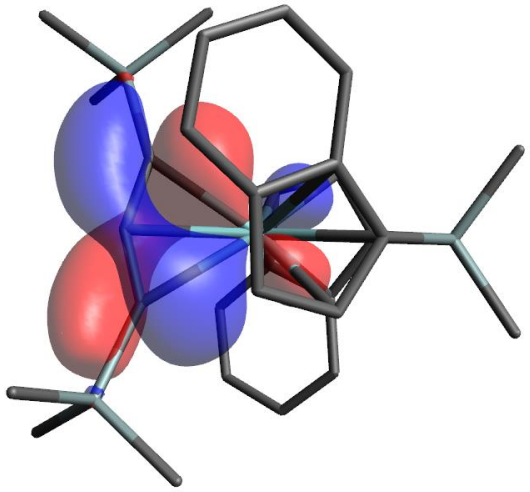	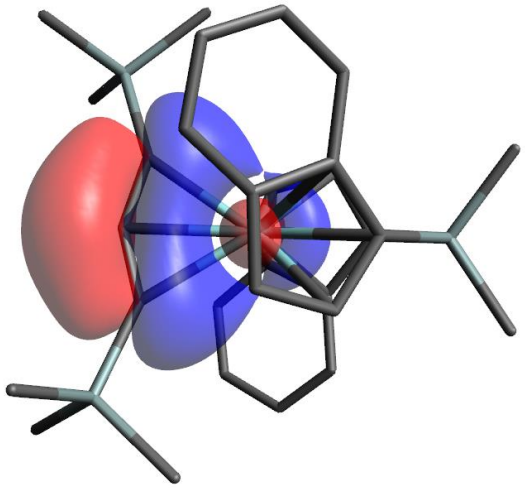

9.3.7 Calculation of deviation from planarity and biradicaloid character of all investigated compounds.

Table S25. Summary of selected data from optimised structures (B3LYP/GD3BJ/def2tzvp) and CAS(8,9)/def2tzvp calculations.

Metallocene	Si1C1M1	M1C1C2	C2C1Si1	Si2C3M1	M1C3C2	C2C3Si2	∑∢(C1)	∑∢(C3)	dfp (C1)	dfp (C3)	SiC-CSi Dihedral	Occ. φ_4	Occ. φ_5	c_4	c_5	β (%)
Cp_2Ti	140.89	71.36	144.80	140.89	71.36	144.80	357.05	357.05	2.9	2.9	-65.19	1.640	0.354	-0.857	0.359	29.8
$Cp^*_2Ti\_sing$	153.51	72.20	134.12	152.44	67.58	139.80	359.83	359.82	0.2	0.2	-10.38	1.229	0.772	-0.744	0.581	75.8
$Cp^*_2Ti\_trip$	153.73	69.32	136.94	153.70	69.30	136.98	359.99	359.99	0.0	0.0	-0.03					
rac-(ebthi)Ti	145.74	70.62	136.27	145.74	70.62	136.27	352.63	352.63	7.4	7.4	-72.60	1.691	0.302	0.871	-0.322	24.0
rac-(ebi)Ti	144.33	71.06	139.95	144.35	71.06	139.93	355.34	355.34	4.7	4.7	-67.27	1.606	0.393	-0.851	0.389	34.5
rac-(ebthi)Zr	142.83	72.12	135.63	142.83	72.12	135.63	350.58	350.58	9.4	9.4	-82.03	1.916	0.079	-0.944	0.092	1.9
rac-(ebi)Zr	141.15	72.57	140.78	141.15	72.57	140.77	354.50	354.50	5.5	5.5	-76.21	1.902	0.088	-0.937	0.122	3.3
rac-(sbthi)Zr	142.59	72.34	137.89	142.69	72.25	135.17	352.82	350.11	7.2	9.9	-80.39	1.909	0.085	-0.942	0.110	2.7
rac-(sbi)Zr	140.72	72.74	141.66	140.81	72.77	141.50	355.11	355.08	4.9	4.9	-74.75	1.890	0.102	-0.936	0.148	4.9

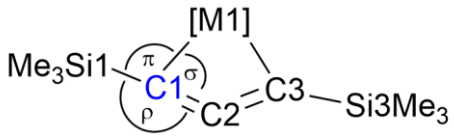

[M1] = *rac*-(ebi)M or *rac*-(ebthi)M
M = Ti or Zr

$$\mathbf{dfp = [360° - (\pi + \rho + \sigma)]}$$

Figure 170: Explanation Figure for calculating dfp values.

9.3.8 Graphical analysis of correlation between the dfp and electronic parameters of the investigated 1-metallacyclobuta-2,3-dienes

Table S26: Comparison of calculated features of 1-metallacyclobuta-2,3-dienes, calculated at the B3LYP/GD3BJ/def2tzvp level of theory.

Metallocene	$\Delta E_{S\text{-}T}$ [kJ/mol]	dfp (C1) [°]	$q_{nat.NBO}$ (allene)	β[a] [%]
Cp_2Ti (**A**)	-24.3	2.9	-0.52	29.8
Cp^*_2Ti (**B**)	9.9	0.2[b]/ 0.0[c]	-0.94[b]/ -0.58[c]	75.8
rac-(ebthi)Ti (**1a**)	-41.4	7.4	-0.74	24.0
rac-(ebi)Ti (**1c**)	-25.2	4.7	-0.62	34.5
rac-(ebthi)Zr (**2a**)	-99.8	9.4	-0.98	1.9
rac-(sbthi)Zr (**2b**)	-96.9	7.2	-0.95	2.7
rac-(ebi)Zr (**2c**)	-81.6	5.5	-0.91	3.3
rac-(sbi)Zr (**2d**)	-78.7	4.9	-0.88	4.9

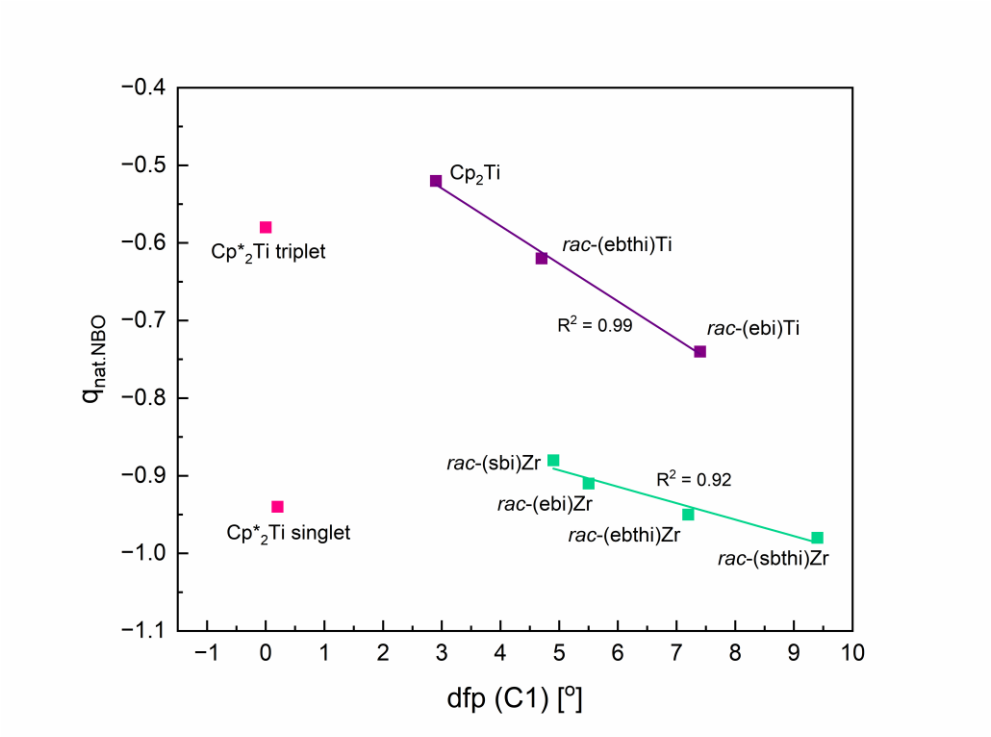

Figure S171. Correlation of dpf (C1) [°] between $q_{nat.NBO}$ for all the complexes in Table S26.

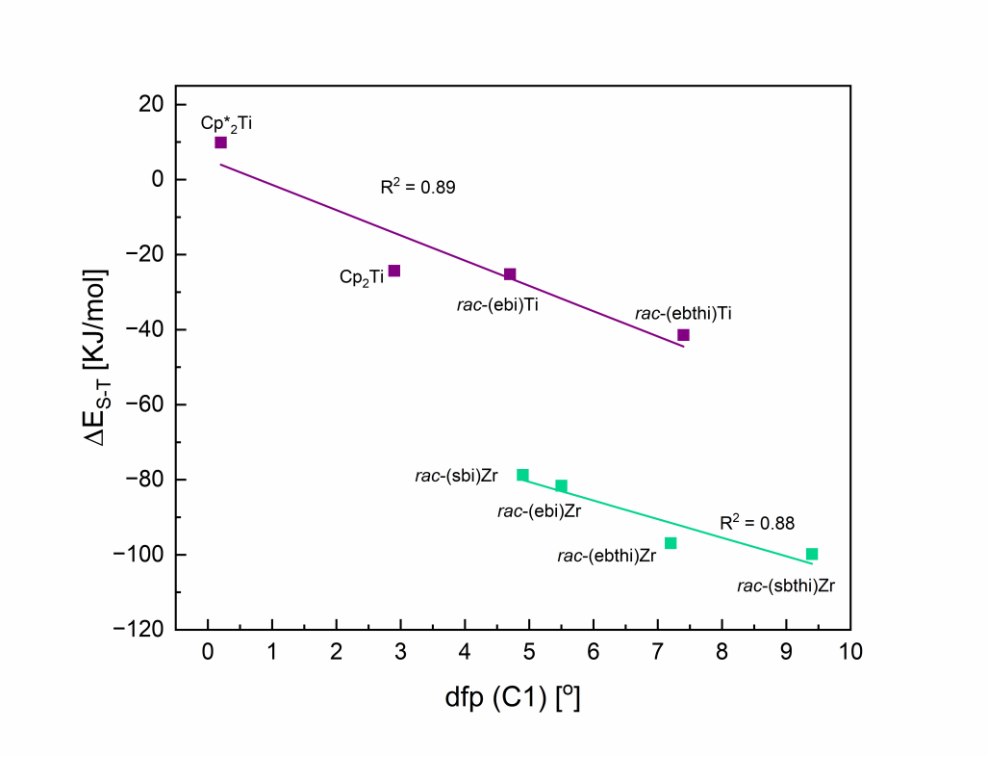

Figure S172. Correlation of dpf (C1) [º] between Δ*E*S-T [kJ/mol] for all the complexes in Table S26.

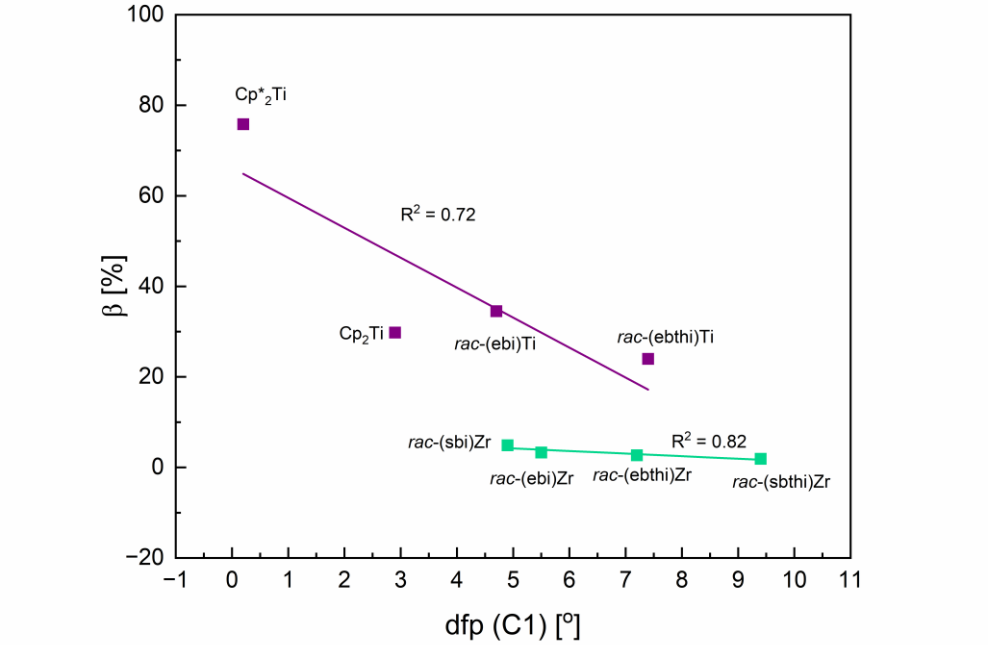

Figure S173. Correlation of dpf (C1) [º] between β [%] for all the complexes in Table S26.

10. References

1 G. M. Diamond, S. Rodewald and R. F. Jordan, Efficient Synthesis of *rac*-(Ethylenebis(indenyl))ZrX_2 Complexes via Amine Elimination, *Organometallics*, 1995, **14**, 5-7.

2 F. Reiß, M. Reiß, A. Spannenberg, H. Jiao, W. Baumann, P. Arndt, U. Rosenthal and T. Beweries, Visiting the Limits between a Highly Strained 1-Zirconacyclobuta-2,3-diene and Chemically Robust Dizirconacyclooctatetraene, *Chem. Eur. J.*, 2018, **24**, 5667-5674.

3 P. Huang, D. Xu, R. M. Reich, F. Kaiser, B. Liu and F. E. Kühn, Et_2Zn-mediated stoichiometric C(sp)-H silyation of 1-alkynes and chlorosilanes, *Tetrahedron Lett.*, 2019, **60**, 1574-1577.

4 G. R. Fulmer, A. J. M. Miller, N. H. Sherden, H. E. Gottlieb, A. Nudelman, B. M. Stoltz, J. E. Bercaw and K. I. Goldberg, NMR Chemical Shifts of Trace Impurities: Common Laboratory Solvents, Organics, and Gases in Deuterated Solvents Relevant to the Organometallic Chemist, *Organometallics*, 2010, **29**, 2176-2179.

5 G. M. Sheldrick, A short history of SHELX, *Acta Cryst., Sect. A: Found. Crystallogr.*, 2008, **64**, 112-122.

6 G. M. Sheldrick, Crystal structure refinement with SHELXL, *Acta Cryst.*, *Sect. C: Struct. Chem.*, 2015, **71**, 3-8.

7 H. Putz and K. Brandenburg, *Diamond-Crystal and Molecular Structure Visualization*, Crystal Impact-GbR, Kreuzherrenstr. 102, 53227, Bonn, Germany, 2018.

8 A. L. Spek, PLATON SQUEEZE: a tool for the calculation of the disordered solvent contribution to the calculated structure factors, *Acta Cryst.*, 2015, **C71**, 9-18.

9 S. Chen, J. Wang and H. Wang, Synthesis, characterization and pyrolysis of a high zirconium content zirconocene-polycarbosilane precursor without Zr-O bond, *Materials & Design*, 2016, **90**, 84-90.

10 F. Reiß, M. Reiß, J. Bresien, A. Spannenberg, H. Jiao, W. Baumann, P. Arndt and T. Beweries, 1-Titanacyclobuta-2,3-diene – an elusive four-membered cyclic allene, *Chem. Sci.*, 2019, **10**, 5319-5325.

11 M. J. Frisch, G. W. Trucks, H. B. Schlegel, G. E. Scuseria, M. A. Robb, J. R. Cheeseman, G. Scalmani, V. Barone, G. A. Petersson, H. Nakatsuji, X. Li, M. Caricato, A. V. Marenich, J. Bloino, B. G. Janesko, R. Gomperts, B. Mennucci, H. P. Hratchian, J. V. Ortiz, A. F. Izmaylov, J. L. Sonnenberg, D. Williams-Young, F. Ding, F. Lipparini, F. Egidi, J. Goings, B. Peng, A. Petrone, T. Henderson, D. Ranasinghe, V. G. Zakrzewski, J. Gao, N. Rega, G. Zheng, W. Liang, M. Hada, M. Ehara, K. Toyota, R. Fukuda, J. Hasegawa, M. Ishida, T. Nakajima, Y. Honda, O. Kitao, H. Nakai, T. Vreven, K. Throssell, J. A., Jr. Montgomery, J. E. Peralta, F. Ogliaro, M. J. Bearpark, J. J. Heyd, E. N. Brothers, K. N. Kudin, V. N. Staroverov, T. A. Keith, R. Kobayashi, J. Normand, K. Raghavachari, A. P. Rendell, J. C. Burant, S. S. Iyengar, J. Tomasi, M. Cossi, J. M. Millam, M. Klene, C. Adamo, R. Cammi, J. W. Ochterski, R. L. Martin, K. Morokuma, O. Farkas, J. B. Foresman and D. J. Fox, *Gaussian 16, Rev. C.01*, Gaussian, Inc., Wallingford, CT, 2016.

12 (a) E. D. Glendening, J. K. Badenhoop, A. E. Reed, J. E. Carpenter, J. A. Bohmann, C. M. Morales, C. R. Landis and F. Weinhold, Theoretical Chemistry Institute, University of Wisconsin, Madison, 2013; (b) J. E. Carpenter and F. Weinhold, Analysis of the geometry

of the hydroxymethyl radical by the "different hybrids for different spins" natural bond orbital procedure, *J. Mol. Struct.: THEOCHEM*, 1988, **169**, 41-62; (c) F. Weinhold and J. E. Carpenter, The Natural Bond Orbital Lewis Structure Concept for Molecules, Radicals, and Radical Ions. In *The structure of small molecules and ions*, Springer, 1988, pp. 227-236; (d) F. Weinhold and C. R. Landis, *Valency and bonding: a natural bond orbital donor-acceptor perspective*, Cambridge University Press, 2005.

13 (a) A. D. Becke, Densit-functional exchange-energy approximation with correct asymptotic behavior, *Phys. Rev. A*, 1988, **38**, 3098-3100; (b) J. P. Perdew, Density-functional approximation for the correlation energy of the inhomogeneous electron gas, *Phys. Rev. B*, 1986, **33**, 8822-8824.

14 (a) S. H. Vosko, L. Wilk and M. Nusair ,Accurate spin-dependent electron liquid correlation energies for local spin density calculations: a critical analysis, *Can. J. Phys.*, 1980, **58**, 1200-1211; (b) C. Lee, W. Yang, R. G. Parr, Development of the Colle-Salvetti correlation-energy formula into a functional of the electron density, *Phys. Rev. B*, 1988, **37**, 785-789; (c) B. Miehlich, A. Savin, H. Stoll and H. Preuss, Results obtained with the correlation energy density functionals of Becke and Lee, Yang and Parr, *Chem. Phys. Lett.*, 1989, **157**, 200-206; (d) A. D. Becke, Becke's three parameter hybrid method using the LYP correlation functional, *J. Chem. Phys.*, 1993, **98**, 5648-5652.

15 F. Weigend and R. Ahlrichs, Balanced basis sets of split valence, triple zeta valence and quadruple zeta valence quality for H to Rn: Design and assessment of accuracy, *Phys. Chem. Chem. Phys.*, 2005, **7**, 3297-3305.

16 (a) S. Grimme, J. Antony, S. Ehrlich and H. Krieg, A consistent and accurate ab *initio* parametrization of density functional dispersion correction (DFT-D) for the 94 elements H-Pu, *J. Chem. Phys.*, 2010, **132**, 154104; (b) S. Grimme, S. Ehrlich and L. Goerigk, Effect oft he damping function in dispersion corrected density functional theory, *J. Comput. Chem.*, 2011, **32**, 1456-1465.

17 T. Lu and Q. Chen, Interaction Region Indicator: A Simple Real Space Function Clearly Revealing Both Chemical Bonds and Weak Interactions, *Chemistry–Methods*, 2021, **1**, 231-239.

18 T. Lu and F. Chen, Multiwfn: A multifunctional wavefunction analyzer, *J. Comput. Chem.*, 2012, **33**, 580-592.

19 R. Dennington, T. A. Keith and J. M. Millam, GaussView, version 6.0. 16. *Semichem Inc. Shawnee Mission KS*, 2016.

20 Mercury: http://www.ccdc.cam.ac.uk/mercury/

21 (a) R. F. Bader, Atoms in Molecules, *Acc. Chem. Res.*, 1985, **18**, 9-15; (b) R. F. Bader, A Quantum Theory of Molecular Structure and Ist Applications, *Chem. Rev.*, 1991, **91**, 893-928; (c) R. F. Bader, *Atoms in Molecules: A Quantum Theory*, Oxford University Press, 1994; (d) R. F. Bader, The Quantum Mechanical Basis of Conceptual Chemistry, *Monatsh. Chem.*, 2005, **136**, 819-854.

22 (a) J. C. Christopher, Essentials of computational chemistry: theories and models. 2004; (b) L. Salem and C. Rowland, The Electronic Properties of Diradicals, *Angew. Chem. Int. Ed. Engl.*, 1972, **11**, 92-111; (c) J.-P. Malrieu and G. Trinquier, A Recipe for Geometry Optimization of Diradicalar Singlet States from Broken-Symmetry Calculations, *J. Phys. Chem. A*, 2012, **116**, 8226-8237.

23 E. Miliordos, K. Ruedenberg and S. S. Xantheas, Unusual Inorganic Biradicals: A Theoretical Analysis, *Angew. Chem. Int. Ed.*, 2013, **52**, 5736-5739.

24 M. Fischer, F. Reiß and C. Hering-Junghans, Titanocene pnictinidene complexes, *Chem. Commun.*, 2021, **57**, 5626-5629.